Quantum Field Modelling in Optical Communication Systems

by

Alwin Ming Wai Tam

Submitted in total fulfilment of

the requirements for the degree of

Master of Engineering Science

Department of Electrical and Electronics Engineering

University of Melbourne

Australia

2011

Abstract

Quantum field theory predicts photons are created from the phase modulator when the optical field experiences a refractive index change, and hence energy are excited from a lossless phase modulator, an effect not included in classical field theory. In high speed optical communication system, a phase modulator is used to impress data onto the phase of the optical field. The phase modulation process requires a refractive index change within the modulating medium; therefore the process of photon excitation from the modulator will inevitably occur.

The scope of this thesis is to develop a quantum field theory of a transverse phase modulator, based upon time dependent Bogoliubov transforms, that includes the phenomenon of photon/energy excitation from the modulator. This model will be used for determining the properties of a phase modulated optical field, and investigate the impact from photon creation from the phase modulator on a range of optical communication systems.

It is found that when an input coherent optical field is subject to phase modulation, it evolve from a coherent state to a two photon coherent squeeze state, for which the mean and variance of the photoelectron count observed by a detector are time dependent. Furthermore, it is shown that the effect of photon creation improves the performance of the optical communication system, and this improvement increases exponentially with a linear increase in bit rate. However, simulation results have shown this improvement is insignificant even when the optical system operates at a bit rate of terabits per second. Therefore the effect of photon creation has a negligible impact on the performance of a high speed optical communication system.

Declaration

This is to certify that:

I. The thesis comprises only my original work.

II. Due acknowledgement has been made in the text to all other material used.

III. The thesis is less than 50,000 words in length, exclusive of table, maps, bibliographies, appendices and footnotes.

Signature:

Date:

Preface

This thesis presents most of the work that I have undertaken during my Masters candidature. The work involve is to construct a quantum field model of a phase modulator in order to determine the quantum effect of photon creation from modulator in optical communication system, an issue which has not been addressed before. Chapter 5 and Chapter 6 closely aligned with the papers of publication that I have co-authored during my candidature. These research papers are listed in Appendix A of this thesis. This thesis can be broadly divided into three parts.

Part 1 presents a background and the motivation of this work. Chapter 2 and Chapter 3 introduce the background theories that are essential to understand the quantum analysis of an optical communication system presented in later Chapters.

Part 2 presents a theoretical quantum field model of a phase modulator that includes the effect of photon creation from the modulator. The model will be used for determining the impact of photon creation in an optical communication system. This will be given by the contents in Chapter 4 and Chapter 5.

Part 3 presents the important results that highlight the impact of photon creation from phase modulator on the properties of the modulated optical field and in a high speed optical communication system. Simulation results that reveal the extent of the impact of this effect in an optical communication system will be presented in order to determine whether the quantum effect of photon creation from modulator is detectable. These results will be shown in Chapter 6 and Chapter 7.

Acknowledgments

I would like to take this opportunity to express my deepest appreciation to my supervisors, Professor Rod Tucker and Dr. Kerry Hinton, for giving me an opportunity to study in University of Melbourne and instructive guidance for my research and paper publications. In addition, I am grateful to Dr Kerry Hinton for his effort in organizing basketball games in a weekly basis, which greatly helped me to release my stresses during my studies, as well as lending me many of his books during my thesis writing without charging me rent. I appreciate Associate Professor Peter Farrell for serving as my research project committee providing valuable insight into my work, and playing some lovely music from his guitar and ukulele to encourage me whenever I am facing some challenges in my research.

As an important part of my life in Australia, I would like to thank the School of Engineering in University of Melbourne for awarding me a Master Research Scholarship (MRS) that is essential to sustain my living cost.

I am also indebt to my friends in University of Melbourne for their support and encourage which creates a friendly and comfortable environment for my study. Last but not least, I would like to thank my parents for their endless support and all the efforts that they have made over the years of my candidature.

Table of Contents

Abstract ii

Declaration iii

Preface iv

Acknowledgements v

Table of Contents vi

List of Figures x

List of Tables xiv

1. Introduction **1**

1.1 The Trend of Optical Communication System 1

1.2 Historical Backgrounds of Particle Creation 3

1.3 Motivations 5

1.4 Thesis Objectives 7

1.5 Thesis Outline 8

2. Overview of Optical Communications **10**

2.1 Phase Modulation Theory 10

2.2 Analysis of Optical Communication Systems 14

2.2.1 Binary Phase Shift Keyed (BPSK) Systems 14

2.2.2 Amplitude Shift Keyed (ASK) Systems 22

2.2.3 Systems performance 26

2.3 Summary 31

3. Introduction to Quantum Field Theory (QFT) 33

3.1 Quantum Field Operators in Vacuum 33

3.2 Quantum State of Optical Field 37

3.3 Summary 42

4. Quantum Field Model of Phase Modulator 43

4.1 Chapter Objectives 43

4.2 Quantum Model of Phase Modulator 44

4.2.1 Field in Modulating Medium 44

4.2.2 Hamiltonian Formalism in Modulating Medium 48

4.2.3 Bogoliubov Transformation of Field Mode 55

4.2.4 Field in Anti-Reflective Coating (ARC) 59

4.3 Conclusions 61

5. Quantum Representation of Phase Modulated Field 63

5.1 Chapter Objectives 63

5.2 Field Mode Solution in Modulating Medium 63

5.2.1 The Quantum Mechanical Scattering Analogy 65

5.2.2 Field Operator Representation 70

5.3 Field Mode Solution in ARC 77

5.4 Continuum Operators and States 80

5.5 Phase Modulated Field Operator 83

5.6 Conclusions 93

6. Properties of Phase Modulated Field **94**

6.1 Chapter Objectives 94

6.2 Power Flow of Phase Modulated Field 95

6.3 Detection of Optical Field 110

6.3.1 Direct Detection of Unmodulated Field 110

6.3.2 Direct Detection of Modulated Field 115

6.4 State Evolution of Modulated Field 122

6.5 Photon Creation in Phase Modulation 137

6.5.1 Spontaneous Emission from Modulator 141

6.5.2 Stimulated Emission from Modulator 150

6.5.3 Energy Exchange between Signal Field and Modulator 152

6.5.4 Dependence of Photon Creation Process 156

6.6 PSD for Sinusoidal Modulation 161

6.7 Conclusions 167

7. Quantum Modelling of Optical Communication Systems **169**

7.1 Chapter Objectives 169

7.2 Quantum Field Model of BPSK system 170

7.2.1 Analysis of BPSK Transmitter 170

7.2.2 Analysis of BPSK Homodyne Receiver 173

7.2.3 Analysis of BPSK Heterodyne Receiver 185

7.3 Quantum Field Model of ASK system 188

7.3.1 Analysis of ASK Transmitter 189

7.3.2 Analysis of ASK Homodyne Receiver 192

7.3.3 Analysis of ASK Heterodyne Receiver 196

7.4 BER Quantum Limit of Communication Systems 198

7.5 BER Quantum Limit and Bit rate Relation 220

7.6 Conclusions 226

8. Conclusions **228**

8.1 Summary 228

8.2 Future Works 229

Bibliography and References **231**

Appendix A: List of Publications 237

List of Figures

Figure 1.1	Block diagram of high speed optical communication system.	3
Figure 2.1	Configuration of phase modulator.	10
Figure 2.2	Characteristics of BPSK modulation.	15
Figure 2.3	Configuration of BPSK transmitter.	16
Figure 2.4	Configuration of balanced coherent receiver.	16
Figure 2.5	Characteristics of ASK modulation.	22
Figure 2.6	Configuration of ASK transmitter for which transmitted data is externally modulated.	23
Figure 2.7	Probability density functions for *Y,* conditioned on *'1'* and *'0'*.	27
Figure 3.1	State diagram of optical field prepared in coherent state.	40
Figure 3.2	Amplitude and phase uncertainty spread of optical field with a) Low photon number b) Large photon number.	41
Figure 4.1	Diagram of AO-TPM.	43
Figure 4.2	TEM wave propagating in *z* direction.	46
Figure 4.3	Time dependent refractive index profile of modulator.	55
Figure 5.1	Refractive index profile of modulating medium.	64
Figure 5.2	Propagation of forward incident field in a time varying *n(t)* profile.	66
Figure 5.3	Propagation of backward incident field in a time varying *n(t)* profile.	67
Figure 5.4	Refractive index profile of ARC.	77
Figure 5.5	Refractive index against distance for a phase modulated system.	85
Figure 5.6	Field decomposition of forward traveling wave in modulating medium.	88
Figure 5.7	Field decomposition of backward propagating wave in modulating medium.	88
Figure 6.1	PSD of unmodulated optical field corrupted by laser phase noise.	96
Figure 6.2	Configuration of optical system.	98

Figure 6.3	Power flow of optical field at the modulator (SCFT).	103
Figure 6.4	Illustration of spontaneous emission out of the .	104
Figure 6.5	Equivalent circuit of transformer analogy.	106
Figure 6.6	Illustration of stimulating photons out of the modulator.	106
Figure 6.7	Equivalent circuit of the transformer analogy.	107
Figure 6.8	Power flow of optical field at the modulator (Energy exchange term positive).	108
Figure 6.9	Power flow of the optical field at the modulator (Energy exchange term negative).	109
Figure 6.10	LC Circuit analogy.	109
Figure 6.11	Direct detection setup for the detection of unmodulated optical field.	111
Figure 6.12	Configuration of the direct detection receiver.	111
Figure 6.13	Frequency response of the ideal InGaAs photodiode.	112
Figure 6.14	Direct detection setup for the detection of modulated optical field.	116
Figure 6.15	Relation between variance product $[\Delta X_1(\omega_S)]^2[\Delta X_2(\omega_S)]^2$ and phase $B(\omega_S,t)$	131
Figure 6.16	Relations between variance and phase $B(\omega_S,t)$ (a) In phase variance (b) Quadrature variance.	132
Figure 6.17	The signal strengths of modulated field and their fluctuations in phase space at $t = T$, in continuum coherent state representation.	133
Figure 6.18	The signal strength of modulated field and their fluctuations in phase space at $t = T$, in two photon coherent state representation (a) $B(\omega_S,T) = 0$. (b) $B(\omega_S,T) \neq 0$.	134
Figure 6.19	Refractive index profile induced from alternating rectangular pulse modulation.	140
Figure 6.20	Temporal profile of $\lvert\beta(\omega,t)\rvert^2$ with $\omega = \omega_S$ for alternating rectangular pulse modulation.	141
Figure 6.21	A photon creation pulse of $\lvert\beta(\omega_S,t)\rvert^2$ due to a transition in $n(t)$.	143

Figure 6.22	Refractive index profile seen by the field during its time of flight inside the modulating medium within (a) time interval A (b) time interval B (c) time interval C (d) time interval D (e) time interval E.	143
Figure 6.23	Figure 6.23: Temporal *profile* of $\|\beta(\omega,\tau)\|2$ *with* $\omega =$ L for an alternating rectangular **pulse pattern.**	148
Figure 6.24	Photoelectron accumulated per second against frequency.	149
Figure 6.25	Temporal profile of photoelectron flux contributed from stimulated emission out of the modulator $F_{\kappa}(t)$	151
Figure 6.26	Temporal profile of photoelectron flux contributed from the process of energy exchange between optical field and excited modulator $F_I(t)$.	152
Figure 6.27	$B(\omega_S,t)$ against time.	154
Figure 6.28	Photoelectron difference between modulated field and input field δY for $T_M = 1\ s$ against input field frequency ω_S.	158
Figure 6.29	Relation between photoelectron difference of modulated and unmodulated optical field δY and photon flight time in modulator T_f.	159
Figure 6.30	Photoelectron difference of modulated and unmodulated field δY for $T_M = 1\ s$ against magnitude of nonlinear refractive index Δv.	160
Figure 6.31	Photoelectron difference of modulated and unmodulated optical field δY for $T_M = 1\ s$ against bit transition rate Ω.	161
Figure 6.32	Refractive index profile induced from sinusoidal control signal.	162
Figure 6.33	Comparison of PSD between QFT (photon creation included) and SCFT (photon creation not included) for sinusoidal modulation.	166
Figure 7.1	Configuration of BPSK transmitter.	171
Figure 7.2	Balanced homodyne receiver structure.	174
Figure 7.3	Beam splitter representation of inefficient photodiode.	177
Figure 7.4	Frequency profile of an imperfect photodiode.	179
Figure 7.5	Block diagram of ASK Transmitter.	189
Figure 7.6	Probability density functions for *Y,* conditioned on *'1'* and *'0'*.	199
Figure 7.7	Refractive index profile for alternating bit pattern.	201

Figure 7.8 Phase of *P(t)* against time. 203

Figure 7.9 Modulation factor *M* against time. 204

Figure 7.10 $|\beta(\omega_S,t)|$ against time for alternating bit pattern. 205

Figure 7.11 Signal space diagram for alternate bit pattern from SCFT, with variable $Z = \eta q\sqrt{F_S F_L T_b}$. 213

Figure 7.12 Signal space diagram for alternate bit pattern (quantum analysis), with variable $Z = \eta q\sqrt{F_S F_L T_b}$ and $\zeta = \frac{1}{T_b}\int_{T_{S1}-T_b}^{T_{S1}} P(t')\left|\beta(\omega_S,t')\right|^2 dt'$. 215

Figure 7.13 Relation between BER improvement and transmitted laser power for the modulation systems considered at *2 Tbps*. (a) BPSK-HO system (b) BPSK-HE system (c) ASK-HO system (d) ASK-HE system. 219

Figure 7.14 Bit transition rate against bit rate. 221

Figure 7.15 Photon flight time in the modulator against bit rate. 222

Figure 7.16 Modulator length against bit rate. 222

Figure 7.17 Refractive index change against bit rate. 223

Figure 7.18 Semi-log plot of quantum ratio against bit-rate for modulation systems considered. 224

List of Tables

Table 1.1	Differences between our analysis and analyses given by previous literatures.	6
Table 2.1	Quantum limit comparison between different modulation systems.	31
Table 6.1	Translation between the phenomenon of spontaneous emission out of the modulator into transformer analogy.	105
Table 6.2	Parameters used in rectangular pulse modulation.	138
Table 6.3	Summary for the descriptions of $\|\beta(\omega_S,t)\|^2$ profile.	147
Table 6.4	Parameters used in sinusoidal modulation.	162
Table 7.1	List of simulation parameters.	201
Table 7.2	Quantum limit comparisons between traditional, SCFT (effect of bit transition included) and QFT analysis for alternating bit pattern.	212

1. Introduction

1.1 The Trend of Optical Communication System

Over the past 20 years, optical communication system has become the primary method for long haul communication. The key advantages of optical communication network over other communication technologies e.g. copper wire network, are its large bandwidth capacity, low attenuation, immunity to interference and high security [1]. Its success is heavily based on the invention of laser, optical fiber, optical receiver and optical modulator.

Recent studies [2,3] have shown that data traffic is doubling every year in the communication network. Optical communication engineers have came up with various solutions to sustain the rapid growth in traffic demand while maintaining a high quality of service. One of the key solutions is to use a phase modulator to externally impress the transmit data onto the optical field [1].

Amplitude shift keying (ASK), which is sometimes referred to intensity modulation, carries digital information by changing the **amplitude** of the optical field generated from the laser. In ASK, the energy carried by a transmit *'1'* bit is greater than that of a transmit *'0'* bit. Currently, ASK is widely used in optical links [1]. For ASK systems that operates at a speed higher than *2 Gb/s*, external phase modulator is used to provide sufficient modulation bandwidth [4,5]. In this thesis, externally modulated systems will be considered.

Another common type of modulation format is phase shift keyed (PSK) system that carries digital information by changing the **phase** of the optical field by the use of a phase modulator. In a Binary PSK (BPSK) system, the phase carried by *'1'* bit

experiences an 180^0 phase offset with respect to *'0'* bit. As we shall see in Chapter 2, a PSK system has a higher signal to noise ratio (SNR) as compared with ASK system, and hence achieve a better system performance with the same transmit power. New modulation format such as differential phase shift keying (DPSK), and Coherent Optical Orthogonal Frequency Division Modulation (CO-OFDM), are types of PSK systems that has been recently develop to improve the optical communication performance at high bit rate *(> 40 Gbps)* [6,7]. Consequently, the role of phase modulator is becoming more important in high speed communication systems. Further details on the properties of ASK and PSK systems will be presented in Chapter 2.

Due to the advent in digital signal processing technology, coherent detection is becoming a popular optical detection scheme [8]. A coherent receiver has an additional laser source, which is refer to as the local oscillator (LO) that down-converts the optical signal to a baseband electrical signal using heterodyne or homodyne detection. The phase of LO field is controlled so that the signal amplitude between a *'0'* bit and *'1'* bit is maximized, and thus optimizes the systems performance [8]. Although the complexity of a coherent receiver is sophisticated as compared with other receiver i.e. direct detection receiver. The configuration of coherent receiver provides signal gain as well as allowing the receiver to be shot noise limited, in which shot noise is the only dominant noise while other noise sources i.e. thermal noise, are effectively suppressed [1]. In this thesis, a coherent receiver will be considered. Figure 1.1 is a block diagram showing the overall structure of the communication system considered in this thesis.

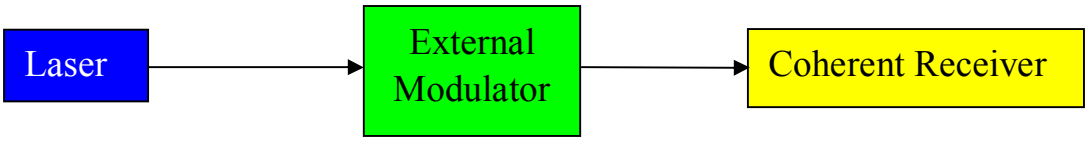

Figure 1.1: Block diagram of high speed optical communication system.

1.2 Historical Backgrounds of Particle Creation

The theoretical concept of particle creation from vacuum has been studied extensively in the fields of Quantum Field Theory in Curved Space Time (QFT-CS) and Quantum Gravity (QG). The process of particle creation from vacuum is different from the process of particle creation due to energy redistribution as a consequence of modulation i.e. energy at a certain frequency mode is removed and redistributed onto other frequencies as described by [9]. The former process excites energy from vacuum thus leads to an energy difference between the energy before and after the modulation process occurs, while the energy remains the same for the later process provided the modulator is lossless. Particle creation from vacuum has continued to be a popular research area in devising methods to experimentally detect the existence of quantum particle production in the area of quantum physics.

The concept of particle creation out of the vacuum was first introduced in 1939 by Schrödinger [10], on the discussion of creating particles due to space-time curvature. In the paper by Husumi in 1953 [11], the presented results show a quantum harmonic oscillator (QHO) with time dependent frequency subjected to a time varying force can excite particles from vacuum. This result is of great importance because it was found that many models in QFT-CS and QG can be simplified down to the problem of time dependent QHO. This has lead to many

interesting researches in particle creation from vacuum in the late 1960s to 1980s, where theoretical analyses have shown particle can be excited from vacuum by:

1. Expansion of universe and non-static gravitational field [12]
2. Cavity subjected to time varying boundary condition [13]
3. Rotating and non-rotating black hole can emit quanta, which is refer to as Hawking's radiation [14].
4. A constantly accelerating observer in a vacuum can register a bath of quanta that have a thermal spectrum, which is known as Unruh radiation. [15].

However, results from these analyses indicates the trace of particle creation is extremely weak and detection of these phenomena is beyond any practical possibility i.e. To observe Unruh radiation that corresponds to a temperature of $1\ K$ requires a constant acceleration in the order of $10^{20}\ ms^{-2}$ [15]. However, it is later shown rapid changes in refractive index effectively corresponds to an acceleration in the order greater than $10^{20}\ ms^{-2}$ [16]. As a result, the effect of particle creation may be discovered under changes in refractive index. Since then, there has been many publications [17, 18, 19, 20, 21] analyzing the number of particles being created due to the changes in refractive index, as well as devising possible ideas in which this effect can be determined experimentally.

In this thesis, we will consider the effect of photon creation subjected to rapid changes in refractive index. This is because the process of phase modulation requires changes in refractive index as discussed in the subsequent section.

1.3 Motivations

In Section 1.1, we have stated high speed optical communication system requires a phase modulator to modulate the optical field. A phase change is established by altering the refractive index of the modulating medium of the phase modulator. Details of the process of phase modulation will be given in Chapter 2. However in the context of QFT, previous literatures [16 - 21] have revealed that changes in refractive index gives rise to the phenomenon of photon creation, as mentioned in Chapter 1.2. As a result, the process of phase modulation excites photons from the modulating medium subjected changes in refractive index.

However, traditional analysis of a phase modulated system [1, 22, 23, 24, 25] cannot address the effect of photon creation from modulator because the optical signal is treated as a classical field. To include the effect of photon creation from phase modulator, the field must be quantized [26, 27]. The difference between classical field and quantum field will be revealed in Chapter 3. Although the effect of photon creation due to changes in refractive index has been studied extensively in QFT, however this has not been considered in an optical communication system. Although a quantum model of phase modulator, recently presented by [9], provides an adequate description on the frequency spectrum of the phase modulated field for which their result resembles to the result predicted by classical field theory [22 – 25], however they did not include the effect of photon creation from modulator. Thus, the model from [9] gives an incomplete quantum description of a phase modulator.

With the increasing popularity of the use of phase modulator in high speed optical communication systems, it is therefore important to give a full quantum field description of a phase modulated field. In this thesis, two common types of modulation formats ASK and BPSK are considered. We will use QFT to describe

these optical systems that will include the quantum effect of photon creation from the phase modulator.

Similar to previous literatures [12, 16, 17, 18, 19, 26], we will mathematically describe the evolution of the phase modulated quantum field using Bogoliubov transformation. However, to determine the effect of photon creation in an optical communication system, two extra constraints need to be considered and this will extend the analyses considered from the previous literatures [12, 16, 17, 18, 19, 26]. Previous analyses consider the state of the quantum field is in a vacuum state for all frequency modes, while due to the presence of a single mode laser source in a communication system, there exist a mode in which the quantum field is described in a coherent state. Besides, previous analyses considers the field is confined inside the time varying refractive index medium, while in a communication system, the optical field propagates out of the time varying medium. The significance of these additional constraints is essential to describe the behavior of a phase modulated system. The additional constraints considered in this thesis are summarized in Table 1.1.

Previous photon creation analyses	**Analysis in this thesis**
Input field in vacuum state	Input field in coherent state
Field confined inside the time varying refractive index medium	Field propagates out of the time varying medium

Table 1.1: Differences between our analysis and analyses given by previous literatures.

Before we close this section, it is worthwhile to mention we specifically consider the effect of photon creation from modulator in this thesis instead of particle creation from modulator in general. This is because in an optical system, the detector is

photosensitive; therefore it is only designed to detect photons and not other types of particle such as mesons and gravitons.

1.4 Thesis Objectives

From the description in Chapter 1.3, it has become clear that the process of phase modulation gives rise to the quantum phenomenon of photon creation. However, the impact of photon creation in a communication system is unclear and the how this effect changes the properties of a phase modulated optical field remains an open question. Therefore the objectives of this thesis are:

1. To develop a quantum field model of optical phase modulator that includes the effect of photon creation from the modulator.
2. Determine how the effect of photon creation from modulator changes the properties of the phase modulated optical field.
3. Reveal possible factors that can influence the process of photon creation from modulator.
4. Determine the impact of photon creation from modulator on the performance of an optical communication system.
5. Give an order of estimate on the significance of the impact of photon creation from modulator and investigate whether this phenomenon is detectable in an optical communication system.

1.5 Thesis Outline

This thesis can be broadly divided into three parts. The first part reviews some of the basic theories of externally modulated system and QFT. The next part involves in the development of a quantum field model of a phase modulator that includes the effect of photon creation from modulator. The last part of the thesis uses the results from the quantum field model that we have constructed in order to determine the impact of photon creation from modulator on the state of the modulated field and in a high speed optical communication system.

In Chapter 2 of this thesis, we will introduce the mechanisms involved in the process of phase modulation. An overview of the operation of ASK and BPSK modulation systems will be presented. Using classical field theory (CFT), we will derive the BER quantum limit that describes the potential performance of the system.

Chapter 3 presents some of the theoretical background of QFT. The properties of coherent state that describes a single mode optical field will be introduced. We will compare the expression of the quantum field with the classical field representation. This is useful for highlighting the shortfall of CFT.

In Chapter 4, we will develop a quantum model of phase modulator with the use of the quantum theory presented in Chapter 3. In this Chapter, we will determine the equation of motion of the field propagating in various media of the phase modulator.

In Chapter 5, we will derive the quantum field representation of the modulated field based on the model presented in Chapter 4. The effect of photon creation from modulator is included in this expression.

In Chapter 6, we will determine the impact of photon creation on the properties of a phase modulated optical field. This Chapter will reveal the factors that influence

the creation of photons. Various numbers of plots will be generated to determine the significance of photon creation from modulator.

In Chapter 7, we will determine the impact of photon creation from modulator on the performance of various optical communication systems. Two main comparisons will be drawn in this Chapter. Firstly, we determine the effect of bit transition on the systems performance by comparing the traditional results presented in Chapter 2 in which the effect of bit transition is neglected, with the results obtained where the effect of bit transition is included but with the effect of photon creation neglected. Subsequently, a comparison between the CFT and QFT will be made, in order to determine the impact of photon creation from modulator on the types of communication systems considered.

The conclusion summarizes the results obtained from Chapter 6 and Chapter 7. Conclusions for the impact of photon creation from modulator on the properties of phase modulated field and various modulation systems considered will be stated. Possible future directions of this research project are also included.

2 Overview of Optical Communications

In this Chapter we review some of the basic principles of phase modulation and optical communications. We shall focus on high speed optical systems in which the optical carrier is modulated by external phase modulator (see Section 1.1). This Chapter is organised as follows. In Section 2.1, we provide a background of the mechanisms involve in the phase modulation process. In Section 2.2, an overview of the operation of various types of modulation systems will be presented. Two simple types of digital modulation formats, amplitude shift keying (ASK) and binary phase shift keying (BPSK), are considered. The performance of optical systems based on these two modulation formats is determined using semi-classical field theory (SCFT), in which the field is expressed as mathematical function while the quantum mechanical nature of light is considered. The potential performance for the optical systems considered can be determined from the bit error rate (BER) quantum limit.

2.1 Phase Modulation Theory

In external phase modulation, the continuous wave (CW) laser is operated in steady state and the phase of the optical carrier (optical field) is regulated by a control signal feeding into the phase modulator as shown in Figure 2.1.

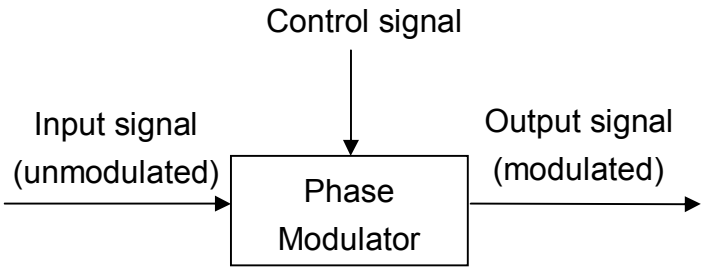

Figure 2.1: Configuration of phase modulator.

The modulator shown in Figure 2.1 is a transverse phase modulator (TPM) in which the control signal propagates in a direction that is orthogonal to the optical signal. Another common type of modulator that is used in optical communication is travelling wave phase modulator (TWPM) in which the control signal propagates in the same direction as the optical field. TWPM is generally more suitable for high speed optical communication [28], but for the simplicity of the analysis, TPM is considered throughout this thesis.

In the modulator, the control signal and the optical field interacts to establish a phase offset for the optical field. This interaction uses nonlinear polarization. The polarization density $p(t)$ of the non-dispersive medium in the modulator can be approximated by [29]

$$\begin{aligned} p(t) &= \varepsilon_0 \chi E_M(t) + 2\chi^{(2)} {E_M}^2(t) + 4\chi^{(3)} {E_M}^3(t) + \ldots \\ &= \varepsilon_0 \chi E_M(t) + p_{NL}(t) \end{aligned} \tag{2.1}$$

where χ is the linear susceptibility, $\chi^{(2)}$ is the second order susceptibility, $\chi^{(3)}$ is the third order susceptibility, and $E_M(t)$ is the electric field amplitude in the modulator. The terms second and higher order in $E_M(t)$ represent the non-linearity of the modulating medium. Both second order and third order nonlinear mechanisms can be used to modulate the optical field. The magnitude of the higher order susceptibilities i.e. $\chi^{(2)}$, $\chi^{(3)}$, are small as compared with the linear susceptibility χ. Therefore the field strength in the modulator i.e. $|E_M(t)|$, must be large for the nonlinear effect to become appreciable.

A TPM that uses optical control signal to control the phase of the input signal (optical carrier) can be used for high speed modulation system. This type of modulator is known as all optical phase modulator (AOPM), and it will be considered in this thesis. AOPM uses optical Kerr effect where the optical control signal is used to change the refractive index of the material so that the phase of the optical carrier is

modified. This is a third order nonlinear process in which the third term in Equation (2.1) dominates, thus the nonlinear polarization density is

$$p_{NL}(t) \approx 4\chi^{(2)} E_T{}^3(t) \tag{2.2}$$

[16 - 20] has reported a large change in refractive index can be induced by a femtosecond pulse laser by exciting the semiconductor media near the band-to-band transition with a response time in the order of femtosecond.

In Figure 2.1, we can identify both optical and control field are fed into the modulator. Thus, the field expression inside the modulator is [29],

$$E_M(t) = E_S(t) + E_C(t) \tag{2.3}$$

where $E_S(t)$ and $E_C(t)$ is the electric field of the optical carrier and the control signal, respectively. For simplicity of the analysis, we assume the optical signal field has an optical angular frequency at ω_S, and thus the expression of $E_S(t)$ is given by

$$E_S(t) = A_S \cos(\omega_S t + \theta_S) \tag{2.4}$$

where A_S is the signal field strength and θ_S is the initial phase angle of the signal field. Next, we consider the expression of the control field to be

$$E_C(t) = A_C(t)\cos(\omega_C t + \theta_C) \tag{2.5}$$

where $A_C(t)$ is the envelop function of the field strength, θ_C is the initial phase angle of control signal field, and ω_C is the angular frequency of the control signal. In order to determine the phase change of the input signal, we shall determine $p_{NL}(t)$ at frequency ω_S by using expression (2.4) and (2.5) in Equation (2.3), and substituting this into Equation (2.2), where after some algebraic manipulation we have

$$\begin{aligned} p_{NL}(\omega_S, t) &= 3\chi^{(3)}\left[A_S{}^2 + 2A_C{}^2(t)\right]A_S \cos(\omega_S t) \\ &= 3\eta_0\chi^{(3)}\left[i_S + 2i_C(t)\right]A_S \cos(\omega_S t) \end{aligned} \tag{2.6}$$

In the second line of Equation (2.6), η_0 is the intrinsic impedance of free space ($\eta_0 = 377\Omega$), while $i_S = A_S^2/\eta_0$ and $i_C(t) = A_C^2(t)/\eta_0$, represent the intensity of the input field and control field respectively. The first term in expression (2.6) represents the effect of self phase modulation (SPM) in which the polarization density is dependent on the intensity of the input signal $E_S(t)$. In TPM, the intensity of the control signal $i_C(t)$ is much greater than the optical signal i_S [5, 29] i.e. $i_C(t)_{MAX} >> i_S$, therefore the effect of SPM (1st term in (2.6)) can be neglected. Expression (2.6) can be expressed in the form

$$\begin{aligned} p_{NL}(\omega_S, t) &= \varepsilon_0 \Delta\chi(t) E_S(t) \\ &= \varepsilon_0 \Delta\chi(t) A_S \cos(\omega_S t) \end{aligned} \tag{2.7}$$

where

$$\Delta\chi(t) = \frac{6\eta_0 \chi^{(3)}}{n\varepsilon_0} i_C(t) \tag{2.8}$$

ε_0 is the free space permitivitty ($\varepsilon_0 = 8.85*10^{-12}$ V/m) and $\Delta\chi(t)$ is the time variation of the change in susceptibility. The relation between the refractive index n and susceptibility is $n^2 = 1+\chi$. By differentiating both sides, the time varying refractive index change $\Delta n(t)$ can be expressed as

$$2n\Delta n(t) = \Delta\chi(t) \tag{2.9}$$

By substituting expression (2.9) into Equation (2.8), the relation between $\Delta n(t)$ and field amplitude of control signal is given by

$$\Delta n(t) = \frac{3\eta_0 \chi^{(3)}}{n^2 \varepsilon_0} i_C(t) \tag{2.10}$$

A change in refractive index $\Delta n(t)$ will create a phase offset of $\Delta\varphi(t)$ to the optical signal, and their relation is given by

$$\Delta\varphi(t) = \frac{2\pi\Delta n(t) L}{\lambda_S} \tag{2.11}$$

where L is the modulator length, and $\lambda_S = 2\pi c_0/\omega_S$ is the wavelength of the input signal, in which c_0 is the speed of light in vacuum ($c_0 = 3*10^8\ ms^{-1}$). By substituting expression (2.11) into Equation (2.10), the relation between $\Delta\varphi(t)$ and $i_C(t)$ is

$$\Delta\varphi(t) = \frac{6\pi\eta_0\chi^{(3)}L}{n^2\lambda_S\varepsilon_0} i_C(t) \tag{2.12}$$

Expression (2.12) is a mathematical description of cross phase modulation (CPM), where the phase of the optical input signal $E_S(t)$, is governed by the intensity of the control signal $E_C(t)$.

2.2 Analysis of Optical Communication Systems

In this subsection, we shall review some of the basic principles of phase shift keyed (PSK) and amplitude shift keyed (ASK) systems. The analysis presented in this Chapter uses SCFT. In SCFT, optical field is modelled as a stream of photons (particle) and each photon has an energy of $\hbar\omega_S$ *(joules)*, where $\hbar$ is the reduced Planck constant *($\hbar = 1.054*10^{-34}$ joules*second)*, and ω_S is the angular frequency of optical field. The analysis in this section follow closely to the traditional optical communication analysis presented in textbooks [22 - 25] and journal articles [1, 30, 31].

2.2.1 Binary Phase Shift Keyed (BPSK) Systems

In a BPSK system, the transmitted data is encoded onto the phase of the optical carrier by the use of phase modulator at the transmitter. When a *'1'* bit is transmitted, the phase of optical carrier is not modified by the modulating signal (control signal),

while if a *'0'* bit is transmitted, the field experiences an additional phase shift of 180^0. The characteristics of BPSK modulation is shown in Figure 2.2.

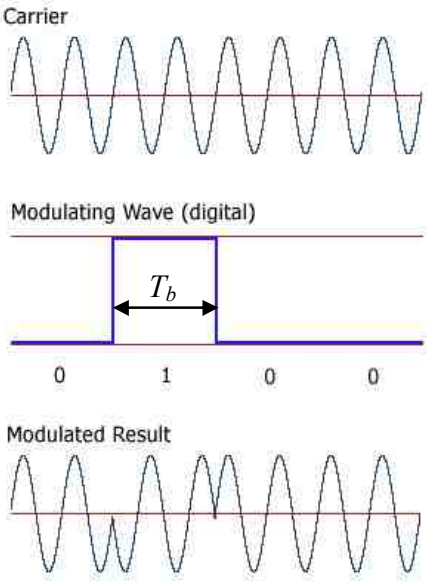

Figure 2.2: Characteristics of BPSK modulation.

T_b in Figure 2.2 represents the bit-rate of the modulating signal. A BPSK transmitter consists of a laser and a phase modulator as shown in Figure 2.2. The laser generates an optical field, and is operating in steady state. The phase of the optical field will be modulated by the phase modulator. The phase change of the optical field is governed by the control signal. From expression (2.12), we can identify the control field is turned on when a *'0'* bit is transmitted to establish an additional phase shift of 180^0, and turned off when a *'1'* bit is transmitted.

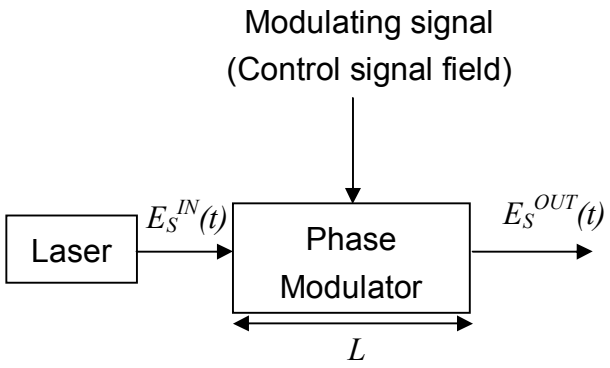

Figure 2.3: Configuration of BPSK transmitter.

The transmitted data impressed into the BPSK modulated signal can be detected by a coherent receiver. A balanced homodyne receiver is considered so that the input signal power can be fully exploited after being divided by the 3 dB coupler [1, 25, 30, 31]. A balanced detector uses two photodiodes for detection. A block diagram of a balanced coherent receiver is shown in Figure 2.4.

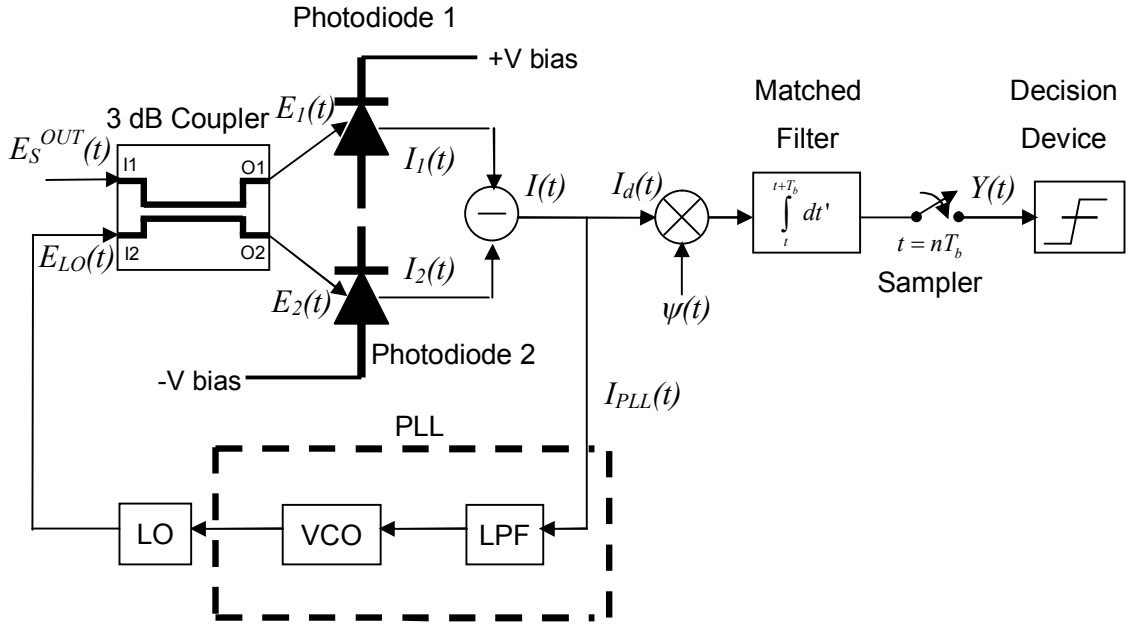

Figure 2.4: Configuration of balanced coherent receiver.

Suppose the transmitter laser generates an optical field at frequency ω_S, thus the field amplitude of the laser $E_S^{IN}(t)$ can be expressed in the form

$$E_S^{IN}(t) = \sqrt{2P_S}\cos(\omega_S t + \theta_S) \tag{2.13}$$

where θ_S is the initial phase angle of the signal field which has been introduced in Equation (2.4), P_S is the mean signal power. In expression (2.13), the field amplitude is normalized so that the RMS expression gives the average power P_S, i.e.

$$\frac{1}{T}\int_0^T \left|E_S^{IN}(t)\right|^2 dt = P_S \tag{2.14}$$

Within the bit interval $0 < t \leq T_b$, the modulated signal $E_S^{OUT}(t)$ has the form [1]

$$E_S^{OUT}(t) = \sqrt{2P_S}\cos(\omega_S t + \theta_S + a\pi) \tag{2.15}$$

where $a = 0$ for a transmit *'1'*, and $a = 1$ for a transmit *'0'*. In the calculation of BER, we shall make the same assumption used in standard communication textbooks [1, 22 - 25], for which the phase of the field is assumed to be in steady state within a bit period T_b, and thus the **dynamical nature of modulation (effect of bit transition) is ignored**.

In coherent detection, a local oscillator (LO) at the receiver generates a strong optical field. The field amplitude of the local oscillator $E_{LO}(t)$ is added onto the signal field amplitude $E_S(t)$ before it arrives at the detector [1]. The expression of the single frequency LO field is given by

$$E_{LO}(t) = \sqrt{2P_L}\cos(\omega_{LO} t + \theta_{LO}) \tag{2.16}$$

where P_L is the mean power of the LO field and ω_{LO} is the frequency of the LO field. θ_{LO} is the phase of the LO field that is controlled by the phase locked loop (PLL) in order to optimize the systems performance (See Figure 2.4). The addition operation between the $E_{LO}(t)$ and $E_S(t)$ is realized by the 3 dB coupler, a lossless network with two inputs and two outputs, as shown in Figure 2.4. The coupler directs half of the

signal field power from port I1 to output port O1 and the other half to output port O2 but with an additional 180^0 phase shift. At port I2, half of the LO field power will be coupled from port I2 to port O1, while the other half is directed towards port O2. Thus, the output field at port O1 is expressed as

$$\begin{aligned} E_1(t) &= \frac{E_S{}^{OUT}(t) + E_{LO}(t)}{\sqrt{2}} \\ &= \sqrt{P_S}\cos(\omega_S t + \theta_S + a\pi) + \sqrt{P_L}\cos(\omega_{LO} t + \theta_{LO}) \end{aligned} \tag{2.17}$$

while the field at port O2 is

$$\begin{aligned} E_2(t) &= \frac{E_S{}^{OUT}(t) - E_{LO}(t)}{\sqrt{2}} \\ &= \sqrt{P_S}\cos(\omega_S t + \theta_S + a\pi) + \sqrt{P_L}\cos(\omega_{LO} t + \theta_{LO}) \end{aligned} \tag{2.18}$$

within a bit period. Each optical field arrives at a p-i-n photodiode, and each signal is converted from optical to electrical form. The fraction of incident photons that contribute to the detector current is called quantum efficiency, denoted by η. The frequency of the incident optical signal generally has a spectral bandwidth in which η is relatively constant and is close to its maximum value [25]. The mean photocurrent *I(t)*, is related to the mean photon flux *F(t)* by

$$I(t) = \eta q F(t) \tag{2.19}$$

The optical field strength $|E(t)|$ is related to the mean photon flux *F(t)* by

$$F(t) = \frac{|E(t)|^2}{\hbar\omega} \tag{2.20}$$

Using expression (2.19) and (2.20), we can relate detector current with the magnitude of the incident field by the following expression

$$I(t) = R|E(t)|^2 \tag{2.21}$$

where R is the photodiode's responsitivity and is related to the quantum efficiency η by $R = \eta q/\hbar\omega$ *(amps/watt)*. By substituting the expression of $E_1(t)$ from expression (2.17) into Equation (2.21), we obtained the expression of $I_1(t)$ during a bit period,

$$I_1(t) = R\left\{\frac{P_S + P_L}{2} + \sqrt{P_S P_L}\cos\left[\left(\omega_S - \omega_{LO}\right)t + \theta_S - \theta_{LO} + a\pi\right]\right\} \quad (2.22)$$

The irrelevant high frequency component $\omega_S + \omega_{LO}$, has been omitted in Equation (2.22) [25]. Similarly, by substituting the expression of $E_2(t)$ from expression (2.18) into Equation (2.21), we have

$$I_2(t) = R\left\{\frac{P_S + P_L}{2} - \sqrt{P_S P_L}\cos\left[\left(\omega_S - \omega_{LO}\right)t + \theta_S - \theta_{LO} + a\pi\right]\right\} \quad (2.23)$$

From the coherent receiver configuration shown in Figure 2.4, we can identify the signal current $I(t)$ is determined by subtracting $I_1(t)$ in Equation (2.22) from $I_2(t)$ in Equation (2.23), in which we have

$$\begin{aligned} I(t) &= I_1(t) - I_2(t) \\ &= 2R\sqrt{P_S P_L}\cos\left[\left(\omega_S - \omega_L\right)t + \theta_S - \theta_{LO} + a\pi\right] \\ &= 2\sqrt{I_S I_L}\cos\left[\omega_{IF}t + \theta_S - \theta_{LO} + a\pi\right] \quad 0 < t \le T_b \end{aligned} \quad (2.24)$$

$\omega_{IF} = \omega_S - \omega_{LO}$ is the intermediate frequency, while I_S and I_L represents the mean current contributed by the modulated signal and local oscillator power, respectively i.e. $I_S = RP_S$, $I_L = RP_L$.

From Figure 2.4, we can identify the signal current is divided into two components, $I_{PLL}(t)$ and $I_d(t)$, where $I_{PLL}(t) = K_e I(t)$ and $I_d(t) = (1-K_e)I(t)$ in which K_e is a proportional constant ranges between *0* and *1*. $I_{PLL}(t)$ represents the portion of the signal current being fed to the phase locked loop (PLL). The magnitude of the current $I_{PLL}(t)$ is used for controlling the angle θ_{LO} to a desired value of θ_S i.e. $\theta_{LO} = \theta_S$. Provided $(\Delta\nu_S + \Delta\nu_{LO})T_b$ is small, where $\Delta\nu_S$ and $\Delta\nu_{LO}$ is the *3 dB* spectral bandwidths of the signal and LO laser respectively, the current that is drawn from the PLL is small i.e. $I_{PLL}(t) \sim 0$, and thus K_e is small [32]. For high speed modulation

systems, T_b is small, which implies the detected signal current $I_d(t)$ is roughly equals to the signal current $I(t)$ i.e. $I_d(t) \approx I(t)$. Therefore the mean current detected can be expressed as

$$\begin{aligned} I_d(t) &\approx I(t) \\ &= 2\sqrt{I_S I_L}\cos(\omega_{IF} t + a\pi) \\ &= 2\eta q\sqrt{F_S F_L}\cos(\omega_{IF} t + a\pi) \end{aligned} \tag{2.25}$$

In the last line of Equation (2.25), we have expressed the current I_S and I_L in terms of mean photon flux using the relation in Equation (2.19).

The coherent receiver can be classified into two types, homodyne and heterodyne receiver. For homodyne receiver, we have $\omega_{IF} = 0$ ($\omega_S = \omega_{LO}$), while in the case of heterodyne receiver, we have $\omega_{IF} \neq 0$ ($\omega_S \neq \omega_{LO}$). The signal $\psi(t)$ in Figure 2.4 is different for homodyne and heterodyne receiver. For homodyne receiver, we have [1]

$$\psi_{HO}(t) = \frac{1}{\sqrt{T_b}} \tag{2.26}$$

while for heterodyne receiver we have [1]

$$\psi_{HE}(t) = \sqrt{\frac{2}{T_b}}\cos(\omega_{IF} t) \tag{2.27}$$

We can identify from Figure 2.4, that the detector current $I_d(t)$ is mixed with signal $\psi(t)$, and fed into the matched filter before the transmitted data is sampled. A matched filter optimises the signal to noise ratio and hence the performance of the system. Mathematical analysis from [22] show the matched filter can be realized by an integrate and dump block for BPSK systems, in which the signal current is accumulated within the bit period. This electrical signal is sampled at time $t = T_b$ and the accumulated signal strength Y is measured. This signal strength is removed after time T_b in order to detect the next bit being sent. The signal strength Y detected from the transmitted data at time $t = T_b$, is represented by

$$Y = \int_0^{T_b} I_d(t)\psi(t)\,dt \tag{2.28}$$

By substituting expressions (2.25) and (2.26) into Equation (2.28), the mean signal strength of the received data detected from the BPSK homodyne (BPSK-HO) system at time $t = T_b$ is,

$$\begin{aligned} Y_{BPSK-HO} &= \int_0^{T_b} \frac{1}{\sqrt{T_b}} 2\eta q\sqrt{F_S F_L}\cos(a\pi)dt \\ &= 2\eta q\sqrt{F_S F_L T_b}\cos(a\pi) \end{aligned} \tag{2.29}$$

When $a = 0$, a *'1'* bit is received within the bit interval in Equation (2.29), where we have

$$Y_{BPSK-HO}[1] = 2\eta q\sqrt{F_S F_L T_b} \tag{2.30}$$

$Y_{BPSK\text{-}HO}[1]$ represents the mean signal strength detected for a *'1'* bit. If $a = 1$, a *'0'* bit is received during the bit interval in Equation (2.29), and we have

$$Y_{BPSK-HO}[0] = -2\eta q\sqrt{F_S F_L T_b} \tag{2.31}$$

where $Y_{BPSK\text{-}HO}[0]$ represents the mean signal strength detected for a *'0'* bit.

Similarly, by substituting expressions (2.25) and (2.27) into Equation (2.28), the mean signal strength of the transmitted data detected from the BPSK heterodyne (BPSK-HE) system at time $t = T_b$ is,

$$\begin{aligned} Y_{BPSK-HE} &= \sqrt{\frac{2}{T_b}} 2\eta q\sqrt{F_S F_L}\int_0^{T_b} \cos(\omega_{IF}t + a\pi)\cos(\omega_{IF}t)dt \\ &= \eta q\sqrt{2F_S F_L T_b}\cos(a\pi) \end{aligned} \tag{2.32}$$

where the double frequency term $2\omega_{IF}$ is averaged out to 0 from the time integral given that $\omega_{IF} >> 1/T_b$. When a *'1'* bit is transmitted within a bit interval, $a = 0$ in Equation (2.32), and we get

$$Y_{BPSK-HE}[1] = \eta q\sqrt{2F_S F_L T_b} \tag{2.33}$$

where $Y_{BPSK\text{-}HE}[1]$ represents the mean signal strength detected for a *'1'* bit. Else if a *'0'* bit is transmitted within a bit interval, $a = 1$ in Equation (2.32), and we have

$$Y_{BPSK-HE}[0] = -\eta q\sqrt{2F_S F_L T_b} \tag{2.34}$$

where $Y_{BPSK\text{-}HE}[0]$ represents the mean signal strength detected for a *'0'* bit.

2.2.2 Amplitude Shift Keyed (ASK) Systems

In this section, we shall determine the signal strength detected by the coherent receiver for a ASK system. In an ASK system, the transmitted data is encoded onto the amplitude of the optical carrier. When a *'1'* bit is transmitted, the field strength of the optical carrier (signal) will be high and vice-versa when a *'0'* bit is transmitted. The characteristics of ASK modulation is shown in Figure 2.5.

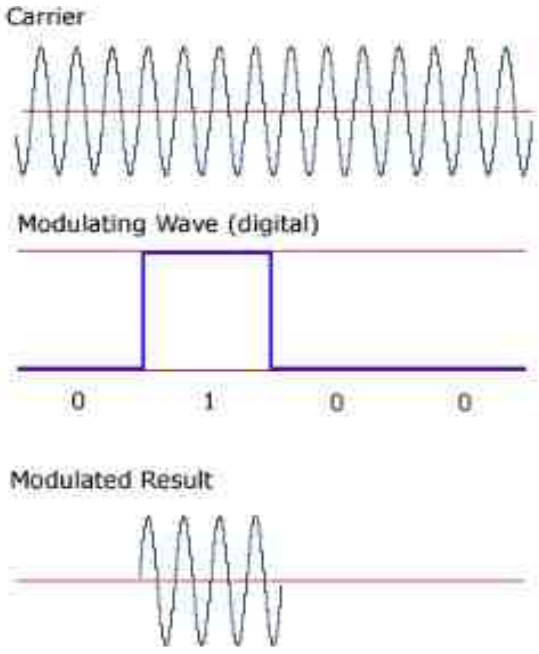

Figure 2.5: Characteristics of ASK modulation.

The transmitted data can be encoded onto the optical carrier by operating the transmit laser at steady state and impressing the transmitted data onto the optical carrier

externally using Mach Zehnder interferometer (MZI). In this thesis, external modulation is considered. The configuration of a MZI is shown in Figure 2.6.

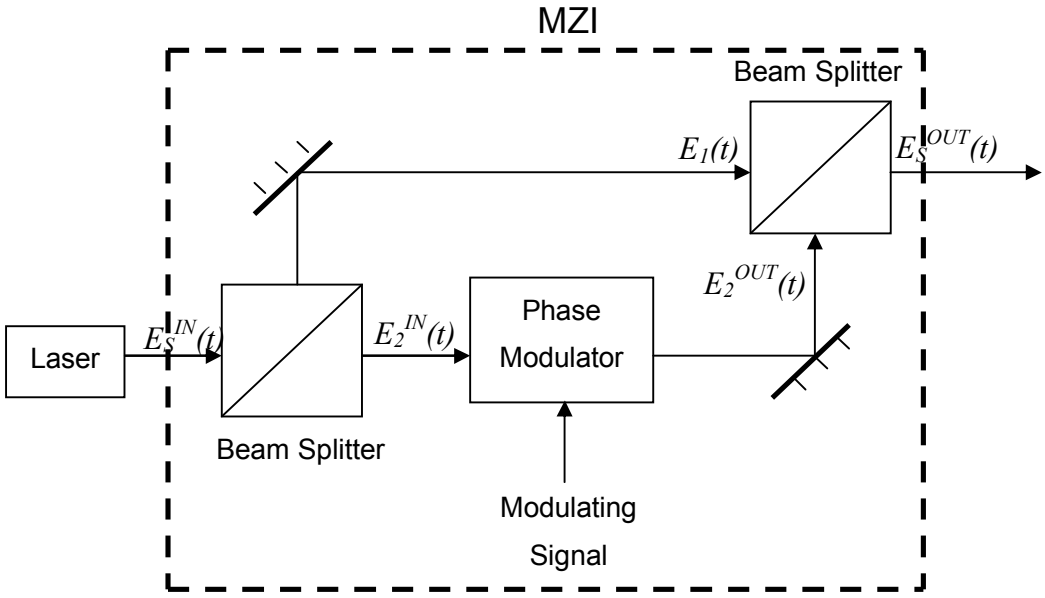

Figure 2.6: Configuration of ASK transmitter for which transmitted data is externally modulated.

The MZI uses the interference between two phase offset components of the optical carrier. In this device the optical field $E_S^{IN}(t)$ given by Equation (2.13), is equally divided into two component by the 50:50 beam splitter. The magnitude of the transmission and reflection coefficient $|R|$ and $|T|$ for a 50:50 beam splitter is $1/\sqrt{2}$ ($|R| = |T| = 1/\sqrt{2}$). Thus half of the optical field power will travel in arm 1 while the other half will travel in arm 2. The phase difference between the reflection coefficient φ_R and the transmission coefficient φ_T is $\pi/2$ ($\varphi_R - \varphi_T = \pi/2$) [33]. The optical field in arm 1 is represented by,

$$E_1(t) = RE_S^{IN}(t) = i\sqrt{P_S}\cos(\omega_S t + \theta_S) \tag{2.35}$$

while the optical field in arm 2 is

$$E_2^{IN}(t) = TE_S^{IN}(t) = \sqrt{P_S}\cos(\omega_S t + \theta_S) \tag{2.36}$$

where P_S is the mean signal power, and $i = \sqrt{-1}$. In this analysis, we have chosen the transmission coefficient phase angle φ_T to be *0* for simplicity. The phase modulator placed at arm 2 is used to control the interference process by regulating the phase delay between arm 1 and arm 2. The modulator in arm 2 operates similarly to the BPSK system, for which the optical signal $E_2^{OUT}(t)$ will experience an additional 180^0 phase shift when a *'0'* bit is transmitted and no phase shift when a *'1'* bit transmitted. The field expression at the output of the modulator in arm 2 $E_2^{OUT}(t)$ in a bit interval T_b is given by,

$$E_2^{OUT}(t) = \sqrt{P_S}\cos(\omega_S t + \theta_S + a\pi) \quad 0 < t \le T_b \tag{2.37}$$

where $a = 0$ when a *'0'* bit is transmitted and $a = 1$ when a *'1'* bit is transmitted.

The field components will recombine at the output of the second beam splitter, thus the optical signal transmitted $E_S^{OUT}(t)$ is given by

$$\begin{aligned} E_S^{OUT}(t) &= TE_1(t) + RE_2^{OUT}(t) \\ &= i\sqrt{\frac{P_S}{2}}\left[\cos(\omega_S t + \theta_S) + \cos(\omega_S t + \theta_S + a\pi)\right] \\ &= ia'\sqrt{2P_S}\cos(\omega_S t + \theta_S) \quad 0 < t \le T_b \end{aligned} \tag{2.38}$$

In the second line of (2.38), we can identify $E_S^{OUT}(t) = 0$ for $a = 1$ and $i(2P_S)^{1/2}\cos(\omega_S t + \theta_S)$ for $a = 0$. Thus, $a' = 0$ when a *'0'* bit is sent and $a' = 1$ when a *'1'* bit is sent.

The transmitted information modulated by ASK format can be detected by a coherent receiver. The coherent receiver structure for ASK system is the same as BPSK system, as shown in Figure 2.4. The only difference between ASK and BPSK analysis for coherent detection arises from the incident signal field, for which $E_S^{OUT}(t)$ for ASK system in Equation (2.38) is expressed differently from BPSK system in Equation (2.15). By using the field expression in Equation (2.38) and following the

similar procedure Subsection 2.2.1, after some mathematical manipulation we can determine the detected current $I_d(t)$ for ASK system to be

$$\begin{aligned} I_d(t) &\approx 2a' R E_S(t) E_{LO}(t) \\ &= a' 2\eta q \sqrt{F_S F_L} \cos(\omega_{IF} t) \end{aligned} \tag{2.39}$$

where the expression of the LO field $E_{LO}(t)$, is given by Equation (2.16), and ω_{IF} is the intermediate frequency that represents the difference between signal field frequency and LO field frequency $(\omega_{IF} = \omega_S - \omega_{LO})$. The approximation in Equation (2.39) implies the amount of signal current drawn by the PLL is small, thus most of the signal current is fed to the matched filter, as shown in Figure 2.4.

By substituting expressions (2.39) and (2.26) into Equation (2.28), the signal strength of the transmitted data detected from ASK homodyne system (ASK-HO) at time $t = T_b$ is given by

$$\begin{aligned} Y_{ASK-HO} &= \int_0^{T_b} I_d(t) \psi_{HO}(t) dt \\ &= a' 2\eta q \sqrt{F_S F_L T_b} \end{aligned} \tag{2.40}$$

where $\omega_{IF} = 0$ in (2.39) for homodyne detection. For *a' = 1*, a *'1'* bit is transmitted, and the mean signal strength is

$$Y_{ASK-HO}[1] = 2\eta q \sqrt{F_S F_L T_b} \tag{2.41}$$

while for *a' = 0*, a *'0'* bit is transmitted, and the mean signal strength is

$$Y_{ASK-HO}[0] = 0 \tag{2.42}$$

Similarly, by substituting expressions (2.39) and (2.27) into Equation (2.28), the transmitted data detected from ASK heterodyne system (ASK-HE) at time $t = T_b$ is,

$$\begin{aligned} Y_{ASK-HE} &= \int_0^{T_b} I_d(t) \psi_{HE}(t) dt \\ &= a' \eta q \sqrt{2 F_S F_L T_b} \end{aligned} \tag{2.43}$$

where $\omega_{IF} \neq 0$ in (2.39) for heterodyne detection. For *a'* = 1, a *'1'* bit is transmitted, and the mean signal strength is

$$Y_{ASK-HE}[1] = \eta q \sqrt{2F_S F_L T_b} \tag{2.44}$$

while for *a' = 0,* a *'0'* bit is transmitted, and the mean signal strength is

$$Y_{ASK-HE}[0] = 0 \tag{2.45}$$

2.2.3 Systems performance

The bit error rate (BER), which measures the mean number of errors over an extended time interval $(>>T_b)$, is commonly used to describe the performance of an optical system. A lower BER indicates the system is less error prone. In this subsection, we shall review the BER calculation of various optical communication systems (BPSK-HO, BPSK-HE, ASK-HO, ASK-HE) using the signal strength expressions derived in Section 2.2.1 and Section 2.2.2.

The transmitted signal is generally corrupted by the noise in the system. In this subsection, we assume the communication channel and the receiver are lossless and noiseless. However, even in the absence of extraneous noise, it is impossible to detect an optical signal with complete certainty. In the SCFT model, this is attributed to the random nature of photon arrival. In fact the output power of the laser yields the **mean** photon flux over a period of time, and does NOT give the **actual** photon flux at each time instant [25]. The number of photons that fall onto the detector in T seconds is represented by Poisson distribution [1, 25]

$$P(N|1) = \frac{(FT)^N \exp(-FT)}{N!} \tag{2.46}$$

where $P(N|1)$ represents the photon number N detected given that a *'1'* bit is transmitted, and F is the mean photon flux that falls onto the detector. Since the photocurrent at the receiver is generated from the photon flux arriving at the detector,

therefore the statistics of photocurrent is also characterized by Poisson distribution. The noise statistics of photocurrent is known as shot noise.

The receiver will determine whether a *'1'* bit or a *'0'* bit is received based on the received signal strength Y and the threshold Y^{th} set by the decision device. Figure 2.7 shows when the received signal strength exceeds the threshold Y^{th}, the receiver will consider a bit *'1'* was received, while if the received signal strength is below Y^{th}, it will consider a bit *'0'* was received. The probability density function $P(Y|'1')$ in Figure 2.7 represents the received signal strength given that a *'1'* bit is sent, while $P(Y|'0')$ represents the received signal strength given that a *'0'* bit is sent. The received signal has a statistical deviation of $\sigma[0]$ and $\sigma[1]$, around the mean values $Y[1]$ and $Y[0]$ respectively, as the signal is corrupted by noise. A detection error is made when the receiver considers a bit *'1'* is received while a bit *'0'* is transmitted, i.e. $P[(Y < Y^{th})|'1']$, or when a bit *'0'* is received while a bit *'1'* is transmitted i.e. $P[(Y > Y^{th})|'0']$. The probability of an error is represented by the shaded area in Figure 2.7.

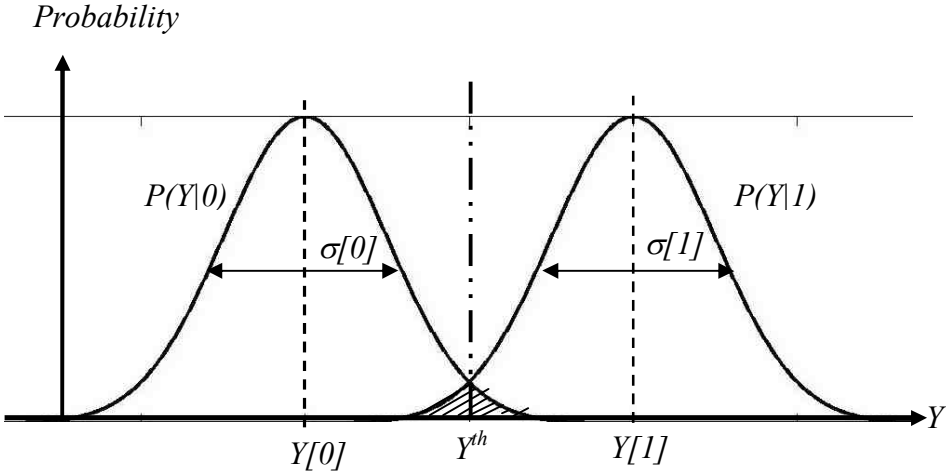

Figure 2.7: Probability density functions for Y, conditioned on *'1'* and *'0'*.

Because shot noise is the only noise sources included in this analysis, the probability distribution of *P(Y|1)* and *P(Y|0)* in Figure 2.7 are Poisson distributed.

We shall determine the BER quantum limit for modulation systems that use a coherent receiver. The quantum limit represents the relationship between the lower limit of the received power and BER in an optical communication system because only shot noise is considered, while other extraneous noise such as thermal noise, dark current noise etc. is neglected in the analysis. With balanced coding, the probability of transmitting a ***'1'* bit and *'0'* bit is equally probable**, and the BER is given by [25]

$$BER = \frac{1}{2}\left[P\left(Y > Y^{th} \mid '0'\right) + P\left(Y < Y^{th} \mid '1'\right)\right] \tag{2.47}$$

From mathematical statistics, it is well known that Poisson distribution can be well approximated by Gaussian distribution provided the mean photon flux of the field detected by the photodiode is large [34]. This condition applies to **coherent detection** because the photon flux of the LO field is large i.e. large F_L. As a result, *P(Y|1)* and *P(Y|0)* can be approximated by Gaussian distribution for coherent detection. It is convenient to introduced the Q-function, which describes the normalized Gaussian tail probability, and is defined as [25]

$$Q(\gamma) = \frac{1}{\sqrt{2\pi}} \int_{\gamma}^{\infty} \exp\left(\frac{-\xi^2}{2}\right) d\xi \tag{2.48}$$

Provided $\gamma >> 1$, we have an approximation of $Q(\gamma)$ [25]

$$Q(\gamma) \approx \frac{1}{\gamma\sqrt{2\pi}} \exp\left(-\frac{\gamma^2}{2}\right) \tag{2.49}$$

For the modulation format considered in this thesis (BPSK-HO, BPSK-HE, ASK-HO, ASK-HE), the probability of transmitting a *'1'* and *'0'* is equally probable and that the

impact of mistaking a *'0'* for a *'1'* is the same as its converse [1]. Under this condition, the BER in Equation (2.47) can be re-expressed as [1]

$$BER = Q(\gamma) = Q\left(\frac{Y^{th} - Y[0]}{\sigma[0]}\right) = Q\left(\frac{Y^{th} - Y[1]}{\sigma[1]}\right) \tag{2.50}$$

where Y^{th} is the threshold, *Y[1]* and *Y[0]* is the signal strength detected for bit *'1'* and bit *'0'* respectively, $\sigma[0]$ and $\sigma[1]$ is the shot noise deviation for bit *'1'* and bit *'0'* respectively. Using Equation (2.50), the threshold value Y^{th} can be determined as

$$Y^{th} = \frac{Y[0]\sigma[1] + Y[1]\sigma[0]}{\sigma[0] + \sigma[1]} \tag{2.51}$$

Y^{th} is set so that the shaded area under the probability density function *P(Y|1)* and *P(Y|0)* are equal in Figure 2.7, and the error probability is minimized [25].

By substituting the threshold value expression in expression (2.51) into Equation (2.50), the BER for coherent detection can be expressed as

$$BER = Q(\gamma) = Q\left(\frac{Y[1] - Y[0]}{\sigma[1] + \sigma[0]}\right) \tag{2.52}$$

where the parameter γ is defined by

$$\gamma = \frac{Y[1] - Y[0]}{\sigma[1] + \sigma[0]} \tag{2.53}$$

γ^2 can be identified as the signal to noise ratio SNR [1, 25]. Using the expression of the Q-function in Equation (2.49), we can identify the BER is exponentially related to the SNR. This implies an increase in SNR will lead to an exponential decrease in BER, and hence the communication system performance improves significantly.

For coherent receiver, the power spectral density (PSD) of shot noise for either a *'0'* bit or *'1'* bit transmitted is given by [1]

$$\sigma_{shot}{}^2[1] = \sigma_{shot}{}^2[0] = \eta q^2 F_L \tag{2.54}$$

where F_L is the mean photon flux of the LO field. The PSD of shot noise is the same regardless of whether transmitted signal is modulated via ASK or PSK, or whether the coherent receiver is homodyne or heterodyne. Provided shot noise is the only noise considered, the BER expressions of various modulation systems can be determined by substituting expression (2.54), and the mean signal strength expression for the corresponding modulation systems derived in Subsection 2.2.2, into Equation (2.52), where we obtained the following

$$\begin{aligned} BER_{BPSK-HO} &= Q\left[\frac{2\eta q\sqrt{F_S F_L T_b} - \left(-2\eta q\sqrt{F_S F_L T_b}\right)}{2\sqrt{\eta q^2 F_L}}\right] \\ &= Q\left(\sqrt{4\eta F_S T_b}\right) \end{aligned} \tag{2.55}$$

$$\begin{aligned} BER_{BPSK-HE} &= Q\left[\frac{q\eta\sqrt{2F_S F_L T_b} - \left(-q\eta\sqrt{2F_S F_L T_b}\right)}{2\sqrt{\eta q^2 F_L}}\right] \\ &= Q\left(\sqrt{2\eta F_S T_b}\right) \end{aligned} \tag{2.56}$$

$$\begin{aligned} BER_{ASK-HO} &= Q\left[\frac{2q\eta\sqrt{F_S F_L T_b} - 0}{2\sqrt{\eta q^2 F_L}}\right] \\ &= Q\left(\sqrt{\eta F_S T_b}\right) \end{aligned} \tag{2.57}$$

$$\begin{aligned} BER_{ASK-HE} &= Q\left[\frac{\eta q\sqrt{2F_S F_L T_b} - 0}{2\sqrt{\eta q^2 F_L}}\right] \\ &= Q\left(\sqrt{\frac{\eta F_S T_b}{2}}\right) \end{aligned} \tag{2.58}$$

When $\eta = 1$ (maximum quantum efficiency), expressions (2.55) - (2.58) corresponds to the BER quantum limit of the modulation systems considered, and the systems performance is optimized.

Using expression of the Q function in Equation (2.49) and expressions (2.55) - (2.58), we can determine the required minimum photon number in a bit period to achieve a given BER. This result is shown in Table 2.1.

Modulation format	BER equation	Quantum limit $BER = 10^{-9}$ (ph/bit)	Quantum limit BER = 10^{-15} (ph/bit)
BPSK-HO	$Q\left(\sqrt{4F_S T_b}\right)$	9	16
BPSK-HE	$Q\left(\sqrt{2F_S T_b}\right)$	18	32
ASK-HO	$Q\left(\sqrt{F_S T_b}\right)$	36	64
ASK-HE	$Q\left(\sqrt{\frac{F_S T_b}{2}}\right)$	72	128

Table 2.1: Quantum limit comparison between different modulation systems.

From Table 2.1, we can identify the quantum limit of BPSK-HO is the smallest followed by BPSK-HE, ASK-HO and ASK-HE. The smaller the quantum limit, the better the sensitivity of the receivers. In addition, Table 2.1 shows achieving a lower BER requires more photons i.e. greater power is required from transmit laser. This can be understood from the fact that increasing the transmit laser power increases the SNR (γ). By increasing the power by less than 2 times, the BER reduces by *6* orders of magnitude (10^{-9} to 10^{-15}) due to the nonlinearity of Q function.

2.3 Summary

A transverse AOPM is considered in this thesis to modulate the optical field for high speed communication systems. The process of phase modulation uses optical Kerr effect, a nonlinear mechanism in which the phase of the signal field is controlled by the intensity of the control signal by varying the refractive index of the modulator. The relation between the phase change and the intensity of the control signal in

Equation (2.12) will be used for the development of the quantum field model in Chapter 4.

The analysis of various optical systems that uses ASK and BPSK modulation format were considered in this Chapter using SCFT. Similar to the traditional optical communication analysis [1, 22 - 25], the dynamical nature of modulation that includes the effect of bit transition delay has been ignored. A summary of quantum limit giving the minimum photon number required to achieve a specific BER is presented in Table 2.1. These results will be used to compare the BER quantum limit determined from quantum field theory (QFT) in Chapter 7.

3 Introduction to Quantum Field Theory (QFT)

In Chapter 2, the optical field has been treated semi-classically in which the field is expressed as algebraic function while the detector's response has been modelled as though the light consists of discrete quanta. In this Chapter, quantum field theory (QFT) is used to give a full and appropriate description of the quantum nature of light generated from the transmit laser. In QFT the field is represented by a matrix operator that operates on quantum state vectors to describe observable quantities, e.g. power flow of optical field. We begin by giving a summary of quantum representation for optical field propagating in vacuum. We shall also discuss the properties of coherent state that describes the optical field generated from a laser.

3.1 Quantum Field Operators in Vacuum

In QFT the field is expressed as operators instead of algebraic function as in semi-classical field theory (SCFT). However similar to SCFT, the optical field operator in QFT is also governed by Maxwell's equation [35]

$$\begin{aligned} &\nabla \mathrm{X}\hat{E} = -\frac{d\hat{B}}{dt} \\ &\frac{1}{\mu_0}\nabla \mathrm{X}\hat{B} = \varepsilon_0 \frac{d\hat{E}}{dt} \\ &\varepsilon_0 \nabla \bullet \hat{E} = 0 \\ &\nabla \bullet \hat{B} = 0 \end{aligned} \tag{3.1}$$

where $\hat{B}$ is the magnetic field density operator, $\hat{E}$ is the electric field operator, $\varepsilon_0 = 8.85*10^{-12} V/m$ is the free space electric permittivity and $\mu_0 = 4\pi*10^{-7} H/m$ is the free space magnetic permeability, ∇ is the differential gradient operator ($= \boldsymbol{i}\partial/\partial x + \boldsymbol{j}\partial/\partial y + \boldsymbol{k}\partial/\partial z$). In this Chapter we consider the field propagating in vacuum, thus the extra

terms due to bound charges and current sources are omitted in Equation (3.1). The optical field is assumed to be transverse electromagnetic (TEM) field propagating in the *z* direction, which satisfies the Coulomb gauge condition [35]

$$\nabla \bullet \hat{A} = 0 \tag{3.2}$$

where $\hat{A}$ is the magnetic vector potential operator. $\hat{A}$ is related to $\hat{B}$ field operator by,

$$\hat{B} = \nabla X \hat{A} \tag{3.3}$$

while the relation between $\hat{A}$ and $\hat{E}$ is

$$\hat{E} = \frac{\partial \hat{A}}{\partial t} \tag{3.4}$$

From expression (3.2) and (3.4), it can be determined that

$$\nabla \bullet \hat{E} = 0 \tag{3.5}$$

By introducing the curl operator (∇X) to both sides of the first equation in expression (3.1) (Faraday's law), replacing $\nabla X \hat{B}$ on the right hand side of the equation by the 2nd equation in expression (3.1), and using the identity $\nabla X \left(\nabla X \hat{E} \right) = \nabla \left(\nabla \bullet \hat{E} \right) - \nabla^2 \hat{E}$, we arrive at the wave equation

$$\nabla^2 \hat{E} = -\varepsilon_0 \mu_0 \frac{\partial^2 \hat{E}}{\partial t^2} \tag{3.6}$$

To quantize the optical field propagating in the *z* direction, it is appropriate to assume the general expression of $\hat{E}(z,t)$ has the form

$$\hat{E}(z,t) = \sum_m \hat{q}_m(t) Z_m(z) \tag{3.7}$$

where *m* is a mode index integer and represents the mode component of the field, and $\hat{q}_m(t)$ is an operator denoted by the hat above it. By substituting expression (3.7) into Equation (3.6), we arrived at the following differential equations that holds for each field mode component

$$\nabla^2 Z_m(z) + k_m^2 Z_m(z) = 0 \tag{3.8}$$

$$\frac{\partial^2 \hat{q}_m}{\partial t^2} + \omega_m{}^2 \hat{q}_m(t) = 0 \tag{3.9}$$

where k_m is the propagation constant associated with the mode index m and can be expressed as $k_m = \omega_m/(\varepsilon_0\mu_0)^{1/2}$. It is obvious that the solution of spatial component $Z_m(z)$ in Equation (3.8) has the form of plane waves i.e.

$$Z_m(z) = \exp(ik_m z) \tag{3.10}$$

There is one complication however that in optical communication system, the field is not confined within a cavity. Therefore, the mode summation in Equation (3.7) should instead be replaced by an integral [35]. In this Chapter, we shall simplify the problem by employing the concept of "box normalization", in which space is covered by an infinite set of large finite size cubic boxes [33]. This configuration allows periodic boundary conditions to be imposed so that the field is assumed to be the same value at opposite sides of the box, thus only fields with wavelength $\lambda = \frac{mL}{2}$ exist [35]. As a result, the field solution can be represented by the summation in Equation (3.7) where the mode index is discrete (m is an integer). We shall remove the unphysical limitation on the finite size boxes in Chapter 5 by allowing the field mode index to be continuous.

It is well known that the solution of optical field propagating in the z direction $\hat{E}(z,t)$ is [33, 35]

$$\hat{E}(z,t) = \left(\frac{\hbar\omega_m}{2\varepsilon_0 V}\right)^{1/2} \sum_{m=0}^{\infty} \hat{a}_m \exp(ik_m z - i\omega_m t) + \hat{a}_m{}^{+} \exp(-ik_m z + i\omega_m t) \tag{3.11}$$

In this the temporal field component is

$$\hat{q}_m(t) = \left(\frac{\hbar\omega_m}{2\varepsilon_0 V}\right)^{1/2} \left[\hat{a}_m \exp(-i\omega_m t) + \hat{a}_m{}^{+} \exp(i\omega_m t)\right] \tag{3.12}$$

and the spatial component is

$$Z_m(z) = \exp(ik_m z) \tag{3.13}$$

It is shown in Equation (3.11) that the optical field is a real vector field. The propagation constant k_m is related to the length of the box cavity L by $k_m = 2\pi m/L$, and is also related to the angular frequency of the field ω_m by $\omega_m = |k_m|c_0$. $\hat{a}_m$ and $\hat{a}_m^+$ are the annihilation and creation operator respectively.

We have the following relations when $\hat{a}_m$ and $\hat{a}_m^+$ operate on the number state of the field $|N_m\rangle$ [33]

$$\hat{a}_m |N_m\rangle = \sqrt{N_m}\,|N_m - 1\rangle \tag{3.14}$$

$$\hat{a}_m^+ |N_m\rangle = \sqrt{N_m + 1}\,|N_m + 1\rangle \tag{3.15}$$

where N_m describes the number of photons from the field at mode m. The photon number operator $\widehat{N}_m$ which can be expressed as $\widehat{N}_m = \hat{a}_m^+ \hat{a}_m$, gives the photon number of the field when operates on number state $|N_m\rangle$

$$\widehat{N}_m |N_m\rangle = \hat{a}_m^+ \hat{a}_m |N_m\rangle = N_m |N_m\rangle \tag{3.16}$$

The annihilation and creation operator, $\hat{a}_m^+$ and $\hat{a}_m$, satisfies the commutation relation

$$\left[\hat{a}_m, \hat{a}_n^+\right] = \hat{a}_m \hat{a}_n^+ - \hat{a}_n^+ \hat{a}_m = \delta_{mn} \tag{3.17}$$

It is shown from [33, 35] that the commutation relation in expression (3.17) as well as the constant $(\hbar\omega/2\varepsilon_0 V)^{1/2}$ gives the corresponding field Hamiltonian (energy operator) of the form

$$\widehat{H} = \sum_{m=0}^{\infty} \hbar\omega_m \left(\hat{a}_m^+ \hat{a}_m + \frac{1}{2}\right) \tag{3.18}$$

Note that the first term in Equation (3.18) represents the energy density of the optical field, while the last term represents the energy density due to vacuum fluctuation.

In SCFT, the expression of the electric field strength of the optical field is [33]

$$E(z,t)=\left(\frac{\hbar\omega_m}{2\varepsilon_0 V}\right)^{1/2}\sum_{m=0}^{\infty}c_m\exp\left(ik_m z-i\omega_m t\right)+c_m{}^{*}\exp\left(-ik_m z+i\omega_m t\right) \qquad (3.19)$$

By comparing the QFT expression in (3.11) with the SCFT expression in (3.19), we can identify the Fourier coefficients c_m and its conjugate $c_m{}^{*}$ in Equation (3.19) is replaced by the annihilation and creation operator $\hat{a}_m$ and $\hat{a}_m{}^{+}$. An immediate consequence of treating the Fourier coefficients as complex numbers rather than operators is that the vacuum energy (last term in Equation (3.18)) does not appear in the energy density expression in SCFT [35].

3.2 Quantum State of Optical Field

Recalling from Section 3.1, the field in QFT is treated as an operator that operates on a quantum state vector that characterizes the properties of the field. The state that closely resemble to the property of optical field generated from the laser is known as the coherent state [33]. In this Section we shall discuss the properties of the coherent state generated by a single mode laser.

A single mode coherent state vector $|\rho_m\rangle$ corresponds to a linear superposition of the number states $|N_m\rangle$

$$\left|\rho_m\right\rangle=\exp\left(\frac{-\left|\rho_m\right|^2}{2}\right)\sum_{N=0}^{\infty}\frac{\rho_m{}^{N}}{(N!)^{1/2}}\left|N_m\right\rangle \qquad (3.20)$$

where ρ_m is a complex number. We shall neglect the mode index (subscript m) that is attached to state vector $|N_m\rangle$ in the following expressions for simplicity. It is easy to verify from Equation (3.20) that the ket state vector $|\rho\rangle$ is normalized, i.e.

$$\left\langle\rho\middle|\rho\right\rangle=\exp\left(-\left|\rho\right|^2\right)\sum_{N=0}^{\infty}\frac{\rho^{*N}\rho^{N}}{N!}=1 \qquad (3.21)$$

The coherent states are the right eigenstates of annihilation operator $\hat{a}$, which can be verified using expression (3.14) and (3.20)

$$\hat{a}\left|\rho\right\rangle = \exp\left(\frac{-\left|\rho\right|^2}{2}\right)\sum_{N=0}^{\infty}\frac{\rho^N}{\left(N!\right)^{1/2}}N^{1/2}\left|N-1\right\rangle = \rho\left|\rho\right\rangle \tag{3.22}$$

Similarly using expression (3.14) and (3.20), it is easy to verify the creation operator $\hat{a}^+$ satisfy the eigen-equation

$$\left\langle\rho\right|\hat{a}^+ = \left\langle\rho\right|\rho^* \tag{3.23}$$

However, the state $|\rho>$ is not a right eigenstate of the creation operator.

The mean photon number of the optical field in state $|\rho>$ is obtained by calculating the expectation value of the number operator $\widehat{N}$ with respect to state $|\rho>$. Using Equation (3.22) and Equation (3.23) we have

$$\left\langle\rho\right|\widehat{N}\left|\rho\right\rangle = \left\langle\rho\right|\hat{a}^+\hat{a}\left|\rho\right\rangle = \left|\rho\right|^2 = N \tag{3.24}$$

N represents the mean photon number optical field, thus Equation (3.24) shows the mean photon number of the optical field N can be represented by $|\rho|^2$. The variance of photon number of the optical field is given by the following relation

$$\left(\Delta N\right)^2 = \left\langle\widehat{N}^2\right\rangle - \left\langle\widehat{N}\right\rangle^2 \tag{3.25}$$

The first term in Equation (3.25) is calculated by re-ordering the $\hat{a}\hat{a}^+$ term using the commutation relation in expression (3.17),

$$\begin{aligned}\left\langle\widehat{N}^2\right\rangle &= \left\langle\rho\right|\hat{a}^+\hat{a}\hat{a}^+\hat{a}\left|\rho\right\rangle \\ &= \left\langle\rho\right|\hat{a}^+\hat{a}^+\hat{a}\hat{a} + \hat{a}^+\hat{a}\left|\rho\right\rangle \\ &= \left|\rho\right|^4 + \left|\rho\right|^2\end{aligned} \tag{3.26}$$

Thus, using the result in Equation (3.26) and the definition of the variance of photon number arrival rate in Equation (3.25), we have

$$\left(\Delta N\right)^2 = \left|\rho\right|^4 + \left|\rho\right|^2 - \left(\left|\rho\right|^2\right)^2 = \left|\rho\right|^2 = N \tag{3.27}$$

We see that one of the important property of the field prepared in coherent state is the **mean photon number *N* is equal to its variance**. The fractional uncertainty in the photon number of coherent state is,

$$\frac{\Delta N}{\left\langle \widehat{N} \right\rangle} = \frac{1}{|\rho|} = \frac{1}{\sqrt{N}} \tag{3.28}$$

The fractional uncertainty decreases with increasing coherent state amplitude $|\rho|$.

The probability distribution of detecting N photons in a single mode optical field is obtained from the definition

$$\begin{aligned} P(N) &= \left|\langle N|\rho\rangle\right|^2 \\ &= \exp\left(-|\rho|^2\right)\sum_{M=0}^{\infty}\sum_{N=0}^{\infty}\frac{\rho^M}{(M!)^{1/2}}\frac{\rho^{*N}}{(N!)^{1/2}}\langle N|M\rangle \\ &= \exp\left(-|\rho|^2\right)\frac{|\rho|^{2N}}{N!} \\ &= \exp\left(-\left\langle \widehat{N} \right\rangle\right)\frac{\left\langle \widehat{N} \right\rangle^N}{N!} \end{aligned} \tag{3.29}$$

The final line in Equation (3.29) is a Poisson probability distribution. This agrees with the photon arrival statistics derived from SCFT [1, 25]. In fact the mean photon number equal to its corresponding variance $\left\langle \widehat{N} \right\rangle = (\Delta N)^2$, is a property of the Poisson distribution.

It is useful to introduce the in phase and quadrature operator $\widehat{X}_1$ and $\widehat{X}_2$ to describe the property of the coherent state, where it is defined as

$$\widehat{X}_1 = \frac{1}{2}\left(\hat{a}^+ + \hat{a}\right) \tag{3.30}$$

$$\widehat{X}_2 = \frac{1}{2i}\left(\hat{a} - \hat{a}^+\right) \tag{3.31}$$

Using the commutation relation in expression (3.17) and the definition of variance in Equation (3.25), it follows that the quadrature variances are

$$(\Delta X_1)^2 = (\Delta X_2)^2 = \frac{1}{4} \tag{3.32}$$

The coherent state is known as the minimum uncertainty state in which both in-phase and quadrature variance are minimized, where we have

$$(\Delta X_1)^2 (\Delta X_2)^2 = \frac{1}{16} \tag{3.33}$$

Figure 3.1 is a state diagram showing the electric-field property of the coherent state. The phasor characterizes the mean signal strength and the phase of the optical field. The circle in Figure 3.1 is commonly referred to as the uncertainty contour. It represents the uncertainty in which the phasor lies. The uncertainty area's circular symmetry shows that a field prepared in coherent state has equal uncertainty (i.e. variance) in the in-phase and quadrature component. The amplitude contribution reproduces the result for the photon number variance [33]

$$(\Delta N)^2 = \left[\left(\langle \hat{N} \rangle^{1/2} + \frac{1}{4} \right)^2 - \left(\langle \hat{N} \rangle^{1/2} - \frac{1}{4} \right)^2 \right]^2 = \langle \hat{N} \rangle \tag{3.34}$$

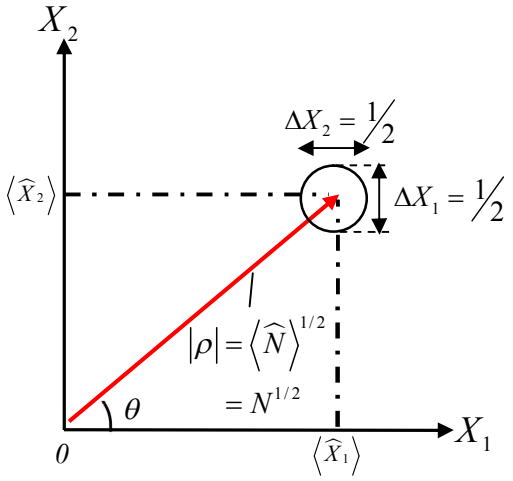

Figure 3.1: State diagram of optical field prepared in coherent state.

Note that there is also an uncertainty associated with the phase of the field. Provided the amplitude (photon number) of the field is large ($|\rho| >> 1$), the arc rule gives the approximate expression

$$\Delta\varphi = \frac{1}{2|\rho|} = \frac{1}{2\langle \hat{N} \rangle} \tag{3.35}$$

The product of photon-number and phase uncertainty is therefore

$$\Delta N \Delta\varphi = \frac{1}{2} \tag{3.36}$$

From expression (3.35), we can identify the phase uncertainty of the field can be neglected as the photon number is large. This has a similar property with the amplitude uncertainty given by Equation (3.28). Figure 3.2 shows the amplitude and phase uncertainty spread resembles to that of a classical stable wave as photon number increases.

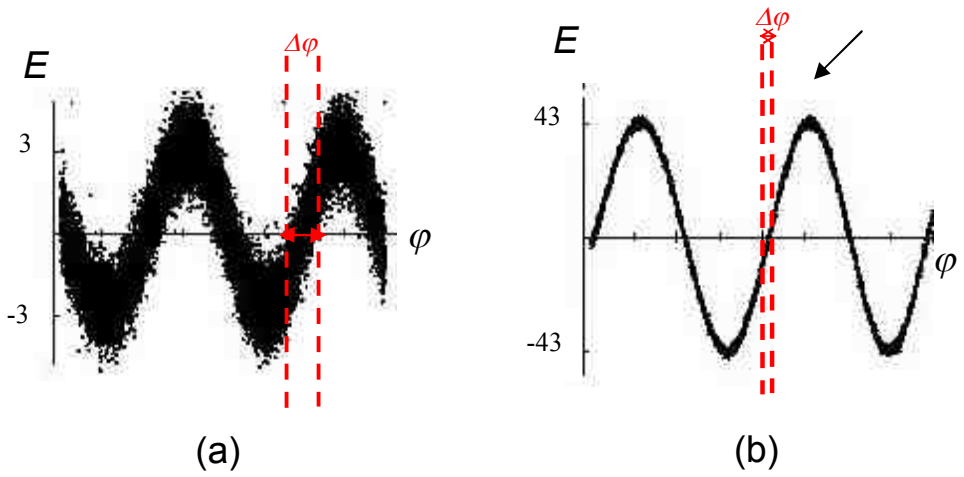

Figure 3.2: Amplitude and phase uncertainty spread of optical field with a) Low photon number b) Large photon number.

3.3 Summary

In QFT the representation of optical field is promoted from mathematical function to an operator. The mean and variance of the observed field amplitude is determined by calculating the "expectation value" of the state with respect to the number operator. The optical field generated from the laser is best described by coherent state. The coherent state is an eigenstate of the annihilation operator as shown in Equation (3.22), where this will be used extensively in Chapter 5, Chapter 6 and Chapter 7. The photon number statistics has a **Poisson distribution** in which the mean is equivalent to its variance for field prepared in coherent state. It is a minimum uncertainty state in which the in-phase and quadrature variance are minimized. The amplitude and phase uncertainty spread resembles to that of a classical stable wave as photon number increases.

4 Quantum Field Model of Phase Modulator

4.1 Chapter Objectives

In this Chapter, we will use the theory presented in Chapter 2 and Chapter 3 to determine the equation of motion of the modulated field in the modulator. Although a quantum representation of a phase modulator has been presented in [9], their model did not include the effect of photon creation that arises from the time variation of refractive index indicated by [16 - 21].

The objective of this Chapter is to develop a quantum model that describes the behavior of a phase modulated field which incorporates the phenomenon of photon creation. The optical field is modulated by an all optical phase modulator (AOPM). As we have explained in Chapter 2, the phase of the modulated field is controlled by the intensity of the optical control signal. A diagram of an AOPM is shown in Figure 4.1. The anti-reflective coatings (ARC) are added at the front and back end of the modulator to reduce signal losses due to reflection of optical signal.

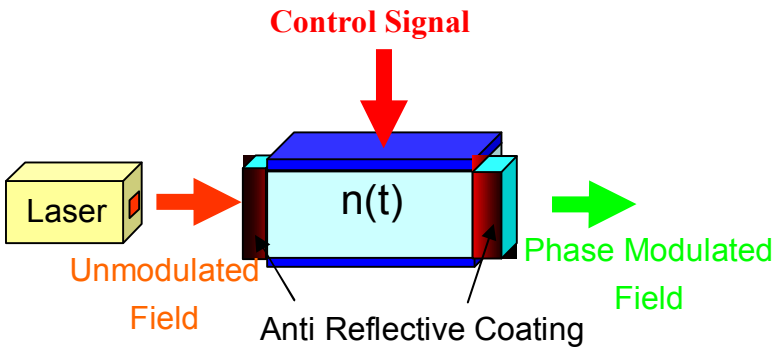

Figure 4.1: Diagram of AO-TPM.

4.2 Quantum Model of Phase Modulator

In this Section, a quantum field representation of the laser field propagating through the phase modulator is presented. From Figure 4.1, we can identify the modulator consists of two different types of media; a modulating medium whose refractive index is dependent on the intensity of the control signal strength, and the ARC whose refractive index varies spatially along the propagating direction z. In the following Subsections, we shall determine the corresponding equation of motion that describes the characteristics of the optical field propagating in each of these regions.

4.2.1 Field in Modulating Medium

In Chapter 2, we discussed an all optical phase modulator (AOPM) that uses cross phase modulation (XPM) so that the control optical field creates a time dependent dielectric medium $\varepsilon(t)$, to impress phase encoded data onto the optical carrier. In this Section, we determine the equation of motion that governs the field propagation in a modulating medium whose dielectric and hence refractive index $n(t)$ is time dependent. Similar to the analysis of field propagating in vacuum in Chapter 3, the field operator that describes the optical carrier propagating inside the time dependent modulating medium is governed by the Maxwell's equation. We will use the following assumptions to simplify the problem:

1. The modulator lossless i.e. no loss in energy due to energy reflection and signal attenuation.
2. The ARC and modulating medium are non-dispersive.
3. The modulator has no bound charges or current source.
4. The intensity of the optical carrier has negligible effect on the refractive index change.

5. The maximum rate of change of refractive index is much smaller than the carrier frequency of the optical field.
6. The waveguide effects in the communication link are ignored.

Based on these assumptions, we can write the Maxwell's equation of the form,

$$\begin{aligned} \nabla X\, \hat{E} &= -\frac{\partial \hat{B}}{\partial t} \\ \nabla X\, \hat{B} &= \mu_0 \frac{\partial \left[\varepsilon(t) \hat{E} \right]}{\partial t} \\ \nabla \bullet \left[\varepsilon(t) \hat{E} \right] &= 0 \\ \nabla \bullet \hat{B} &= 0 \end{aligned} \tag{4.1}$$

where $\hat{E}(z,t)$ is the electric field operator and $\hat{B}(z,t)$ is the magnetic flux density operator of the optical signal, μ_0 is the free space magnetic permeability constant (= $4\pi * 10^{-7}$ *H/m [Henry/meter]*), ∇ is the differential gradient operator (= $\boldsymbol{i}\partial/\partial x + \boldsymbol{j}\partial/\partial y + \boldsymbol{k}\partial/\partial z$), and $\varepsilon(t)$ is the time dependent electric permittivity. The spatial and time dependence for $\hat{E}(z,t)$ and $\hat{B}(z,t)$ operators have been suppressed in Equation (4.1) for clarity.

By introducing the curl operator (∇X) to both sides of the first equation in expression (4.1) (Faraday's law), replacing $\nabla X \hat{B}$ on the right hand side of the equation by the 2nd equation in (4.1), and using the identity $\nabla X \left(\nabla X \hat{E} \right) = \nabla \left(\nabla \bullet \hat{E} \right) - \nabla^2 \hat{E}$, we arrive at the wave equation

$$\nabla \left(\nabla \bullet \hat{E} \right) - \nabla^2 \hat{E} = -\mu_0 \frac{\partial^2 \left(\varepsilon(t) \hat{E} \right)}{\partial t^2} \tag{4.2}$$

Expression (4.2) is the equation of motion of the optical field inside the modulating medium. From the third line in expression (4.1), we have $\nabla \bullet \hat{E} = 0$. As a result, the first term in the left hand side of Equation (4.2) vanishes, for which we arrived at

$$\nabla^2 \hat{E} = \mu_0 \frac{\partial^2 \left(\varepsilon(t) \hat{E} \right)}{\partial t^2} \tag{4.3}$$

Since the waveguide effect of the modulating medium is ignored, the optical field is characterized by transverse electromagnetic (TEM) wave [36, 37].

Similar to Chapter 3, the problem can be simplified by assuming the field propagate in the z direction, and thus the gradient operator can therefore be reduced to $\nabla \rightarrow \boldsymbol{k}\partial/\partial z$. For simplicity, $\hat{E}(z,t)$ and $\hat{B}(z,t)$ field vector operators are orientated along the x and y axes respectively as shown in Figure 4.2.

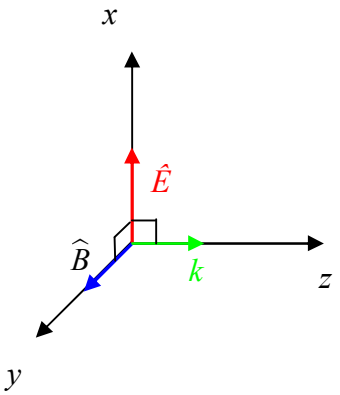

Figure 4.2: TEM wave propagating in z direction.

Using the simplifications from above, expression (4.3) can be rewritten as

$$\frac{\partial^2 \hat{E}}{\partial z^2} = \mu_0 \frac{\partial^2 \left(\varepsilon(t) \hat{E} \right)}{\partial t^2} \tag{4.4}$$

The form of Equation (4.4) can be further simplified by working with the electric flux density operator $\hat{D}(z,t)$, which is defined as

$$\hat{D}(z,t) = \varepsilon(t) \hat{E}(z,t) \tag{4.5}$$

By expressing (4.5) in terms of $\hat{D}(z,t)$, we have

$$\frac{\partial^2 \widehat{D}}{\partial z^2} - \left(\frac{n(t)}{c_0}\right)^2 \frac{\partial^2 \widehat{D}}{\partial t^2} = 0 \tag{4.6}$$

where c_0 is the speed of light in the free space ($c_0 = 1/[\mu_0\varepsilon_0]^{1/2} = 3*10^{-8}\ ms^{-1}$) and $n(t)$ is the time dependent refractive index and is related to $\varepsilon(t)$ by $n(t) = [\varepsilon(t)/\varepsilon_0]^{1/2}$.

In general, the field operator $\widehat{D}(z,t)$ can be represented as a superposition of field modes which takes the form

$$\widehat{D}(z,t) = \sum_m \hat{q}_m^{\ MM}(t) Z_m^{\ MM}(z) \tag{4.7}$$

where the subscript m is an integer that denotes the mode of the field, $\hat{q}_m^{\ MM}(t)$ is the time dependent field operator and $Z_m^{\ MM}(z)$ is the spatial mode function of the $\widehat{D}(z,t)$ field. By the use of 'box normalization" introduced in Chapter 3, the field can be represented by a summation of field modes instead of an integral.

By substituting (4.7) into the wave equation in (4.6) and using the method of separation of variables, Equation (4.6) can be reduced into two ordinary differential equations (ODEs). One of the ODE governs the spatial component of the field mode $Z_m^{\ MM}(z)$ and is given by

$$\frac{d^2 Z_m^{\ MM}}{dz^2} + k_m^{\ 2} Z_m^{\ MM}(z) = 0 \tag{4.8}$$

where k_m represents the wave-number inside the modulating medium associated with the mode index m. The mode index is related to the wave-number in the vacuum k_{0m} by $k_m = nk_{0m}$, where n is the refractive index of the media in the absence of the control signal. From Chapter 3, we have shown the solution of $Z_m^{\ MM}(z)$ in Equation (4.8) has the form of plane waves, i.e. $Z_m^{\ MM}(z) = \exp(ik_m z)$. Therefore, the general solution of field operator $\widehat{D}(z,t)$ can be rewritten as

$$\widehat{D}(z,t) = \sum_m \hat{q}_m^{\,MM}(t)\exp(ik_m z) \tag{4.9}$$

The other ODE that governs the time evolution of the field operator in the modulating medium is given by

$$\frac{d^2\hat{q}_m^{\,MM}}{dt^2} + \omega_m^{\,2}(t)\hat{q}_m^{\,MM}(t) = 0 \tag{4.10}$$

where $\omega_m(t) = k_m c_0/n(t)$ is the time dependent angular frequency of the field. Expression (4.10) that governs the equation of motion of $\hat{q}_m^{\,MM}(t)$ is also known as the time dependent oscillator equation which has been studied extensively in the QFT literatures [11, 12]. The solution structure of $\hat{q}_m^{\,MM}(t)$, is more complicated as compared with the spatial dependence of the field $Z_m^{\,MM}(z)$, and will be discussed in more details in the following subsection.

4.2.2 Hamiltonian Formalism in Modulating Medium

The solution of $\hat{q}_m^{\,MM}(t)$ is governed by the structure of the field Hamiltonian operator. The Hamiltonian operator $\hat{H}$ is an energy operator that enables the expectation value of the energy inside the modulating medium to be determined for energy state-vector $|E\rangle$. In this Section, we shall determine the identities that govern the solution structure of $\hat{q}_m^{\,MM}(t)$ based on the expression of the Hamiltonian.

The Hamiltonian operator is derived by applying a quantization procedure in classical Hamiltonian mechanics. The procedures of deriving the Hamiltonian operator are shown as follows [38]:

1. Construct the corresponding Lagrangian operator from the equation of motion using field Euler-Lagrangian equation.
2. Derive the Hamiltonian operator from the Lagrangian operator using Legendre

transforms.

3. Apply quantization procedure by replacing canonical variables by noncommuting operators.

A. Expression of Field Lagrangian

From Hamiltonian mechanics, the classical version of the equation of motion in (4.10) for which $\hat{q}_m^{MM}$ is replace with a classical variable q_m^{MM}, can be constructed using the field Euler-Lagrange equation [38]

$$\frac{\partial}{\partial t}\left(\frac{\partial L_D}{\partial\left(\partial D/\partial t\right)}\right)-\frac{\partial}{\partial z}\left(\frac{\partial L_D}{\partial\left(\partial D/\partial z\right)}\right)+\left(\frac{\partial L_D}{\partial D}\right)=0 \tag{4.11}$$

where L_D is the Lagrangian density. Notice that the electric flux D in expression (4.11) is a classical variable whose expression is similar to that of Equation (4.9) except that it is now dependent on the classical variable q_m^{MM}. The field Lagrangian operator is related to the Lagrangian density operator by $L=\int_V L_D dV$. In order to reproduce the classical version of the equation of motion in Equation (4.10) as well as satisfying the expression (4.11), the field Lagrangian L is expressed as

$$L=\frac{\mu_0}{2k_m^{\,2}}\int_V\left(\frac{\partial D}{\partial t}\right)^2-\left(\frac{c_0}{n(t)}\right)^2\left(\frac{\partial D}{\partial z}\right)^2 dV \tag{4.12}$$

Using Equation (4.12), we can determine the expression of the canonical conjugate momentum $W(z,t)$, where we have

$$W(z,t)=\frac{\partial L_D}{\partial\left(\partial D/\partial t\right)}=\frac{\mu_0}{k_m^{\,2}}\frac{\partial D}{\partial t} \tag{4.13}$$

By substituting the general expression of $D(z,t)$ in Equation (4.9) into the definition of $W(z,t)$ in Equation (4.13), we arrive at

$$W(z,t) = \sum_m w_m{}^{MM}(t)\exp(ik_m z) \tag{4.14}$$

where

$$w_m{}^{MM}(t) = \frac{\mu_0}{k_m{}^2}\frac{dq_m{}^{MM}}{dt} \tag{4.15}$$

From expression (4.14) and (4.15), it can be realized that the canonical conjugate momentum field $W(z,t)$ corresponds to the magnetic flux density $B(z,t)$. When Equation (4.9) is substituted into Equation (4.12), using the relation $\varepsilon(t)/\varepsilon_0 = n^2(t)$ and $k_m = -k_{-m}$, as well as applying the spatial integral expression,

$$\int_V \exp\left[\pm i(k_m - k_n)z\right]dV = V\delta_{m,n} \tag{4.16}$$

where V is the volume of the modulating medium, it is easy to verify that L can be re-expressed in terms of the temporal component of the field

$$L = \frac{V}{2}\sum_m \frac{\mu_0}{k_m{}^2}\frac{\partial q_m{}^{MM}}{\partial t}\frac{\partial q_{-m}{}^{MM}}{\partial t} - \frac{q_m{}^{MM}(t)\,q_{-m}{}^{MM}(t)}{\varepsilon(t)} \tag{4.17}$$

B. Expression of Classical Hamiltonian

The classical Hamiltonian H can be determined by performing the Legendre transformation on L [35]

$$H(t) = \int_V W(z,t)\frac{\partial D}{\partial t}dV - L(z,t) \tag{4.18}$$

Using expressions (4.16) and (4.17), the classical Hamiltonian in the modulating medium $H(t)$ can be expressed as

$$H(t) = \frac{V}{2}\sum_{m=-\infty}^{\infty}\frac{\mu_0}{k_m{}^2}\frac{\partial q_m{}^{MM}}{\partial t}\frac{\partial q_{-m}{}^{MM}}{\partial t} + \frac{q_m{}^{MM}(t)\,q_{-m}{}^{MM}(t)}{\varepsilon(t)} \tag{4.19}$$

C. Quantization of Hamiltonian systems

In order to transit from classical field theory (CFT) to quantum field theory (QFT), we replace the canonical field $D(z,t)$, $W(z,t)$ by noncommutating field operators $\widehat{D}(z,t)$, $\widehat{W}(z,t)$ for which they satisfy the standard equal time commutation relation [38],

$$[\widehat{D}(z,t),\widehat{D}(z',t)]=[\widehat{W}(z,t)^{+},\widehat{W}(z',t)^{+}]=0 \tag{4.20}$$

$$[\widehat{D}(z,t),\widehat{W}(z',t)]=i\hbar\delta_{z,z'} \tag{4.21}$$

where the commutator bracket is defined as *[A,B] = AB – BA*. In order to satisfy the commutation relation in expression (4.20) and (4.21), we find the corresponding commutation relations for the temporal component of the mode operators

$$[\hat{q}_m^{\,MM}(t),\hat{q}_n^{\,MM}(t)]=[\widehat{w}_m^{\,MM+}(t),\widehat{w}_n^{\,MM+}(t)]=0 \tag{4.22}$$

$$[\hat{q}_m^{\,MM}(t),\widehat{w}_n^{\,MM}(t)]=\frac{i\hbar}{V}\delta_{m,-n} \tag{4.23}$$

By replacing the classical variable $q_m^{\,MM}$ by the quantum operator $\hat{q}_m^{\,MM}$ in the classical Hamiltonian in Equation (4.19), and using the equation of motion in (4.10), the relations between the $\widehat{D}(z,t)$ and $\widehat{E}(z,t)$ from Equation (4.5), as well as the relation between $\widehat{E}(z,t)$ and $\widehat{B}(z,t)$ field operator in Equation (4.1), we can express the Hamiltonian field operator in the modulating media as

$$\widehat{H}(t)=\frac{1}{2}\int\varepsilon(t)\widehat{E}^{2}(z,t)+\widehat{B}^{2}(z,t)dV \tag{4.24}$$

The expression of $\widehat{H}(t)$ in Equation (4.19) can be used to determine the average total energy inside the volume of the modulating medium by calculating the expectation value $\langle E|\widehat{H}(t)|E\rangle$. Unlike the scenario for the field propagating in a vacuum, the expression of the Hamiltonian for modulating medium is explicitly dependent on time.

In QFT, it is convenient to introduce the annihilation and creation operators of the phase modulated field, $\hat{b}_m(t)$ and $\hat{b}_m^{+}(t)$, that can be expressed in terms $\hat{q}_m^{MM}(t)$ and $\hat{w}_m^{MM}(t)$

$$\hat{b}_m(t) = \left(\frac{V}{2\hbar\omega(t)\varepsilon(t)}\right)^{1/2} \hat{q}_m^{MM}(t) + i\left(\frac{\omega(t)\varepsilon(t)V}{2\hbar}\right)^{1/2} \hat{w}_m^{MM}(t) \qquad (4.25)$$

$$\hat{b}_m^{+}(t) = \left(\frac{V}{2\hbar\omega(t)\varepsilon(t)}\right)^{1/2} \hat{q}_{-m}^{MM}(t) - i\left(\frac{\omega(t)\varepsilon(t)V}{2\hbar}\right)^{1/2} \hat{w}_{-m}^{MM}(t) \qquad (4.26)$$

Because the modulating medium has a time varying index, therefore the coefficient in front of $\hat{q}_m^{MM}(t)$ and $\hat{w}_{-m}^{MM}(t)$ in Equation (4.25) and (4.26) are time dependent. Despite that $\hat{b}_m(t)$ and $\hat{b}_m^{+}(t)$ are time dependent inside the modulating medium, they continue to satisfy the equal time commutation relations [12]

$$[\hat{b}_m^{+}(t), \hat{b}_n(t)] = [\hat{b}_m(t)^{+}, \hat{b}_n(t)^{+}] = 0 \qquad (4.27)$$

$$[\hat{b}_m(t), \hat{b}_n^{+}(t)] = \delta_{m,n} \qquad (4.28)$$

where the subscripts *m* and *n*, indicate different modes which the parameters are associated with. Expression (4.27) and (4.28) can be verified from the commutation relation in (4.25) and (4.26). By substituting (4.25) and (4.26) into (4.19), and using the commutation relation in (4.28), the Hamiltonian operator can re-expressed in terms of $\hat{b}_m(t)$ and $\hat{b}_m^{+}(t)$ where it takes the form

$$\hat{H}(t) = \sum_{m=0}^{\infty} \hbar\omega_m(t)\left(\hat{b}_m^{+}(t)\hat{b}_m(t) + \frac{1}{2}\right) \qquad (4.29)$$

The field Hamiltonian in (4.29) is the same as the Hamiltonian for a time dependent harmonic oscillator presented by [39]. Using the Hamiltonian expression in (4.29), we can determine the general form of the field mode in the modulating medium.

Using the definition of $\hat{b}_m(t)$ and $\hat{b}_m^{+}(t)$ operator from expression (4.25) and (4.26) respectively in the modulating medium, the temporal component of the electric flux density operator $\hat{q}_m^{MM}(t)$ can be expressed as

$$\hat{q}_m^{MM}(t) = \left(\frac{\hbar\omega_m(t)\varepsilon(t)}{2V}\right)^{1/2}\left[\hat{b}_m(t) + \hat{b}_{-m}^{+}(t)\right] \tag{4.30}$$

From Equation (4.30), one can easily verified that

$$\hat{q}_m^{MM*}(t) = \hat{q}_{-m}^{MM}(t) \tag{4.31}$$

By substituting the expression of $\hat{q}_m^{MM}(t)$ from Equation (4.30) into the expression of $\hat{D}(z,t)$ in (4.9), we can rewrite $\hat{D}(z,t)$ as

$$\hat{D}(z,t) = \sum_{m=-\infty}^{\infty}\left(\frac{\hbar\omega_m(t)\varepsilon(t)}{2V}\right)^{1/2}\left[\hat{b}_m(t)\exp(ik_m z) + \hat{b}_{-m}^{+}(t)\exp(-ik_m z)\right] \tag{4.32}$$

We will now show that the time dependent annihilation and creation operators, $\hat{b}_m(t)$ and $\hat{b}_m^{+}(t)$, can be re-expressed in terms of the time independent operator (unmodulated) annihilation and creation operator introduced in Chapter 3 using

$$\hat{b}_m(t) = \hat{a}_m f_m(t) \tag{4.33}$$

where $f_m(t)$ is a time dependent function yet to be determined. In Chapter 3, we have shown the time independent annihilation and creation operator, $\hat{a}_m$ and $\hat{a}_m^{+}$, satisfies the usual commutation relations

$$\left[\hat{a}_m, \hat{a}_n\right] = \left[\hat{a}_m^{+}, \hat{a}_n^{+}\right] = 0 \tag{4.34}$$

$$\left[\hat{a}_m, \hat{a}_n^{+}\right] = \delta_{m,n} \tag{4.35}$$

For simplicity, it is convenient to rewrite $\hat{q}_m^{MM}(t)$ as

$$\hat{q}_m^{MM}(t) = \hat{a}_m u_m(t) + \hat{a}_{-m}^{+} u_m^{*}(t) \tag{4.36}$$

where $u_m(t)$ is related to $f_m(t)$ by

$$u_m(t) = \left(\frac{\hbar\omega_m(t)\varepsilon(t)}{2V}\right)^{1/2} f_m(t) \tag{4.37}$$

Furthermore, by substituting expression (4.36) into the equation of motion for $\hat{q}_m^{MM}(t)$ in Equation (4.10), we can determine $u_m(t)$ is governed by the ODE

$$\frac{d^2 u_m}{dt^2} + \left[\frac{k_m c_0}{n(t)}\right]^2 u_m(t) = 0 \tag{4.38}$$

Similarly, the general solution of the temporal component of the canonical conjugate momentum operator $\hat{w}_m^{MM}(t)$ can be determined by substituting Equation (4.36) into Equation (4.15)

$$\hat{w}_m^{MM}(t) = \frac{\mu_0}{k_m^{\,2}}\left(\hat{a}_m \frac{du_m}{dt} + \hat{a}^{+}_{-m} \frac{du_m^{*}}{dt}\right) \tag{4.39}$$

where $\mu_0 = 4\pi*10^{-7} H/m$ is the free space magnetic permeability. In order to satisfy the commutation relations between $\hat{q}_m^{MM}(t)$ and $\hat{w}_n^{MM}(t)$ in Equation (4.22) and Equation (4.23), the mode function $u_m(t)$ must obey the normalization condition

$$u_m(t)\frac{du_m^{*}}{dt} - \frac{du_m}{dt}u_m^{*}(t) = i\frac{\hbar k_{0m}^{\,2}}{\mu_0 V} \tag{4.40}$$

where k_{0m} is the propagation constant in free space . The normalization condition in Equation (4.40) can be verified by substituting the expressions (4.39) and (4.36) into (4.21), as well as using the commutation relation of $\hat{a}_m$ and $\hat{a}_m^{+}$ in expression (4.34)

and (4.35). The expression on the left of Equation (4.40) is the Wronskian of two independent solutions $u_m(t)$ and $u_m^*(t)$, and hence it is time independent [40].

4.2.3 Bogoliubov Transformation of Field Mode

In this Subsection, we shall determine the evolution of the field propagating in the modulating medium whose refractive index is time varying. For simplicity, the refractive index profile *n(t)* is assumed to be changing dynamically between the time interval $-T < t < T$, while it is asymptotically static in the remote past $(t < -T)$ and remote future $(t > T)$ as shown in Figure 4.3.

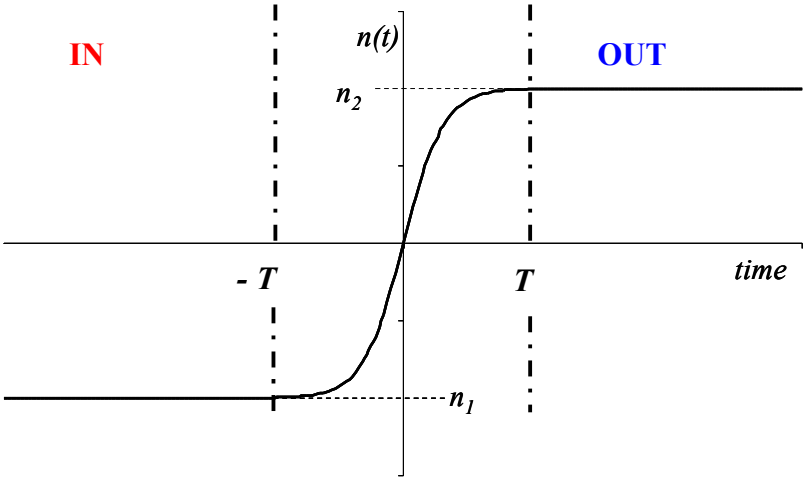

Figure 4.3: Time dependent refractive index profile of modulator.

In Figure 4.3 there are two time regions in which the refractive index *n(t)* is constant. We shall call the static region in the remote past $t < -T$ as the 'in' region while the static region in the remote future $t > T$ as the 'out' region. The 'in' region corresponds to the situation when the modulator is in steady state with refractive index n_1. Therefore the expression of field mode is governed by the ODE,

$$\frac{d^2 u_m^{\ in}}{dt^2} + \left(\frac{k_m c_0}{n_1}\right)^2 u_m^{\ in}(t) = 0 \qquad t < T \tag{4.41}$$

where $u_m^{\ in}(t)$ represents the solution of the field mode in the 'in' region. Similarly, in the 'out' region *(t > T)* the modulator is in steady state with refractive index n_2. The field mode is governed by the ODE,

$$\frac{d^2 u_m^{\ out}}{dt^2} + \left(\frac{k_m c_0}{n_2}\right)^2 u_m^{\ out}(t) = 0 \qquad t > T \tag{4.42}$$

where $u_m^{\ out}(t)$ represents the solution of the field mode in the 'out' region.

The solutions in Equation (4.43) and Equation (4.44) can be expressed in the form of simple complex exponential,

$$u_m^{\ in}(t) = C_m^{\ in} \exp\left(-i\omega_m^{\ in} t\right) \tag{4.43}$$

$$u_m^{\ out}(t) = C_m^{\ out} \exp\left(-i\omega_m^{\ out} t\right) \tag{4.44}$$

where $\omega_m^{\ in} = k_m c_0/n_1$ and $\omega_m^{\ out} = k_m c_0/n_2$ are the angular frequency of the field at the remote past and remote future respectively. The constant in front of expression (4.43) and (4.44) is to ensure the normalization condition in Equation (4.40) is satisfied.

During the time interval when the modulating medium is time dependent $-T < t < T$, the refractive index, *n(t)*, is changing and the field mode solution $u_m(t)$ cannot be described in terms of simple complex exponential *exp(iωt)*, but rather it evolves into some complicated form. In Chapter 5, the representation of $u_m(t)$ inside the interval for which *n(t)* is time varying will be discussed in more detail. In the 'out' region, the refractive index remains static at n_2 and $u_m(t)$ can be re-expressed in terms of complex exponential. However the expression of $u_m^{\ out}(t)$ (field mode

solution in the 'out' region) consist of positive and negative frequency components as a consequence of dynamic change in $n(t)$ during the time period $-T < t < T$ [26]. The field in the 'out' region is therefore given by

$$\begin{aligned} u_m(t>T) &= \alpha_m u_m^{out}(t) + \beta_m u^*{}_m^{out}(t) \\ &= C_m^{out}\left[\alpha_m \exp\left(-i\omega_m^{out}t\right) + \beta_m \exp\left(i\omega_m^{out}t\right)\right] \\ &= \left(\frac{\hbar\omega_m^{out}}{2\varepsilon_2 V}\right)^{1/2}\left[\alpha_m \exp\left(-i\omega_m^{out}t\right) + \beta_m \exp\left(i\omega_m^{out}t\right)\right] \end{aligned} \tag{4.45}$$

where α_m and β_m are the time independent Bogoliubov coefficients and $C_m^{out} = (\hbar\omega_m^{out}/2\varepsilon_2 V)^{1/2}$.

By substituting expression (4.45) into (4.36), $\hat{q}_m^{MM}(t)$ in the 'out' region $(t > T)$ can therefore be expressed as

$$\begin{aligned} \hat{q}_m^{MM}(t>T) &= \left(\frac{\hbar\omega_m^{out}}{2\varepsilon_2 V}\right)^{1/2}\left\{\hat{a}_m\left[\alpha_m \exp\left(-i\omega_m^{out}t\right) + \beta_m \exp\left(i\omega_m^{out}t\right)\right] + H.c.\right\} \\ &= \left(\frac{\hbar\omega_m^{out}}{2\varepsilon_2 V}\right)^{1/2}\left[\hat{b}_m \exp\left(-i\omega_m^{out}t\right) + \hat{b}_{-m}^{+} \exp\left(i\omega_m^{out}t\right)\right] \end{aligned} \tag{4.46}$$

where $\hat{b}_m$ and $\hat{b}_{-m}^{+}$ are the annihilation and creation operator in the 'out' region and H.c. is an abbreviation for Hermitian conjugate. Thus, the general expression of the electric flux operator can therefore be expressed as

$$\hat{D}(z,t) = \sum_{m=-\infty}^{\infty}\left(\frac{\hbar\omega_m^{out}\varepsilon_2}{2V}\right)^{1/2}\left[\hat{b}_m \exp\left(ik_m z - i\omega_m^{out}t\right) + H.c.\right] \tag{4.47}$$

The 'out' operators $\hat{b}_m$ are related to the 'in' operators $\hat{a}_m$ through the expressions

$$\hat{b}_m = \alpha_m \hat{a}_m + \beta_m^{*}\hat{a}_{-m}^{+} \tag{4.48}$$

$$\hat{b}_{-m}^{+} = \alpha_m^{*}\hat{a}_{-m}^{+} + \beta_m \hat{a}_m \tag{4.49}$$

Likewise, one can reverse the transformation in expression (4.48) and (4.49) to obtain

$$\hat{a}_m = \alpha_m^{*}\hat{b}_m - \beta_m^{*}\hat{b}_{-m}^{+} \tag{4.50}$$

$$\hat{a}_m^{+} = \alpha_m \hat{b}_m - \beta_m \hat{b}_{-m}^{+} \tag{4.51}$$

Equations (4.48) - (4.51) are known as the **Bogoliubov transform**. Given that the spatial component is represented as plane waves i.e. $exp(ik_m z)$, the Bogoliubov coefficients are both diagonal and isotropic, thus the field modes inside the modulating medium, corresponding to different values of k_m, are independent of one another [26]. By substituting Equation (4.45) into Equation (4.40), it can be verified the Bogoliubov coefficients satisfy the identity

$$|\alpha_m|^2 - |\beta_m|^2 = 1 \tag{4.52}$$

Using the identity in Equation (4.52), the commutation relation of the 'in' operators, $\hat{a}_m$ and $\hat{a}_m^{+}$ in expression (4.34) and (4.35), and the relation in (4.50) and (4.51), we can verified the operators $\hat{b}_m$ and $\hat{b}_m^{+}$ satisfied the commutation relations as $\hat{a}_m$ and $\hat{a}_m^{+}$, where we have

$$[\hat{b}_m, \hat{b}_n] = [\hat{b}_m^{+}, \hat{b}_n^{+}] = 0 \tag{4.53}$$

$$[\hat{b}_m, \hat{b}_n^{+}] = \delta_{m,n} \tag{4.54}$$

In Chapter 3.2, we have shown the Hamiltonian operator $\hat{H}$ for the field in the vacuum is time independent. This implies the 'in' vacuum state vector $|0_{in}\rangle$ is an eigenstate of the 'in' operator $\hat{a}_m$ for all time t (i.e. $\hat{a}_m|0_{in}\rangle = 0$). This condition is satisfied when the Bogoliubov coefficient is given by [40],

$$|\alpha_m| = 1 \qquad |\beta_m| = 0 \tag{4.55}$$

and the field mode $u_m(t)$ can be expressed in terms of simple complex exponentials i.e. $exp(-i\omega t)$, at all time.

However in a modulating medium whose refractive index is time varying, the expression of the Hamiltonian becomes time dependent as shown in Equation (4.29).

An immediate consequence of this is the 'in' vacuum state vector $|0_{in}>$ is not in an eigenstate of the out annihilation operator $\hat{b}_m$ [26, 40]. This can be verified from Equation (4.48), where $\hat{b}_m$ is dependent on $\hat{a}_m^+$ when β_m coefficient is non-zero, and since $|0_{in}>$ is not an eigenstate of $\hat{a}_m^+$, thus $|0_{in}>$ is not an eigenstate of $\hat{b}_m$. Therefore $|0_{in}>$ is not an energy eigenstate for the modulated field and thus this results in the quantum phenomenon of photon creation from modulator as shown in Chapter 6.

4.2.4. Field in Anti-Reflective Coating (ARC)

In Figure 4.1 we have shown ARCs are added at the front and back end of the modulator and the detector to reduce signal losses due to reflection of optical signal being transmitted. This is achieved by varying the dielectric permittivity smoothly in the propagation direction [41]. Therefore the ARC is an inhomogeneous medium, whose dielectric permittivity is spatially dependent. In this Subsection, we shall determine the equation of motion that governs the propagation of the optical field inside the ARC. In order to simplify the problem, we shall assume the optical field strength of the control signal decays rapidly at the boundary of the modulating medium and the ARC so that it does not alter the refractive index of the ARC. As a result, it is appropriate to assume the refractive index and hence the electric permittivity of ARC is time independent. The quantum Maxwell's equations that governs the characteristics of optical field propagating inside the ARC is expressed as

$$\begin{aligned} \nabla X \hat{E} &= -\frac{\partial \hat{B}}{\partial t} \\ \nabla X \hat{B} &= \mu_0 \frac{\partial \left[\varepsilon(z) \hat{E} \right]}{\partial t} \\ \nabla \bullet \left[\varepsilon(z) \hat{E} \right] &= 0 \\ \nabla \bullet \hat{B} &= 0 \end{aligned} \tag{4.56}$$

Since the field propagates in the z direction, therefore by following a similar procedure as in Section 4.2, the Maxwell's equation can be reduced to a wave equation,

$$\frac{\partial^2 \widehat{E}}{\partial z^2} - \left(\frac{n(z)}{c_0}\right)^2 \frac{\partial^2 \widehat{E}}{\partial t^2} = 0 \tag{4.57}$$

where the z dependent dielectric permittivity is related to the refractive index by $n(z)=[\varepsilon(z)/\varepsilon_0]^{1/2}$. The electric field $\widehat{E}(z,t)$ is polarized along the x direction and propagates along the z direction as shown in Figure 4.2.

We assume the general solution of the $\widehat{E}(z,t)$ field can be written as the product of the temporal component and spatial component, where we have

$$\widehat{E}(z,t) = \sum_m \hat{q}_m^{\,ARC}(t) Z_m^{\,ARC}(z) \tag{4.58}$$

$\hat{q}_m^{\,ARC}(t)$ is the temporal component of the $\widehat{E}(z,t)$ field, while $Z_m^{\,ARC}(z)$ is the spatial component of the field inside the ARC, and the subscript m denotes the mode that the field are associated with. Using the method of separation of variables, we obtain the ODE that governs the temporal component of the $\widehat{E}(z,t)$ field

$$\frac{d^2 \hat{q}_m^{\,ARC}}{dt^2} + \omega_m{}^2 \hat{q}_m^{\,ARC}(t) = 0 \tag{4.59}$$

where $\omega_m = k_{0m}c_0$ is the angular frequency of the field. The equation of motion for $\hat{q}_m^{\,ARC}(t)$ in Equation (4.59) is identical to the equation that governs the field propagating in the vacuum presented in Chapter 3, which is expressed in terms of complex exponential, i.e.

$$\hat{q}_m^{\,ARC}(t) = \left(\frac{\hbar\omega_m}{2\varepsilon_0 V}\right)^{1/2} \left[\hat{a}_m \exp(-i\omega_m t) + \hat{a}_{-m}^{\,+} \exp(i\omega_m t)\right] \tag{4.60}$$

Thus, the field representation can be expressed in the general form

$$\hat{E}(z,t)=\sum_{m=0}^{\infty}\left(\frac{\hbar\omega_m}{2\varepsilon_0 V}\right)^{1/2}\left[\hat{a}_m\exp(-i\omega_m t)Z_m{}^{ARC}(z)+\hat{a}_{-m}{}^{+}\exp(i\omega_m t)Z_{-m}{}^{ARC}(z)\right] \quad (4.61)$$

By substituting the first term in Equation (4.61) into the wave equation in Equation (4.57), we obtain the ODE for $Z_m{}^{ARC}(z)$

$$\frac{d^2 Z_m{}^{ARC}(z)}{dz^2}+k_m(z)^2 Z_m{}^{ARC}(z)=0 \quad (4.62)$$

where the z dependent wave-number is define as $k_m(z) = n(z)\omega_m/c_0 = n(z)k_{m0}$. Equation (4.62) agrees with the theory of field propagation inside an inhomogeneous medium presented by [41]. It is sufficient to consider the first term in Equation (4.61) when deriving (4.62) because substituting the second term would yield similar result, but with $Z_m{}^{ARC}(z)$ replaced with $Z_{-m}{}^{ARC}(z)$, and thus the solution of the second term is merely a complex conjugate of the first term. Expression (4.59) and (4.62) are the equation of motions that governs the time evolution and spatial dependence of the optical field as it propagates through the ARC. However, the solution structure of the spatial component $Z_m{}^{ARC}(z)$ governed by Equation (4.62) is more complicated, and will be discussed in detail in Chapter 5.

4.3 Conclusions

A quantum field description of optical field propagating through the modulator has been developed. The AOPM consists of two media, a modulating medium for which refractive index changes when a control optical field is applied, and ARCs at the front and backend of the modulator to minimize reflection losses by having a spatially varying index profile. The equations of motion of the field operator inside these media are derived from the Maxwell's equations.

It is shown that inside the modulating medium, the time evolution of the optical field modes can be describe by an oscillator whose angular frequency $\omega(t)$ is time dependent, while the spatial component can be represented by plane wave $exp(ikz)$. We have derived the Hamiltonian operator inside the modulating medium in order to determine the conditions that the field mode solution must satisfy. From this, we have shown the structure of the annihilation and creation operator represented by $\hat{a}_m$ and $\hat{a}_m^+$ within the 'in' region (before the modulator is turned on) evolves to $\hat{b}_m$ and $\hat{b}_m^+$ in the 'out' region. The 'in' field operator $\hat{a}_m$ and $\hat{a}_m^+$ is related to the 'out' operator $\hat{b}_m$ and $\hat{b}_m^+$ through the Bogoliubov transform.

In the ARC, the temporal component of the optical field is represented by complex exponential $exp(i\omega t)$, while the spatial component is represented in a complicated form. The solution of the spatial component in the ARC will be presented in Chapter 5.

5 Quantum Representation of Phase Modulated Field

5.1 Chapter Objectives

This Chapter presents a detail calculation on the quantum field representation of a phase modulated optical field based on the model specified in Chapter 4. In Chapter 4, we showed the modulator consists of two types of media, a modulating medium whose refractive index is time dependent and anti-reflective coating (ARC) whose refractive index changes with distance.

The rest of this Chapter is organized as follows. In Section 5.2, we derived the field operator that describes the field propagating in the modulating medium. In Section 5.3, we derived the field operator that describes the field propagating in the ARC. In Section 5.4, we remove the simplification of box normalization introduced in Chapter 3, to give a travelling wave representation of an optical field. In Section 5.5, we will use the results in Section 5.2, Section 5.3 and Section 5.4 to derive an expression of a phase modulated optical field. We shall work in Heisenberg picture throughout this Chapter in which the state of phase modulated field remains in a coherent state at all time while the field operator evolves in time.

5.2 Field Mode Solution in Modulating Medium

In this Section, we shall derive the quantum field representation inside the modulating medium whose refractive index changes when a control signal is applied, as discussed in Chapter 4. In Chapter 4, we have shown the electric flux operator propagating in the modulating medium in the z direction, can be represented by plane waves i.e.

$$\hat{D}(z,t) = \sum_{m=-\infty}^{\infty} \hat{q}_m^{\,MM}(t)\exp(ik_m z) \tag{5.1}$$

where the subscript m is the mode index. The time component $\hat{q}_m^{\,MM}(t)$ is governed by the equation of motion,

$$\frac{d^2\hat{q}_m^{\,MM}}{dt^2} + \left[\frac{k_m c_0}{n(t)}\right]^2 \hat{q}_m^{\,MM}(t) = 0 \tag{5.2}$$

Provided the refractive index profile changes dynamically within some time interval with a static 'in' and static 'out' region, as revealed in Figure 5.1 (or Figure 4.3), we have shown in Chapter 4 the expression of $\hat{q}_m^{\,MM}(t)$ can be written in the general form,

$$\hat{q}_m^{\,MM}(t) = \sum_{m=-\infty}^{\infty} \hat{a}_m u_m(t) + \hat{a}_{-m}^{+} u_m^{*}(t) \tag{5.3}$$

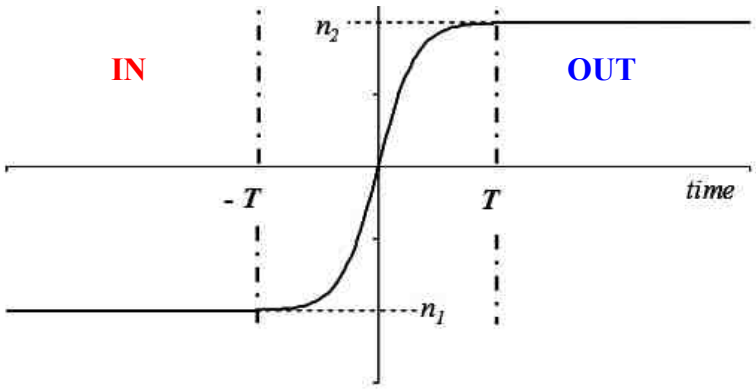

Figure 5.1: Refractive index profile of modulating medium.

In Chapter 4, we have seen the field mode in the 'out' region ($t > T$) is expressed as

$$u_m(t > T) = C_m^{\,out}\left[\alpha_m \exp\left(-i\omega_m^{\,out} t\right) + \beta_m \exp\left(i\omega_m^{\,out} t\right)\right] \tag{5.4}$$

where α_m and β_m are the Bogoliubov coefficients, and $C_m^{\,out} = (\hbar\omega_m^{\,out}/2\varepsilon_2 V)^{1/2}$. Thus in the 'out' region, $\hat{q}_m^{\,MM}(t)$ can be re-expressed as

$$\hat{q}_m^{MM}(t>T)=\sum_{m=-\infty}^{\infty}\left(\frac{\hbar\omega_m^{out}\varepsilon_2}{2V}\right)^{1/2}\left[\hat{b}_m\exp\left(-i\omega_m^{out}t\right)+\hat{b}_{-m}^{+}\exp\left(i\omega_m^{out}t\right)\right] \quad (5.5)$$

The modulated field annihilation and creation operator, $\hat{b}_m$ and $\hat{b}_{-m}^{+}$, is related to the unmodulated field operator, $\hat{a}_m$ and $\hat{a}_m^{+}$, via the Bogoliubov transformation i.e.

$$\hat{b}_m=\alpha_m\hat{a}_m+\beta_m^{*}\hat{a}_{-m}^{+} \quad (5.6)$$

$$\hat{b}_m^{+}=\alpha_m^{*}\hat{a}_m^{+}+\beta_m\hat{a}_{-m} \quad (5.7)$$

By substituting expression (5.3) into the equation of motion in (5.2), we can identify the mode function $u_m(t)$ is governed by the ODE,

$$\frac{d^2u_m}{dt^2}+\left[\frac{k_mc_0}{n(t)}\right]^2u_m(t)=0 \quad (5.8)$$

In this Section, we shall determine the closed form expression of the Bogoliubov coefficients, and hence the representation of the quantum field operator of a phase modulated optical field. In the following subsection, an analogy between the field propagating in the modulating medium and the quantum mechanical scattering will be drawn. The expression of the scattering coefficients will be determined from this analogy, and by relating the scattering coefficients with the Bogoliubov coefficients, the expression of the Bogoliubov coefficients can be determined.

5.2.1 The Quantum Mechanical Scattering Analogy

The equation of motion for $u_m(t)$ in Equation (5.8) can be realized as the same type of equation as the one-dimensional potential Schrödinger equation which takes the form

$$\frac{d^2\xi}{dz^2}+\left(E-V(z)\right)\xi=0 \quad (5.9)$$

where $V(z)$ is the barrier potential in the z direction, E is the energy of the particle and ξ is the probability amplitude of the particle. It can be shown that by replacing the spatial co-ordinate z by time t, and the energy potential function $E - V(z)$ by $\omega^2(t)$, Equation (5.9) coincides with Equation (5.8). The similarities between Equation (5.8) and Equation (5.9) allow us to construct a mathematical analogy between the problems of particle creation due to time dependent refractive index, with the one-dimensional scattering problem through a potential barrier.

In this thesis, we will adopt the quantum scattering method proposed by [39] to identify the relation between the scattering coefficients and the Bogoliubov coefficients so that the field mode solution $u_m(t)$ can be determined.

Similar to the analogy of scattering problem in quantum mechanics, because of the presence of time dependent barrier subjected to the transitions of $n(t)$ during the period $-T < t < T$, we admit two asymptotic solutions to the field mode in Equation (5.8). One solution describes the incident field propagating forward in time which has some probability of scattering backward in time, as shown in Figure 5.2.

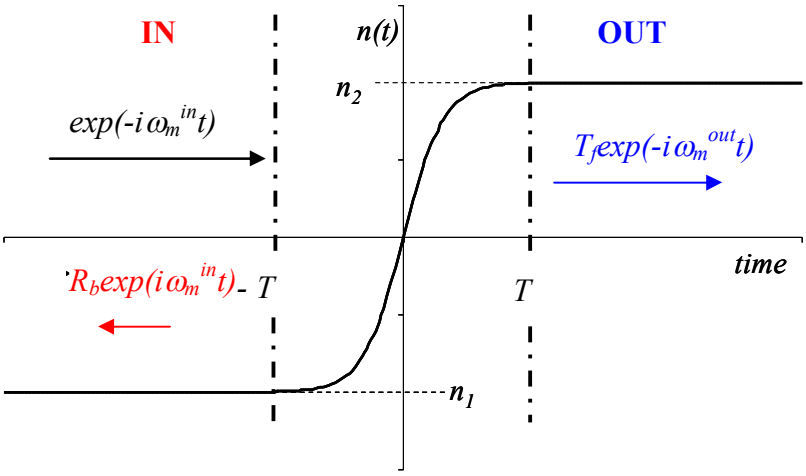

Figure 5.2: Propagation of forward incident field in a time varying $n(t)$ profile.

We can express the forward propagating solution $\varphi_f(t)$ as

$$\begin{aligned}\varphi_f(t) &= C_m^{\,in}\left[\exp\left(-i\omega_m^{\,in}t\right)+R_b\exp\left(i\omega_m^{\,in}t\right)\right] && t<T\\ &= C_m^{\,out}T_f\exp\left(-i\omega_m^{\,out}t-i\Omega_m\right) && t>T\end{aligned} \tag{5.10}$$

where R_b is the scattering coefficient that governs the probability of the incident field reflected backward in time and T_f represents the probability of the field transmitted forward in time. Ω_m is the phase offset due to transition of refractive index from n_1 to n_2. The other solution $\varphi_b(t)$ corresponds to the incident field propagating backward in time with some probability scattered forward in time, as shown in Figure 5.3.

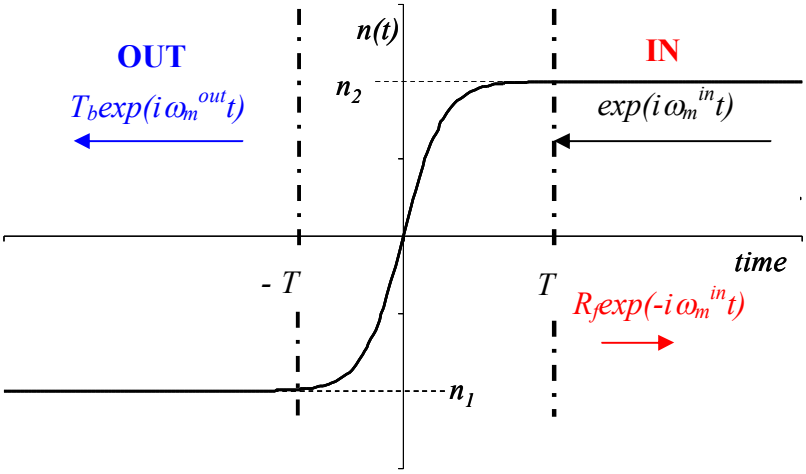

Figure 5.3: Propagation of backward incident field in a time varying *n(t)* profile

The backward propagating solution $\varphi_b(t)$ takes the form

$$\begin{aligned}\varphi_b(t) &= C_m^{\,in}T_b\exp\left(i\omega_m^{\,in}t+i\Omega_m\right) && t<T\\ &= C_m^{\,out}\left[\exp\left(i\omega_m^{\,out}t\right)+R_f\exp\left(-i\omega_m^{\,out}t\right)\right] && t>T\end{aligned} \tag{5.11}$$

where T_b governs the probability of transmitting the incident field backward in time and R_f represents the reflection coefficient that reflects the field forward in time. Similar to the field mode solutions $u_m(t)$, the asymptotic solutions, $\varphi_f(t)$ and $\varphi_b(t)$ satisfy the time dependent ODE in Equation (5.8). In the remote past and remote future, $\varphi_f(t)$ and $\varphi_b(t)$ in Equation (5.10) and Equation (5.11), is expressed as

simple complex exponential *exp(iωt)*, because in these regions the refractive index is time invariant. When the refractive index is changing from n_1 to n_2 during the period $-T < t < T$, $\varphi_f(t)$ and $\varphi_b(t)$ cannot be described as simple complex exponential.

The four complex scattering coefficients in Equation (5.10) and Equation (5.11) can be used to construct a scattering matrix which is defined as

$$S = \begin{pmatrix} R_b & T_f \\ T_b & R_f \end{pmatrix} \tag{5.12}$$

Various relations between the scattering coefficients can be obtained by entering a pair of asymptotic solutions into the Wronskian operator. The Wronskian operator is defined as [42]

$$W\left[\gamma_1, \gamma_2\right] = \gamma_1 \frac{d\gamma_2}{dt} - \frac{d\gamma_1}{dt}\gamma_2 = constant \tag{5.13}$$

By computing the following Wronskians at $t = -T$ and $t = T$, and equating these results [39] leads to the following relations

$$W\left[\varphi_f^*, \varphi_f\right]: \quad \left|T_f\right|^2 + \left|R_b\right|^2 = 1 \tag{5.14}$$

$$W\left[\varphi_b^*, \varphi_b\right]: \quad \left|T_b\right|^2 + \left|R_f\right|^2 = 1 \tag{5.15}$$

$$W\left[\varphi_f^*, \varphi_b\right]: \quad R_b^* T_b = -T_f^* R_f \tag{5.16}$$

$$W\left[\varphi_f^*, \varphi_b\right]: \quad R_b T_b^* = -T_f R_f^* \tag{5.17}$$

$$W\left[\varphi_f, \varphi_b\right]: \quad T_b = T_f \tag{5.18}$$

Equations (5.14) - (5.18) shows that the *S* matrix is a symmetrical and unitary matrix i.e.

$$S^+ S = 1 \tag{5.19}$$

Although the asymptotic solutions, $\varphi_f(t)$ and $\varphi_b(t)$, as well as the field mode representation, $u_m(t)$ is governed by the ODE in Equation (5.8), there is a

subtle difference between them. Initial condition that governs the behavior of the field mode solution at certain point in time is not specified in the asymptotic solutions in Equation (5.10) and Equation (5.11). In contrast to the asymptotic solutions, the field mode solution $u_m(t)$ requires initial condition to determine its expression. Therefore, the field mode representation can be derived from the asymptotic solution once the initial condition is specified [39].

In the 'IN' region in Figure 5.2, the field has not experience changes in refractive index, thus it is appropriate to consider the field mode obeys the initial condition

$$u_m^{\ *}(t) = C_m^{\ in} \exp\left(i\omega_m^{\ in} t\right) = \frac{\varphi_b(t)}{T_b} \qquad t < T \tag{5.20}$$

Hence in the 'out' region, $t > T$, where changes of refractive index has taken place, we can use the relation in Equation (5.11) to deduce the expression of the field mode, where we have

$$u_m^{\ *}(t) = C_m^{\ out}\left[\frac{1}{T_b}\exp\left(i\omega_m^{\ out} t\right) + \frac{R_f}{T_b}\exp\left(-i\omega_m^{\ out} t\right)\right] \qquad t > T \tag{5.21}$$

By comparing Equation (5.21) with the Bogoliubov transform in expression (5.4), we have finally established the relation between the scattering coefficients and the Bogoliubov coefficients, where we have

$$\alpha_m = \frac{1}{T_b^{\ *}} \tag{5.22}$$

$$\beta_m = \frac{R_f^{\ *}}{T_b^{\ *}} \tag{5.23}$$

Expression (5.23) shows the β_m coefficient is non-zero because the transition in refractive index effectively acts as a potential barrier that reflects a portion of the field backward in time, thus gives rise to a non-zero R_f. As we shall see in Chapter 6, a non-zero β_m represents the quantum phenomenon of photon creation from modulator.

5.2.2 Field Operator Representation

In this Subsection, the expression of the scattering coefficients, R_f and T_b, will be derived. Using the relation between the scattering coefficients and the Bogoliubov coefficients in Equation (5.22) and Equation (5.23), the field operator representation in the modulating medium can be determined. By using the initial condition in Equation (5.20), the expression of the field mode $u_m(t)$ for general time can be found by solving the ODE in Equation (5.8), where we shall reproduce this for convenience

$$\frac{d^2u_m}{dt^2}+\left(\frac{k_m c_0}{n(t)}\right)^2 u_m(t)=0 \tag{5.24}$$

All the parameters in expression (5.24) take its usual meaning defined earlier. This equation has been studied extensively in quantum field theory (QFT), where if $\omega_m(t)=k_m c_0/n(t)$ exhibits a linear profile i.e. $\omega_m(t) = A + Bt$, the field solution can be expressed in terms of Bessel function [41], while if $\omega_m(t)$ has the form of monotonically increasing step function $\omega_m(t) = A + B\tanh(pt)$, the field solution is represented by hypergeometric series [43, 44]. Despite of the extensive investigations of Equation (5.24), it cannot be exactly solved for all arbitrary expressions of $\omega_m(t)$ [41].

In quantum mechanics, Wentzel-Kramers-Briullouin (WKB) approximation method is a commonly used technique to give an approximate closed form solution for the equation of motion in (5.24), such that an approximate representation of the field can be determined from some arbitrary function of $\omega_m(t)$ for whom the exact solution might be unknown. Similar to the approach used in [41], but with the spatial co-ordinate z replace with time t, the equation of motion in (5.24) will be solved by representing the exact solution as an infinite power series expansion of WKB approximation solution i.e.

$$u_m(t) = \sum_{j=0}^{\infty} \left(\frac{1}{k_m c_0} \right)^j b_{m,j}(t) \exp\left(-ik_m c_0 \psi(t)\right) \tag{5.25}$$

where $b_{m,j}(t)$ is the j^{th} order time dependent coefficients, $\psi(t)$ is a time dependent function that appears at the phase component of the field. We shall now omit the mode index m in Equation (5.25) temporarily for clarity. The time dependent parameters $b_j(t)$ and $\psi(t)$ can be solved by substituting expression (5.25) into Equation (5.24), where we will obtain an equation of the type

$$\left(1/kc_0 \right)^2 A(t) + \left(1/kc_0 \right) B(t) + C(t) + \left(kc_0\right) D(t) + \left(kc_0\right)^2 E(t) + \ldots = 0 \tag{5.26}$$

where the time dependent coefficients i.e. $A(t)$, $B(t)$, $C(t)$..., are expressions that involves time dependent function $b_j(t)$ and $\psi(t)$. To equate the LHS to RHS we require $A(t) = B(t) = C(t) \ldots = 0$. This equating process gives rise to a series of 1st order differential equations where we have

$$\frac{1}{n^2(t)} - \left[\psi'(t)\right]^2 = 0 \tag{5.27}$$

$$\frac{db_0}{dt} + \frac{b_0(t)}{2} \frac{\psi''(t)}{\psi'(t)} = 0 \tag{5.28}$$

$$\frac{db_1}{dt} + \frac{b_1(t)}{2} \frac{\psi''(t)}{\psi'(t)} = \frac{1}{2i} \frac{d^2 b_0}{dt^2} \frac{1}{\psi'(t)} \tag{5.29}$$

and more… for higher order jth term

where $\psi'(t)$ and $\psi''(t)$ denotes the first and second order time derivatives of $\psi(t)$ respectively. The differential equations in (5.27), (5.28) and (5.29) can be derived from the condition by equating $A(t) = 0$, $B(t) = 0$, and $C(t) = 0$, respectively. These differential equations allow the unknown parameter $b_j(t)$ and $\psi(t)$ to be solved recursively. Solving Equation (5.27) determines the expression of $\psi(t)$ in terms of $\omega(t)$, then use this to solve for $b_0(t)$ from Equation (5.28). After that, these

expressions are used in Equation (5.29) to determine $b_1(t)$, and similarly, the higher order $b_j(t)$ term (i.e. for $j > 1$) can be determined from the recursive relation

$$\frac{db_j}{dt} + \frac{b_j(t)}{2}\frac{\psi''(t)}{\psi'(t)} = \frac{1}{2i}\frac{d^2 b_{j-1}}{dt^2}\frac{1}{\psi'(t)} \tag{5.30}$$

By solving the differential equations in (5.27), (5.28) and (5.29) recursively, we get

$$\psi(t) = \pm\int_{-\infty}^{t} \frac{1}{n(\tau)} d\tau \tag{5.31}$$

$$b_0(t) = C\sqrt{n(t)} \tag{5.32}$$

$$b_1(t) = -iC\sqrt{n(t)}\int_{-\infty}^{t} \sqrt{n(\tau)}\frac{d}{d\tau}\left(\frac{dn/d\tau}{4n^{1/2}(\tau)}\right)d\tau \tag{5.33}$$

where C is a constant parameter. Note that C is dependent on the mode index m as shown later in this Section. Furthermore, the time integral in expression (5.31) and (5.33) range from -∞ to time t, implies the field is confined inside the modulating medium $n(t)$. Analysis of field propagation through a finite size modulating medium will be presented later in Chapter 5.5.

From now on, we shall invoke the mode index subscript m once again. By substituting the expressions (5.31), (5.32) and (5.33) into Equation (5.25), a 1st order approximate expression of the field mode that propagates forward in time, as denoted by the + subscript $u_{m+}(t)$, can be determined for some arbitrary form of $\omega_m(t)$ where we have

$$u_{m+}(t) \approx \left(\frac{\hbar\omega_m(t)\varepsilon(t)}{2V}\right)^{1/2}\left[1 + i\int_{-\infty}^{t}\left(\frac{1}{\omega_m(\tau)}\right)^{1/2}\frac{d}{d\tau}\left(\frac{d\omega_m/d\tau}{4\omega_m^{3/2}(\tau)}\right)d\tau\right]\exp\left(-i\int_{-\infty}^{t}\omega_m(\tau)d\tau\right) \tag{5.34}$$

where the relation $\omega_m(t)=k_m c_0/n(t)$ has been used to replace all $n(t)$ terms with $\omega_m(t)$. In order to reproduce the time dependent factor $(\hbar\omega_m(t)\varepsilon(t)/2V)^{1/2}$ in Equation (5.34), the constant parameter C_m is given by $C_m=(\hbar k_m c_0\varepsilon_0/2V)1/2$. The approximation is

only valid provided the higher order terms in expression (5.25) and (5.26) are negligible. The necessary condition which governs the validity of the approximate solution for all time t in Equation (5.26) is given by [41]

$$\left(\frac{d\omega/dt}{\omega^2(t)}\right)_{\max} << 1 \tag{5.35}$$

Equation (5.35) is known as the adiabatic condition, which states under the condition when the ratio of the maximum rate of change of angular frequency $d\omega/dt$ is much smaller than the square of the optical field frequency $\omega^2(t)$, it is appropriate to approximate the exact solution as WKB power series expansion in expression (5.26). In standard optical communication system, the maximum modulation rate is much smaller than its carrier frequency, and hence $d\omega/dt << \omega^2(t)$ [22 - 24]. Therefore, we can conclude the approximate expression in (5.34) is sufficient to represent the optical field mode in the context of optical communication system.

By considering the refractive index profile in Figure 5.1, the refractive index remains constant at n_2 in the 'out' region ($t > T$). Therefore for $t > T$, the time dependent factor $(\hbar\omega_m(t)\varepsilon(t)/2V)^{1/2}$ in (5.34) is constant. Consequentially in the 'out' region ($t > T$), expression (5.34) becomes

$$u_{m+}(t>T)=\left(\frac{\hbar\omega_m^{out}\varepsilon_2}{2V}\right)^{1/2}\left[1+i\int_{-T}^{T}\left(\frac{1}{\omega_m(\tau)}\right)^{1/2}\frac{d}{d\tau}\left(\frac{d\omega_m/d\tau}{4\omega_m^{3/2}(\tau)}\right)d\tau\right]\exp\left(-i\omega_m^{out}(t-2T)-i\int_{-T}^{T}\omega_m(\tau)d\tau\right) \tag{5.36}$$

The time integral in (5.36) now spans from $-T$ *to* T, the refractive index is constant in the 'in' and 'out', thus the integral vanishes in those two regions. By comparing the conjugate of Equation (5.36) with the forward time propagating component i.e 1st term in Equation (5.21), and using the relation in (5.22), we have obtained the expression of the Bogoliubov coefficient α_m

$$\alpha_m=\frac{1}{T_b^*}=1+i\int_{-T}^{T}\left(\frac{1}{\omega_m(\tau)}\right)^{1/2}\frac{d}{d\tau}\left(\frac{d\omega_m/d\tau}{4\omega_m^{3/2}(\tau)}\right)d\tau \tag{5.37}$$

By comparing the expression in (5.36) with (5.21), the value of the constant C_m^{out} in (5.21) is found to be $C_m^{out} = \left(\hbar\omega_m^{out} \varepsilon_2 \big/ 2V \right)^{1/2} \exp\left(-i \int_{-T}^{T} \omega(\tau) d\tau \right)$.

Equation (5.23) show the expression of Bogoliubov coefficient β_m, is derived from the reflection coefficient R_f. Consider the conjugate field mode solution represented by the zeroth order WKB (i.e. b_0 is the only term considered in (5.25)), we have

$$u_{m,0}^{*}(t) = \left(\frac{\hbar\omega_m(t)\varepsilon(t)}{2V} \right)^{1/2} \exp\left(i \int_{-\infty}^{t} \omega_m(\tau) d\tau \right) \tag{5.38}$$

The second subscript *'0'* in Equation (5.38) denotes the field mode is approximated to zeroth order. The zeroth order WKB solution is known as a reflectionless solution for which the reflection of field mode inside an inhomogenous medium is neglected [45]. The 1st order approximate expression for R_f is determined by introducing a reflection term in Equation (5.38) i.e.,

$$u_m^{*}(t) = \left(\frac{\hbar\omega_m(t)\varepsilon(t)}{2V} \right)^{1/2} \left[\exp\left(i \int_{-\infty}^{t} \omega_m(\tau) d\tau \right) + R_f(t) \exp\left(-i \int_{-\infty}^{t} \omega_m(\tau) d\tau \right) \right] \tag{5.39}$$

By substituting Equation (5.39) into the ODE in Equation (5.24), we arrived at the differential equation

$$\frac{dR_f}{dt} = i \frac{1}{\omega^{1/2}(t)} \frac{d}{dt} \left(\frac{d\omega/dt}{4\omega^{3/2}(t)} \right) \exp\left(2i \int_{-\infty}^{t} \omega_m(\tau) d\tau \right) \tag{5.40}$$

The second order derivative term d^2R_f/dt^2 has been neglected in Equation (5.40), which is appropriate provided the adiabatic condition in Equation (5.35) is satisfied for all time. By solving the ODE in Equation (5.40), the representation of the 1st order approximation of R_f is

$$R_f(t) = i\int_{-\infty}^{t}\left(\frac{1}{\omega_m(\tau)}\right)^{1/2}\frac{d}{d\tau}\left(\frac{d\omega_m/d\tau}{4\omega_m^{3/2}(\tau)}\right)\exp\left(2i\int_{-\infty}^{\tau}\omega_m(\tau)d\tau\right)d\tau \qquad (5.41)$$

In the 'in' and 'out' region, R_f in Equation (5.41) reduces to a constant because the refractive index does not vary in time, and hence the integral vanishes for $t < 0$ and $t > T$. Since the adiabatic condition in Equation (5.35) is satisfied, therefore $1/T_b \sim 1$, and thus we have the expression of β_m from Equation (5.23),

$$\begin{aligned}\beta_m &\approx R_f^{*}(t>T)\\ &= -i\int_{-T}^{T}\left(\frac{1}{\omega_m(\tau)}\right)^{1/2}\frac{d}{d\tau}\left(\frac{d\omega_m/d\tau}{4\omega_m^{3/2}(\tau)}\right)\exp\left(-2i\int_{-\infty}^{\tau}\omega_m(t')dt'\right)d\tau\end{aligned} \qquad (5.42)$$

From the expression of Bogoliubov coefficients in (5.37) and (5.42), one can verify they approximately satisfy the Bogoliubov identity introduced in Chapter 4,

$$|\alpha_m|^2 - |\beta_m|^2 = 1 \qquad (5.43)$$

The identity in Equation (5.43) is exactly satisfied if the solution is approximated to an infinite order [26], and provided the adiabatic condition in Equation (5.35) holds, the differences between the 1st order approximation and the exact solution of the Bogoliubov coefficients becomes negligible.

However, if the refractive index of the modulating medium changes abruptly where $d\omega/dt >> \omega^2(t)$ (i.e. condition (5.35) is not satisfied), the Bogoliubov coefficients, α_m and β_m, cannot be expressed in terms of Equation (5.37) and (5.42), respectively. In fact, if the refractive index of the modulating medium changes instantaneously from n_1 to n_2, the magnitude of the scattering coefficients, R_f and T_b, is represented by the Fresnels equation,

$$|R_f| = \frac{n_1 - n_2}{n_1 + n_2} \qquad (5.44)$$

$$|T_b| = \frac{2\sqrt{n_1 n_2}}{n_1 + n_2} \qquad (5.45)$$

Using the relation in (5.22) and (5.23), the corresponding magnitude of the Bogoliubov coefficients for an **instantaneous change in refractive index** is

$$\alpha_m = \frac{n_1 + n_2}{2\sqrt{n_1 n_2}} \tag{5.46}$$

$$\beta_m = \frac{n_1 - n_2}{2\sqrt{n_1 n_2}} \tag{5.47}$$

In Chapter 6, we show that the photon creation is governed by β_m, thus Equation (5.47) gives the upper bound for photon creation when the adiabatic condition in Equation (5.35) is not satisfied, i.e. $d\omega/dt >> \omega^2(t)$.

After the expression of α_m and β_m Bogoliubov coefficients is determined in (5.37) and (5.42), the electric flux density operator $\widehat{D}(z,t)$ can be determined using expression (5.1), (5.3) and (5.4), where we have

$$\begin{aligned}\widehat{D}(z,t) = \sum_m \left(\frac{\hbar\omega_m^{\ out}\varepsilon_2}{2V}\right)^{1/2} \hat{a}_m \Bigg(\alpha_m \exp\left[ik_m z - \left(i\omega_m(t-2T) + i\int_{-T}^{T}\omega_m(\tau)\,d\tau\right)\right] \\ + \beta_m \exp\left[ik_m z + \left(i\omega_m(t-2T) + i\int_{-T}^{T}\omega_m(\tau)\,d\tau\right)\right]\Bigg) + H.c.\end{aligned} \tag{5.48}$$

The expression of modulated field annihilation and creation operator, $\hat{b}_m$ and $\hat{b}_m^{\ +}$ in Equation (5.48) is defined in expression (5.6) and (5.7) respectively, while *H.c.* is an abbreviation for Hermitian conjugate. Thus, the electric field operator $\widehat{E}(z,t)$ in the modulating medium can be derived from $\widehat{D}(z,t)$ using the relation

$$\begin{aligned}\widehat{E}(z,t) &= \frac{\widehat{D}(z,t)}{\varepsilon(t)} \\ &= \sum_m \left(\frac{\hbar\omega_m^{\ out}}{2\varepsilon_2 V}\right)^{1/2} \hat{a}_m \Bigg(\alpha_m \exp\left[ik_m z - \left(i\omega_m(t-2T) + i\int_{-T}^{T}\omega_m(\tau)\,d\tau\right)\right] \\ &\quad + \beta_m \exp\left[ik_m z + \left(i\omega_m(t-2T) + i\int_{-T}^{T}\omega_m(\tau)\,d\tau\right)\right]\Bigg) + H.c.\end{aligned} \tag{5.49}$$

The field operator $\hat{E}(z,t)$ in Equation (5.49) will be used to derive the phase modulated field operator in Section 5.5.

5.3 Field Mode Solution in ARC

In this Section, we shall derive the quantum field representation inside an ARC whose refractive index gradually varies with position in order to reduce the reflection loss from the modulator. Figure 5.4 shows an ARC with a refractive index profile that monotonically increases from n_1 and n_2.

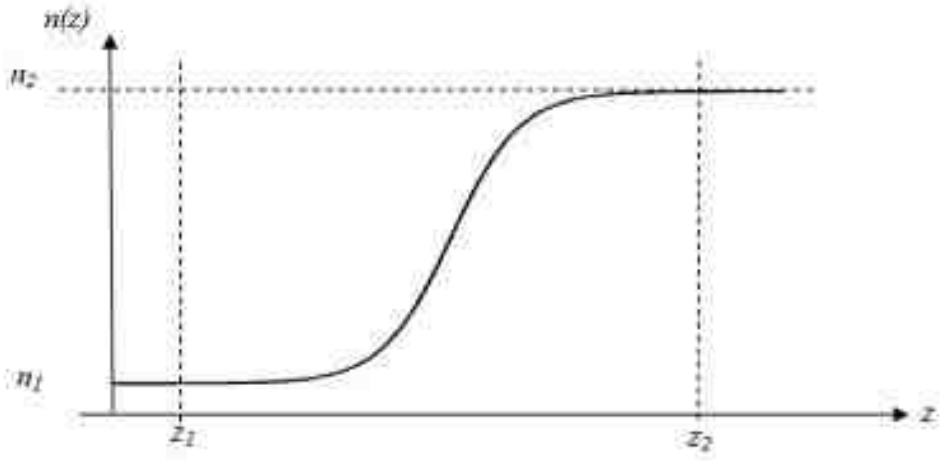

Figure 5.4: Refractive index profile of ARC.

In Chapter 4, we have shown the general solution of the electric field operator $\hat{E}(z,t)$ is represented by

$$\hat{E}(z,t)=\sum_{m=0}^{\infty}\left(\frac{\hbar\omega_m}{2\varepsilon_0 V}\right)^{1/2}\left[\hat{a}_m\exp(-i\omega_m t)Z_m{}^{ARC}(z)+\hat{a}_{-m}{}^{+}\exp(i\omega_m t)Z_{-m}{}^{ARC}(z)\right] \qquad (5.50)$$

The spatial component of the electric field operator $Z_m{}^{ARC}(z)$, is governed by the ODE,

$$\frac{d^2 Z_m^{ARC}}{dz^2} + k_m(z) Z_m^{ARC}(z) = 0 \tag{5.51}$$

where $k_m(z)$ is the spatially varying propagation constant that is related to the refractive index $n(z)$ by $k_m(z) = n(z)\omega_m/c_0$. By comparing expression (5.51) with Equation (5.24), we can identify these ODEs are of the same type where the former is dependent on z while the latter is dependent on t. Therefore, the spatial component can be approximated by WKB approximation given that the refractive index is varying slowly with respect to the optical wavelength. Expressing this in mathematical form we have [41]

$$\left|\frac{dn}{dz}\right|_{\max} = \frac{2\pi n^2}{\lambda_0} \tag{5.52}$$

where λ_0 is the optical wavelength in free space. By following a similar procedure in Subsection 5.2.2, the zeroth order WKB solution of $Z_m^{ARC}(z)$ is,

$$Z_{m,0}^{ARC}(z) = \frac{K_m}{\sqrt{k_m(z)}}\left[T_f(z)\exp\left(i\int_{-\infty}^{z} k_m(\xi)\,d\xi\right) + R_b(z)\exp\left(-i\int_{-\infty}^{z} k_m(\xi)\,d\xi\right)\right] \tag{5.53}$$

where $T_f(z)$ represents the amplitude transmission coefficient that determines the portion of the incoming signal being transmitted, and $R_b(z)$ determines the reflection losses of the incoming signal. The second subscript *'0'* in Equation (5.53) denotes the spatial dependence of the optical field is approximated by the zeroth order WKB solution. In an optical communication system, the ARC is designed to ensure the condition in Equation (5.52) is satisfied, so that a reflection loss is minimized. As a result, we assume $T_f(z) \approx 1$ and $R_b(z) \approx 0$, where there is effectively no reflection loss in the optical system. By substituting Equation (5.53) into Equation (5.50), the approximate solution of the electric field operator $\widehat{E}(z,t)$ is given by

$$\begin{aligned}\hat{E}(z,t) &= \sum_m \hat{q}_m^{\,ARC}(t) Z_m^{\,ARC}(z) \\ &= \sum_m \hat{e}_m^{\,+}(z,t) + \hat{e}_m^{\,-}(z,t) \\ &= \sum_m \frac{1}{\sqrt{n(z)}} \left(\frac{\hbar\omega_m}{2\varepsilon_0 V}\right)^{1/2} \hat{a}_m \exp\left(i\int_{-\infty}^{z} k_m(\xi)\,d\xi - i\omega_m t\right) + H.c.\end{aligned} \tag{5.54}$$

where the constant K_m in Equation (5.53) is chosen to be $K_m = (\omega_m/c_0)^{1/2}$, so that $K_m/\sqrt{k_m(z)} = 1/\sqrt{n(z)}$, and *H.c.* is the Hermitian conjugate. By comparing the expression of $\hat{E}(z,t)$ in Equation (5.54) at $z > z_2$ (refractive index is static at n_2), with the field propagating in free space where $n(z) = 1$, we can identify the electric field operator has been **reduced** by a factor of $\sqrt{n_2}$ for field propagating in the ARC. However by using Faraday's law $\nabla X \hat{E} = -\dfrac{\partial \hat{B}}{\partial t}$, it can be verified that the magnetic flux density operator $\hat{B}(z,t)$ of the field propagating in ARC, has been **increased** by a factor of $\sqrt{n_2}$ at $z > z_2$ as compared with the field propagating in free space.

We shall determine the power flow of an optical field in an ARC at $z > z_2$, and compare this with the field propagating in free space. For simplicity, we assumed the field propagates in the vacuum for $z < z_1$ i.e. $n_1 = 1$. The power flow of the field is characterized by the Poynting vector operator $\hat{S}(z,t)$, which is defined as [33]

$$\hat{S}(z,t) = \varepsilon_0 c_0^{\,2} A\left[\hat{E}^{-}(z,t) X \hat{B}^{+}(z,t) - \hat{B}^{-}(z,t) X \hat{E}^{+}(z,t)\right] \tag{5.55}$$

The minus superscript in Equation (5.55) denotes the field components are associated with $\hat{a}_m$, while the positive superscript denotes the field components are associated with $\hat{a}_m^{+}$. By setting $n(z) = 1$ of field operator $\hat{E}(z,t)$ in expression (5.54), using the Faraday's law to determine $\hat{B}(z,t)$ from $\hat{E}(z,t)$, and substituting the results into Equation (5.55), the Poynting vector in free space (i.e. at $z = z_1$) is [33]

$$\hat{S}(z_1,t) = 2\varepsilon_0 c_0 A \hat{E}^{-}(z_1,t)\hat{E}^{+}(z_1,t) \tag{5.56}$$

Using the result in Equation (5.54), it is evident that $\widehat{E}(z_2,t)=\frac{1}{\sqrt{n_2}}\widehat{E}(z_1,t)$ and $\widehat{B}(z_2,t)=\sqrt{n_2}\,\widehat{B}(z_1,t)$. Using Equation (5.55), the Poynting vector at $z = z_2$ is expressed as,

$$\begin{aligned}\hat{S}(z_2,t) &= \varepsilon_0 c_0{}^2 A\left[\widehat{E}^{-}(z_2,t)X\widehat{B}^{+}(z_2,t)-\widehat{B}^{-}(z_2,t)X\widehat{E}^{+}(z_2,t)\right]\\ &= \varepsilon_0 c_0{}^2 A\left[\frac{1}{\sqrt{n_2}}\widehat{E}^{-}(z_1,t)X\sqrt{n_2}\widehat{B}^{+}(z_1,t)-\sqrt{n_2}\widehat{B}^{-}(z_1,t)X\frac{1}{\sqrt{n_2}}\widehat{E}^{+}(z_1,t)\right]\\ &= 2\varepsilon_0 c_0 A\widehat{E}^{-}(z_1,t)\widehat{E}^{+}(z_1,t)\\ &= \hat{S}(z_1,t)\end{aligned} \quad (5.57)$$

The result in Equation (5.57) shows the Poynting vector, and hence the power flow of the optical field is the same regardless of the refractive index of the material. Therefore we can conclude although the electric field amplitude $\widehat{E}(z,t)$ and magnetic flux density $\widehat{B}(z,t)$ are different for media with different refractive index, the power flow of the field are the same i.e. independent of the refractive index of the material.

5.4 Continuum Operators and States

The optical field expression developed so far uses "box normalization", for which the field is assumed to be confined inside a cavity enclosing by a volume V in order to simplify the results. The existence of the cavity gives rise to a sum of discrete set of modes, and this is known as the standing wave representation [35]. However in an optical communication system, no identifiable cavity is present (see Figure 4.1). In this section, we shall remove the unphysical limitation of optical field confined inside cavity, and follow the approach in [46] in developing a field operator that gives a travelling wave representation for field propagating in free space.

Using the definition of the propagation constant $k_m = 2\pi m/L$, the mode spacing Δk can be expressed as

$$\Delta k = k_m - k_{m-1} = \frac{2\pi}{L} \tag{5.58}$$

It is often more convenient to describe the field in terms of frequency. Therefore translating the mode spacing in terms of angular frequency we have

$$\Delta\omega = \frac{2\pi c_0}{L} \tag{5.59}$$

The mode becomes continuous in the limit of $L \to \infty$ and hence $\Delta\omega \to 0$. The conversion from sum to integral in the field expression (i.e. Equation (5.1)) is

$$\sum_m \to \int_0^\infty \frac{L}{2\pi} dk \to \frac{1}{\Delta\omega} \int_0^\infty d\omega \tag{5.60}$$

The continuous mode annihilation operators, designated as $\hat{a}(\omega)$ is related to its discrete counterpart $\hat{a}_m$ by

$$\hat{a}_m \to (\Delta\omega)^{1/2} \hat{a}(\omega) \tag{5.61}$$

The discrete Kronecker delta is related to the continuous Dirac delta function by

$$\delta_{mn} = \Delta\omega\delta(\omega - \omega') \tag{5.62}$$

Using expression (5.61) and (5.62), the continuous annihilation and creation operator satisfy the commutation relation

$$\left[\hat{a}(\omega), \hat{a}^+(\omega')\right] = \delta(\omega - \omega') \tag{5.63}$$

In Chapter 3, we have shown by using the electric field operator that characterizes field propagation in free space with the use of 'box normalization' employed, is expressed as

$$\hat{E}(z,t) = \left(\frac{\hbar\omega_m}{2\varepsilon_0 V}\right)^{1/2} \sum_{m=0}^{\infty} \hat{a}_m \exp(ik_m z - i\omega_m t) + \hat{a}_m^{+} \exp(-ik_m z + i\omega_m t) \tag{5.64}$$

By applying the expression in (5.60), (5.61) and (5.62) into Equation (5.64), the discrete electric field mode operator can be converted into the continuous mode electric field operator, where we have

$$\begin{aligned}\hat{E}(z,t) &= \hat{E}^{-}(z,t) + \hat{E}^{+}(z,t) \\ &= \frac{1}{(\Delta\omega)^{1/2}} \int_0^{\infty} d\omega \left(\frac{\hbar\omega}{2\varepsilon_0 V}\right)^{1/2} \hat{a}(\omega) \exp(ik_0 z - i\omega t) + H.c. \\ &= \int_0^{\infty} d\omega \left(\frac{\hbar\omega}{4\pi\varepsilon_0 c_0 A}\right)^{1/2} \hat{a}(\omega) \exp(ik_0 z - i\omega t) + H.c.\end{aligned} \tag{5.65}$$

Similarly by using expressions (5.60), (5.61) and (5.62) as well as the result in Equation (5.49), the continuous mode electric field operator in the modulating medium is expressed as

$$\begin{aligned}\hat{E}^{MM}(z,t) &= \hat{E}^{MM-}(z,t) + \hat{E}^{MM+}(z,t) \\ &= \int_0^{\infty} d\omega \left(\frac{\hbar\omega_m^{\ out}}{4\pi\varepsilon_2 c_0 A}\right)^{1/2} \hat{a}(\omega) \left(\alpha(\omega) \exp\left[ikz - \left(i\omega(t-2T) + i\int_{-T}^{T} \omega(\tau)\, d\tau\right)\right]\right. \\ &\quad \left. + \beta(\omega) \exp\left[ikz + \left(i\omega(t-2T) + i\int_{-T}^{T} \omega(\tau)\, d\tau\right)\right]\right) + H.c.\end{aligned} \tag{5.66}$$

where the Bogoliubov coefficients in continuous mode form, $\alpha(\omega)$ and $\beta(\omega)$, can be expressed as

$$\alpha(\omega) = 1 + i\int_{-T}^{T} \left(\frac{1}{\omega(\tau)}\right)^{1/2} \frac{d}{d\tau}\left(\frac{d\omega/d\tau}{4\omega^{3/2}(\tau)}\right) d\tau \tag{5.67}$$

$$\beta(\omega) = -i\int_{-T}^{T} \left(\frac{1}{\omega(\tau)}\right)^{1/2} \frac{d}{d\tau}\left(\frac{d\omega/d\tau}{4\omega^{3/2}(\tau)}\right) \exp\left(-2i\int_{-\infty}^{\tau} \omega(t')\, dt'\right) d\tau \tag{5.68}$$

While if we apply the above procedure to the ARC field expression in Equation (5.54), we obtain the continuous mode electric field operator of the form

$$\hat{E}^{ARC}(z,t) = \frac{1}{\sqrt{n(z)}} \left(\frac{\hbar\omega}{4\pi\varepsilon_0 c_0 A}\right)^{1/2} \hat{a}(\omega) \exp\left(i\int_{-\infty}^{z} k(\xi)\, d\xi - i\omega t\right) + H.c. \tag{5.69}$$

Similar to its discrete counterpart, the continuum coherent state is expressed as [46]

$$\left|\{\rho(\omega)\}\right\rangle = \exp\left(\int_0^\infty -\frac{1}{2}\left|\rho(\omega)\right|^2 + \rho(\omega)\hat{a}^+(\omega)d\omega\right)\left|0\right\rangle \tag{5.70}$$

where the vacuum state has the usual property

$$\hat{a}(\omega)\left|0\right\rangle = 0 \tag{5.71}$$

Using the identity in Equation (5.71) and the definition of $\left|\{\rho(\omega)\}\right\rangle$ in Equation (5.70), it can be verified the continuum coherent state is an eigenstate of the annihilation operator,

$$\hat{a}(\omega)\left|\{\rho(\omega)\}\right\rangle = \rho(\omega)\left|\{\rho(\omega)\}\right\rangle \tag{5.72}$$

Therefore, the mean total number of photon flux associated with the continuum coherent state is

$$\left\langle \hat{N} \right\rangle = \left\langle \{\rho(\omega)\}\right|\int_0^\infty \hat{a}^+(\omega)\hat{a}(\omega)d\omega\left|\{\rho(\omega)\}\right\rangle = \int_0^\infty \left|\rho(\omega)\right|^2 d\omega \tag{5.73}$$

In this Section, we have shown the presence of the cavity can be effectively removed by introducing an artificial cavity with an infinite length in the *z* direction. The mode spacing Δk therefore becomes infinitely small, and hence gives rise to a continuous representation of the mode in the *z* direction. As a result, continuous field mode operator and continuum state are employed to give a travelling wave representation of an optical field.

5.5 Phase Modulated Field Operator

As we have previously mentioned, the modulator consist of two types of media, the ARC and a modulating medium. In Section 5.2, we have derived the field operator that characterizes an optical field propagating in the modulating medium, while in Section 5.3, the field operator that describes field propagation in ARC has been

derived. In this Section, we shall use these results together with the theory of continuum mode analysis in Section 5.4 to give a travelling wave representation of the phase modulated field operator.

Figure 5.5 shows the refractive index profile dependence in spatial direction z at the transmitter of an all optical phase modulated system. The refractive index profile of the modulator material in a phase modulated system shown in Figure 5.5 can be divided into 5 regions of interest. In region 1 and 5, the optical field is propagating in free space, while in region 2 and 4, the field propagates in the ARC. Region 3 represents the modulating medium of the modulator whose refractive index is governed by the time varying control signal; therefore the value of refractive index changes with time. In this derivation, we shall assume the ARC in Region 2 and 4 are ideal so that all optical power from the incoming signal is transmitted through the media. In addition, we shall simplify the problem by assuming the control signal has negligible impact on the ARCs, as a result the refractive index of the ARC is assumed to be time independent. Since photons are excited from the modulating medium subjected to changes in refractive index $n(t)$ [16], therefore the above assumption neglects the effect of photon creation in the ARC. Furthermore, by making the assumption of no bound charges and current sources at the modulator, the field expression needs to be matched at the boundary between different regions [36] i.e. at $z = z_1$, $z = z_2$, $z = z_3$, $z = z_4$ and $z = z_5$.

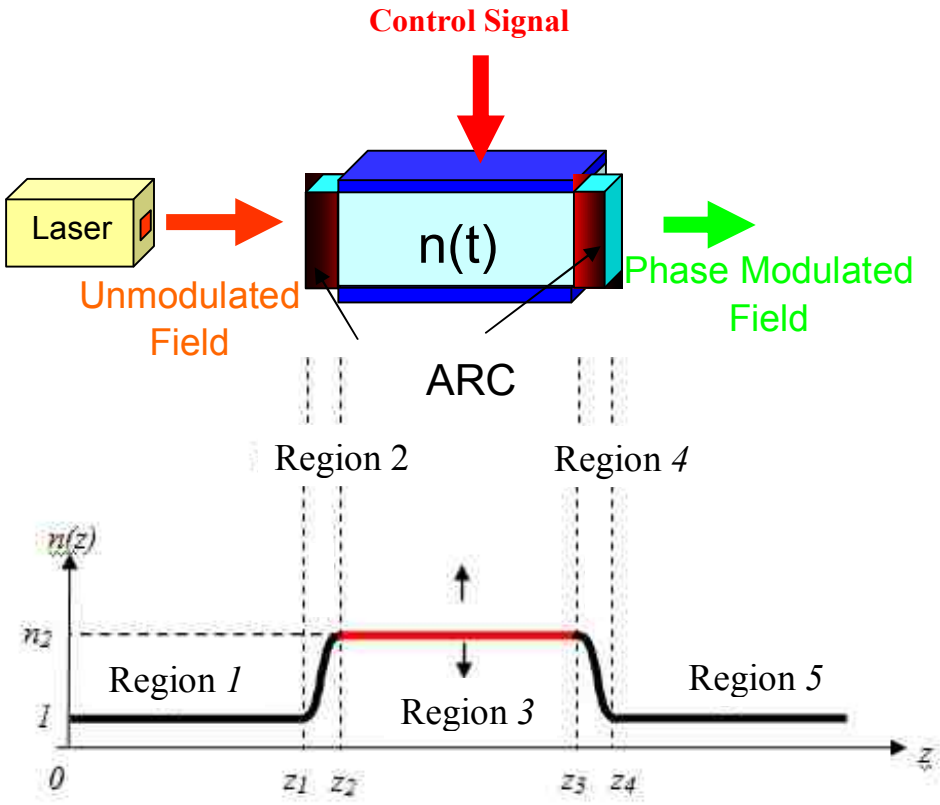

Figure 5.5: Refractive index against distance for a phase modulated system.

Region 1:

In region 1, the field propagates in free space, for which the travelling wave representation of electric field operator $\hat{E}_1(z,t)$ is given by Equation (5.65), where the subscript '1' denotes the field expression in region 1. We begin by considering the field expression at the boundary of region 1 and region 2 at $z = z_1$. With the use of Equation (5.65), we have the field expression at $z = z_1$ and time $t' = t + T_{f1}$

$$\hat{E}_1(z_1,t') = \int_0^\infty d\omega \left(\frac{\hbar\omega}{4\pi\varepsilon_0 c_0 A}\right)^{1/2} \hat{a}(\omega)\exp(i\varphi_1 - i\omega t') + H.c. \qquad (5.74)$$

where T_{f1} is the flight time of the field propagating from the laser at $z = 0$ to the boundary of ARC at $z = z_1$ which can be expressed as $T_{f1} = z_1/c_0$.

Region 2:

In region 2, the field propagates in the ARC whose refractive index is gradually increasing over the z direction as shown in Figure 5.5. By employing expression (5.69) derived in Section 5.4, which characterizes the field propagation in the ARC, the field expression in region 2 is given by

$$\hat{E}_2(z,t)=\int_0^{\infty} d\omega \frac{K_2}{\sqrt{n(z)}}\left(\frac{\hbar\omega}{4\pi\varepsilon_0 c_0 A}\right)^{1/2}\hat{a}(\omega)\exp\left(i\int_{z_1}^{z}k(\xi)d\xi-i\omega t\right)+H.c. \quad z_1\le z<z_2 \quad (5.75)$$

where K_2 is a constant. Note that the lower limit of the phase integral in Equation (5.75) is chosen to be z_1 instead of -∞ as in Equation (5.69), because the field description in expression (5.75) holds only when the spatial distance z is in between z_1 and z_2.

By matching the boundary at $z = z_1$ and time $t' = t + T_{f1}$ i.e. $\hat{E}_1(z_1,t')=\hat{E}_2(z_1,t')$, the value of K_2 is evaluated to be

$$K_2=\exp(i\varphi_1) \quad (5.76)$$

where $\varphi_1 = k_0 z_1$ By using Equation (5.75) and Equation (5.76), the field expression at $z = z_2$ and time $t'' = t + T_{f1} + T_{f2}$, is given by

$$\hat{E}_2(z_2,t'')=\int_0^{\infty} d\omega \frac{1}{\sqrt{n}}\left(\frac{\hbar\omega}{4\pi\varepsilon_0 c_0 A}\right)^{1/2}\hat{a}(\omega)\exp(i\varphi_1+i\varphi_2-i\omega t'')+H.c. \quad z_1\le z<z_2 \quad (5.77)$$

where T_{f2} is the photon flight time in region 2, the propagation phase delay in ARC φ_2 is $\varphi_2=\int_{z_1}^{z_2}k(\xi)d\xi$, and n is the refractive index at z_2.

Region 3:

In region 3, the field propagates in the modulating medium whose refractive index is time dependent. In Section 5.4, the travelling wave representation for an optical field propagating in the modulating medium is introduced in Equation (5.66). However,

the representation in Equation (5.66) applies to the time interval when the refractive index becomes static after some dynamical changes i.e. $t > T$ in Figure 5.1. In this Section, we considered the situation that is more general for which the refractive index may not necessary have a static region. By using the result in Equation (5.66), and the expression of the field mode in Equation (5.34), the travelling wave representation of the field operator in the modulating medium is expressed as

$$\hat{E}^{MM}(z,t) = \int_0^\infty d\omega \left(\frac{\hbar\omega_m^{out}}{4\pi\varepsilon_2 c_0 A}\right)^{1/2} \hat{a}(\omega)\left(\alpha(\omega,t)\exp\left[ikz - i\int_{-\infty}^{t}\omega(\tau)d\tau\right] + \beta(\omega,t)\exp\left[ikz + i\int_{-\infty}^{t}\omega(\tau)d\tau\right]\right) + H.c. \tag{5.78}$$

where from Equation (5.34) and (5.41), we can verify the time dependent Bogoliubov coefficients is expressed as

$$\alpha(\omega,t) = \frac{1}{T_b(t)} = 1 + i\int_{-\infty}^{t}\left(\frac{1}{\omega(\tau)}\right)^{1/2}\frac{d}{d\tau}\left(\frac{d\omega/d\tau}{4\omega^{3/2}(\tau)}\right)d\tau \tag{5.79}$$

$$\beta(\omega,t) = -i\int_{-\infty}^{t}\left(\frac{1}{\omega(\tau)}\right)^{1/2}\frac{d}{d\tau}\left(\frac{d\omega/d\tau}{4\omega^{3/2}(\tau)}\right)\exp\left(-2i\int_{-\infty}^{\tau}\omega(t')dt'\right)d\tau \tag{5.80}$$

Assume there is a time interval $t < T$, for which no changes in refractive index has taken place in the modulating medium i.e. similar to the 'in' region in Figure 5.1. Using expression (5.79) and (5.80) we have $\alpha(\omega,t) = 1$ and $\beta(\omega,t) = 0$, within that time interval as $d\omega/dt = 0$ for $t < T$. Consider there is a forward propagating optical field at $t < T$. For $t \geq T$, changes in refractive index takes place and the forward propagating field is decomposed into two field components as shown in Equation (5.78). The field component that is dependent on $\alpha(\omega,t)$, propagates in the $+z$ direction, as shown by the red arrow in Figure 5.6, while the other component that is dependent on $\beta(\omega,t)$, propagates in the $-z$ direction, as illustrated by the blue arrow in Figure 5.6.

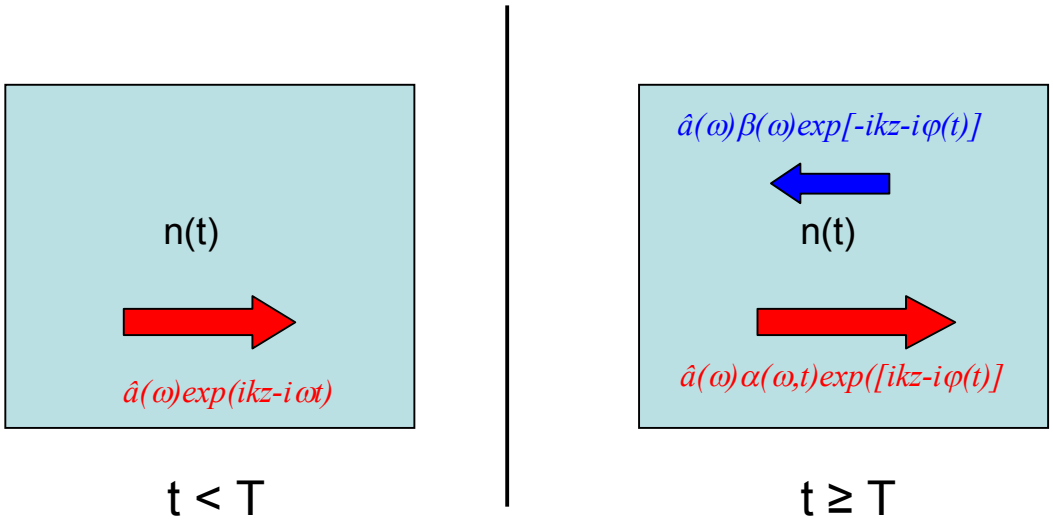

Figure 5.6: Field decomposition of forward traveling wave in modulating medium.

Similarly, when we consider an optical field propagating in the $-z$ direction (backward propagating) for $t < -T$, it decomposes into a field component that is dependent on $\alpha(\omega,t)$ propagating in the $-z$ direction, as shown by the blue arrow in Figure 5.7, and another component that is dependent on $\beta(\omega,t)$ propagating in the $+z$ direction, as shown by the red arrow in Figure 5.7.

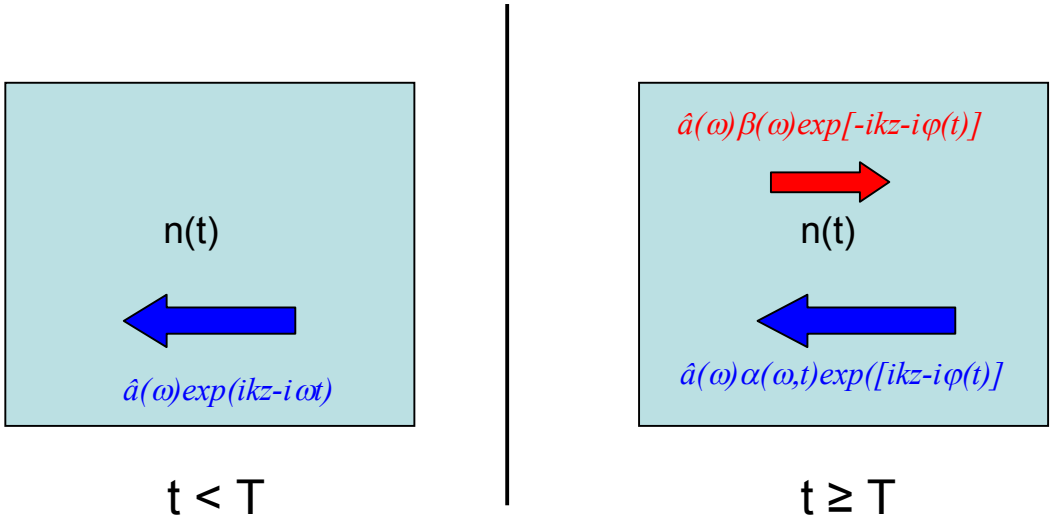

Figure 5.7: Field decomposition of backward propagating wave in modulating medium.

Only the field component that propagates in the $+z$ direction will be considered in the phase modulated field expression because they propagate towards the detector. i.e. red arrow in Figure 5.6 and Figure 5.7. Thus, the general expression of the electric field operator that propagates towards the detector ($+z$ direction) in region 3 is

$$\begin{aligned}\hat{E}_3(z,t) &= \int_0^\infty d\omega \left(\frac{\hbar\omega(t)}{4\pi\varepsilon(t)c_0 A}\right)^{1/2} \hat{a}(\omega)\left\{K_3\alpha(\omega,t)\exp\left[ikz - i\int_{t''}^{t}\omega(\tau)d\tau\right]\right. \\ &\left. + K_3^{*}\beta(\omega,t)\exp\left[-ikz + i\int_{t''}^{t}\omega(\tau)d\tau\right]\right\} + H.c. \qquad (5.81)\\ &= \int_0^\infty d\omega \left(\frac{\hbar\omega(t)}{4\pi\varepsilon(t)c_0 A}\right)^{1/2} K_3\left[\hat{a}(\omega)\alpha(\omega,t) + \hat{a}^{+}(\omega)\beta^{*}(\omega,t)\right]\exp\left[ikz - i\int_{t''}^{t}\omega(\tau)d\tau\right] + H.c. \\ &= \int_0^\infty d\omega \left(\frac{\hbar\omega(t)}{4\pi\varepsilon(t)c_0 A}\right)^{1/2} K_3\hat{b}(\omega,t)\exp\left[ikz - i\int_{t''}^{t}\omega(\tau)d\tau\right] + H.c. \quad z_2 \le z < z_3\end{aligned}$$

where K_3 is a constant. The second line in Equation (5.81) is obtained by grouping the complex exponential terms $\exp\left[ikz - i\int_{t''}^{t}\omega(\tau)d\tau\right]$. From Equation (5.86), we can identify the modulated field annihilation operator $\hat{b}(\omega,t)$, is related to unmodulated field annihilation and creation operator, $\hat{a}(\omega)$ and $\hat{a}^{+}(\omega)$, by the time dependent Bogoliubov transformation

$$\hat{b}(\omega,t) = \alpha(\omega,t)\hat{a}(\omega) + \beta(\omega,t)\hat{a}^{+}(\omega) \qquad (5.82)$$

Similarly the modulated field creation operator $\hat{b}^{+}(\omega,t)$, buried in the Hermitian conjugate (*H.c.*) term in Equation (5.81), is expressed as

$$\hat{b}^{+}(\omega,t) = \alpha^{*}(\omega,t)\hat{a}^{+}(\omega) + \beta^{*}(\omega,t)\hat{a}(\omega) \qquad (5.83)$$

Notice that the lower limit of the phase integral is selected to be time t'' in Equation (5.81), where $t'' = t + T_{f1} + T_{f2}$, because we have assumed the optical field enters the modulating medium at t''. By using Equation (5.81), the field operator for region 3 is given by

$$\hat{E}_3(z_2,t'') = \int_0^\infty d\omega \left(\frac{\hbar\omega(t'')}{4\pi\varepsilon(t'')c_0 A} \right)^{1/2} K_3 \hat{a}(\omega) \exp(ikz_2) + H.c. \qquad (5.84)$$

By comparing expression (5.84) with Equation (5.81), we can identify the Bogoliubov coefficients has the value $\alpha(\omega,t) = 1$ and $\beta(\omega,t) = 0$ in Equation (5.84) at time t''. This is because the lower limit of the integral in Equation (5.79) and Equation (5.80) are set to t'', which describes the optical field has not experience any time variation in refractive index before it enters the modulating medium.

By matching the boundary condition at $z = z_2$ i.e. $\hat{E}_2(z_2,t'') = \hat{E}_3(z_2,t'')$, with the use of expression (5.77) and (5.81), and the relation $\varepsilon(t'')/\varepsilon_0 = n^2(t'')$ and $\omega(t'') = kc_0/n(t'')$, the constant K_3 is evaluated to be

$$\begin{aligned} K_3 &= \frac{n^{3/2}(t'')}{n} \exp(i\varphi_1 + i\varphi_2 - ikz_2 - i\omega t'') \\ &\approx \sqrt{n} \exp(i\varphi_1 + i\varphi_2 - ikz_2 - i\omega t'') \end{aligned} \qquad (5.85)$$

In the last line of expression (5.85), we have assume $n(t'') \approx n$. Notice that K_3 is proportional to $n^{3/2}(t'')$ and thus it is time dependent as a consequence of assuming the refractive of the ARC is time independent. By using the expression of K_3 in Equation (5.85) and expression (5.81), the field at the boundary $z = z_3$ and time t''', where $t''' = t + T_{f1} + T_{f2} + T_{f3}$, is expressed as

$$\hat{E}_3(z_3,t''') = \int_0^\infty d\omega \frac{1}{\sqrt{n}} \left(\frac{\hbar\omega}{4\pi\varepsilon_0 c_0 A} \right)^{1/2} \hat{b}(\omega,t''') \exp\left(i\varphi_1 + i\varphi_2 + i\varphi_3 - i\omega t'' - i\int_{t''}^{t'''} \omega(\tau)\, d\tau \right) + H.c. \qquad (5.86)$$

where T_{f3} is the photon flight time in region 3 and φ_3 is the propagation delay and is expressed as $\varphi_3 = k(z_3 - z_2)$. By assuming the temporal change in refractive index Δn, is much smaller than the refractive index of the material n i.e. $\Delta n << n$, we can assume T_{f3} as a constant, with the expression $T_{f3} = nL/c_0$, where L is the length of the modulating medium.

Region 4:

In region 4, the optical field propagates in the ARC. Unlike the ARC in region 2, the refractive index in region 4 is monotonically decreasing from *n* to *1* with respect to distance *z*, as shown in Figure 5.5. By assuming the refractive index of ARC is time independent, and with the use of expression (5.69), the field operator in region 4 is expressed as

$$\hat{E}_4(z,t)=\int_0^{\infty} d\omega \frac{1}{\sqrt{n(z)}}\left(\frac{\hbar\omega}{4\pi\varepsilon_0 c_0 A}\right)^{1/2} K_4\hat{b}(\omega,t''')\left(\exp\left(i\int_{z_3}^{z} k(\xi)d\xi - i\omega t\right)+H.c.\right) \quad z_3 \le z < z_4 \quad (5.87)$$

where K_4 is a constant. Because the field has been modulated before it propagates in region 4 at time *t'''*, therefore the modulated field annihilation operator $\hat{b}(\omega,t''')$, is used in expression (5.87). The field expression at boundary $z = z_3$, is

$$\hat{E}_4(z_3,t''')=\int_0^{\infty} d\omega \frac{1}{\sqrt{n}}\left(\frac{\hbar\omega}{4\pi\varepsilon_0 c_0 A}\right)^{1/2} \hat{b}(\omega,t''')\exp(-i\omega t''')+H.c. \quad (5.88)$$

By matching the boundary condition at $z = z_3$ i.e. $\hat{E}_3(z_3,t''')=\hat{E}_4(z_3,t''')$, with the use of expression (5.87) and (5.88), K_4 is evaluated to be

$$K_4=\exp\left(i\varphi_1+i\varphi_2+i\varphi_3-i\omega(t''-t''')-i\int_{t''}^{t'''}\omega(\tau)d\tau\right) \quad (5.89)$$

Using Equation (5.87) and Equation (5.89), the general expression of an optical field propagating in region 4 is

$$\hat{E}_4(z,t)=\int_0^{\infty} d\omega \frac{1}{\sqrt{n}}\left(\frac{\hbar\omega}{4\pi\varepsilon_0 c_0 A}\right)^{1/2} \hat{b}(\omega,t''')\exp\left(i\int_{z_3}^{z} k(\xi)d\xi+i\varphi_1+i\varphi_2+i\varphi_3-i\omega t-i\omega(t''-t''')-i\int_{t''}^{t'''}\omega(\tau)d\tau\right)+H.c. \quad (5.90)$$

Thus, the field expression at $z = z_4$ and at time $t'''' = t + T_{f1} + T_{f2} + T_{f3} + T_{f4}$, is given by

$$\hat{E}_4(z_4,t'''') = \int_0^{\infty} d\omega \frac{1}{\sqrt{n(z_4)}} \left(\frac{\hbar\omega}{4\pi\varepsilon_0 c_0 A}\right)^{1/2} \hat{b}(\omega,t''') \exp\left(i\varphi_1 + i\varphi_2 + i\varphi_3 + i\varphi_4 - i\omega t'''' - i\omega(t''-t''') - i\int_{t''}^{t'''} \omega(\tau)\,d\tau\right) + H.c. \quad (5.91)$$

where the propagation phase delay φ_4 is $\varphi_4 = \int_{z_3}^{z_4} k(\xi)\,d\xi$ and $n(z_4) = 1$.

Region 5:

In region 5, the optical field leaves the modulator and propagates in free space. The general expression in region 5 is represented by

$$\hat{E}_5(z,t) = \int_0^{\infty} d\omega \left(\frac{\hbar\omega}{4\pi\varepsilon_0 c_0 A}\right)^{1/2} K_5 \hat{b}(\omega,t''') \exp(ik_0 z - i\omega t) + H.c. \quad z \geq z_4 \quad (5.92)$$

where K_5 is a constant. Since the field enters region 5 at time t'''', thus using Equation (5.92), the field expression at the boundary $z = z_4$ is

$$\hat{E}_5(z_4,t'''') = \int_0^{\infty} d\omega \left(\frac{\hbar\omega}{4\pi\varepsilon_0 c_0 A}\right)^{1/2} K_5 \hat{b}(\omega,t''') \exp(ik_0 z_4 - i\omega t'''') + H.c. \quad (5.93)$$

By matching the boundary condition at $z = z_4$ i.e. $\hat{E}_4(z_4,t'''') = \hat{E}_5(z_4,t'''')$, with the use of expression (5.91) and (5.93), K_5 is evaluated to be

$$K_5 = \exp\left(i\varphi_1 + i\varphi_2 + i\varphi_3 + i\varphi_4 - i\omega(t''-t''') - i\int_{t''}^{t'''} \omega(\tau)\,d\tau\right) \quad (5.94)$$

Using Equation (5.91) and Equation (5.94), the general expression of an optical field propagating in region 5 is

$$\hat{E}_5(z,t) = \int_0^{\infty} d\omega \left(\frac{\hbar\omega}{4\pi\varepsilon_0 c_0 A}\right)^{1/2} \hat{b}(\omega,t''') \exp\left(ik_0 z + i\varphi_1 + i\varphi_2 + i\varphi_3 + i\varphi_4 - i\omega t - i\omega(t''-t''') - i\int_{t''}^{t'''} \omega(\tau)\,d\tau\right) + H.c. \quad (5.95)$$

The field operator in region 5 $\hat{E}_5(z,t)$ represents the phase modulated field at the output of the modulator $\hat{E}_{out}(z,t)$. For the purpose of convenience, we shall translate the time scale from t'''' in Equation (5.93) to t i.e. $t'''' = t + T_{f1} + T_{f2} + T_{f3}$

$+ T_{f4} \rightarrow t$. Furthermore, we assume the photon flight time between the laser and the modulator as well as in the ARCs is small so that $T_{f1} \approx T_{f2} \approx T_{f4} \approx 0$. Thus, the field operator for a phase modulated optical field is can be expressed as

$$\widehat{E}_{out}(z,t) = \int_0^{\infty} \left(\frac{\hbar\omega}{4\pi\varepsilon_0 c_0 A} \right)^{1/2} \left\{ \hat{b}(\omega,t) \exp\left[ik_0 z + i\varphi_{out} - iW(\omega,t) \right] + H.c. \right\} d\omega \quad (5.96)$$

where φ_{out} is the propagation phase delay from the transmit laser to the output of the modulator which has the expression $\varphi_{out} = \varphi_1 + \varphi_2 + \varphi_3 + \varphi_4$, and $W(\omega,t)$ is the time varying modulated phase angle and is expressed as

$$W(\omega,t) = \omega t - \omega T_f + \int_{t-T_f}^{t} \omega(\tau)\, d\tau \quad (5.97)$$

T_f represents the photon flight time in the modulator and is equivalent to T_{f3} defined earlier in the section.

5.6 Conclusions

In this Chapter, we have derived the phase modulated field operator in Equation (5.96), which characterizes an optical field propagating through a modulator. The field operator is derived by matching the boundary condition of the general solutions between two dissimilar media. The quantum field representation will be used extensively in Chapter 6 to examine how the properties of modulated optical field are altered as a consequence of photon creation from modulator. It is also useful in deducing the impact of photon creation on various types of communication systems studied in Chapter 7.

6 Properties of Phase Modulated Field

6.1 Chapter Objectives

The quantum field expression of modulated field has been derived in Chapter 5. It is shown that the field expression is dependent on the time dependent Bogoliubov coefficients $\alpha(\omega,t)$ and $\beta(\omega,t)$. The objective of this Chapter is to use the phase modulated field expression in Chapter 5 to investigate the quantum statistical properties of phase modulated field that includes the quantum effect of photon creation from modulator. This will assist in the understanding of why photon creation occurs in the modulation process, as well as realizing the impact of photon creation in an optical system.

The rest of this Chapter is organized as follows. In Section 6.2, we analyze the power flow of the optical field at the input and output of the phase modulator in order to explain why photon/energy is excited during the modulation process. In Section 6.3, the difference between the detector response of unmodulated field and modulated field is resolved so that the change in statistical property as a result of photon creation can be determined. In Section 6.4, we investigate how the state of the field is modified due to the effect of photon creation. In Section 6.5, we examine the extent of the effect of photon creation in an optical system from numerical simulation, and to identify the parameters that influences this process. In Section 6.6, we determine the power spectral density (PSD) of a sinusoidal phase modulated field by including the effect of photon creation.

6.2 Power Flow of Phase Modulated Field

In this Section, we shall determine the power flow differences between the input and output of the phase modulator. This enables us to realize the impact of photon creation due to phase modulation as well as understand the mechanisms involved for triggering this process.

Throughout this Chapter, a single mode laser will be considered. In Chapter 5, we have discussed the state of the optical field is generally represented by continuum coherent state $|\{\rho_{in}(\omega)\}\rangle$ which can be expressed as [46]

$$\begin{aligned}\left|\left\{\rho_{in}(\omega)\right\}\right\rangle &= \hat{D}_{\rho}\left[\rho_{in}(\omega)\right]|0\rangle \\ &= \exp\left[\int_{0}^{\infty}\rho_{in}{}^{*}(\omega)\hat{a}^{+}(\omega)-\rho_{in}(\omega)\hat{a}(\omega)d\omega\right]|0\rangle\end{aligned} \tag{6.1}$$

where $\hat{D}_{\rho}$ is the displacement operator which is represented by

$$\hat{D}_{\rho}\left[\rho_{in}(\omega)\right] = \exp\left[\int_{0}^{\infty}\rho_{in}{}^{*}(\omega)\hat{a}^{+}(\omega)-\rho_{in}(\omega)\hat{a}(\omega)d\omega\right] \tag{6.2}$$

$\hat{a}(\omega)$ and $\hat{a}^{+}(\omega)$ in expression (6.1) and (6.2) is the annihilation and creation operator associated with angular frequency ω, and they satisfy the usual commutation relation

$$\begin{aligned}\left[\hat{a}(\omega),\hat{a}^{+}(\omega')\right] &= \hat{a}(\omega)\hat{a}^{+}(\omega')-\hat{a}^{+}(\omega')\hat{a}(\omega) \\ &= \delta(\omega-\omega')\end{aligned} \tag{6.3}$$

$\rho_{in}(\omega)$ in Equation (6.1) is the normalized amplitude wavepacket function that characterizes a single mode laser which can be expressed as [46]

$$\rho_{in}(\omega) = (2\pi F_S)^{1/2}\exp(i\theta_S)\delta(\omega-\omega_S) \tag{6.4}$$

where F_S is the mean photon flux at signal frequency ω_S, θ_S is the initial phase angle of the field, ω_S is the frequency of the optical field. The Dirac delta function in Equation (6.4) implies all the power of the optical field is concentrated at frequency

ω_S. The continuum coherent state is an eigenstate annihilation operator $\hat{a}(\omega)$ which satisfies the eigen-equation

$$\begin{aligned}\hat{a}(\omega)\left|\{\rho_{in}(\omega)\}\right\rangle &= \rho_{in}(\omega)\left|\{\rho_{in}(\omega)\}\right\rangle \\ &= (2\pi F_S)^{1/2}\exp(i\theta_S)\delta(\omega-\omega_S)\left|\{\rho_{in}(\omega)\}\right\rangle\end{aligned} \tag{6.5}$$

The wavepacket function presented in Equation (6.4) assumes the bandwidth of the laser is infinitely narrow as indicated by the Dirac delta function. However for a practical laser, the frequency spectrum of the optical field is distributed at signal frequency ω_S and has a Lorentzian lineshape [1]. This is a consequence of spontaneous emission inside the active region of the laser medium. For a distributed feedback (DFB) laser that outputs a *1500 nm* optical field, the *3 dB* linewidth of the Lorentzian lineshape $\Delta\nu$ is approximately *50 MHz* [1]. Figure 6.1 illustrates the power spectral density (PSD) of unmodulated optical field that is corrupted by laser phase noise.

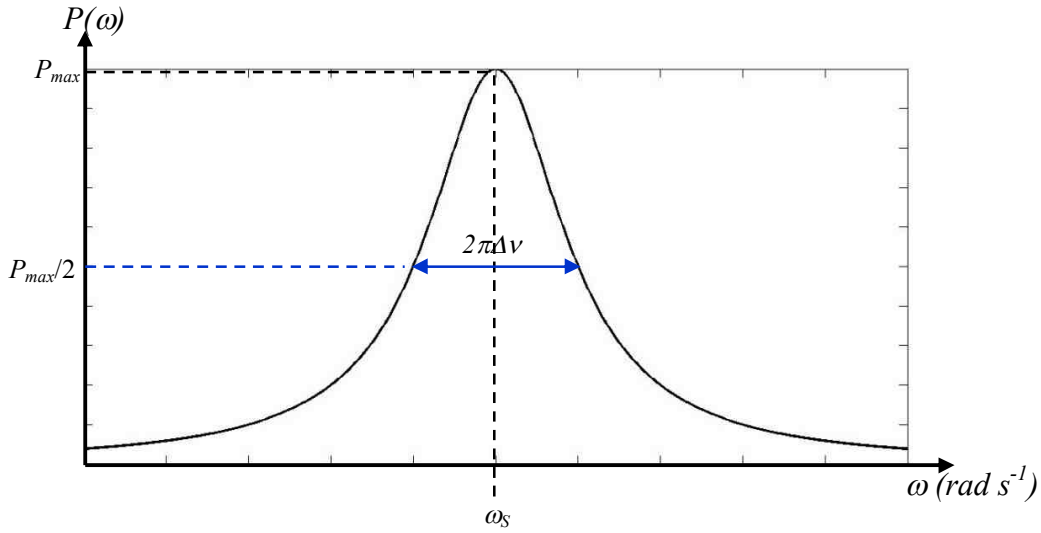

Figure 6.1: PSD of unmodulated optical field corrupted by laser phase noise.

The spread in the frequency spectrum results from laser phase noise $\varphi_{SN}(\omega,t)$. $\varphi_{SN}(\omega,t)$ is a random variable, and using the laser phase noise model from [1, 47, 48, 49], the phase noise is commonly characterized by the Wiener process

$$\varphi_{SN}(\omega,t) = \int_{-\infty}^{t} \frac{\partial \varphi_{SN}}{\partial \tau} d\tau \tag{6.6}$$

The time derivative of phase noise $d\varphi_{SN}/dt$ can be modelled as a zero-mean white Gaussian process with a power spectral density (PSD) that is related to the *3 dB* linewidth $\Delta\nu$ by

$$S_{\partial\varphi_{SN}/\partial t} = 2\pi\Delta\nu \tag{6.7}$$

In order to incorporate the laser phase noise into the analysis, we shall introduce the phase noise annihilation operator $\hat{a}_{\varphi}(\omega,t)$

$$\hat{a}_{\varphi}(\omega,t) = \hat{a}(\omega)\exp\left(i\varphi_{SN}(\omega,t)\right) \tag{6.8}$$

It is easy to verify that the phase noise annihilation and creation operator, $\hat{a}_{\varphi}(\omega,t)$ and $\hat{a}_{\varphi}^{+}(\omega,t)$, satisfies the equal time commutation relation, where we have

$$\left[\hat{a}_{\varphi}(\omega,t), \hat{a}_{\varphi}^{+}(\omega',t)\right] = \delta(\omega-\omega') = \left[\hat{a}(\omega), \hat{a}^{+}(\omega')\right] \tag{6.9}$$

Expression (6.9) shows the equal time commutation relation between $\hat{a}_{\varphi}(\omega,t)$ and $\hat{a}_{\varphi}^{+}(\omega,t)$, is identical to the commutation relation of $\hat{a}(\omega)$ and $\hat{a}(\omega)$. The continuous field mode operator of the optical field $\hat{E}(z,t)$ can be expressed in terms of $\hat{a}_{\varphi}(\omega,t)$ and $\hat{a}_{\varphi}^{+}(\omega,t)$ as

$$\begin{aligned}\hat{E}(z,t) &= \hat{E}^{+}(z,t) + \hat{E}^{-}(z,t) \\ &= \int_{0}^{\infty}\left(\frac{\hbar\omega}{4\pi\varepsilon_0 c_0 A}\right)^{1/2}\left[\hat{a}_{\varphi}(\omega,t)\exp\left(ik_0 z - i\omega t\right) + H.c.\right]d\omega\end{aligned} \tag{6.10}$$

where k_0 is the free space propagation constant, ε_0 is the free space dielectric permittivity ($\varepsilon_0 = 8.85*10^{-12}$ *V/m*), and c_0 is the speed of light in free space (c_0 =

$3*10^8\ ms^{-1}$), A is the cross section area that the field propagates through, and *H.c.*is an abbreviation for Hermitian conjugate.

In order to determine the power flow of the phase modulated field, we shall consider an optical phase modulator located at some fixed distance D from the laser, as shown in Figure 6.2.

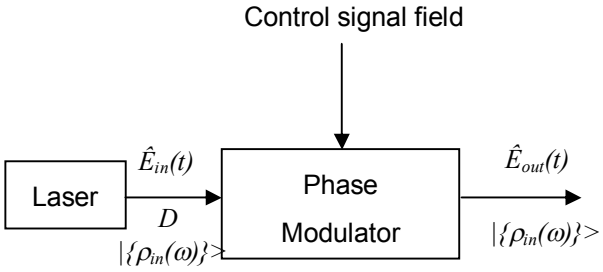

Figure 6.2: Configuration of optical system.

The expression of the field operator at the input terminal of the modulator $\hat{E}_{in}(t)$ is given by

$$\begin{aligned}\widehat{E}_{in}(t) &= \widehat{E}(D,t) \\ &= \int_0^\infty \hat{e}_{in}^{+}(\omega,t) + \hat{e}_{in}^{-}(\omega,t)\,d\omega \\ &= \int_0^\infty \left(\frac{\hbar\omega}{4\pi\varepsilon_0 c_0 A}\right)^{1/2} \left[\hat{a}_\varphi(\omega,t)\exp(i\varphi_{in} - i\omega t) + H.c.\right] d\omega\end{aligned} \tag{6.11}$$

where $\varphi_{in} = k_0 D$, and $\hat{e}_{in}^{+}(\omega,t)$ is expressed as

$$\hat{e}_{in}^{+}(\omega,t) = \left(\frac{\hbar\omega}{4\pi\varepsilon_0 c_0 A}\right)^{1/2} \hat{a}_\varphi(\omega,t)\exp(i\varphi_{in} - i\omega t) \tag{6.12}$$

Notice that expression (6.11) is very similar to Equation (6.10), except that the phase offset due to field propagation *i.e.* $k_0 z$, is replaced by a constant phase φ_{in}. This is because the distance between the modulator and the laser does not vary.

At the output terminal of the optical modulator, the optical field is phase modulated. The phase offset due to modulation is dependent on the control signal feeding into the control terminal of phase modulator. In this analysis, we shall adopt the Heisenberg picture in which the field operator changes from $\hat{E}_{in}(t)$ to $\hat{E}_{out}(t)$ due to modulation, but the state of the field remains unchanged at $|\{\rho_{in}(\omega)\}>$, as shown in Figure 6.1. Hence the state of the phase modulated field continues to be described by a continuum coherent state with a wavepacket function given by Equation (6.4). The expression of the phase modulated field at the output of the modulator has been derived in Chapter 5, and it is represented by

$$\begin{aligned}\hat{E}_{out}(t) &= \int_0^\infty \hat{e}_{out}^{+}(\omega,t) + \hat{e}_{out}^{-}(\omega,t)d\omega \\ &= \int_0^\infty \left(\frac{\hbar\omega}{4\pi\varepsilon_0 c_0 A}\right)^{1/2} \left\{\hat{b}(\omega,t)\exp\left(-i\left[W(\omega,t)-\varphi_{out}\right]\right) + H.c.\right\} d\omega\end{aligned} \tag{6.13}$$

where $\hat{b}(\omega,t)$ is the annihilation operator of the phase modulated field, and $W(\omega,t)$ is the modulated phase angle. By comparing the first line with the second line of Equation (6.13), it is shown that $\hat{e}_{out}^{+}(\omega,t)$ can be expressed as

$$\hat{e}_{out}(\omega,t) = \left(\frac{\hbar\omega}{4\pi\varepsilon_0 c_0 A}\right)^{1/2} \left\{\hat{b}(\omega,t)\exp\left(-i\left[W(\omega,t)-\varphi_{out}\right]\right)\right\} \tag{6.14}$$

In expression (6.13), we have assumed the modulator is lossless and no field energy is reflected back to the laser from the modulator. The time varying modulated phase angle $W(\omega,t)$ is represented by

$$W(\omega,t) = \omega t - \omega T_f + \int_{t-T_f}^{t} \omega(\tau)\,d\tau \tag{6.15}$$

where T_f is the photon flight time in the modulator. The instantaneous angular frequency $\omega(\tau)$, that is inside the integral of expression (6.15) is expressed as

$$\omega(t) = \frac{n\omega}{n(t)} \tag{6.16}$$

where n is the material refractive index of the modulating medium, $n(t)$ is the time varying index due to the excitation of the modulating medium from the control signal field in Figure 6.2, and ω is the frequency of the field prior to modulation i.e. frequency of the unmodulated field. We can relate the modulated field annihilation operator $\hat{b}(\omega,t)$ with the unmodulated phase noise annihilation and creation operator, $\hat{a}_\varphi(\omega,t)$ and $\hat{a}_\varphi^{+}(\omega,t)$, by the Bogoliubov transform introduced in Chapter 5, where we have

$$\hat{b}(\omega,t) = \alpha(\omega,t)\hat{a}_\varphi(\omega,t) + \beta^*(\omega,t)\hat{a}_\varphi^{+}(\omega,t) \tag{6.17}$$

$\alpha(\omega,t)$ and $\beta(\omega,t)$ are the time dependent Bogoliubov coefficients. In Chapter 5.2, we have derived their approximate expression to 1st order to be

$$\alpha(\omega,t) = 1 + i\int_{t-T_f}^{t}\left(\frac{1}{\omega(\tau)}\right)^{1/2}\frac{d}{d\tau}\left(\frac{d\omega/d\tau}{4\omega^{3/2}(\tau)}\right)d\tau \tag{6.18}$$

$$\beta(\omega,t) = -i\int_{t-T_f}^{t}\left(\frac{1}{\omega(\tau)}\right)^{1/2}\frac{d}{d\tau}\left(\frac{d\omega/d\tau}{4\omega^{3/2}(\tau)}\right)\exp\left(-2i\left[\omega\tau - \omega T_f + \int_{\tau-T_f}^{\tau}\omega(t')dt'\right]\right)d\tau \tag{6.19}$$

where $d\omega/dt$ is the rate of change of instantaneous frequency and using expression (6.16), it can be verified that

$$\frac{d\omega}{dt} = \frac{dn}{dt}\frac{\omega}{n^2(t)} \tag{6.20}$$

As we have explained in Section 5.2, the approximation in expression (6.18) and (6.19) is accurate provided the adiabatic condition is satisfied i.e.

$$\left.\frac{d\omega}{dt}\right|_{\max} << \omega_S{}^2 \tag{6.21}$$

In fact the condition in Equation (6.21) applies to most phase modulated system [22-24], thus expression (6.18) and (6.19) gives an accurate result. The modulated field

annihilation operator **must** satisfy the same commutation relation as the unmodulated field operator in Equation (6.3) [12]. Thus we have,

$$\begin{aligned}\left[\hat{b}(\omega,t),\hat{b}^{+}(\omega',t)\right] &= \hat{b}(\omega,t)\hat{b}^{+}(\omega',t)-\hat{b}^{+}(\omega',t)\hat{b}(\omega,t)\\ &= \left[\alpha(\omega,t)\alpha^{*}(\omega',t)\hat{a}_{\varphi}(\omega)\hat{a}_{\varphi}^{+}(\omega')-\beta^{*}(\omega',t)\beta(\omega,t)\hat{a}_{\varphi}^{+}(\omega')\hat{a}_{\varphi}(\omega)\right]\\ &= \left[\left|\alpha(\omega,t)\right|^{2}-\left|\beta(\omega,t)\right|^{2}\right]\delta(\omega-\omega')\\ &= \delta(\omega-\omega')\end{aligned} \tag{6.22}$$

where $\alpha(\omega,t)$ and $\beta(\omega,t)$ satisfies the identity

$$\left|\alpha(\omega,t)\right|^{2}-\left|\beta(\omega,t)\right|^{2}=1 \tag{6.23}$$

The mean optical field power flowing through the input terminal is described by the energy flux operator. The energy flux operator $\hat{S}(t)$ is defined as [33]

$$\hat{S}(t)=2\varepsilon_{0}c_{0}A\hat{E}^{-}(t)\hat{E}^{+}(t) \tag{6.24}$$

The signal power flowing into the input terminal of the modulator $P_{in}(t)$ can be calculated from the expectation value of the 'in' energy flux operator $\hat{S}_{in}(t)$

$$\begin{aligned}P_{in}(t) &= \left\langle\{\rho_{in}(\omega)\}\middle|\hat{S}_{in}(t)\middle|\{\rho_{in}(\omega)\}\right\rangle\\ &= 2\varepsilon_{0}c_{0}A\left\langle\{\rho_{in}(\omega)\}\middle|\hat{E}_{in}^{-}(t)\hat{E}_{in}^{+}(t)\middle|\{\rho_{in}(\omega)\}\right\rangle\\ &= \left\langle\{\rho_{in}(\omega)\}\middle|\frac{\hbar}{2\pi}\int_{0}^{\infty}\int_{0}^{\infty}(\omega\omega')^{1/2}\hat{a}_{\varphi}^{+}(\omega,t)\hat{a}_{\varphi}(\omega',t)\exp\left(i(\omega-\omega')t\right)d\omega d\omega'\middle|\{\rho_{in}(\omega)\}\right\rangle\end{aligned} \tag{6.25}$$

By using the expression in (6.4), (6.5), and the commutation relation in Equation (6.3), and performing the double integration over frequency, expression (6.25) can be simplified to

$$P_{in}(t)=\hbar\omega_{S}F_{S} \tag{6.26}$$

Similarly, the signal power that leaves the output terminal of the modulator can be calculated from the expectation value of the 'out' energy flux operator $\hat{S}_{out}(t)$, where we have

$$
\begin{aligned}
P_{out}(t) &= \left\langle \{\rho_{in}(\omega)\} \middle| \hat{S}_{out}(t) \middle| \{\rho_{in}(\omega)\} \right\rangle \\
&= 2\varepsilon_0 c_0 A \left\langle \{\rho_{in}(\omega)\} \middle| \hat{E}_{out}^{-}(z,t)\hat{E}_{out}^{+}(z,t) \middle| \{\rho_{in}(\omega)\} \right\rangle \\
&= \left\langle \{\rho_{in}(\omega)\} \middle| \frac{\hbar}{2\pi} \int_0^\infty \int_0^\infty (\omega\omega')^{1/2} \hat{b}^{+}(\omega,t)\hat{b}(\omega',t) \exp\left(i\left[W(\omega,t) - W(\omega',t)\right]\right) d\omega d\omega' \middle| \{\rho_{in}(\omega)\} \right\rangle
\end{aligned}
\tag{6.27}
$$

By using the expressions in (6.5), (6.17), the commutation relation in Equation (6.22), and performing the double integration over frequency, the expression of the power flow at the output of the modulator in Equation (6.27) can be simplified to

$$
\begin{aligned}
P_{out}(t) = \hbar\omega_S F_S \Big\{ & 1 + 2\left|\beta(\omega_S,t)\right|^2 + 2\sqrt{1+\left|\beta(\omega_S,t)\right|^2}\left|\beta(\omega_S,t)\right| \cos\left[2\left(\theta_S + \varphi_{SN}(\omega_S,t)\right) + A(\omega_S,t) + B(\omega_S,t)\right] \Big\} \\
& + \frac{\hbar}{2\pi}\int_0^\infty \omega \left|\beta(\omega,t)\right|^2 d\omega
\end{aligned}
\tag{6.28}
$$

where $A(\omega_S,t)$ and $B(\omega_S,t)$ is the phase of Bogoliubov coefficients, $\alpha(\omega_S,t)$ and $\beta(\omega_S,t)$, respectively, and is dependent on the signal frequency ω_S. In this, we have used the Bogoliubov identity in Equation (6.23) to express $|\alpha(\omega_S,t)|$ in terms of $|\beta(\omega_S,t)|$.

By comparing the expression in Equation (6.28) with Equation (6.25), we see that the first term in Equation (6.28) corresponds to the average power flow at the input of the modulator. Therefore the remaining terms associated with $\beta(\omega,t)$, corresponds to the power difference between the input field and the output field. It is obvious the average power flow of the optical field at the modulator input is NOT the same as the modulator output ($P_{in} \neq P_{out}$), even if we have assumed the modulator is lossless and no energy is reflected from the modulator. Thus, we can conclude that energy is added to the field during the modulation process if the $\beta(\omega,t)$ dependent terms are positive. If the $\beta(\omega,t)$ dependent terms are negative, energy is removed from the modulated field during the modulation process.

This differs from the SCFT analysis (field represented by function instead of operator) presented in many optical systems literature [1, 22 - 24, 29], where the power of the field at the input and the output of the modulator is the same ($P_{in} = P_{out}$)

provided the modulator is lossless. Figure 6.3 is a diagram showing the power flow of the optical field at the modulator using SCFT.

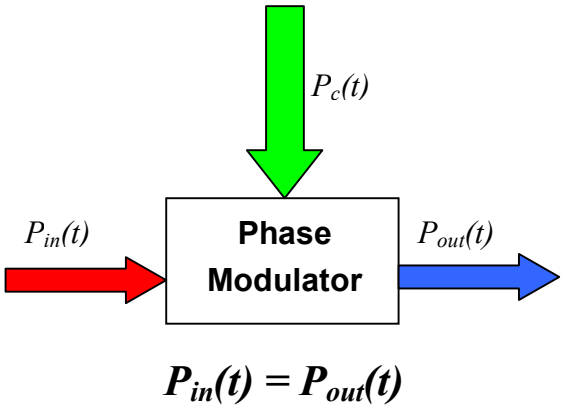

Figure 6.3: Power flow of optical field at the modulator (SCFT).

where P_c in Figure 6.3 represents the power flow of the control signal. The result obtained from SCFT is different from QFT because SCFT does not include the effect of photon creation from modulator.

At the first glance in Equation (6.28), it appears that when the output power flow is greater than the input power flow (i.e. $P_{oui} > P_{in}$) due to $\beta(\omega,t) > 0$, this seems to violates the principle of energy conservation. According to [26], the mismatch in power flow can be accounted for by noting that an external agent alters the refractive index of the modulator. Therefore, it is the energy coupling between the control field and the input field that accounts for the energy difference between the input and the output of modulator by either creating photons from the excited modulating medium or removing photons from the signal field by the excited modulating medium.

By analyzing the $\beta(\omega,t)$ terms in Equation (6.28), we can identify the last term in Equation (6.28) corresponds to an increase in power due to photon creation out of the modulator. This is because this term is positive and the number of photons created is

governed by $|\beta(\omega,t)|^2$ (magnitude of the Bogoliubov coefficient) which is independent on photon flux of the optical field F_S, thus in the absence of the signal field i.e. $F_S = 0$, this term does not vanish. In order to distinguish from other $\beta(\omega,t)$ terms in Equation (6.28), we shall name this process as the spontaneous emission out of the modulator. In general similar to the spontaneous emission of the laser, the photons created in this process do not necessary radiate along the direction of propagation of the optical field (z direction), but can radiate in all directions as shown in Figure 6.4. This is because for vacuum fields which enter the modulator at different directions, i.e. different angles of incidence, also consists of the last term in Equation (6.28) [19].

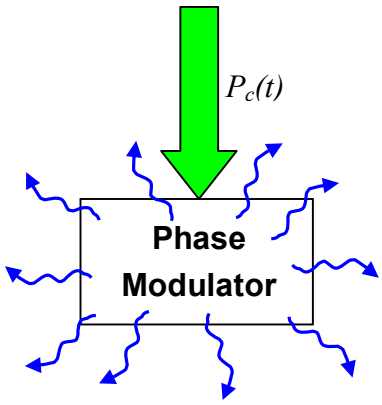

Figure 6.4: Illustration of spontaneous emission out of the modulator.

Furthermore, the frequency integral in Equation (6.28) implies this process is not constrained to the optical frequency ω_S, but applies to all frequencies. Although the limits of the frequency integral ranges from 0 to ∞, the integral is convergent as $\beta(\omega,t)$ decays more rapidly as compared with the linear increase in frequency ω (see Figure 6.24 in Section 6.5). The expression of $\beta(\omega,t)$ in Equation (6.19) shows it is non-zero at the instant when $d\omega/dt \neq 0$, when the instantaneous frequency of the field operator is varying with time. Since $\omega(t) = kc_0/n(t)$, therefore $d\omega/dt$ is non-zero when the refractive index of the modulator $n(t)$ is time varying, thus photons are created during

the transitions of $n(t)$. Since the refractive index profile is governed by the field strength of the control signal, the phenomenon of spontaneous emission out of the modulator requires work to be done by the external (modulating) agent to change the refractive index of the modulator via. the control signal. The process of photon creation is similar to the operation of electrical transformer, in which a voltage is induced in the secondary circuit in order to oppose the change in magnetic flux due to a voltage change at the primary circuit. The change in magnetic flux is an analogue to the change in refractive index i.e. $dn/dt \rightarrow d\phi/dt$, because a voltage induced from $d\phi/dt$ is similar to photon flux induced from dn/dt. Therefore the modulator behaves as an inductor. As shown in Figure 6.5, diode rectifier is placed in between the transformer and the load at the secondary circuit so that a positive voltage is always established across the secondary load irrespective to an increase or decrease in magnetic flux. This is analogous to spontaneous emission from the modulator i.e. $|\beta(\omega_S,t)|^2 > 0$, regardless to an increase or a decrease in refractive index change. Therefore, a transformer circuit is a reasonable electrical analogy for the effect of spontaneous emission out of the modulator. Table 6.1 translates the physical process of photon creation out of the modulator into the transformer analogy.

Photon Creation	**Transformer Analogy**
Control signal power P_c	Primary voltage source $V1$
Change in refractive index dn/dt	Change in magnetic flux $d\phi/dt$
Photon flux created $\int\|\beta(\omega,t)\|^2 d\omega$	Voltage across secondary load V_L

Table 6.1: Translation between the phenomenon of spontaneous emission out of the modulator into transformer analogy.

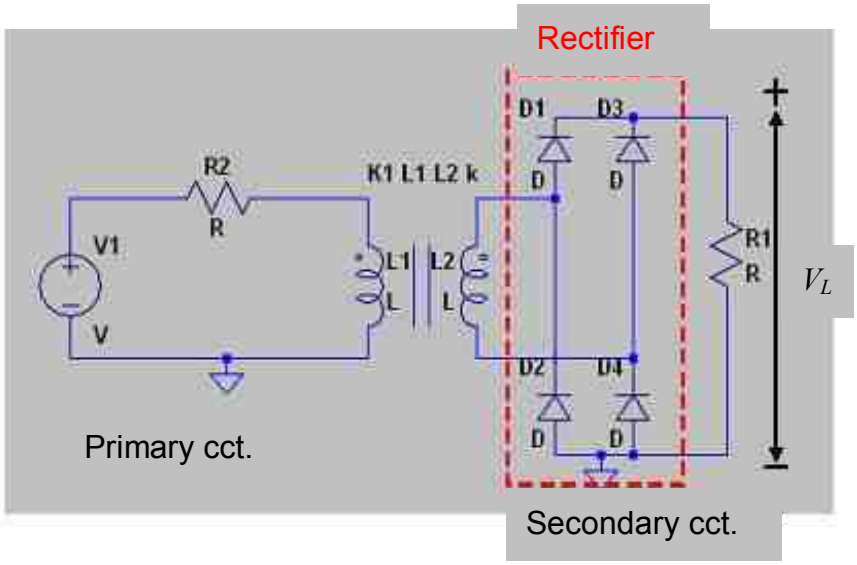

Figure 6.5: Equivalent circuit of transformer analogy.

The phenomenon of spontaneous emission out of the modulator is in fact due to the excitation of the field vacuum state during the transition of the modulator, and this has been widely studied in QFT literature [12, 16 - 21, 44].

The second term in Equation (6.28) is always positive. It describes the process of photon creation stimulated out of the modulator by the optical field, because it is equivalent to the last term of Equation (6.28) being multiplied by the optical field photon flux F, at the optical frequency ω_S. The photons generated from this process replicate the photons from the optical field, as it has the same photon energy and travel in the same direction as the seed photons, as shown in Figure 6.6.

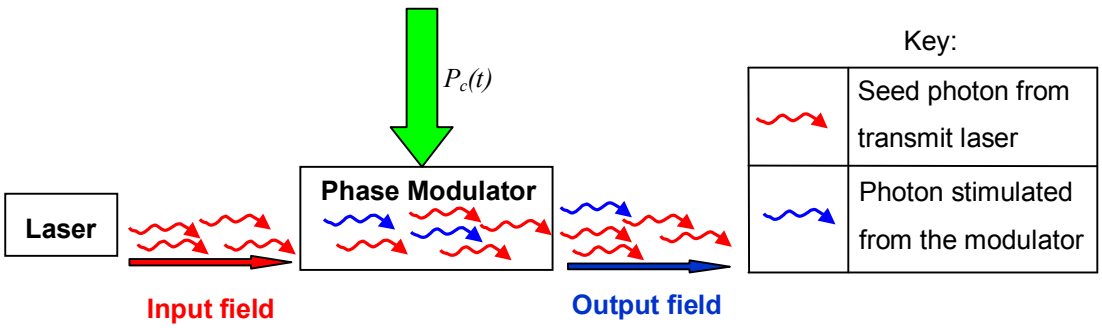

Figure 6.6: Illustration of stimulating photons out of the modulator.

The electric analog of the stimulated process can be represented by transformer circuit shown in Figure 6.7. An amplifier is added in between the diode rectifier and the secondary load in to describe photons are stimulated from the modulator by the optical field.

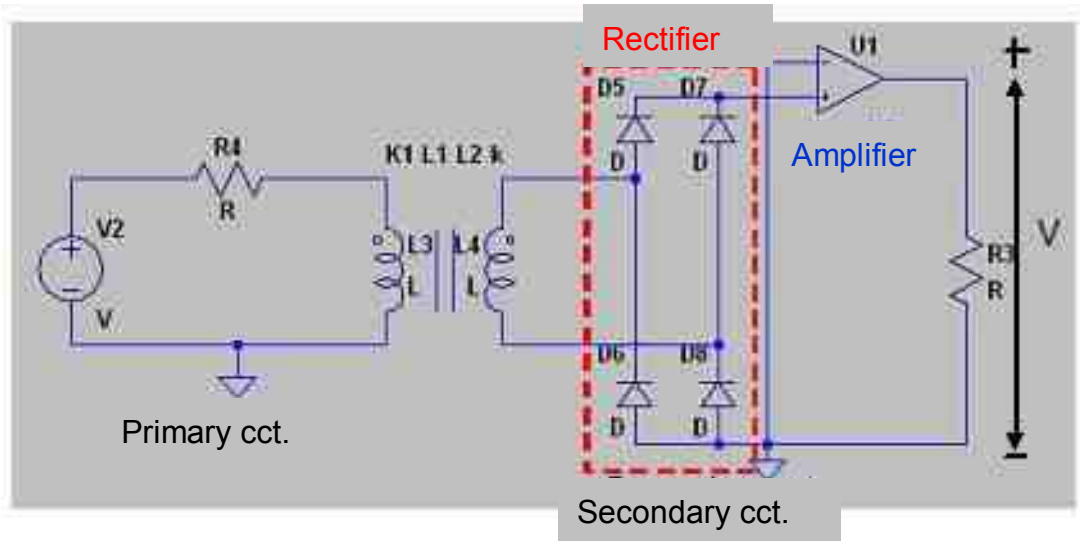

Figure 6.7: Equivalent circuit of the transformer analogy.

We see that when $\beta(\omega_S,t) > 0$, the cosine term (third term) in (6.28) can be either positive or negative depending on the phase angle $2\theta_S + A(\omega_S,t) + B(\omega_S,t)$. This term represents an energy exchange between the optical field and the modulator, which can result in both $P_{out} > P_{in}$ as well as $P_{out} < P_{in}$. At times when the phase angle is $-\pi/2 < 2[\theta_S + \varphi_{SN}(t)] + A(\omega_S,t) + B(\omega_S,t) < \pi/2$, the mean photon flux increases. At other times the mean photon flux decreases. The photons created from the energy exchange process have the same frequency and propagate in the same direction as the input field as it is dependent on F_S. From the results shown in Section 6.5, we shall see the instantaneous magnitude of the energy exchange term dominates over the second term and the last term in Equation (6.28). Therefore, the sign of the energy exchange term

primarily determines whether the power flow at the output of the modulator is greater or less than the modulator input at a particular instant. When the energy exchange term is positive, we have $P_{in} < P_{out}$, and the modulating agent (i.e. control signal) provides additional energy to the output field via the excited modulating medium as explained by [26]. In the case when the energy exchange term is negative, we have $P_{in} > P_{out}$, and some of the input field energy is removed by the excited modulating medium. An excited modulating medium excites and removes energy from the input optical field because the vacuum state of the field is being excited via the refractive index change. This is illustrated in Figure 6.8 and Figure 6.9, where Figure 6.8 illustrates the power flow of the field at the modulator when the energy exchange term is positive, while Figure 6.9 is a power flow diagram of the field at the modulator given that the energy exchange term is negative.

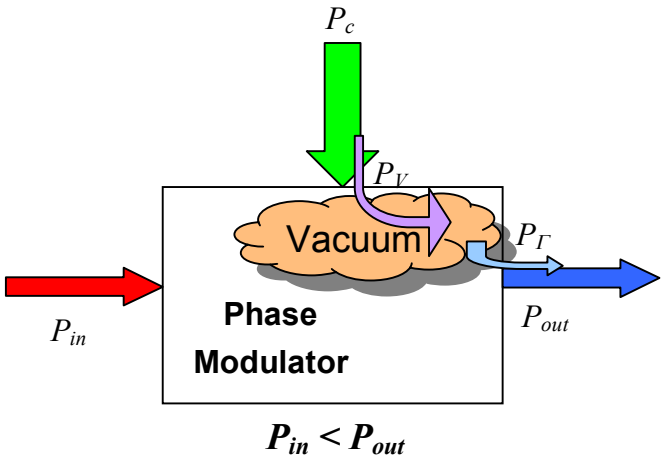

Figure 6.8: Power flow of optical field at the modulator (Energy exchange term positive).

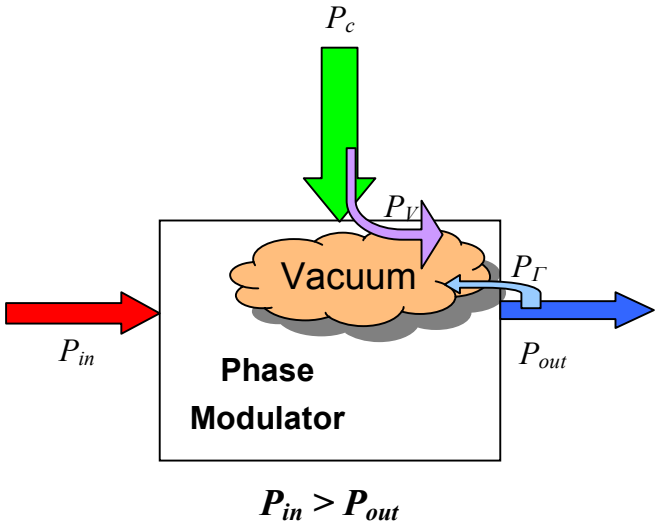

Figure 6.9: Power flow of the optical field at the modulator (Energy exchange term negative).

The interaction between the control signal and the optical field in the modulator is characterized by the purple arrow in Figure 6.8 and Figure 6.9, in which a small portion of the power from the control signal, P_V, excites the vacuum state of the field via. the modulator which then gives rise to the power flow difference, P_Γ, between the input and the output of the modulator. The oscillating nature of the energy exchange term means that there are repeating cycles of energy storage into and release from the modulating medium, driven by the control signal. This is analogous to energy storage and release by a driven LC circuit in which the energy in the system oscillates between the inductor (L) and capacitor (C), as shown in Figure 6.10. S

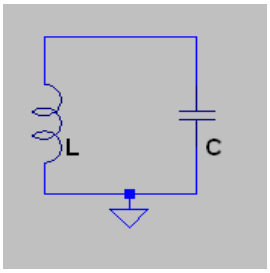

Figure 6.10: LC Circuit analogy.

6.3 Detection of Optical Field

In this Section, we shall consider the direct detection response for unmodulated and modulated optical field. The detector response will be determined from the expression of signal mean and noise variance of the detected field. By comparing the detector response of unmodulated and modulated field, the impact of photon creation from modulator due to phase modulation can be determined. In order to identify this impact and simplify the problem, we have made the following assumptions:

1. The receiver is shot noise limited. Other noises such as dark current noise, relative intensity noise and thermal noise are neglected in this analysis.
2. The modulator is lossless.
3. The photodiode is ideal in which the conversion between photons and photoelectrons is maximized within the passband of the photodiode.

6.3.1 Direct Detection of Unmodulated Field

In this Subsection, the direct detection response for unmodulated field will be determined. A direct detection system is considered because it is one of the simplest detection schemes. The configuration of a back-to-back direct detection system is shown in Figure 6.11, in which the optical field generated from the transmit laser, is directly fed into the receiver. We use the term 'back-to-back' to name the configuration with the receiver located immediately next to the transmitter, thus the distance between transmit laser and direct detection receiver is negligible i.e. $d \approx 0\ m$ in Figure 6.11.

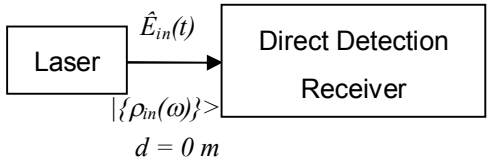

Figure 6.11: Direct detection setup for the detection of unmodulated optical field.

The configuration of the direct detection receiver is shown in Figure 6.12.

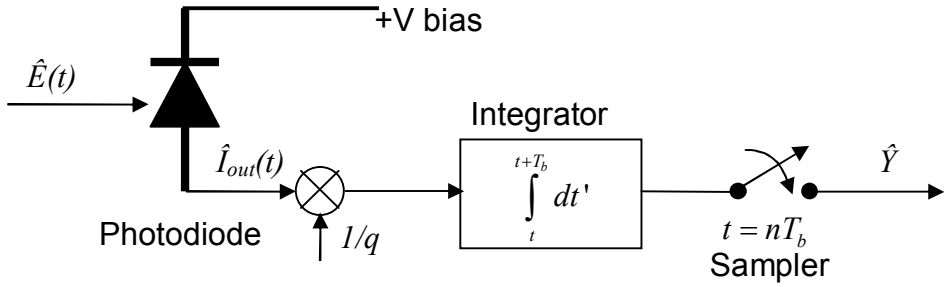

Figure 6.12: Configuration of the direct detection receiver.

The direct detection receiver consists of three important components, a photodiode, an integrator and a sampler. The photodiode converts the incoming photons from the optical field into photoelectrons, and thus the power of optical field gives rise to an electrical current. The integrator accumulates the photoelectrons over some time interval, while the sampler samples the photoelectrons accumulated during the measurement/detection time interval.

A photodiode behaves as a band-pass filter (BPF) which has a lower and upper cutoff frequency. This implies the photoelectric process i.e. conversion of photons to electrons, will take place only over a finite range of photon energies [25]. Throughout this chapter, an InGaAs photodiode is considered, where the lower limit *3 dB* frequency is $\omega_L = 1.1*10^{15}\ rad\ s^{-1}$, while the upper limit *3 dB* frequency is $\omega_U = 1.88*10^{15}\ rad\ s^{-1}$ [25]. Therefore, the passband (3 dB bandwidth) of the photodiode is

$B = \omega_U - \omega_L = 7.8*10^{14}\ rad\ s^{-1}$. In order to simplify the analysis, we assume the InGaAs photodiode has an ideal BPF response. Thus, the frequency response $\eta(\omega)$ is *1* within the passband of the photodiode, and *0* outside the photodiode passband. The signal frequency ω_S lies within the passband of the photodiode so that the field can be detected at maximum efficiency. A plot of the frequency response for an ideal InGaAs photodiode is shown in Figure 6.13.

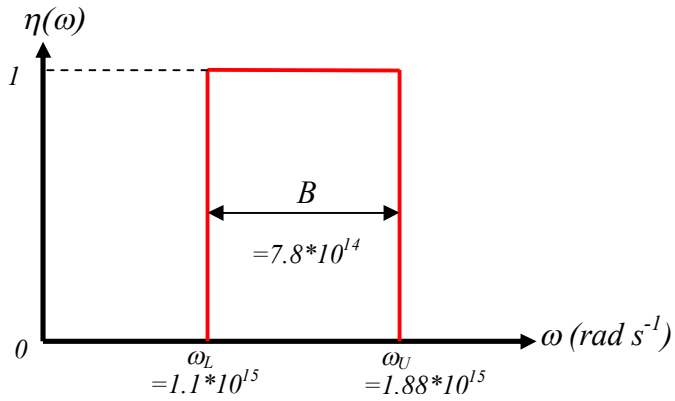

Figure 6.13: Frequency response of the ideal InGaAs photodiode.

For an ideal photodiode, the photocurrent operator associated with the detection of unmodulated field $\hat{I}_{in}(t)$ is defined as [33]

$$\begin{aligned}\hat{I}_{in}(t) &= 2\varepsilon_0 c_0 A \int_0^\infty \int_0^\infty \left(\frac{\eta(\omega) q}{\hbar\omega}\right)^{1/2} \left(\frac{\eta(\omega') q}{\hbar\omega'}\right)^{1/2} \hat{e}_{in}^{-}(\omega,t)\hat{e}_{in}^{+}(\omega',t) d\omega d\omega' \\ &= 2\varepsilon_0 c_0 A \int_0^\infty \int_0^\infty R^{1/2}(\omega) R^{1/2}(\omega') \hat{e}_{in}^{-}(\omega,t)\hat{e}_{in}^{+}(\omega',t) d\omega d\omega'\end{aligned} \tag{6.29}$$

where $R(\omega)$ is the responsitivity of a perfect photodiode and has the expression $R(\omega) = \eta(\omega)q/\hbar\omega$, where q is the charge of the electron and has the value $q = 1.6*10^{-19}\ C$. By expressing $\hat{e}_{in}^{+}(\omega,t)$ and $\hat{e}_{in}^{-}(\omega,t)$ in terms of unmodulated annihilation and creation operator $\hat{a}(\omega)$ and $\hat{a}^{+}(\omega)$, using Equation (6.12) and Equation (6.8), respectively, and applying $\hat{a}(\omega)$ and $\hat{a}^{+}(\omega)$ onto the bra-ket state vector $|\{\rho_{in}(\omega)\}>$ and

$<\{\rho_{in}(\omega)\}|$, we find with the help of eigen-equation (6.5) that the expectation value of the photocurrent $<\hat{I}_{in}(t)>$ from the detector is

$$\begin{aligned}\left\langle \hat{I}_{in}(t)\right\rangle &= \left\langle \{\rho_{in}(\omega)\}\right| \frac{q}{2\pi}\int_0^\infty\int_0^\infty \hat{a}^+(\omega)\hat{a}(\omega')\exp\left(i(\omega-\omega')t\right)d\omega d\omega' \left|\{\rho_{in}(\omega)\}\right\rangle \\ &= qF_S\end{aligned} \tag{6.30}$$

As the photocurrent enters the integrator, photoelectrons will be accumulated. After some measuring time period T_M, the number of photoelectrons accumulated will be sampled. After the sampling process, the photoelectrons stored in the device will be discharged. We shall introduce a detection operator $\hat{Y}_{in}$ to characterize the number of photoelectrons accumulated, where we have

$$\hat{Y}_{in}(T_S, T_M) = \frac{1}{q}\int_{T_S}^{T_S+T_M} \hat{I}_{in}(t)\,dt \tag{6.31}$$

where T_S is the start time of a measurement, and T_M is the duration of the measurement time. By expressing $\hat{I}_{in}(t)$ in terms of $\hat{a}(\omega)$ and $\hat{a}^+(\omega)$ from Equation (6.30), and operating the associated operator onto the continuum coherent state vector in Equation (6.5), the mean of photoelectron count detected by the receiver from an unmodulated optical field over the measurement/detection time T_M is given by

$$\begin{aligned}\left\langle \hat{Y}_{in}(T_S,T_M)\right\rangle &= \frac{1}{q}\frac{q}{2\pi}\int_{T_S}^{T_S+T_M} dt\int_0^\infty\int_0^\infty \left\langle \{\rho_{in}(\omega)\}\right|\hat{a}^+(\omega)\hat{a}(\omega')\left|\{\rho_{in}(\omega)\}\right\rangle \exp\left(i(\omega-\omega')t\right)d\omega d\omega' \\ &= F_S T_M\end{aligned} \tag{6.32}$$

where F_S is the mean photon flux. $<\hat{Y}_{in}(T_S,T_M)>$ represents the mean signal strength of unmodulated field and expression (6.32) shows $<\hat{Y}_{in}(T_S,T_M)>$ corresponds to the mean photon number count in time interval T_M.

In quantum optics, the noise variance of the number of photoelectrons in the detector current due to an unmodulated optical field can be readily obtained from the expression [33]

$$\left[\Delta Y_{in}\left(T_S,T_M\right)\right]^2=\left\langle \hat{Y}_{in}{}^2\left(T_S,T_M\right)\right\rangle-\left\langle \hat{Y}_{in}\left(T_S,T_M\right)\right\rangle^2 \tag{6.33}$$

By employing the definition of $\hat{Y}_{in}\left(T_S,T_M\right)$ in Equation (6.31) and expressing it in terms of $\hat{a}(\omega)$ and $\hat{a}^+(\omega)$ using expression (6.29), (6.12) and (6.8), making use of the commutation relation in Equation (6.9) and the eigen-equation in Equation (6.5), as well as performing the frequency integration, we obtain after some laborious algebraic manipulation,

$$\begin{aligned}
\left\langle \hat{Y}_{in}{}^2\left(T_S,T_M\right)\right\rangle=&\left(\frac{2\varepsilon_0c_0A}{q}\right)^2\int_{T_S}^{2T_S+T_M}dt\int_{T_S}^{T_S+T_M}dt'\int_0^\infty d\omega\int_0^\infty d\omega'\int_0^\infty d\omega''\int_0^\infty d\omega'''R^{1/2}(\omega)R^{1/2}(\omega')R^{1/2}(\omega'')R^{1/2}(\omega''')\\
&*\left\langle\left\{\rho_{in}(\omega)\right\}\left|\hat{e}_{in}^{\ -}(\omega,t)\hat{e}_{in}^{\ +}(\omega',t)\hat{e}_{in}^{\ -}(\omega'',t')\hat{e}_{in}^{\ +}(\omega''',t')\right|\left\{\rho_{in}(\omega)\right\}\right\rangle\\
\approx&\left(\frac{2\varepsilon_0c_0A}{q}\right)^2\int_{T_S}^{2T_S+T_M}dt'\int_{T_S}^{T_S+T_M}dt''\int_0^\infty\int_0^\infty\int_0^\infty\int_0^\infty R^{1/2}(\omega)R^{1/2}(\omega')R^{1/2}(\omega'')R^{1/2}(\omega''')\left\langle\hat{e}_{in}^{\ -}(\omega,t)\hat{e}_{in}^{\ -}(\omega'',t')\hat{e}_{in}^{\ +}(\omega',t)\hat{e}_{in}^{\ +}(\omega''',t')\right\rangle d\omega d\omega' d\omega'' d\omega'''\\
&+2\varepsilon_0c_0A\left\{\int_t^{t+T_M}dt'\int_t^{t+T_M}dt''\int_0^\infty\int_0^\infty d\omega d\omega'''R^{1/2}(\omega)R^{1/2}(\omega''')\left\langle\left\{\rho_{in}(\omega)\right\}\left|\hat{e}_{in}^{\ -}(\omega,t)\hat{e}_{in}^{\ +}(\omega''',t')\right|\left\{\rho_{in}(\omega)\right\}\right\rangle\delta(t'-t'')\right.\\
=&\left\langle\hat{Y}_{in}(T_S,T_M)\right\rangle^2+\left\langle\hat{Y}_{in}(T_S,T_M)\right\rangle
\end{aligned} \tag{6.34}$$

The noise variance calculation in (6.34) is obtained by using the approximation

$$\int_0^\infty\exp\left[i\omega\left(t-t'\right)+i\left(\varphi_{SN}\left(\omega,t\right)-\varphi_{SN}\left(\omega,t'\right)\right)\right]d\omega\approx 2\pi\delta\left(t-t'\right) \tag{6.35}$$

This approximation is reasonable as the bandwidth of the single mode laser is generally much smaller than the signal frequency ω_S [1, 33, 35] i.e. $2\pi\Delta\nu << \omega_S$, as shown in Figure 6.1. The Dirac delta function in Equation (6.35) implies the statistics of phase noise variance is roughly time independent i.e. variance at time t_1 is independent on the variance at time t_2. By substituting expression (6.31) into Equation (6.34), the noise variance detected from unmodulated field is given by

$$\begin{aligned}
\left[\Delta Y_{in}\left(T_S,T_M\right)\right]^2&=\left\langle\hat{Y}_{in}\left(T_S,T_M\right)\right\rangle\\
&=F_ST_M
\end{aligned} \tag{6.36}$$

Notice that the mean number of photoelectrons detected in Equation (6.32) is equal to the variance of the photoelectron count given in Equation (6.36). In Chapter 3, we have stated if the field is prepared in coherent state, the mean photon number and the

photon number variance are equal. Since each photoelectron is generated as a consequence of the incoming photon, thus we can conclude the state of the unmodulated field is characterized by continuum coherent state. In addition, the mean and variance in Equation (6.32) and Equation (6.36) is independent on the time T_S when the measurement is taken, which implies the arrival of photoelectron is a stationary random process [22].

According to [33, 35], the SNR of the unmodulated field is defined as

$$SNR_{in} = \frac{\left\langle \hat{Y}_{in}(t) \right\rangle^2}{\left[\Delta Y_{in}(t) \right]^2} \tag{6.37}$$

As a result, by substituting expression (6.32) and (6.36) into Equation (6.37), the SNR of the unmodulated field is given by

$$SNR_{in} = F_S T_M = \left\langle \hat{Y}_{in}(t) \right\rangle \tag{6.38}$$

Expression (6.38) shows the SNR of the unmodulated field corresponds to the mean number of photoelectrons detected.

6.3.2 Direct Detection of Modulated Field

In this Subsection, the direct detection response for modulated field will be determined. Figure 6.14 shows an optical system for the detection of a modulated optical field, in which the receiver is located immediately next to the transmitter (back to back).

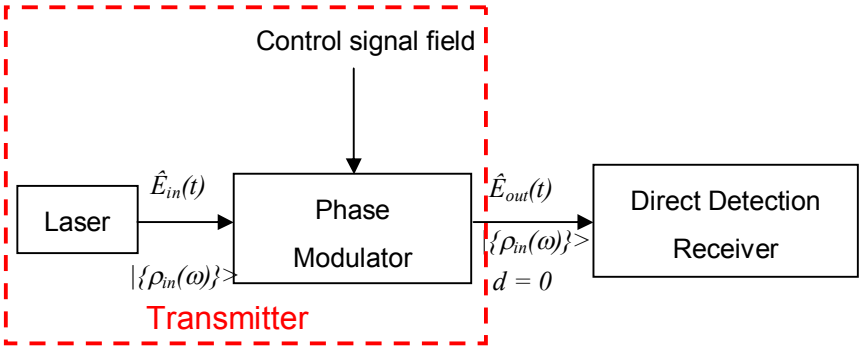

Figure 6.14: Direct detection setup for the detection of modulated optical field.

Notice that the configuration in Figure 6.14 is very similar to Figure 6.12, except that a phase modulator is placed in between the transmit laser and the direct detection receiver so that the optical field is phase modulated before it reaches the detector. If extra photons are created, an additional number of photoelectrons will be detected at the receiver, and likewise the photoelectron count will reduce if photons are removed from the incoming signal. For an ideal photodiode, the photocurrent operator associated to the detection of phase modulated field $\hat{I}_{out}(t)$ is [33]

$$\hat{I}_{out}(t) = 2\varepsilon_0 c_0 A \int_0^\infty \int_0^\infty R^{1/2}(\omega)\hat{e}_{out}^{-}(\omega,t)R^{1/2}(\omega')\hat{e}_{out}^{+}(\omega',t)d\omega d\omega' \qquad (6.39)$$

where $\hat{e}_{out}^{+}(\omega,t)$ is related to the modulated field annihilation operator $\hat{b}(\omega,t)$, as indicated in expression (6.14). By expressing $\hat{e}_{out}^{+}(\omega,t)$ in terms of unmodulated annihilation and creation operator $\hat{a}(\omega)$ and $\hat{a}^{+}(\omega)$, from expression (6.14) and (6.17), using the commutation relation in expression (6.3), and finally applying $\hat{a}(\omega)$ and $\hat{a}^{+}(\omega)$ onto the state vector $|\{\rho_{in}(\omega)\}>$ and $<\{\rho_{in}(\omega)\}|$ with the help of eigen-equation (6.5), the expectation value of the photocurrent $<\hat{I}_{out}(t)>$ is

$$\begin{aligned}\left\langle \hat{I}_{out}(t)\right\rangle &= \left\langle \{\rho_{in}(\omega)\}\left|\frac{q}{2\pi}\int_0^\infty\int_0^\infty \hat{b}^+(\omega,t)\hat{b}(\omega',t)\exp\left(i\left[W(\omega,t)-W(\omega',t)\right]\right)d\omega d\omega'\right|\{\rho_{in}(\omega)\}\right\rangle \\ &= qF_S\left\{1+2\left|\beta(\omega_S,t)\right|^2+2\sqrt{1+\left|\beta(\omega_S,t)\right|^2}\left|\beta(\omega_S,t)\right|\cos\left[2\left(\theta_S+\varphi_{SN}(\omega_S,t)\right)+A(\omega_S,t)+B(\omega_S,t)\right]\right. \\ &\quad \left.+\frac{q}{2\pi}\int_{\omega_L}^{\omega_U}\left|\beta(\omega,t)\right|^2 d\omega\right\}\end{aligned} \tag{6.40}$$

The expression in (6.40) is almost identical to the expression of the power flow for modulated optical field in Equation (6.28). However, there is one subtle difference between the last term of expression (6.40) and (6.28). The integration limits of the spontaneous emission term (last term) in Equation (6.28) ranges from frequency -∞ to ∞. In contrast, integration limits of expression (6.40) ranges from ω_L *to* ω_U because the photodiode is bandwidth limited, as shown in Figure 6.13.

Similar to the unmodulated field detection analysis in Subsection 6.3.1, we introduce a detection operator $\hat{Y}_{out}(T_S, T_M)$ to characterize the number of photoelectrons detected from the phase modulated field, which is defined as

$$\hat{Y}_{out}\left(T_S, T_M\right) = \frac{1}{q}\int_{T_S}^{T_S+T_M} \hat{I}_{out}\left(t\right)dt \tag{6.41}$$

where T_S is the start time of a measurement. By expressing $\hat{I}_{out}(t)$ in terms of $\hat{a}(\omega)$ and $\hat{a}^+(\omega)$ using expressions (6.39), (6.14), (6.17) and (6.8), and applying $\hat{a}(\omega)$ and $\hat{a}^+(\omega)$ onto the bra-ket continuum coherent state vector, $<\{\rho_{in}(\omega)\}|$ and $|\{\rho_{in}(\omega)\}>$ respectively, the expectation value of the number of photoelectrons detected by the receiver is given by

$$\begin{aligned}\left\langle \hat{Y}_{out}\left(T_S,T_M\right)\right\rangle &= F_S T_M + \int_{T_S}^{T_S+T_M}\left\{2F_S\left[\left|\beta(\omega_S,t)\right|^2+\sqrt{1+\left|\beta(\omega_S,t)\right|^2}\left|\beta(\omega_S,t)\right|\cos\left[2\left(\theta_S+\varphi_{SN}(\omega_S,t)\right)+A(\omega_S,t)-B(\omega_S,t)\right]\right]\right. \\ &\quad \left.+\frac{1}{2\pi}\int_{\omega_L}^{\omega_U}\left|\beta(\omega,t)\right|^2 d\omega\right\}dt\end{aligned} \tag{6.42}$$

The first term in Equation (6.42) corresponds to the photoelectrons detected from the unmodulated optical field. As a result, the remaining terms that is dependent on the

Bogoliubov coefficients $\beta(\omega,t)$, appears as a consequence of photon creation/annihilation from the modulator during the modulation process.

The effect of photon creation from modulator in optical detection can be clarified by computing the difference between mean photoelectrons resulting from modulated and input unmodulated fields. The difference can be expressed as

$$\begin{aligned}\delta Y &= \left\langle \hat{Y}_{out} \right\rangle - \left\langle \hat{Y}_{in} \right\rangle \\ &= \int_{T_S}^{T_S+T_M} 2F_S \left[\left|\beta(\omega_S,t)\right|^2 + \sqrt{1+\left|\beta(\omega_S,t)\right|^2}\,\left|\beta(\omega_S,t)\right| \cos\left[2\left(\theta_S + \varphi_{SN}(\omega_S,t)\right) + A(\omega_S,t) - B(\omega_S,t)\right]\right] dt \\ &\quad + \frac{1}{2\pi}\int_{T_S}^{T_S+T_M} dt \int_{\omega_L}^{\omega_U} \left|\beta(\omega,t)\right|^2 d\omega\end{aligned} \tag{6.43}$$

From Equation (6.43), we can identify the difference in mean photoelectron count is governed by $|\beta(\omega,t)|$ and the photon flux of the optical field F_S. By comparing δY in Equation (6.43) with the $\beta(\omega,t)$ components from the power flow expression in Equation (6.28), we can identify the first term in Equation (6.43) corresponds to the effect of stimulated emission out of the modulator as the spontaneous process $|\beta(\omega,t)|^2$ increases by a factor of F_S at an input frequency of ω_S. The second term in Equation (6.43) is associated with the energy exchange between the optical field and the modulator as its magnitude is dependent on the phase of the Bogoliubov coefficients. The last term in Equation (6.43) corresponds to the phenomenon of spontaneous emission out of the modulator because it is independent on F_S, which implies the process is not limited to the input frequency of the optical field ω_S.

The noise variance of the number of photoelectrons detected from the modulated can be readily obtain from the expression [33, 35]

$$\left[\Delta Y_{out}\left(T_S,T_M\right)\right]^2 = \left\langle \hat{Y}_{out}{}^2\left(T_S,T_M\right)\right\rangle - \left\langle \hat{Y}_{out}\left(T_S,T_M\right)\right\rangle^2 \tag{6.44}$$

By employing the definition of $\hat{Y}_{out}\left(T_S,T_M\right)$ in Equation (6.42) and expressing it in terms of $\hat{a}(\omega)$ and $\hat{a}^+(\omega)$ using expressions (6.41), (6.14) and (6.8), making use of the commutation relation in (6.9) and the eigen-equation in (6.5), as well as performing

the frequency integration, we obtain the expression of noise variance after some laborious algebraic manipulation,

$$\begin{aligned}\left[\Delta Y_{out}(T_S,T_M)\right]^2 &= \left(\frac{2\varepsilon_0 c_0 A}{q}\right)^2 \int_{T_S}^{T_S+T_M} dt \int_{T_S}^{T_S+T_M} dt' \int_0^\infty d\omega \int_0^\infty d\omega' \int_0^\infty d\omega'' \int_0^\infty d\omega''' R^{1/2}(\omega) R^{1/2}(\omega') R^{1/2}(\omega'') R^{1/2}(\omega''') \\ &\quad * \left\langle \left\{ \rho_{in}(\omega) \right\} \left| \hat{e}_{out}^{-}(\omega,t) \hat{e}_{out}^{+}(\omega',t) \hat{e}_{out}^{-}(\omega'',t') \hat{e}_{out}^{+}(\omega''',t') \right| \left\{ \rho_{in}(\omega) \right\} \right\rangle \\ &= F_S T_M + 2\left(\frac{1}{2\pi} \int_0^{T_S+T_M} dt \int_{\omega_L}^{\omega_U} \left|\beta(\omega,t)\right|^2 d\omega \right)^2 + \frac{1}{2\pi} \int_{T_S}^{T_S+T_M} dt \int_{\omega_L}^{\omega_U} \left|\beta(\omega,t)\right|^2 d\omega d\omega''' + F_S \left\{ \int_{T_S}^{T_S+T_M} 2\left[4\left|\beta(\omega_S,t)\right|^2 + 3 \right] \left|\beta(\omega_S,t)\right|^2 \right. \\ &\quad \left. + 2\left(4\left|\beta(\omega_S,t)\right|^2 + 1 \right) \left|\beta(\omega_S,t)\right| \sqrt{1+\left|\beta(\omega_S,t)\right|^2} \cos\left[2\left[\theta_S + \varphi_{SN}(\omega_S,t) \right] + A(\omega_S,t) + B(\omega_S,t) \right] \right\}\end{aligned} \tag{6.45}$$

where expression (6.45) is obtained by using the approximation

$$\int_0^\infty \exp\left[iW(\omega,t) - iW(\omega,t') + i\left(\varphi_{SN}(\omega,t) - \varphi_{SN}(\omega,t') \right) \right] d\omega \approx 2\pi\delta(t-t') \tag{6.46}$$

This approximation is reasonable when the frequency bandwidth of $W(\omega,t)$, denoted by ω_M, and the bandwidth of the laser phase noise $2\pi\Delta\nu$, is much smaller than the signal frequency (center frequency) i.e. $\omega_S >> \omega_M + 2\pi\Delta\nu$ [1, 22 - 24].

The expression of signal amplitude $<\hat{Y}_{out}(T_S,T_M)>$, in Equation (6.42), is no longer equivalent to the noise variance $[\Delta\hat{Y}_{out}(T_S,T_M)>]^2$, in Equation (6.45). As a result, the state of modulated field cannot be characterized as a coherent state since its statistical nature is different from the unmodulated field. In fact as we shall see in Section 6.4, the statistical nature expressed in Equation (6.42) and (6.45) can be described by field prepared in a two-photon coherent state [50]. The difference between the mean photoelectron number and the variance of photoelectron is

$$\begin{aligned}&\left(\Delta Y_{out}(T_S,T_M)\right)^2 - \left\langle \hat{Y}_{out}(T_S,T_M) \right\rangle \\ &= F_S \left\{ \int_{T_S}^{T_S+T_M} 4\left[2\left|\beta(\omega_S,t)\right|^2 + 1 \right] \left|\beta(\omega_S,t)\right|^2 + 8\left|\beta(\omega_S,t)\right|^3 \sqrt{1+\left|\beta(\omega_S,t)\right|^2} \cos\left[2\left[\theta_S + \varphi_{SN}(\omega_S,t) \right] + A(\omega_S,t) + B(\omega_S,t) \right] \right. \\ &\quad \left. + 2\left(\frac{1}{2\pi} \int_{T_S}^{T_S+T_M} dt \int_{\omega_L}^{\omega_U} \left|\beta(\omega,t)\right|^2 d\omega \right)^2 \right.\end{aligned} \tag{6.47}$$

Unlike the statistical nature of the unmodulated field, the mean and variance in Equation (6.42) and (6.45) depends on the start time of measurement i.e. T_S dependent,

which implies the arrival of photoelectron is a non-stationary random process when a modulated field is detected [22].

The mean signal amplitude detected expressed in Equation (6.42) and the noise variance detected from the modulated field, in Equation (6.45), consist of terms that are phase dependent. Furthermore, this phase component is dependent on random variable $\phi_{SN}(\omega,t)$. The coherence time t_c is a measure of the rate of phase drift due to the phase noise. The transmit laser coherence time is related to the *3 dB* laser linewidth by [1, 33]

$$t_c = \frac{1}{\pi \Delta \nu} \tag{6.48}$$

Provided the measurement time T_M is much greater than the coherence time in (6.48) (i.e. $T_M >> t_c$), we can assume the probability density function (PDF) of $\phi_{SN}(\omega_S,t)$ is uniformly distributed between *0* and 2π for which we have,

$$p_{\varphi_{SN}}(\varphi_{SN}) = \frac{1}{2\pi} \qquad 0 \le \varphi_{SN} < 2\pi \tag{6.49}$$

where

$$\int_0^{2\pi} p_{\varphi_{SN}}(\varphi_{SN}) d\varphi_{SN} = 1 \tag{6.50}$$

Because the cosine component in expressions (6.42) and (6.45) are dependent on $\phi_{SN}(\omega_S,t)$, thus it is also a random variable. We shall define the random variable U as

$$U = \cos\left[2\left(\theta_S + \varphi_{SN}(\omega_S,t)\right) + A(\omega_S,t) + B(\omega_S,t)\right] \tag{6.51}$$

By using the expression of $p_{\varphi_{SN}}(\varphi_{SN})$ in Equation (6.49), the PDF of random variable U is expressed as [34],

$$p_U(U) = \frac{2}{\pi\sqrt{1-U^2}} \qquad |U| < 1 \tag{6.52}$$

in which,

$$\int_{-1}^{1} p_U(U)\,dU = 1 \tag{6.53}$$

The time averaged value of *U(t)* is evaluated as [34]

$$\overline{U(t)} = \int_{-1}^{1} U p_U(U)\,dU = 0 \tag{6.54}$$

where the overbar denotes the long time average.

As we shall see later in Section 6.5, the product, $|\beta(\omega_S,t)|F_S >> \max[\beta(\omega,t)]B$, thus the terms that is independent of F_S can be neglected from the mean expression in (6.42) and the variance expression in (6.45). Therefore, by using the result in Equation (6.54), we can simplify the expression of long time averaged signal and the noise amplitude in expression (6.42) and (6.45) into

$$\overline{\left\langle \hat{Y}_{out}(T_S,T_M)\right\rangle} \approx F_S\left(T_M + \int_{T_S}^{T_S+T_M} 2\left|\beta(\omega_S,t)\right|^2 dt\right) \tag{6.55}$$

$$\overline{\left[\Delta Y_{out}(T_S,T_M)\right]^2} \approx F_S\left(T_M + \int_{T_S}^{T_S+T_M} 2\left[4\left|\beta(\omega_S,t)\right|^2+3\right]\left|\beta(\omega_S,t)\right|^2 dt\right) \tag{6.56}$$

where the overbar denotes long time averaged since $T_M >> t_c$. Expression (6.55) and (6.56) shows the effect of photon creation out of the modulator increases both signal and noise variance as $|\beta(\omega_S,t)|^2 > 0$. Using expression (6.42) and (6.45) the approximate SNR expression for modulated field can be deduced as

$$\begin{aligned} SNR_{out} &= \frac{\overline{\left\langle \hat{Y}_{out}(t)\right\rangle}^2}{\overline{\left[\Delta Y_{out}(t)\right]^2}} \\ &= \frac{F_S\left(T_M + \int_{T_S}^{T_S+T_M} 2\left|\beta(\omega_S,t')\right|^2 + \sqrt{1+\left|\beta(\omega_S,t')\right|^2}\left|\beta(\omega_S,t')\right|\cos\left[2\left(\theta_S+\varphi_{SN}(\omega_S,t')\right)+A(\omega_S,t')-B(\omega_S,t')\right]dt'\right)^2}{T_M + \int_{T_S}^{T_S+T_M} 2\left[4\left|\beta(\omega_S,t')\right|^2+3\right]\left|\beta(\omega_S,t')\right|^2 dt' + 2\left(4\left|\beta(\omega_S,t)\right|^2+1\right)\left|\beta(\omega_S,t)\right|\sqrt{1+\left|\beta(\omega_S,t)\right|^2}\cos\left[2\left[\theta_S+\varphi_{SN}(\omega_S,t)\right]+A(\omega_S,t)+B(\omega_S,t)\right]} \\ &\approx F_S T_M - \frac{2}{T_M}\int_{T_S}^{T_S+T_M}\left|\beta(\omega_S,t')\right|^2 dt' \end{aligned} \tag{6.57}$$

In the last line of Equation (6.57), we have used the result in Equation (6.54), neglect the terms that are of higher order to $|\beta(\omega_S,t)|^2$ given that $|\beta(\omega_S,t)| << 1$ (see Section 6.5), as well as using the first order Taylor series approximation. Using expression (6.57) and (6.38), the differences between the SNR of the modulated field and the unmodulated field is

$$\begin{aligned}\Delta SNR &= SNR_{in} - SNR_{out} \\ &= \frac{2}{T_M}\int_{t}^{t+T_M} \left|\beta\left(\omega_S, t'\right)\right|^2 dt'\end{aligned} \tag{6.58}$$

A positive value of SNR difference in (6.58) implies the **SNR of unmodulated field is greater than the SNR of modulated field**. This implies the increase in noise power is greater than the increase in signal power due to the effect of photon creation from modulator.

6.4 State Evolution of Modulated Field

In Section 6.3, we have shown the effect of photon creation increases both noise variance and the mean photoelectron number in the detection process. In fact the Equation (6.47) shows the variance of the photoelectron count is greater than the mean of the photoelectron count. As a result, the modulated field cannot be characterized by coherent state during the period when photons are created out of the modulator i.e. $\beta(\omega,t) \neq 0$. This is different to the result presented by [9], which claims the modulated field is described by a tensor product of coherent states. This difference appears because their model did not include the effect of photon creation from modulator. In this Section, we shall determine the time evolution of the state of modulated field by including the effect of photon creation from the modulator.

By considering the commutation relation between $\hat{a}_{\varphi}(\omega,t)$ and $\hat{a}_{\varphi}^{+}(\omega,t)$ of the input field in Equation (6.3), we can identify it is equivalent to that of $\hat{b}(\omega,t)$ and $\hat{b}^{+}(\omega,t)$ in expression (6.22). Therefore the Bogoliubov transformation in expression (6.17) is a linear canonical transformation [50]. For simplicity of the analysis, we neglect the effect of phase noise so that $\hat{a}_{\varphi}(\omega,t)$ reduces to $\hat{a}(\omega)$ using Equation (6.8). According to a theorem from Von Neumann, every canonical transformation involving finitely many particle labels can be represented as a unitary transformation, in which $\hat{a}(\omega)$ and $\hat{a}^{+}(\omega)$, is related to $\hat{b}(\omega,t)$ and $\hat{b}^{+}(\omega,t)$, by [51, 52]

$$\hat{b}(\omega,t)\exp\left(iA(\omega,t)\right)=\hat{s}\left[\zeta(\omega,t)\right]\hat{a}(\omega)\hat{s}^{+}\left[\zeta(\omega,t)\right] \tag{6.59}$$

$$\hat{b}^{+}(\omega,t)\exp\left(-iA(\omega,t)\right)=\hat{s}\left[\zeta(\omega,t)\right]\hat{a}^{+}(\omega)\hat{s}^{+}\left[\zeta(\omega,t)\right] \tag{6.60}$$

where $A(\omega,t)$ is the phase of $\alpha(\omega,t)$ expressed in (6.18), $\hat{s}[\zeta(\omega,t)]$ is the continuum squeezed operator. $\zeta(\omega,t)$ is the squeezed wavepacket function that can be expressed as [33, 46]

$$\zeta(\omega,t)=z(\omega,t)\exp\left[i\vartheta(\omega,t)\right] \tag{6.61}$$

The magnitude and phase of the squeeze parameter, $z(\omega,t)$ and $\vartheta(\omega,t)$, is related to the Bogoliubov coefficients by [33]

$$\sinh\left[z(\omega,t)\right]=\left|\beta(\omega,t)\right| \tag{6.62}$$

$$\vartheta(\omega,t)=B(\omega,t)-A(\omega,t) \tag{6.63}$$

where $B(\omega,t)$ is the phase of $\beta(\omega,t)$. In Chapter 4.2, we have shown the Bogliubov coefficients are diagonal and isotropic, therefore the continuum squeezed operator $\hat{s}[\zeta(\omega,t)]$ defined in [33, 46, 53] can be expressed as

$$\hat{s}\left[\{\zeta(\omega,t)\}\right]=\exp\left(\int_{0}^{\infty}\frac{1}{2}\zeta^{*}(\omega,t)\left[\hat{a}(\omega)\right]^{2}-\frac{1}{2}\zeta(\omega,t)\left[\hat{a}^{+}(\omega)\right]^{2}d\omega\right) \tag{6.64}$$

Equation (6.64) shows the squeezed operator is an unitary operator where $\hat{s}(\omega,t)\hat{s}^{+}(\omega,t) = \hat{s}^{+}(\omega,t)\hat{s}(\omega,t) = 1$. From expression (6.61), (6.62) and (6.64), we can see that when $\beta(\omega,t) = 0$, we have $\hat{s}[\zeta(\omega,t)] = 1$.

Assume the modulator is initially in a steady state with $n(t = 0) = n_1$, so that the optical field is unmodulated at $t = 0$. The state of unmodulated field is characterized by the wavepacket function $\rho_{in}(\omega)$ (defined in Equation (6.5)), where the Dirac delta function in expression (6.5) implies the photon flux is associated with the carrier frequency ω_S. In order to determine the mean photon flux of the unmodulated field, it is useful to introduce the continuous mode photon flux operator, which is defined as [33, 46]

$$\widehat{F}_{in} = \frac{1}{2\pi}\int_0^\infty\int_0^\infty \hat{a}^{+}(\omega)\hat{a}(\omega')\,d\omega d\omega' \tag{6.65}$$

The field is modulated for $t > 0$. The modulated phase angle for $t > 0$ is governed by $W(\omega,t)$ that is expressed in Equation (6.15), while the annihilation operator evolves from $\hat{a}(\omega) \to \hat{b}(\omega,t)$. As a result, the photon flux operator for modulated field can be represented by

$$\widehat{F}_{out}(t) = \frac{1}{2\pi}\int_0^\infty\int_0^\infty \hat{b}^{+}(\omega,t)\hat{b}(\omega',t)\exp\left[i\left[W(\omega,t) - W(\omega',t)\right]\right]d\omega d\omega' \tag{6.66}$$

where

$$\widehat{F}_{out}(t=0) = \widehat{F}_{in} = \frac{1}{2\pi}\int_0^\infty\int_0^\infty \hat{a}^{+}(\omega)\hat{a}(\omega')\,d\omega d\omega' \tag{6.67}$$

The time evolution of the state of modulated field can be determined by using the Schrödinger picture. Schrödinger picture is a direct contrast to the Heisenberg picture in which the state of the field evolves with time while the field operator is time independent. The benefit of adopting Schrödinger picture is the probability

distribution that describes the photon arrival statistics can be determined, which is not as clearly shown when Heisenberg picture is adopted. The same answer should be obtained regardless of whether Heisenberg picture or Schrödinger picture is employed. Thus, we have the relation

$$\left\langle \left\{\rho_{in}(\omega)\right\} \middle| \widehat{F}_{out}(t) \middle| \left\{\rho_{in}(\omega)\right\} \right\rangle = \left\langle \left\{\rho^{\zeta}{}_{out}(\omega,t)\right\} \middle| \widehat{F}_{in} \middle| \left\{\rho^{\zeta}{}_{out}(\omega,t)\right\} \right\rangle \qquad (6.68)$$

where $|\rho^{\zeta}{}_{out}(\omega,t)>$ is the state vector of the phase modulated field, $|\{\rho_{in}(\omega)\}>$ is the state vector of unmodulated field (coherent state vector), $\widehat{F}_{in}$ and $\widehat{F}_{out}(t)$ are the photon flux operator for unmodulated and modulated field, respectively. The left hand side of Equation (6.68) is the Heisenberg picture representation in which the time evolution of the field is entirely encapsulated by the operator, while the left hand side of Equation (6.68) is the Schrödinger picture representation in which the time evolution of the field is completely encapsulated by the state vector.

For clarity, we shall divide the derivation of the state of modulated field into two steps. The first step only considers the time evolution of modulated phase angle in which the effect of photon creation is suppressed i.e. $\hat{a}(\omega) = \hat{b}(\omega,t)$. We shall include the effect of photon creation in the second step. By neglecting the effect of photon creation, $\widehat{F}_{out}(t)$ can be expressed as

$$\widehat{F}_{out}(t) = \frac{1}{2\pi}\int_0^{\infty}\int_0^{\infty} \hat{a}(\omega)\hat{a}(\omega')\exp\left[i\left[W(\omega,t) - W(\omega',t)\right]\right]d\omega d\omega' \qquad (6.69)$$

The mean photon flux can therefore be expressed as,

$$\begin{aligned}
&\left\langle \left\{\rho_{in}(\omega)\right\} \middle| \widehat{F}_{out}(t) \middle| \left\{\rho_{in}(\omega)\right\} \right\rangle \\
&= \frac{1}{2\pi}\int_0^{\infty}\int_0^{\infty} \left\langle \left\{\rho_{in}(\omega)\right\} \middle| \exp\left[iW(\omega,t)\right]\hat{a}^{+}(\omega)\hat{a}(\omega')\exp\left[-iW(\omega',t)\right] \middle| \left\{\rho_{in}(\omega)\right\} \right\rangle d\omega d\omega' \\
&= \frac{1}{2\pi}\int_0^{\infty}\int_0^{\infty} \left\langle \left\{\rho_{out}(\omega,t)\right\} \middle| \hat{a}^{+}(\omega)\hat{a}(\omega') \middle| \left\{\rho_{out}(\omega,t)\right\} \right\rangle d\omega d\omega' \\
&= \left\langle \left\{\rho_{out}(\omega,t)\right\} \middle| \widehat{F}_{in} \middle| \left\{\rho_{out}(\omega,t)\right\} \right\rangle
\end{aligned} \qquad (6.70)$$

By comparing the second line and third line of Equation (6.70), we can deduce the state of modulated field $|\{\rho_{out}(\omega,t)\}\rangle$, with the effect of photon creation suppressed, is related to the state of unmodulated field $|\{\rho_{in}(\omega)\}\rangle$ by

$$\begin{aligned}\left|\{\rho_{out}(\omega,t)\}\right\rangle &= \exp\left[-iW(\omega,t)\right]\left|\{\rho_{in}(\omega)\}\right\rangle \\ &= \exp\left[(2\pi F_S)^{1/2}\left[\exp\left(iW(\omega_S,t)-i\theta\right)\hat{a}^{+}(\omega_S)-\exp\left(-iW(\omega_S,t)+i\theta\right)\hat{a}(\omega_S)\right]\right]|0\rangle\end{aligned} \tag{6.71}$$

In the second line of Equation (6.71), we have expanded $|\{\rho_{in}(\omega)\}\rangle$ using expression (6.1) and (6.5). Notice that in the second line of expression (6.71), the frequency argument of the modulated phase angle $W(\omega,t)$ and the annihilation and creation operator is associated with signal frequency ω_S. By representing $exp[-iW(\omega_S,t)]$ as an integral of complex exponential, we have

$$\exp\left[iW(\omega_S,t)\right]=\int_0^{\infty}\Lambda(\omega_S,\omega')\exp\left(-i\omega' t\right)d\omega' \tag{6.72}$$

$\Lambda(\omega_S,\omega')$ is the normalized classical spectral amplitude for a single frequency phase modulated optical field, which can be determined by computing the Fourier transform of $exp[iW(\omega_S,t)]$. $\Lambda(\omega_S,\omega')$, consist of two frequency arguments, ω_S and ω'. The first argument represents the input carrier field frequency, and the second argument represents the frequency profile around the carrier. $\Lambda(\omega_S,\omega')$ is a normalized function because $exp[-iW(w_S,t)]*exp[iW(w_S,t)] = 1$, therefore by expressing $exp[iW(\omega_S,t)]$ in terms of $\Lambda(\omega_S,\omega')$ from Equation (6.72), we have the normalization condition

$$\int_0^{\infty}\left|\Lambda(\omega_S,\omega')\right|^2 d\omega=1 \tag{6.73}$$

The output state vector in Equation (6.71) can be rewritten into the standard form

$$\begin{aligned}\left|\{\rho_{out}(\omega,t)\}\right\rangle &= \exp\left[\int_0^{\infty}\rho_{out}{}^{*}(\omega,t)\hat{a}^{+}(\omega)-\rho_{out}(\omega,t)\hat{a}(\omega)d\omega\right]|0\rangle \\ &= \hat{D}_{\rho}\left[\rho_{out}(\omega,t)\right]|0\rangle\end{aligned} \tag{6.74}$$

where the time dependent displacement operator in the last line of Equation (6.74) is expressed as

$$\hat{D}_\rho\left[\rho_{out}(\omega,t)\right]=\exp\left[\int_0^\infty \rho_{out}{}^*(\omega,t)\hat{a}^+(\omega)-\rho_{out}(\omega,t)\hat{a}(\omega)d\omega\right] \tag{6.75}$$

From expression (6.72) and (6.75), the time dependent wavepacket function of modulated field $\rho_{out}(\omega,t)$, can be written in the form [46]

$$\begin{aligned}\rho_{out}(\omega,t)&=(2\pi F_S)^{1/2}\exp\left(-iW(\omega,t)+i\theta\right)\delta(\omega-\omega_S)\\&=(2\pi F_S)^{1/2}\exp(i\theta)\left[\int_0^\infty \Lambda(\omega,\omega')\exp(-i\omega' t)d\omega'\right]\delta(\omega-\omega_S)\end{aligned} \tag{6.76}$$

where $\delta(\omega-\omega_S)$ represent the spectral amplitude $\Lambda(\omega,\omega_S)$ is distributed over a range of frequencies around frequency ω_S. This corresponds to the result presented by [9].

We now include the effect of photon creation in order to give a complete representation of the state of modulated field. With the effect of photon creation included in the analysis, the annihilation and creation operator, $\hat{a}(\omega)$ and $\hat{a}^+(\omega)$, in expression (6.71) is replaced with $\hat{b}(\omega,t)$ and $\hat{b}^+(\omega,t)$, respectively. By expressing $\hat{b}(\omega,t)$ and $\hat{b}^+(\omega,t)$ in terms of $\hat{a}(\omega)$ and $\hat{a}^+(\omega)$ from expression (6.59) and (6.60), and after some algebraic manipulation, the state of modulated field that includes the effect of photon creation can be represented by

$$\begin{aligned}\left|\left\{\rho^{\zeta}_{out}(\omega_S t)\right\}\right\rangle&=\exp\left[-iW(\omega_S,t)\right]\exp\left[(2\pi F_S)^{1/2}\left[\exp(-i\theta)\hat{b}(\omega_S,t)-\exp(i\theta)\hat{b}(\omega_S,t)\right]|0\rangle\right]\\&=\exp\left[-iW(\omega_S,t)\right]\exp\left[(2\pi F_S)^{1/2}\left[\exp(-i\theta)\hat{s}\left[\zeta(\omega_S,t)\right]\hat{a}^+(\omega_S)\hat{s}^+\left[\zeta(\omega_S,t)\right]-\exp(i\theta)\hat{s}\left[\zeta(\omega_S,t)\right]\hat{a}^+(\omega_S)\hat{s}^+\left[\zeta(\omega_S,t)\right]\right]|0\rangle\right]\\&=\hat{s}\left[\zeta(\omega_S,t)\right]\exp\left[(2\pi F_S)^{1/2}\left[\exp(-i\theta)\hat{a}(\omega_S)-\exp(i\theta)\hat{a}(\omega_S)\right]\right]|0\rangle\\&=\hat{s}\left[\zeta'(\omega t)\right]\hat{D}_\rho\left[\rho_{out}(\omega t)\right]|0\rangle\end{aligned} \tag{6.77}$$

where the time dependent displacement operator $\hat{D}_\rho\left[\rho_{out}(\omega,t)\right]$ is given by (6.75), while the squeeze function is given by,

$$\zeta'(\omega,t)=\int_0^\infty \zeta(\omega,t)\delta(\omega-\omega_S)d\omega \tag{6.78}$$

The final line in expression (6.77) shows the modulated field state corresponds to the definition of the continuum two photon coherent squeeze state [50, 54]. An evidence of this is shown from the detection of phase modulated field where the mean and variance photoelectron count in Equation (6.42) and Equation (6.45), corresponds to the statistical description of a two photon coherent state [54]. We can conclude that when photon is created from the modulator as a consequence of phase modulation, we get $\beta(\omega,t) \neq 0$, and thus using Equation (6.61) - (6.64) we get $\hat{s}[\zeta(\omega,t)] \neq 1$ even at the lowest order approximation for $\beta(\omega,t)$ shown in Equation (6.19), and the state of the optical field evolves from continuum coherent input state $|\{\rho_{in}(\omega)\}\rangle$ to continuum two photon coherent output state $|\{\rho^{\zeta}_{out}(\omega,t)\}\rangle$, a quantum effect not included by [9].

We shall now investigate the properties of the two photon coherent state, which will be useful in the description of photon arrival statistics for the modulated field. From the expression of the squeeze function in Equation (6.78), we can identify $|\{\rho^{\zeta}_{out}(\omega,t)\}\rangle$ is an eigenstate of $\hat{a}(\omega)$ except at $\omega = \omega_S$ in which $\hat{s}[\zeta(\omega,t)] \neq 1$. The two photon coherent state is an eigenstate of the modulated field annihilation operator $\hat{b}(\omega,t)$ at frequency ω_S. This can be verified by operating $\hat{b}(\omega,t)$ onto the output state $|\{\rho^{\zeta}_{out}(\omega,t)\}\rangle$. Using expression (6.59), (6.77) and (6.78), we obtained

$$\begin{aligned}\hat{b}(\omega,t)\left|\{\rho^{\zeta}_{out}(\omega,\omega',t)\}\right\rangle &= \exp\left[iA(\omega,t)\right]\hat{s}\left[\zeta(\omega,t)\right]\hat{a}(\omega)\hat{s}^{+}\left[\zeta(\omega,t)\right]\hat{s}\left[\zeta(\omega,t)\right]\hat{D}_{\rho}\left[\rho_{out}(\omega,t)\right]|0\rangle \\ &= \exp\left[iA(\omega,t)\right]\hat{s}\left[\zeta(\omega,t)\right]\hat{a}(\omega)\left|\{\rho_{out}(\omega,t)\}\right\rangle \\ &= \exp\left[iA(\omega_S,t)\right]\rho_{out}(\omega,t)\left|\{\rho^{\zeta}_{out}(\omega,t)\}\right\rangle\end{aligned} \tag{6.79}$$

where the eigenfunction $\rho_{out}(\omega,t)$ is defined in Equation (6.76), and $A(\omega_S,t)$ is the phase of $\alpha(\omega_S,t)$ in expression (6.18). The two photon coherent state is a squeezed state for which the uncertainty in one direction in phase space is reduced while the uncertainty in the orthogonal direction increases. In order to describe the effect of

squeezing, it is useful to introduce two mutual orthogonal operators $\hat{X}_1(\omega)$ and $\hat{X}_2(\omega)$. In Schrodinger picture, $\hat{X}_1(\omega)$ and $\hat{X}_2(\omega)$ is defined as

$$\hat{X}_1(\omega) = \frac{1}{2\sqrt{2\pi}}\left[\hat{a}(\omega) + \hat{a}^+(\omega)\right] \tag{6.80}$$

$$\hat{X}_2(\omega) = \frac{1}{2i\sqrt{2\pi}}\left[\hat{a}(\omega) - \hat{a}^+(\omega)\right] \tag{6.81}$$

In Heisenberg representation, the expression of modulated field operator is represented by Equation (6.13). Because in Schrödinger representation, the time evolution of the field is characterized by the field state, the modulated field operator is obtained by setting $t = 0$ in Equation (6.13). Thus we have,

$$\hat{E}^s{}_{out}(t) = \int_0^\infty \left(\frac{\hbar\omega}{4\pi\varepsilon_0 c_0 A}\right)^{1/2} \left[\hat{a}(\omega)\exp\left(i\varphi_{out}\right) + H.c.\right] d\omega \tag{6.82}$$

where the superscript *'s'* in Equation (6.82) denotes the field represented in Schrodinger representation and φ_{out} is the propagation phase delay. By expressing $\hat{a}(\omega)$ and $\hat{a}^+(\omega)$ in terms of $\hat{X}_1(\omega)$ and $\hat{X}_2(\omega)$ in Equation (6.80) and Equation (6.81), we have

$$\hat{E}^s{}_{out}(t) = \int_0^\infty \left(\frac{\hbar\omega}{4\pi\varepsilon_0 c_0 A}\right)^{1/2} \left[\hat{X}_1(\omega)\cos\left(\varphi_{out}\right) + \hat{X}_2(\omega)\sin\left(\varphi_{out}\right)\right] d\omega \tag{6.83}$$

In expression (6.83), it is evident that $\hat{X}_1(\omega)$ and $\hat{X}_2(\omega)$ describes the field amplitude of the in phase and quadrature component of the optical field. Because $\hat{b}(\omega,t)$ is an eigenstate of $|\rho^{\zeta}{}_{out}(\omega,t)>$ at frequency ω_S, therefore it is convenient to express $\hat{a}(\omega)$ in terms of $\hat{b}(\omega,t)$. Using expression (6.17), and the identity in (6.23) we have

$$\hat{a}(\omega) = \alpha^*(\omega,t)\hat{b}(\omega,t) - \beta^*(\omega,t)\hat{b}^+(\omega,t) \tag{6.84}$$

By employing the relation in Equation (6.84), the eigen-equation in (6.79), and the expression of the modulated field wavepacket function in expression (6.76), the expectation value of the in phase component and the quadrature component respectively, are

$$\begin{aligned}\left\langle \hat{X}_1(\omega)\right\rangle &= \left\langle \left\{\rho^{\zeta}{}_{out}(\omega,t)\right\}\left|\frac{1}{2\sqrt{2\pi}}\left[\hat{a}(\omega)+\hat{a}^{+}(\omega)\right]\right|\left\{\rho^{\zeta}{}_{out}(\omega,t)\right\}\right\rangle \\ &= F_S^{1/2}\left\{\left|\alpha(\omega_S,t)\right|\cos\left[W(\omega_S,t)-\theta+A(\omega_S,t)\right]-\left|\beta(\omega_S,t)\right|\cos\left[W(\omega_S,t)-\theta+B(\omega_S,t)\right]\right\}\end{aligned} \tag{6.85}$$

$$\begin{aligned}\left\langle \hat{X}_2(\omega)\right\rangle &= \left\langle \left\{\rho^{\zeta}{}_{out}(\omega,t)\right\}\left|\frac{1}{2i\sqrt{2\pi}}\left[\hat{a}(\omega)-\hat{a}^{+}(\omega)\right]\right|\left\{\rho^{\zeta}{}_{out}(\omega,t)\right\}\right\rangle \\ &= F_S^{1/2}\left\{\left|\alpha(\omega_S,t)\right|\sin\left[W(\omega_S,t)-\theta+A(\omega_S,t)\right]+\left|\beta(\omega_S,t)\right|\sin\left[W(\omega_S,t)-\theta+B(\omega_S,t)\right]\right\}\end{aligned} \tag{6.86}$$

The variance of the in phase $\left[\Delta X_1(\omega)\right]^2$ and quadrature component $\left[\Delta X_2(\omega)\right]^2$ at carrier frequency ω_S are expressed as

$$\begin{aligned}\left[\Delta X_1(\omega_S)\right]^2 &= \left\langle \left\{\rho^{\zeta}{}_{out}(\omega,t)\right\}\left|\frac{1}{4(2\pi)}\left[\hat{a}(\omega_S)+\hat{a}^{+}(\omega_S)\right]^2\right|\left\{\rho^{\zeta}{}_{out}(\omega,t)\right\}\right\rangle - \frac{1}{4(2\pi)}\left[\left\langle \left\{\rho^{\zeta}{}_{out}(\omega,t)\right\}\left|\hat{a}(\omega_S)+\hat{a}^{+}(\omega_S)\right|\left\{\rho^{\zeta}{}_{out}(\omega,t)\right\}\right\rangle\right]^2 \\ &= \frac{1}{4}\left|\alpha(\omega_S,t)-\beta(\omega_S,t)\right|^2\end{aligned} \tag{6.87}$$

$$\begin{aligned}\left[\Delta X_2(\omega_S)\right]^2 &= \left\langle \left\{\rho^{\zeta}{}_{out}(\omega,t)\right\}\left|\frac{-1}{4(2\pi)}\left[\hat{a}(\omega_S)-\hat{a}^{+}(\omega_S)\right]^2\right|\left\{\rho^{\zeta}{}_{out}(\omega,t)\right\}\right\rangle - \left(\frac{-1}{4(2\pi)}\right)\left[\left\langle \left\{\rho^{\zeta}{}_{out}(\omega,t)\right\}\left|\hat{a}(\omega_S)+\hat{a}^{+}(\omega_S)\right|\left\{\rho^{\zeta}{}_{out}(\omega,t)\right\}\right\rangle\right]^2 \\ &= \frac{1}{4}\left|\alpha(\omega_S,t)+\beta(\omega_S,t)\right|^2\end{aligned} \tag{6.88}$$

Equations (6.85) - (6.88) is an approximate expressions because the phase angle $A(\omega_S,t)$ is small and thus can be neglected as explained earlier. The variance product between Equation (6.87) and Equation (6.88) is

$$\begin{aligned}\left[\Delta X_1(\omega_S)\right]^2\left[\Delta X_2(\omega_S)\right]^2 &= \frac{1}{4}\left|\alpha(\omega_S,t)-\beta(\omega_S,t)\right|^2\frac{1}{4}\left|\alpha(\omega_S,t)+\beta(\omega_S,t)\right|^2 \\ &= \frac{1}{16}\left[\left|\alpha(\omega_S,t)\right|^4-\alpha^2(\omega_S,t)\beta^2(\omega_S,t)-\alpha^{*2}(\omega_S,t)\beta^{*2}(\omega_S,t)+\left|\beta(\omega_S,t)\right|^4\right] \\ &\geq \frac{1}{16}\left[\left|\alpha(\omega_S,t)\right|^2-\left|\beta(\omega_S,t)\right|^2\right]^2 \\ &\geq \frac{1}{16}\end{aligned} \tag{6.89}$$

From Equation (6.89), we can identify the variance product is minimized i.e. $\left[\Delta X_1(\omega_S)\right]^2\left[\Delta X_2(\omega_S)\right]^2 = 1/16$, when $\alpha(\omega_S,t)$ and $\beta(\omega_S,t)$ are real. For other values of $\alpha(\omega_S,t)$ and $\beta(\omega_S,t)$ (i.e. $\alpha(\omega_S,t)$ and $\beta(\omega_S,t)$ are imaginary), the uncertainty product of two photon coherent state are greater than *1/16*. A coherent state is a minimum

uncertainty state because the variance product is minimized to *1/16* at all time [33]. As a result, we can conclude the **two photon coherent state is generally NOT a minimum uncertainty state**.

For simplicity of the analysis, we assume $\alpha(\omega_S,t)$ to be real because the imaginary component of $\alpha(\omega,t)$ is small for $d\omega/dt << \omega_S^2$, as shown in expression (6.18). Therefore, the product variance is governed by the phase of $\beta(\omega_S,t)$ denoted by $B(\omega_S,t)$. A plot of variance product in Equation (6.89) with respect to phase $B(\omega_S,t)$ is shown in Figure 6.15.

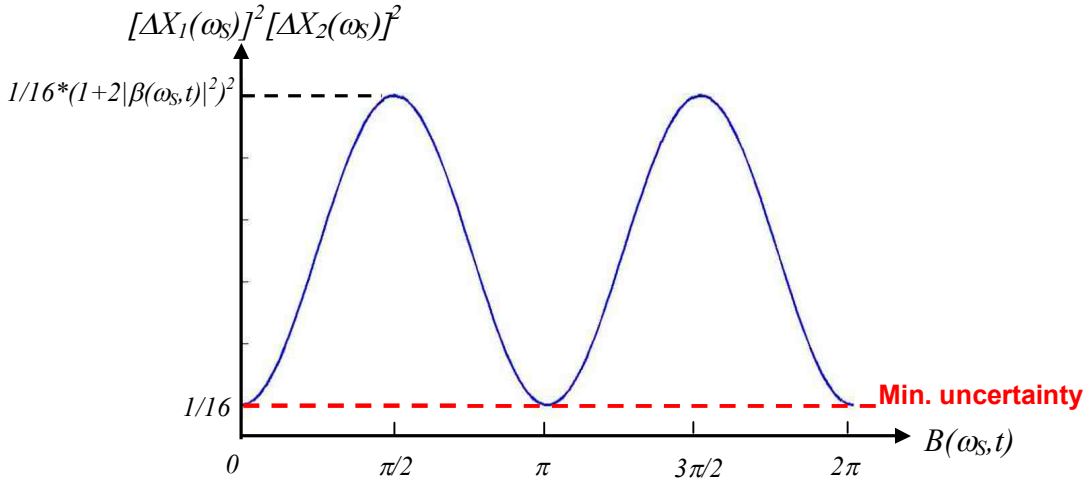

Figure 6.15: Variance product $[\Delta X_1(\omega_S)]^2[\Delta X_2(\omega_S)]^2$ against phase $B(\omega_S,t)$.

From expression (6.87) and (6.88), we can identify the variance of the in phase and quadrature component are not equivalent, therefore the two photon coherent state is a squeezed state [50]. A plot of $\left[\Delta X_1(\omega_S)\right]^2$ and $\left[\Delta X_2(\omega_S)\right]^2$ with respect to $B(\omega_S,t)$ is shown in Figure 6.16(a) and (b).

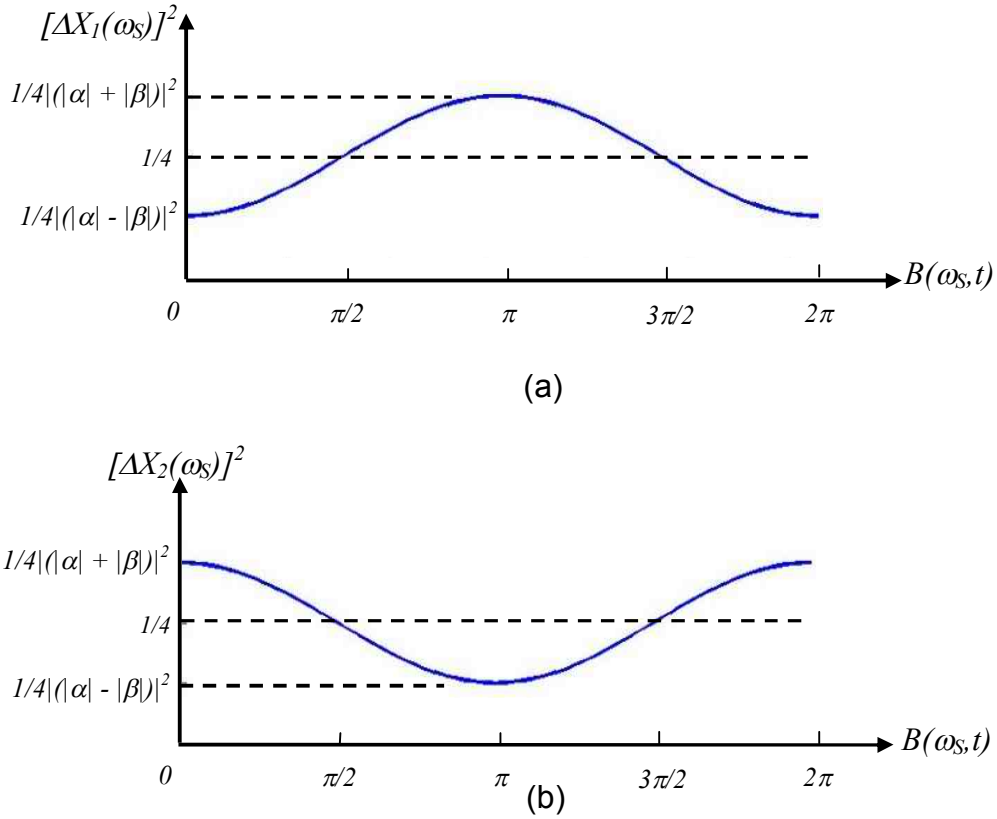

Figure 6.16: Variance against phase $B(\omega_S,t)$ (a) In phase component (b) Quadrature.

In Figure 6.16(a) and (b), we can identify when the variance of a quadrature components increases beyond *1/4* at some angle $B(\omega_S,t)$, the other component is reduced below *1/4* i.e. if $\left[\Delta X_1(\omega_S)\right]^2 < \frac{1}{4}$ then $\left[\Delta X_2(\omega_S)\right]^2 > \frac{1}{4}$ and vice-versa. When the modulated field is at minimum uncertainty state i.e. $B(\omega_S,t) = m\pi$, this corresponds to the extrema of $\left[\Delta X_1(\omega_S)\right]^2$ and $\left[\Delta X_2(\omega_S)\right]^2$.

Neglecting the effect of photon creation by setting $|\beta(\omega_S,t)| = 0$ in expression (6.87) and (6.88), we find the phase modulated field is described by coherent state. In other words, the two photon coherent state $|\{\rho^{\zeta}_{out}(\omega,t)\}>$ reduces to the standard coherent state $|\{\rho_{out}(\omega,t)\}>$ when photon creation is neglected in the analysis. The influence of photon creation on the state of the field is shown in the Argand diagrams of Figure 6.17 and Figure 6.18. These Figures illustrate the mean and the variance of

the two quadrature components of modulated field described by coherent state $|\{\rho_{out}(\omega,t)\}>$ and two photon coherent state $|\{\rho^{\zeta}_{out}(\omega,,t)\}>$, respectively.

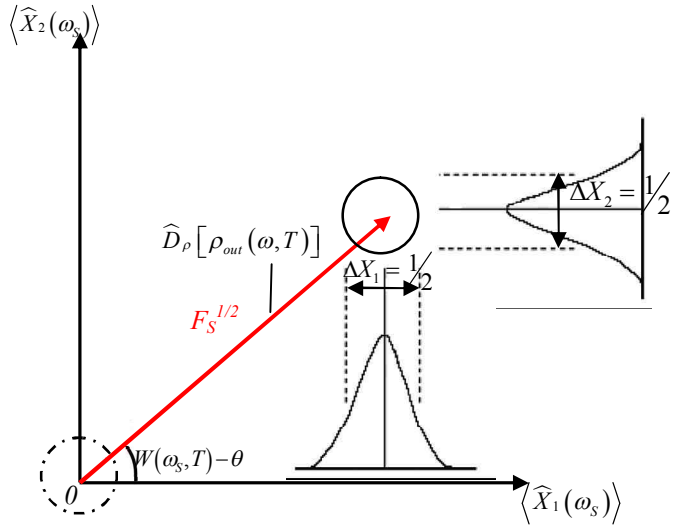

Figure 6.17: The signal strengths of modulated field and their fluctuations in phase space at $t = T$, in continuum coherent state representation.

Figure 6.17 is a snapshot of the field state in phase space at $t = T$ with $|\beta(\omega_S,t)|^2$ set to zero. It shows the displacement operator $\hat{D}_\rho[\rho_{out}(\omega,T)]$ translates the vacuum fluctuation contour centered at the origin $(0,0)$ to the position $(F_S^{1/2}\cos[W(\omega_S,T)\theta], F_S^{1/2}\sin[W(\omega_S,T)-\theta])$ while the shape of vacuum fluctuation contour is unchanged with quadrature variances $[\Delta X_1(\omega_S)]^2 = [\Delta X_2(\omega_S)]^2 = \frac{1}{4}$. Thus, the state of modulated field is in a minimum uncertainty state at all time i.e. $[\Delta X_1(\omega_S)]^2[\Delta X_2(\omega_S)]^2 = \frac{1}{16}$, when the effect of photon creation is neglected. The magnitude of the displaced state vector retains at $F_S^{1/2}$ i.e. $\sqrt{\langle \hat{X}_1(\omega)\rangle^2 + \langle \hat{X}_2(\omega)\rangle^2} = F_S^{1/2}$ at all time. The mean and the variance (fluctuations) of modulated field in Figure 6.17 is obtained by setting $|\beta(\omega_S,t)| = 0$ in Equations (6.85) - (6.88).

Figure 6.18(a) is a phase-space representation of modulated field with the effect of photon creation included (i.e. $|\beta(\omega_S,t)| > 0$) in which the angle $B(\omega_S,T)$ is assumed to be 0.

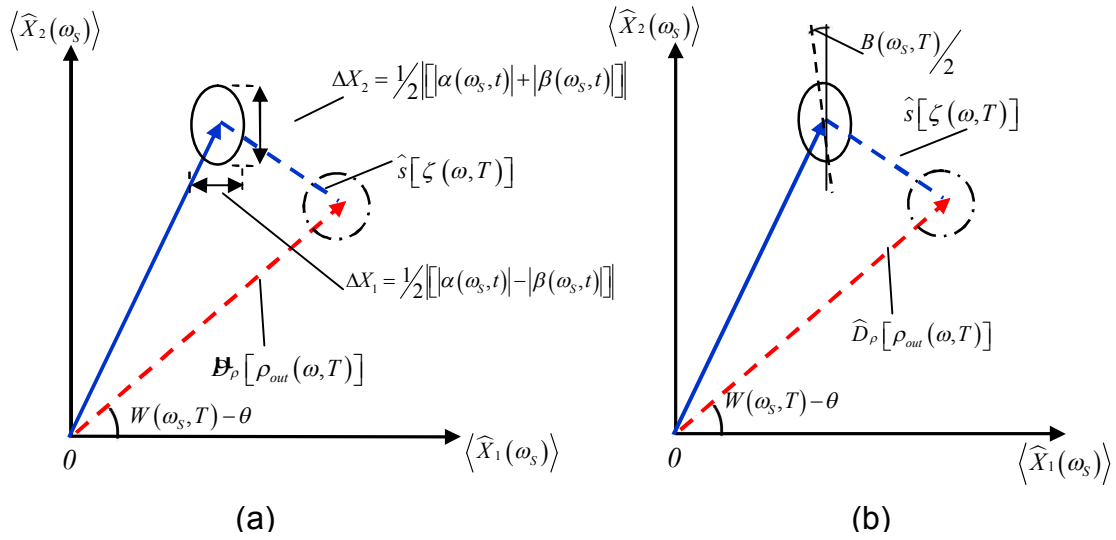

Figure 6.18: The signal strength of modulated field and their fluctuations in phase space at $t = T$, in two photon coherent state representation (a) $B(\omega_S,T) = 0$. (b) $B(\omega_S,T) \neq 0$.

From Figure 6.18(a), it can be identified that the wavepacket squeezed operator $\hat{s}[\zeta(\omega,t)]$ changes the shape of the uncertainty contour into an ellipse as well as displaces the center of the uncertainty contour. The major axis and minor axis of the uncertainty contour is given by $[\Delta\hat{X}_2(\omega_S)] = \frac{1}{2}[|\alpha(\omega_S,t)| + |\beta(\omega_S,t)|]$ and $[\Delta\hat{X}_1(\omega_S)] = \frac{1}{2}[|\alpha(\omega_S,t)| - |\beta(\omega_S,t)|]$, respectively. The center of the ellipse is positioned at $[\langle \hat{X}_1(\omega_S) \rangle, \langle \hat{X}_2(\omega_S) \rangle]$, where $\langle \hat{X}_1(\omega_S) \rangle$ and $\langle \hat{X}_2(\omega_S) \rangle$ is given by Equation (6.85) and Equation (6.86) respectively. With the effect of photon creation included, the magnitude of the state vector (blue arrow in Figure 6.18) does not equal to F_S. Figure 6.18b), illustrates the general case when $B(\omega_S,t) \neq 0$. The effect of this is the uncertainty contour is an

ellipse inclined at an angle of $B(\omega_S,t)/2$ [54] i.e major and minor axes of ellipse are not aligned along the $\widehat{X}_1(\omega)$ and $\widehat{X}_2(\omega)$ axes respectively. In Figure 6.18, the time is fixed at $t = T$. In general as time progresses, the mean amplitude, $\left\langle \widehat{X}_1(\omega) \right\rangle$ and $\left\langle \widehat{X}_2(\omega) \right\rangle$, and the inclination angle $B(\omega_S,t)/2$, varies. As a result, the state vector will rotate around the origin at rate given by $W(\omega_S,t)$ with its magnitude changing during the rotation, while the uncertainty contour will be changing in shape and size.

In order to deduce the photon arrival statistics of the modulated field, we need to express the two photon coherent state $|\{\rho^{\zeta}_{out}(\omega,t)\}>$ in the photon number state representation. The two photon coherent state $|\{\rho^{\zeta}_{out}(\omega,t)\}>$ can be represented by an infinite sum of number states [54]

$$\left|\left\{\rho^{\zeta}{}_{out}(\omega,t)\right\}\right\rangle = \sum_{N=0}^{\infty} C_N(\omega,t)\left|\left\{N(\omega)\right\}\right\rangle \tag{6.90}$$

where $C_N(\omega,t)$ is the PDF of photon flux distribution for the phase modulated field and is time dependent because the state of the field evolves in time. $\left|\left\{N(\omega)\right\}\right\rangle$ is the continuum photon number state that is defined as [33]

$$\left|\left\{N(\omega)\right\}\right\rangle = \frac{\left[\int_0^{\infty} \hat{a}^{+}(\omega)\gamma(\omega)d\omega\right]^N}{\sqrt{\left[N(\omega)\right]!}}\left|0\right\rangle \tag{6.91}$$

where $\gamma(\omega)$ is the spectral amplitude of the input (unmodulated) field. The input field is monochromatic with frequency $\omega = \omega_S$, therefore $\gamma(\omega) = \delta(\omega - \omega_S)$. By operating $\hat{b}(\omega,t)$ onto $|\{\rho^{\zeta}_{out}(\omega,t)\}>$, using the relation $\hat{a}^{+}(\omega)\left|\left\{N(\omega)\right\}\right\rangle = \sqrt{N(\omega)+1}\left|\left\{N(\omega)+1\right\}\right\rangle$ and $\hat{a}(\omega)\left|\left\{N(\omega)\right\}\right\rangle = \sqrt{N(\omega)}\left|\left\{N(\omega)-1\right\}\right\rangle$, we have

$$\alpha(t)\sum_{N=0}^{\infty} C_N(t)\sqrt{N}\left\{\left|N-1\right\rangle\right\} + \beta^{*}(t)\sum_{N=0}^{\infty} C_N(t)\sqrt{N+1}\left|\left\{N+1\right\}\right\rangle = \rho_{out}(t)\sum_{N=0}^{\infty} C_N(t)\left|\left\{N\right\}\right\rangle \tag{6.92}$$

where the frequency dependence is suppressed in Equation (6.92) for clarity. The expression on the left hand side is obtained by expressing $\hat{b}(\omega,t)$ in terms of $\hat{a}(\omega)$ using Equation (6.17) and $|\{\rho^{\zeta}_{out}(\omega,t)\}>$ in terms of $|\{N(\omega)\}>$ in Equation (6.90). The right hand side of the expression is determined from Equation (6.79). By applying the orthogonal property of number state $\langle M|N\rangle = \delta_{MN}$ [33], and equating terms with the same photon number state, we obtained the recurrence formula of the probability amplitude $C_N(t)$

$$\begin{aligned}
&\alpha(t)C_1(t) = \rho_{out}(t)C_0(t)\\
&\alpha(t)\sqrt{2}C_2(t) + \beta^*(t)\sqrt{1}C_0(t) = \rho_{out}(t)C_1(t)\\
&.....\\
&\alpha(t)\sqrt{N}C_N(t) + \beta^*(t)\sqrt{N-2}C_{N-2}(t) = \rho_{out}(t)C_{N-1}(t)
\end{aligned} \tag{6.93}$$

The photon number distribution function $|C_N(t)|^2$ can be determined by taking the variable transformation in the last line of Equation (6.93) [54]

$$C_N(t) = A_N(t)(N!)^{-1/2}\left(\frac{\beta^*(t)}{2\alpha(t)}\right)^{N/2} \tag{6.94}$$

where $A_N(t)$ is the transform variable. After some algebraic manipulation shown in [54], $|C_N(t)|^2$ can be solved giving

$$|C_N(t)|^2 = \frac{1}{N!\alpha(t)}\left|\frac{\beta(t)}{2\alpha(t)}\right|^N \exp\left(-F_S + \left|\frac{\beta(t)}{\alpha(t)}\right|F_S\cos\left[2\left(W(t)-\theta+2B(t)\right)\right]\right)\left[H_N\left(\frac{F_S^{1/2}}{\sqrt{2|\alpha(t)||\beta(t)|}}\right)\right]^2 \tag{6.95}$$

where $H_N(z)$ is the Hermite polynomial defined as [55]

$$H_N(z) = \sum_{m=0}^{[N/2]}\frac{(-1)^m N!(2z)^{N-2m}}{m!(n-2m)!} \tag{6.96}$$

Notice that the photon number arrival rate for modulated field is no longer characterized by Poisson distribution that corresponds to a coherent state. After some laborious algebraic manipulation, we can show the mean and variance of the photon flux distribution in Equation (6.95) reproduces the results in Equation (6.43) and

Equation (6.45). It can be verified that if the effect of photon creation is neglected i.e. $\beta(\omega_S,t) = 0$ and $\alpha(\omega_S,t) = 1$, Equation (6.95) reduces to a Poisson distribution [50].

6.5 Photon Creation in Phase Modulation

From Equation (6.43) in Section 6.3, we have shown the only difference between classical [1, 22 - 24] and quantum optical detection response is due to photon creation out of the modulator. The effect of photon creation from modulator can be classified into three different processes, namely spontaneous emission, stimulated emission and the energy exchange process between the optical field and the modulator ('energy exchange process' for short).

To elucidate the extent of the impact from each of these photon creation processes, we shall introduce the parameters V, κ and Γ, to represent the photoelectron count detected from the spontaneous emission, stimulated emission, and the energy exchange process of photon creation. Using Equation (6.43), the expression of V, κ and Γ, are given by

$$V = \frac{1}{2\pi} \int_{T_S}^{T_S+T_M} \int_{\omega_L}^{\omega_U} \left|\beta(\omega,t)\right|^2 d\omega dt \tag{6.97}$$

$$\kappa = 2F_S \int_{T_S}^{T_S+T_M} \left|\beta(\omega_S,t)\right|^2 dt \tag{6.98}$$

$$\Gamma = 2F_S \int_{T_S}^{T_S+T_M} \sqrt{1+\left|\beta(\omega_S,t)\right|^2}\left|\beta(\omega_S,t)\right| \cos\left[2\left(\theta_S+\varphi_{SN}(\omega_S,t)\right)+A(\omega_S,t)-B(\omega_S,t)\right] dt \tag{6.99}$$

where ω_U and ω_L are the frequency cutoff of the photo-detector. In expression (6.97), (6.98) and (6.99), we have shown the effect of photon creation from modulator is described by the Bogoliubov coefficient $\beta(\omega,t)$. From Equation (6.19), we can identify $\beta(\omega,t)$ is governed by the rate of change of instantaneous frequency $d\omega/dt$, which is in turn dependent on the temporal profile of the control signal. Therefore,

the temporal profile of photon creation is dependent on the characteristics of the control signal.

In this Section, the control signal has a rectangular pulse profile, a common modulating/control signal in optical communication system [22 - 24]. The control signal exhibits a rectangular pulse profile that is an ongoing **alternating** pattern, in which the refractive index alternates between n and $n + \Delta n$ (see Figure 6.19). We used this pattern because it simplifies the calculation as compared with a pseudo-random pattern. As we shall see in this Subsection, $\beta(\omega,t)$ is non-zero at each transition of the control signal. Therefore, an alternating rectangular pulse pattern maximizes the photoelectron difference in Equation (6.43) because the number of transitions of the control signal is maximized. The simulation parameters used in this analysis is given by Table 6.2.

Parameters	Notations	Value
Transmit laser power	P_{in}	*1 mW*
Optical carrier wavelength	λ_S	*1550 nm*
Refractive index (unmodulated)	n	*3.5*
Nonlinear refractive index change	Δn	*0.05*
10 - 90% bit transition rate	Ω	$1.8*10^{14}\ s^{-1}$
Pulse duration	T_p	*1 ps*
Photon flight time in modulator	T_f	$0.3*T_b = 0.3\ ps$
Measurement start time	T_S	*0 s*
Measurement time	T_M	*1 s*
Upper limit of photodiode passband	ω_U	$1.88*10^{15}\ rad\ s^{-1}$
Lower limit of photodiode passband	ω_L	$1.1*10^{15}\ rad\ s^{-1}$
Modulator Type		*All optical*

Table 6.2: Parameters used in rectangular pulse modulation.

A semiconductor all optical transverse phase modulator (AOPM) is considered in this analysis. This is because it has a fast response time so that a rectangular pulse with a pulse duration T_p in the order of pico-seconds and a transition rate Ω in the order of femto-seconds could be generated [19]. An ultrafast *(~Tbps)* modulating signal can be generated from an optical pulse of the femtosecond control laser that excites the semiconductor modulating media near the band-to-band transition, so that large change in refractive index Δn with a transition rate in the order of femtosecond can be achieved [16, 19]. For an AOPM, the change in refractive index is induced by the optical Kerr effect, in which the refractive index profile *n(t)* of the phase modulator follows the intensity profile of the control signal $i_C(t)$. In Chapter 2.2, we have shown the refractive index change $\Delta n(t)$ is related to the intensity profile of the control field $i_C(t)$ by

$$\Delta n(t) = \frac{3\eta_0 \chi^{(3)}}{n^2 \varepsilon_0} i_C(t) \tag{6.100}$$

where n is the refractive index of the semiconductor material in the absence of the control field, ε_0 is the free space permittivity $(\varepsilon_0 = 8.85*10^{-12}\ V/m)$, $\chi^{(3)}$ is the third order susceptibility coefficient of the material, and η_0 is the intrinsic impedance in free space $(\eta_0 = 377\,\Omega)$. Given that the intensity of the control laser i_c is ~ *10* MW/cm^2, the semiconductor media of the modulator will have a Δn of *0.5* [19]. Therefore by using Equation (6.100), in order to induce a Δn of *0.05*, the required i_C is ~ *1* MW/cm^2. The additional phase delay $\Delta\varphi$ due to a change in refractive index Δn is given by

$$\Delta\varphi = \frac{2\pi\Delta nL}{\lambda_S} \tag{6.101}$$

where L is the length of the modulator and λ_S is the optical carrier wavelength. Expression (6.101) shows having a large Δn can produce a large phase offset even

when the photon flight time is small. As we shall see in Chapter 7, the modulator length L is small for a *Tbps* optical communication system, therefore having a large Δn is particularly useful because a sufficient phase delay can be produced over a short propagation distance.

Since the refractive index profile $n(t)$ follows the intensity of the control signal $i_C(t)$, as indicated by Equation (6.100), therefore $n(t)$ is expected to have an alternating rectangular pulse profile. A convenient form of $n(t)$ that describes an alternating rectangular pulse profile is given by

$$n(t) = n + \frac{\Delta n}{2}\left\{1 + \sum_{j=0}^{\infty}\left[\tanh\left(2.2\Omega\left(t - 2jT_p\right)\right) - \tanh\left(2.2\Omega\left(t - (2j+1)T_p\right)\right)\right]\right\} \quad (6.102)$$

where j is an integer, and the remaining parameters takes its usual meaning as in Table 6.2. By using the simulation parameters in Table 6.2, a plot of refractive index profile $n(t)$ is shown in Figure 6.19.

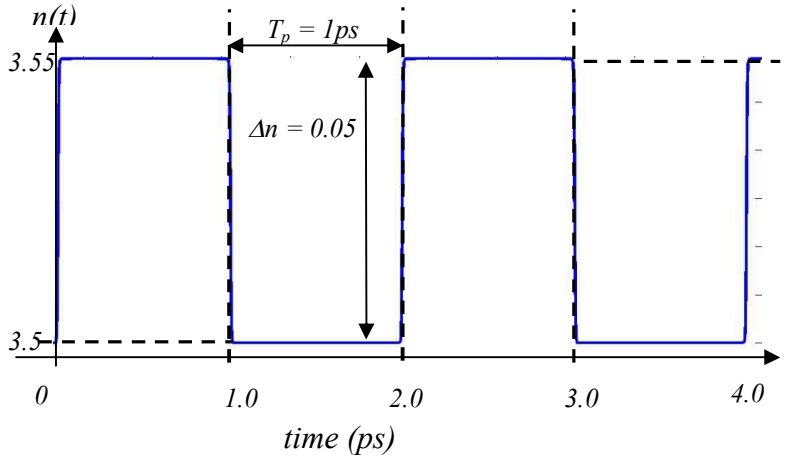

Figure 6.19: Refractive index profile induced from alternating rectangular pulse modulation.

Based on the refractive index profile in Figure 6.19, we shall investigate the characteristics for each of the photon creation processes described in expression

(6.97), (6.98) and (6.99) (i.e. spontaneous emission V, stimulated emission κ and energy exchange from modulator Γ), as well as determining the extent for each of these impacts in the following Subsections.

6.5.1 Spontaneous Emission from Modulator

In this Subsection, we shall determine the photoelectron count accumulated from the process of spontaneous emission out of the modulator V. Since the instantaneous frequency $\omega(t)$ is related to the refractive index profile $n(t)$ by Equation (6.16), thus using Equation (6.19), we can identify $|\beta(\omega_S,t)|^2$ is governed by $n(t)$ profile in Figure 6.19. A plot of the temporal profile of $|\beta(\omega,t)|^2$ for $\omega = \omega_S$, which is derived from the refractive index profile $n(t)$ in Equation (6.102), is shown in Figure 6.20.

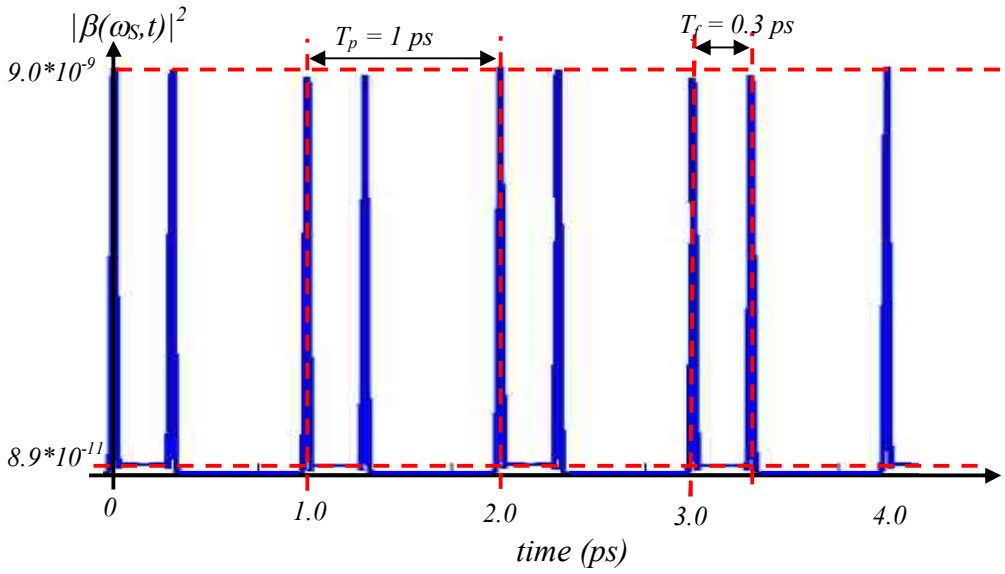

Figure 6.20: Temporal profile of $|\beta(\omega,t)|^2$ with $\omega = \omega_S$ for alternating rectangular pulse modulation.

By comparing Figure 6.20 with Figure 6.19, it is evident that $|\beta(\omega_S,t)|^2$ is non-zero at each transition of the refractive index $n(t)$. As we have explained previously, a non-zero value of $|\beta(\omega_S,t)|^2$ signifies photons are created at time t given that the frequency of the input field is at ω_S. The $|\beta(\omega_S,t)|^2 > 0$ value persists for approximately the photon flight time period inside the modulator T_f. This can be understood from expression (6.19), where the difference of the upper and lower limit of the integral is T_f, thus any variation of $n(t)$ within this period will have a cumulative effect resulting in a non-zero $|\beta(\omega_S,t)|^2$. Furthermore, each transition of $n(t)$ produces a series of identical pulses of $|\beta(\omega_S,t)|^2$ photon flux. This justifies the claim in [19], who uses heuristic reasoning to determine that when the refractive index of a material, $n(t)$, has **a** rectangular pulse profile, two pulses of photons will be emitted from the modulator for a duration of T_f at the transition of $n(t)$. From Figure 6.20, we see that each pulse begins with a large spike at the start of the transition, then reaches a non-zero steady state for sometime, followed by another transient spike that is similar to the previous spike, and then returns back to 0. The claim from [19] overlooks the detail of the photon creation pulse as it does not capture the overshoot feature at the start of the transition. In Section 6.4, we have shown the state of modulated field is characterized by continuum coherent state when $\beta(\omega_S,t) = 0$, and is described by two photon coherent state when $\beta(\omega_S,t) > 0$. Thus, the temporal profile of $\beta(\omega_S,t)$ in Figure 6.20, shows there are some time intervals in which the state of the modulated field can be characterized by continuum coherent state, while there are some time intervals where the field quantum state is described by two photon coherent state.

In order to understand the shape of the profile, we shall divide a photon creation pulse into 5 different time intervals to explain one of its features separately, as shown in Figure 6.21.

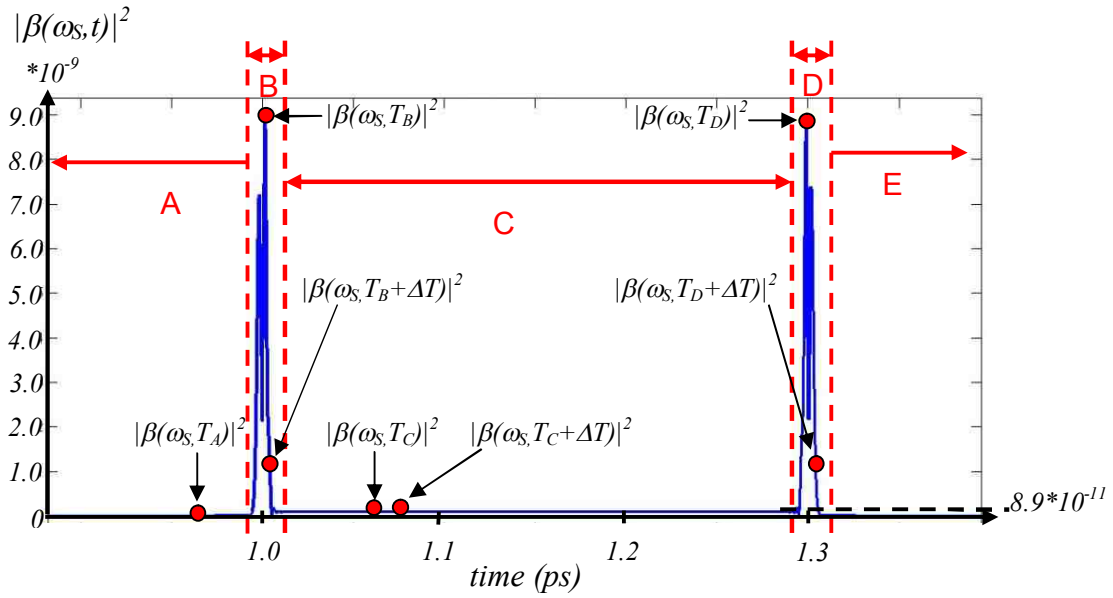

Figure 6.21: A photon creation pulse of $|\beta(\omega_S,t)|^2$ due to a transition in $n(t)$.

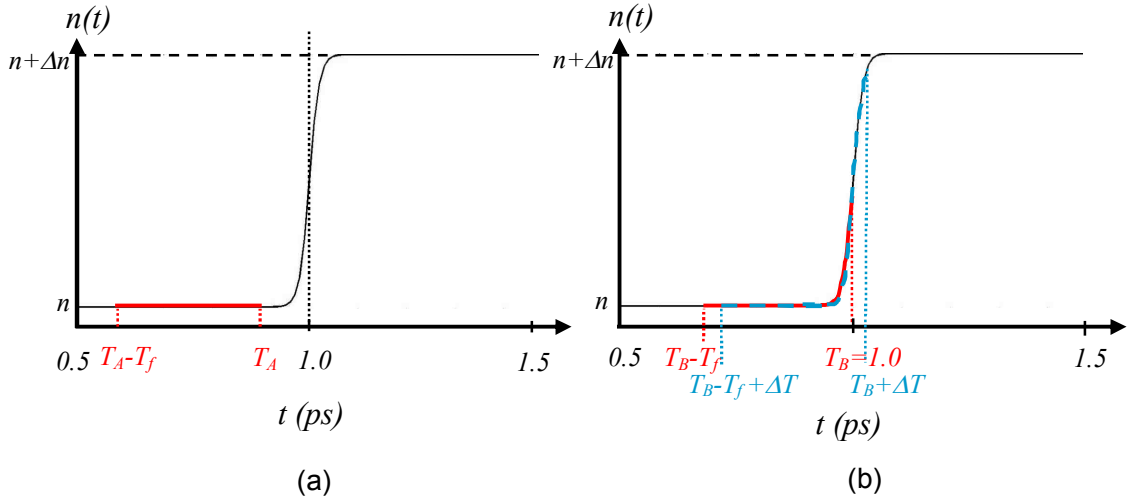

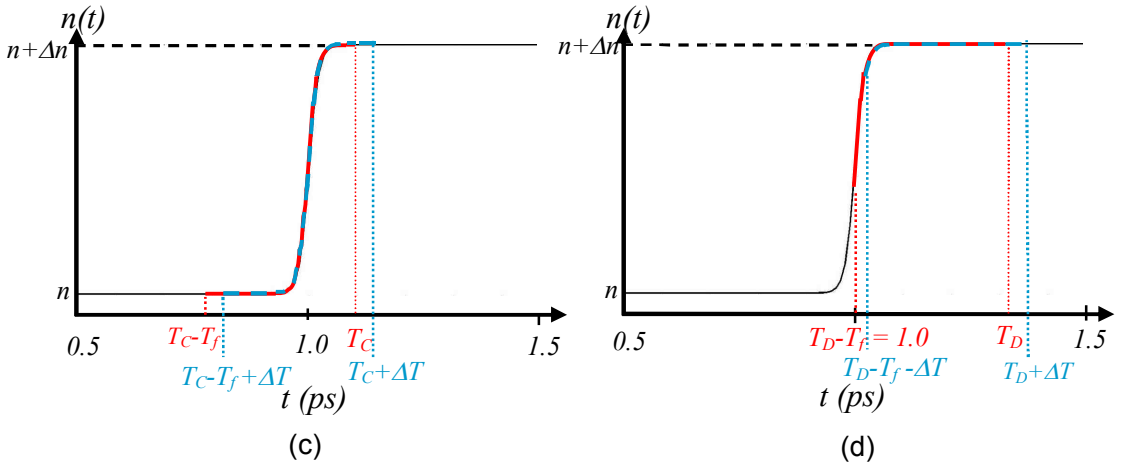

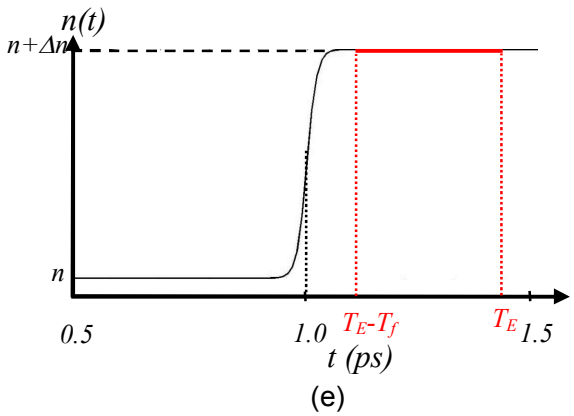

Figure 6.22: Refractive index profile seen by the field during its time of flight inside the modulating medium within (a) time interval A (b) time interval B (c) time interval C (d) time interval D (e) time interval E.

To explain the features of the photon creation pulse, it is useful to refer to the expression of $\beta(\omega_S,t)$ in (6.19), reproduced in the following equation

$$\beta(\omega_S,t) = -i\int_{t-T_f}^{t}\left(\frac{1}{\omega_S(\tau)}\right)^{1/2}\frac{d}{d\tau}\left(\frac{d\omega_S/d\tau}{4\omega_S^{3/2}(\tau)}\right)\exp\left(-2i\left[\omega_S\tau-\omega_S T_f+\int_{\tau-T_f}^{\tau}\omega_S(t')dt'\right]\right)d\tau \quad (6.103)$$

During time interval A, $|\beta(\omega_S,t)|^2 = 0$, thus the state of the field is characterized by coherent state. This can be explained by considering the period in which the field enters the modulating medium at time T_A - T_f and leaves the modulator at T_A, Figure 6.22(a). In this period, the field experiences a static refractive index profile during its time of flight inside the modulating medium, as shown in red in Figure 6.22(a). Because the instantaneous frequency $\omega_S(t)$ is related to $n(t)$ by Equation (6.16), a static $n(t)$ profile gives $d\omega_S/dt = 0$. Therefore, from Equation (6.103) we see $|\beta(\omega_S,T_A)|^2 = 0$, as shown in Figure 6.21.

In time interval B, a large transient spike occurs as shown in Figure 6.21 and the state of the field is characterized by two photon coherent state. This is a consequence of the field entering the modulating medium at time when $n(t)$ is static at

n, such as T_B - T_f in Figure 6.22(b), and leaves the medium when $n(t)$ is time varying at T_B. The change in $n(t)$ experienced by the field within this period is shown by the red line in Figure 6.22(b). During this time period, $|\beta(\omega_S, T_B)|^2$ is non-zero because $d\omega/dt$ is non-zero just before the field leaves the modulating medium. Furthermore, inside the time interval B, $|\beta(\omega_S, t)|^2$ is time varying. We see this by considering the field component that enters the modulator at a later time $t = T_B + \Delta T$, in which the $n(t)$ profile experience by the field is shown by the blue dotted line in Figure 6.22(b). This profile is different from the red profile in Figure 6.22(b), thus $|\beta(\omega_S, T_B+\Delta T)|^2 \neq |\beta(\omega_S, T_B)|^2$, as shown in Figure 6.21. The spike is due to the significant variation of $d\omega/dt$ during the flight time T_f as the field leaves the time dependent medium. In fact, [17] has shown that a $\omega(t)$ profile in which $d\omega/dt$ changes rapidly creates many more photons than profiles without rapid changes in $\omega(t)$. The phase angle of $\beta(\omega_S, t)$, i.e. $B(\omega_S, t)$, is also changing rapidly in this time interval (see Figure 6.27). This means the inclination angle of uncertainty contour in Figure 6.18 is changing with respect to time, and thus the uncertainty contour is rotating about its center point as time progresses.

In time interval C, a constant non-zero value of $|\beta(\omega_S, t)|^2$ value is seen. Within this time interval the state of the field is characterized by two photon coherent state. This corresponds to a time $t = T_C$ - T_f, when the optical field enters the modulating medium when $n(t)$ is relatively static at n, and leaves the medium at $t = T_C$ when $n(t)$ is relatively static at $n + \Delta n$, as shown in red from the $n(t)$ profile in Figure 6.22(c). During this time of flight T_f, the field experiences a step transition of $n(t)$ from n to $n + \Delta n$, thus $|\beta(\omega_S, T_C)|^2$ is non-zero. In time interval C, $|\beta(\omega_S, t)|^2$ has a steady state value. We see this by noting the field entering the modulator at a later time $t = T_C$ - $T_f + \Delta T$, will also experience a step transition of $n(t)$ as shown by the blue dotted line. Since the step profile for $n(t)$, shown by the blue dotted line is the

same as the red solid line in Figure 6.22(c), therefore $|\beta(\omega_S, T_C+\Delta T)|^2 = |\beta(\omega_S, T_C)|^2$ as shown in Figure 6.21. The steady state $|\beta(\omega_S,t)|^2$ value agrees with the analytical result given by [19] for a step profile of $n(t)$. In addition, a steady value of $|\beta(\omega_S,t)|^2$ suggests the phase angle of $\beta(\omega_S,t)$ i.e. $B(\omega_S,t)$, is time invariant and hence the inclination angle of uncertainty contour in Figure 6.18 remains unchanged for the time period C.

During time interval D, another spike in $|\beta(\omega_S,t)|^2$, which is similar to the one in time interval B, is generated and the field state is described by two photon coherent state. This is a consequence of the field entering the modulating medium when $n(t)$ is time varying, such as T_D - T_f, and leaves the medium at T_D when $n(t)$ is relatively stable at $n + \Delta n$, as shown by the red line in Figure 6.22(d). At the time in which the field enters the modulating medium, $d\omega/dt$ is rapidly changing, with $d\omega/dt = 0$ just before the field enters the medium, and $d\omega/dt \neq 0$ just after it enters the modulator. Similar to time interval B, $|\beta(\omega_S,t)|^2$ is time varying during time interval D. This is because the field experiences a different refractive index change if it enters the modulator at some ΔT time later, as shown by the blue dotted line in Figure 6.22(d). As a result, $|\beta(\omega_S, T_D+\Delta T)|^2 \neq |\beta(\omega_S, T_D)|^2$, as shown in Figure 6.21.

In time interval E, the field experiences a static $n(t)$ profile at $n + \Delta n$ during its time of flight inside the modulating medium, as shown by the red line in Figure 6.22(e). As a result, $d\omega_S/dt = 0$, which leads to $|\beta(\omega_S,t)|^2 = 0$, and the field is described by coherent state until the next transition occurs at the trailing edge of the pulse. Referring to Figure 6.20, we see that a leading edge transition in $n(t)$ produces a pair of spikes in $|\beta(\omega_S,t)|^2$, and another pair of spikes is produced at the trailing edge transition in $n(t)$. The profile of $|\beta(\omega_S,t)|^2$ due to a trailing edge transition can be understood by following a similar explanation for a leading edge transition in the paragraphs above. Furthermore, Figure 6.20 shows a trailing edge transition of $n(t)$

produces a similar $|\beta(\omega_S,t)|^2$ pulse as the leading edge transition. A summary for the above descriptions of Figure 6.22 is shown in Table 6.3.

Time interval	$\|\beta(\omega_S,t)\|^2$ characteristics	Field state	Comment
A	Zero	Coherent state	Field enters and leaves the medium when $n(t) = n$.
B	Non-zero transient spike	Two photon coherent state	Field entering the medium when $n(t)$ is static and leaves the medium when $n(t)$ is changing.
C	Non-zero steady state value	Two photon coherent state	Field enters and leaves the medium when $n(t)$ is static, BUT experienced a transition from $n(t) = n$ to $n(t) = n + \Delta n$ during its flight inside the medium.
D	Non-zero transient spike	Two photon coherent state	Field entering the medium when $n(t)$ is changing and leaves the medium when $n(t)$ is static.
E	Zero	Coherent state	Field enters and leaves the medium when $n(t) = n + \Delta n$.

Table 6.3: Summary for the descriptions of $|\beta(\omega_S,t)|^2$ profile.

The $|\beta(\omega_S,t)|^2$ profile in Figure 6.21 can be used to determine the photoelectrons accumulated at the measurement time in the detector T_M, generated by photon creation due to an alternating rectangular pulse pattern.

The frequency integral in Equation (6.97) shows the number of photoelectrons accumulated due to spontaneous emission from the modulator V, is contributed by the optical frequency ω_S as well as other frequencies that is within the passband of the photo-detector. The lower limit of the photo-detector passband is represented by ω_L,

while the upper limit is represented by ω_U, where the value of these parameters is given by Table 6.2. Therefore the profile of $|\beta(\omega,t)|^2$ within the photo-detector passband needs to be known for V to be determined. A plot of $|\beta(\omega,t)|^2$ at the lower limit of the detector passband (i.e. $|\beta(\omega_L,t)|^2$), against time t is shown in Figure 6.23.

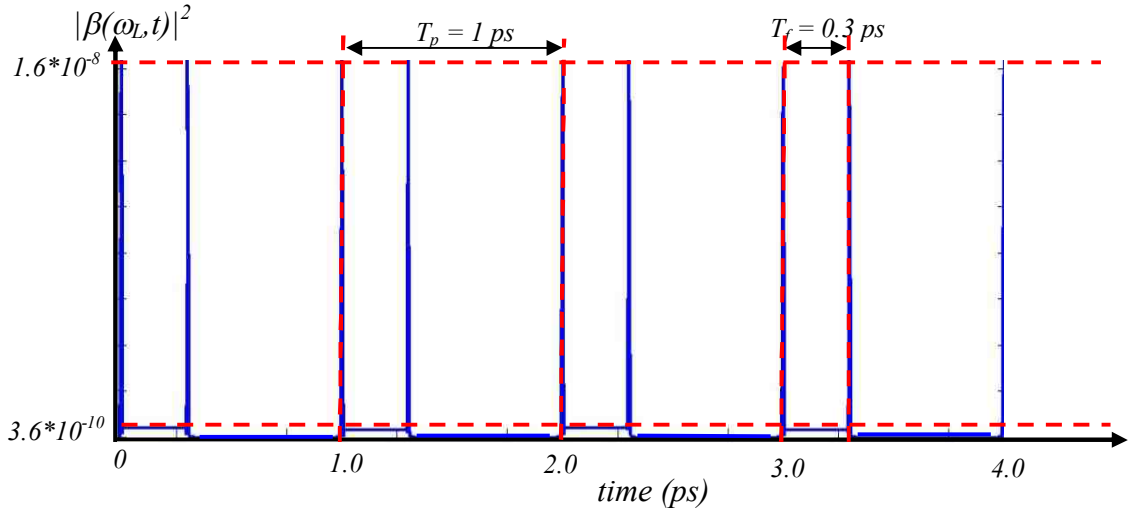

Figure 6.23: Temporal profile of $|\beta(\omega,t)|^2$ with $\omega = \omega_L$ for an alternating rectangular pulse pattern.

From Figure 6.23, it can be seen that the shape of $|\beta(\omega_L,t)|^2$ profile is very similar to $|\beta(\omega_S,t)|^2$ in Figure 6.20. Each photon pulse persists for duration of T_f. The differences between $|\beta(\omega_L,t)|^2$ and $|\beta(\omega_S,t)|^2$ are the amplitude of the overshoot and the non-zero steady state value. In the steady state (region C in Figure 6.21) $|\beta(\omega_S,t)|^2 < |\beta(\omega_L,t)|^2$. A plot of accumulated photoelectron count for one second, due to the effect of spontaneous emission out of the modulator, against frequency that lies within the passband of the photodiode, ω_L to ω_U, is shown in Figure 6.24.

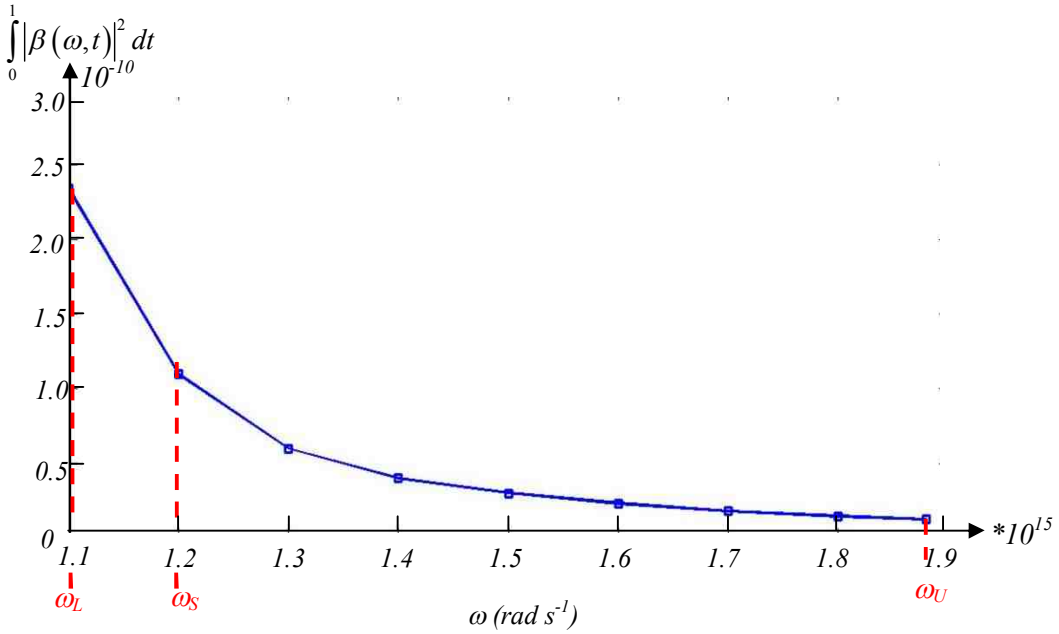

Figure 6.24: Photoelectron accumulated per second against frequency.

The plot is generated by performing the time integration from a number of $|\beta(\omega,t)|^2$ profiles for a set of values of ω over time interval $T_S = 0\ s$ to $T_S + T_M = 1\ s$, where T_M is the measurement time. The area under the curve in Figure 6.24 divided by 2π is the photoelectron count over one second due to spontaneous emission out of the modulator V, as indicated by Equation (6.97). Thus, the value of V is calculated to be

$$V = 8.4 * 10^4 \ electrons \tag{6.104}$$

This corresponds to an average current $<I_V>$ of $\langle I_V \rangle = \frac{Vq}{T_M} = 13.4 * 10^{-15}\ Amps$. The results in Figure 6.24 shows $|\beta(\omega,t)|^2$ decays at a faster rate than $1/\omega$, and is bounded by an upper limit of $(\Delta n)^2 / 4n(n+\Delta n)$ for $\omega \rightarrow 0$ (see Equation (5.47)). Therefore the frequency integral in Equation (6.97) is finite even if the frequency limit of the integral is taken from 0 to ∞. As a result, the process of spontaneous emission out of the modulator requires a finite amount of excitation energy from the external agent.

6.5.2 Stimulated Emission from Modulator

In this Subsection, we shall determine the photoelectron count accumulated from the process of stimulated emission out of the modulator κ. In Table 6.2, we have considered a CW single mode transmit laser that generates an optical field at a wavelength λ_S of *1550nm* (ω_S=*1.2*10*^{15} *rad s*$^{-1}$) with an output power of P_{in} = *1mW*. The mean photon flux F_S of the optical field before modulation is calculated to be

$$F_S = P_{in} / \hbar\omega_S = 7.8 * 10^{15} \ photons / s \tag{6.105}$$

For an ideal photodiode (i.e. quantum efficiency $\eta(\omega)$ = *1* within photodiode passband), the photoelectron flux $F_\kappa(t)$ generated from the process of stimulated emission can be expressed as

$$F_\kappa(t) = 2\left|\beta(\omega_S, t)\right|^2 F_S \tag{6.106}$$

where the subscript κ signifies the contribution from stimulated emission process. The relation between photoelectron flux $F_\kappa(t)$ and the photoelectron count accumulated κ, is given by

$$\kappa = \int_{T_S}^{T_S+T_M} F_\kappa(t)\, dt \tag{6.107}$$

Expression (6.106) can be realized as dividing the power flow of the stimulated emission out of the modulator (second term in Equation (6.28)) by photon energy $\hbar\omega_S$. A plot of the temporal profile of photoelectron flux contributed from stimulated emission from the modulator $F_\kappa(t)$, is shown in Figure 6.25.

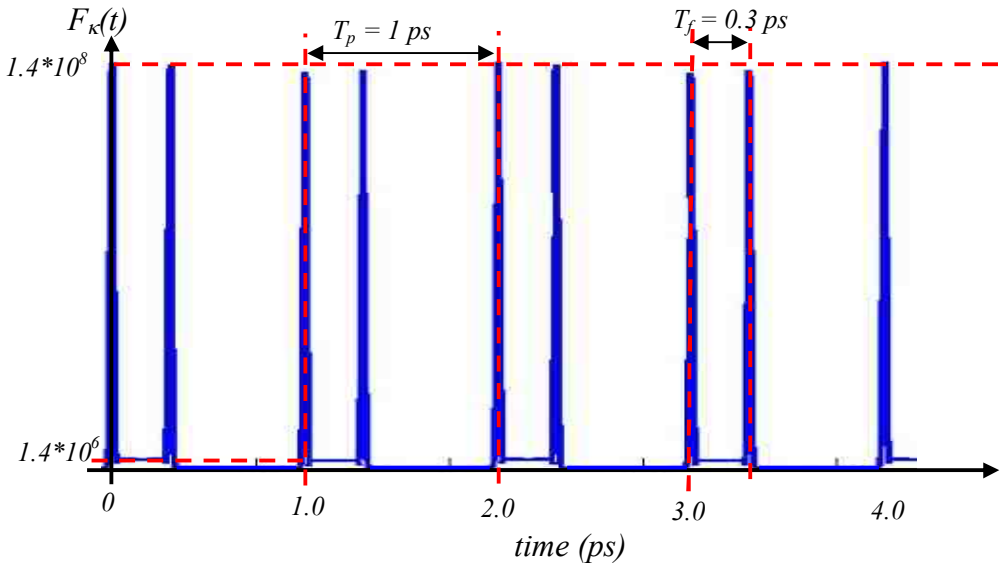

Figure 6.25: Temporal profile of photoelectron flux contributed from stimulated emission out of the modulator $F_\kappa(t)$.

Notice that the shape of the profile from Figure 6.25 is nearly identical to Figure 6.20, where a photon creation pulse of duration of T_f occurs at every transition of $n(t)$, except that Figure 6.25 has been scaled by a factor of $2F_S$.

Using the value of F_S in Equation (6.105) and (6.107), the photoelectrons accumulated per second from the stimulated emission process is calculated to be

$$\kappa = \int_0^1 F_\kappa(t)\,dt = 1.0*10^7 \ electrons \tag{6.108}$$

By comparing expression (6.108) with (6.104), we can identify the photoelectrons accumulated due to the stimulated process is roughly 2 orders of magnitude greater than the spontaneous process, thus we can neglect the spontaneous contribution in the calculation.

6.5.3 Energy Exchange between Signal Field and Modulator

In this Subsection, we shall determine the number of photoelectrons accumulated due to the energy exchange process between optical field and the modulator Γ. For clarity, we shall temporarily neglect the laser phase noise $\varphi_{SN}(\omega,t)$. The photoelectron flux $F_\Gamma(t)$ generated from the energy exchange process can be expressed as

$$F_\Gamma(t) = 2F_S\sqrt{1+\left|\beta(\omega_S,t)\right|^2}\,\left|\beta(\omega_S,t)\right|\cos\left[2\theta_S + A(\omega_S,t) + B(\omega_S,t)\right] \quad (6.109)$$

where the subscript Γ denotes the contribution from the energy exchange process, θ_S is the mean initial phase angle of the optical field, $A(\omega_S,t)$ and $B(\omega_S,t)$ are the phase $\alpha(\omega_S,t)$ and $\beta(\omega_S,t)$.

The relation between photoelectron flux $F_\Gamma(t)$ and the photoelectron count accumulated Γ, is given by

$$\Gamma = \int_{T_S}^{T_S+T_M} F_\Gamma(t)\,dt \quad (6.110)$$

The temporal profile of the photoelectron flux contributed from the energy exchange process is shown in Figure 6.26.

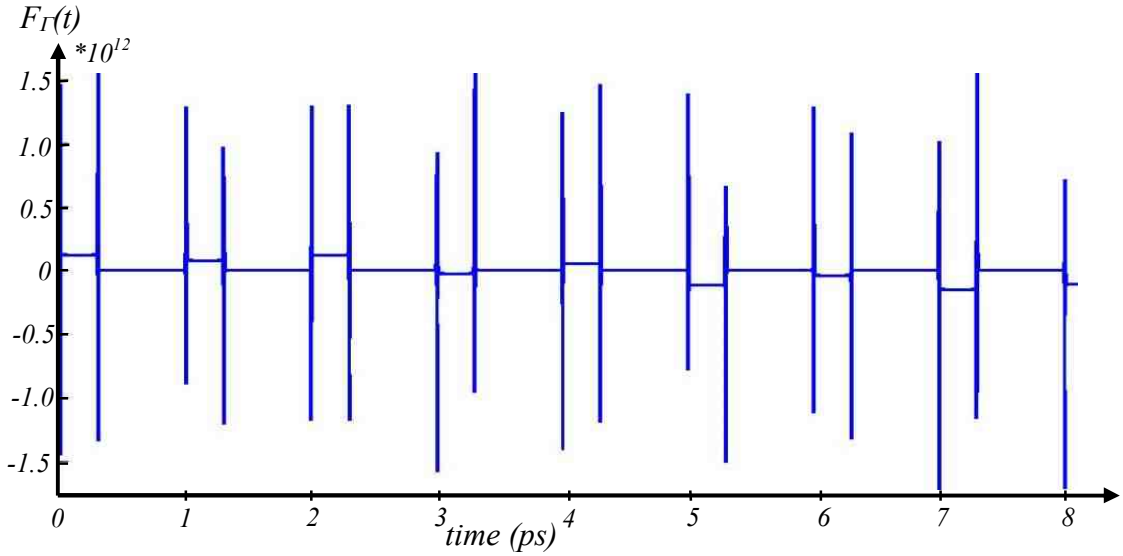

Figure 6.26: Temporal profile of photoelectron flux contributed from the process of energy exchange between optical field and modulator $F_\Gamma(t)$.

Figure 6.26 is generated by setting the mean initial phase angle to zero i.e. $\theta_S = 0$. By comparing Figure 6.26 with Figure 6.25, we can identify the magnitude of the photoelectron pulse contributed from the process of energy exchange is roughly 5 orders of magnitude greater than the stimulated process. As a result, we have $|F_I(t)| >> F_\kappa(t)$.

The total mean photoelectron flux contributed from the interaction between the optical field and the modulator is given by

$$F_T(t) = F_V(t) + F_\kappa(t) + F_\Gamma(t) \tag{6.111}$$

where $F_V(t)$ is the time varying mean photon flux created from the process of spontaneous emission out of the modulator. $F_V(t)$ can be determined by computing the frequency integral in Equation (6.97) i.e.

$$F_V(t) = \frac{1}{2\pi}\int_{\omega_L}^{\omega_U} \left|\beta(\omega,t)\right|^2 d\omega \tag{6.112}$$

From expression (6.112), we see $F_V(t) \geq 0$. Since $\kappa >> V$ (see expressions (6.104) and (6.108)), and both $F_V(t)$ and $F_\kappa(t)$ are always positive, we can therefore conclude $F_\kappa(t) >> F_V(t)$. Since $|F_I(t)| >> F_\kappa(t) >> F_V(t)$, thus the mean total photon flux created at a given time is mainly governed by the energy exchange process i.e. $F_T(t) \approx F_I(t)$. Therefore we simplify Equation (6.111) into

$$\begin{aligned} F_T(t) &\approx F_\Gamma(t) \\ &= 2F_S\sqrt{1+\left|\beta(\omega_S,t)\right|^2}\left|\beta(\omega_S,t)\right|\cos\left[2\theta_S + A(\omega_S,t) + B(\omega_S,t)\right] \end{aligned} \tag{6.113}$$

Due to the dominance of the energy exchange process, the temporal profile of $F_T(t)$ will follow $F_I(t)$ profile in Figure 6.26.

However, the steady state amplitude of each photon creation pulse (time interval C in Figure 6.21) is different and can be negative. This implies different number of

photons will be created at different transitions. This is due to the dependence on the phase angle $2\theta_S + A(\omega_S,t) + B(\omega_S,t)$. The mean input field phase angle is constant at θ_S. From Equation (6.18), the phase of $A(\omega_S,t)$ is the same for every transition. From Equation (6.19), the dependence of $\beta(\omega,t)$ on the complex exponential term inside the time integral indicates $B(\omega_S,t)$ varies from 0 to 2π for every transition. A plot of the variation of $B(\omega_S,t)$ against time is shown in Figure 6.27.

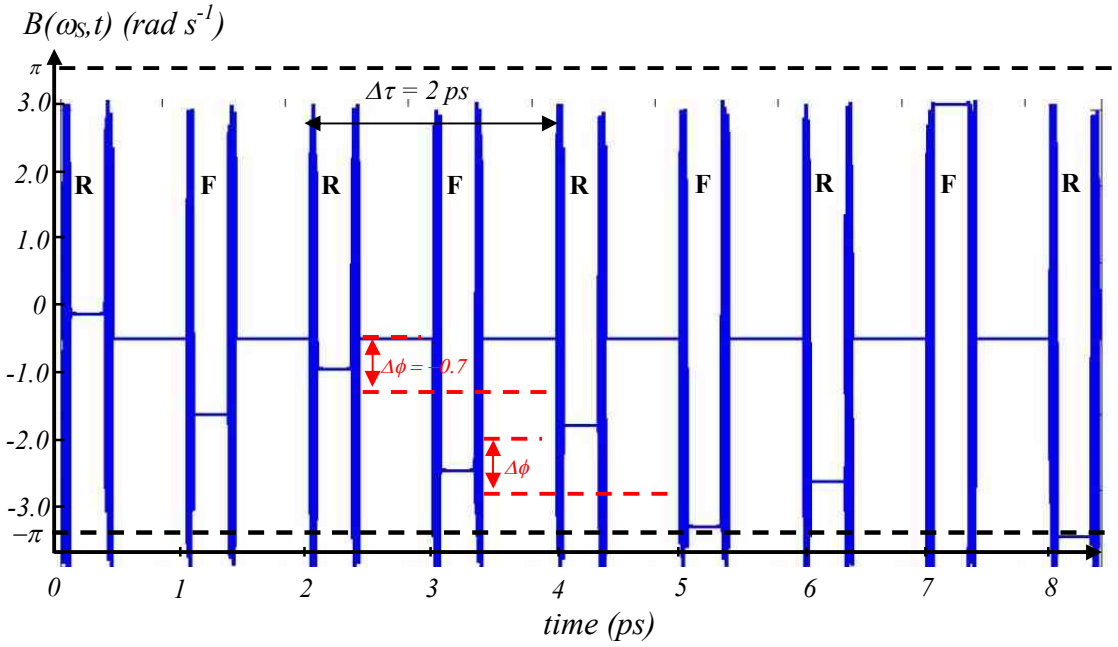

Figure 6.27: $B(\omega_S,t)$ against time.

By comparing Figure 6.27 with the refractive index $n(t)$ profile in Figure 6.19, we can identify the phase variation of $B(\omega_S,t)$ is non-zero when there is a transition in $n(t)$, where 'R' represents a rise transition in $n(t)$, while 'F' represents a fall transition in $n(t)$. For each transition of $n(t)$ the non-zero constant value of $B(\omega_S,t)$ persists for roughly for a duration of T_f before it returns back to zero. At every transition, the phase of $B(\omega_S,t)$ is different, which is responsible for the difference in the steady state amplitude of $F_I(t)$ as shown in Figure 6.26. Furthermore, Figure 6.27 shows $B(\omega_S,t)$

changes by an amount of $\Delta\phi$ for every second transition, which implies $B(\omega_S,t)$ will change by an angle of $\Delta\phi$ for every rise/fall transition. The phase drift of $B(\omega_S,t)$ in Figure 6.27 signifies the non-zero steady state value of $F_\Gamma(t)$ oscillates in between $|F_\Gamma(t)|$ and $-|F_\Gamma(t)|$ in the order *20* pico-seconds (i.e. $2\pi\Delta\tau/\Delta\phi \sim 20ps$). As a result, the positive values of $F_\Gamma(t)$ will cancel out with the negative values of $F_\Gamma(t)$ within the measurement interval $T_M >> t_c$. Although the photo-electron count generated from the energy exchange process $F_\Gamma(t)$ is in general much greater than the stimulated process $F_\kappa(t)$, the average number of photoelectrons accumulated due to the energy exchange process will be small due to this cancellation. Thus we have

$$\Gamma << \kappa \tag{6.114}$$

Short term effects of particle creation or annihilation by field-modulator energy exchange could be large but at the current time there are no known practical situations where such short time scales are relevant. Expression (6.114) show in the time scale of optical detection, the number of photoelectrons accumulated from the energy exchange process can be neglected as it is much smaller than stimulated emission process κ.

If the impact of phase noise $\varphi_{SN}(\omega_S,t)$ is considered, it will give the same result as in Equation (6.114). This is because the measurement time T_M is much greater than the transmit laser coherence time t_c, thus the PDF of $F_\kappa(t)$ is represented by expression (6.52). Using the result in Equation (6.54), it is shown that Γ averages out to *0* over time when the effect of phase noise is included.

Using the expression (6.43), and the result in Equation (6.108), the total mean photoelectron count accumulated in *1* second due to the quantum effect of photon creation from modulator, is given by

$$\begin{aligned}\delta Y &= V + \kappa + \Gamma \\ &\approx \kappa \\ &= 1.0*10^{7}\ photoelectrons\end{aligned} \tag{6.115}$$

In order to determine the effect of photon creation, we shall define the quantum ratio Φ as

$$\Phi = \frac{\left\langle \delta \hat{Y} \right\rangle}{\left\langle \hat{Y}_{in} \right\rangle} \tag{6.116}$$

where $<\hat{Y}_{in}>$ is the mean photoelectron count detected from the unmodulated field. The bigger the value of Φ, the effect of photon creation will become more dominant. By using the result of δY in Equation (6.116), and the expression of $<\hat{Y}_{in}>$ in Equation (6.32), Φ is calculated to be

$$\Phi = \frac{1.0*10^{7}}{7.8*10^{15}} = 1.3*10^{-9} \tag{6.117}$$

From (6.117), we can determine the photon creation has an effect of *1 part to the* 10^9 *(1/*Φ*)*, hence the effect of photon creation is small.

6.5.4 Dependence of Photon Creation Process

In this Subsection we shall determine the factors that govern the process of photon creation out of the modulator. From the power flow expression (6.28) in Section 6.2, it is shown that the process of photon creation is dependent on the Bogoliubov coefficients $\alpha(\omega,t)$ and $\beta(\omega,t)$. From expression (6.18) and (6.19), it is shown that $\alpha(\omega,t)$ and $\beta(\omega,t)$ is dependent on the field frequency $\omega(t)$, the photon flight time of the modulator T_f, and the rate of change of instantaneous frequency $d\omega/dt$ of the field subjected to modulation. In previous Subsections, we have shown the temporal profile of the field frequency $\omega(t)$ is governed by the refractive index profile $n(t)$. The features that govern the profile of $n(t)$ include the transition rate Ω and change in

refractive index Δn. As a result, these factors also have influence on the process of photon creation. In summary, the factors that govern the process of photon creation are

1. The frequency of input optical field (unmodulated) ω_S.
2. Photon flight time in the modulator T_f.
3. 10 – 90% bit transition rate.
4. Magnitude of the change in nonlinear refractive index Δn.

An alternating rectangular pulse refractive index profile given in Equation (6.102) is considered, and the simulation parameters in Table 6.2 will be used to generate the numerical results presented in this Subsection. We shall investigate how the process of photon creation will be influenced by changing the dependent parameters from above one at a time.

Equation (6.43) represents the difference in mean photoelectron count detected between the modulated and unmodulated field, as a consequence of the effect of photon creation from modulator. In Equation (6.115), we have shown this difference is primarily due to the process of stimulated emission out of the modulator κ. We shall begin by determining how the process of photon creation gets affected by changing the optical frequency of the input (unmodulated) field ω_S, while other parameters in Table 6.2 are kept fixed. A plot of the photoelectron count accumulated within the measurement time interval of $T_M = 1\ s$ due to photon creation from the modulator, against frequency of input unmodulated field, is shown in Figure 6.28.

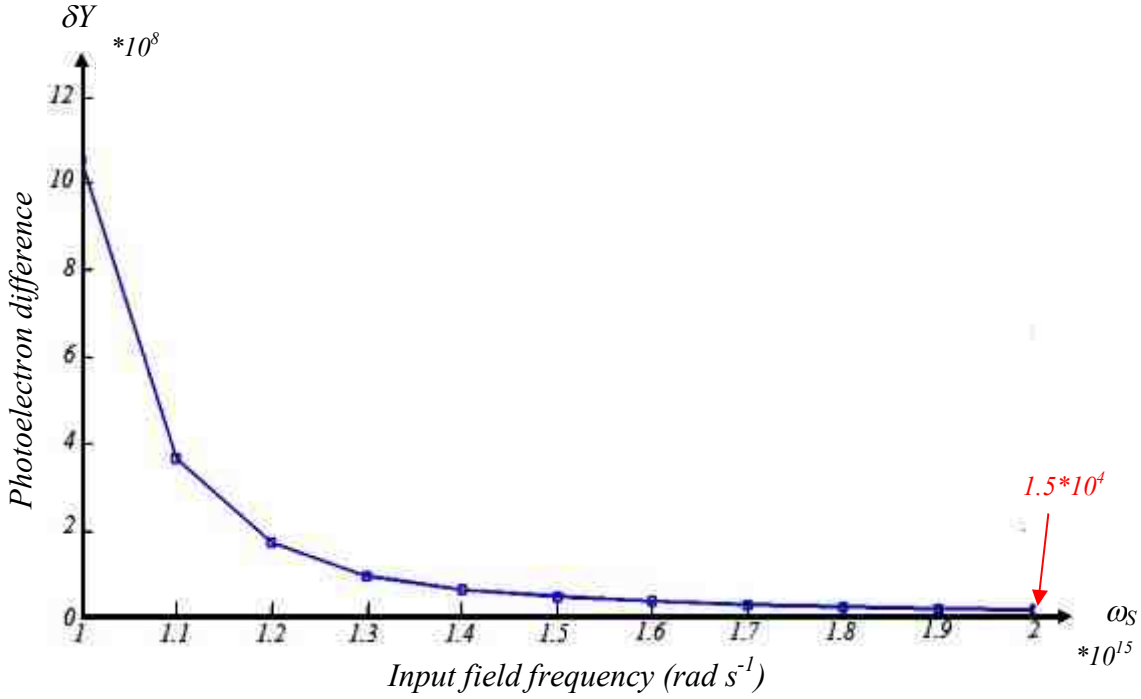

Figure 6.28: Photoelectron difference between modulated field and input field δY for $T_M = 1\ s$ against input field frequency ω_S.

Figure 6.28 shows the difference in photoelectron flux detected between the output (modulated) and input (unmodulated) field decreases exponentially with an increase of the input field frequency. This is because ω_S is inversely related to $\beta(\omega,t)$, as shown in expression (6.19). This makes physical sense because photons associated with higher frequency modes have more energy.

We shall now determine the effect of photon creation with respect to the photon flight time in the modulator T_f. A plot of the mean photoelectron difference detected between the modulated output and the unmodulated input field for $T_M = 1\ s$, against photon flight time in the modulator, is shown in Figure 6.29.

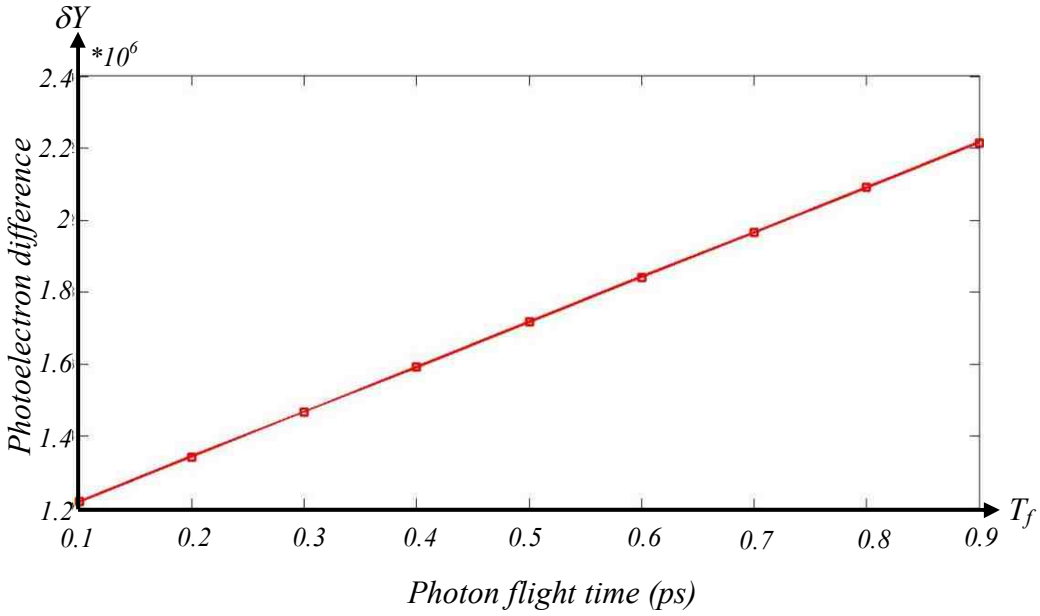

Figure 6.29: Relation between photoelectron difference of modulated and unmodulated optical field δY and photon flight time in modulator T_f.

From Figure 6.29, it is shown that for $T_f < T_p$ i.e. $T_p = 1\ ps$, the mean photoelectron difference increases linearly with respect to T_f. This is because an increase in T_f implies an increase in the length of the modulator. As a result, the interaction length between the modulator and the control signal increases, thus more photons will be created from the modulator.

Figure 6.30 reveals the relation between the mean photoelectron difference detected between the modulated and unmodulated field δY and refractive index change Δn.

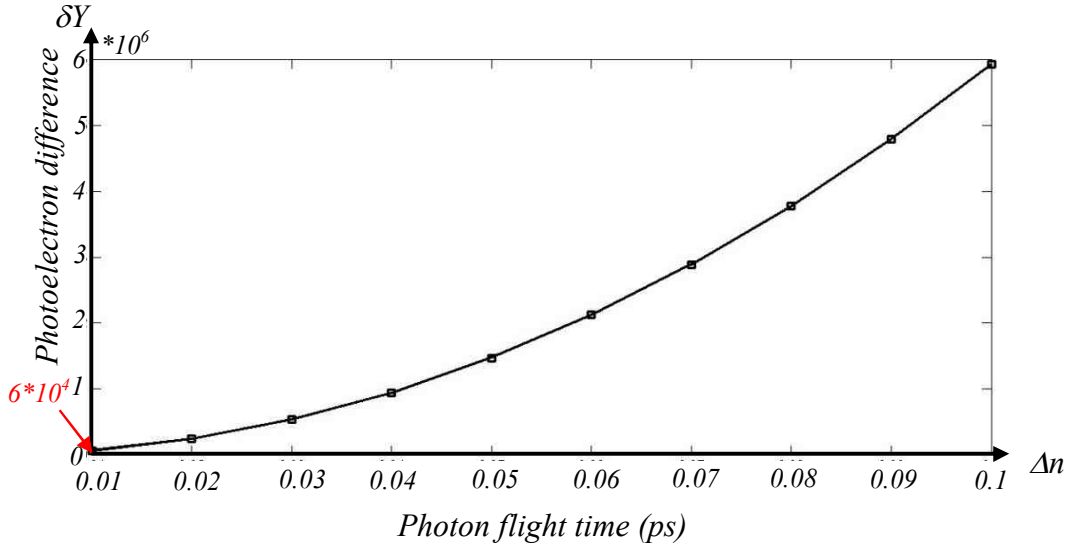

Figure 6.30: Photoelectron difference of modulated and unmodulated field δY for $T_M = 1\ s$ against magnitude of nonlinear refractive index Δn.

Figure 6.30 shows the photon number created from the modulator increases exponentially with respect to an increase in nonlinear refractive index. This trend can be shown from the mathematical expression in Equation (6.102), for which the refractive index profile $n(t)$ is linearly proportional to the nonlinear refractive index Δn. Therefore increasing Δn will lead to an increase in the rate of change in refractive index dn/dt. Since the rate of change in frequency $d\omega/dt$, is related to dn/dt, as indicated by Equation (6.20), therefore using Equation (6.19), we find an increase in dn/dt will lead to an exponential increase in $|\beta(\omega_S,t)|^2$, and thus δY increases exponentially according to expression (6.115).

Finally, we shall determine how changes in bit transition rate will alter the process of photon creation. The relation between the mean photoelectron difference and the bit transition rate is shown in Figure 6.31.

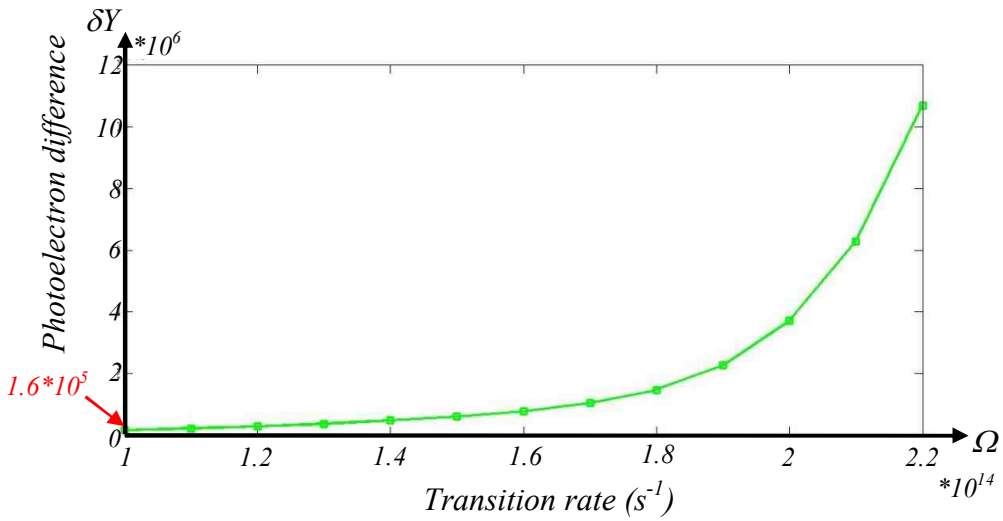

Figure 6.31: Photoelectron difference of modulated and unmodulated optical field δY for $T_M = 1\ s$ against bit transition rate Ω.

Figure 6.31 shows the mean photoelectron difference detected due to photon creation, increases exponentially with respect to an increase in bit transition rate Ω. This is because *dn/dt* is dependent on Ω which can be verified from Equation (6.102). Using Equation (6.19) and Equation (6.20), we can identify an increase *dn/dt* will lead to an exponential increase in $|\beta(\omega_S,t)|^2$, and thus δY increases exponentially according to Equation (6.115). An exponential increase in photon number from Figure 6.31 is valid provided the adiabatic condition in Equation (6.21) is satisfied.

6.6 PSD for Sinusoidal Modulation

The quantum model of phase modulator presented by [9] shows when the carrier signal (optical field) is sinusoidally modulated, the PSD of the modulated field is described by Bessel function, which agrees with the classical modulation theory [22 - 24]. However the quantum model from [9] neglects the effect of photon creation. In this Section, we shall determine the power spectral density (PSD) of a sinusoidal

phase modulated field with the effect of photon creation from modulator included in the analysis.

The simulation parameters used in this analysis is given by Table 6.4 from below.

Parameters	Notations	Value
Transmit laser power	P_{in}	*1 mW*
Optical carrier wavelength	λ_S	*1550 nm*
Refractive index (unmodulated)	n	*3.5*
Nonlinear refractive index change	Δn	*0.05*
Control signal frequency	ζ	$10^{12}\ s^{-1}$
Photon flight time in modulator	T_f	$1/2\zeta = 0.25$ *ps*

Table 6.4: Parameters used in sinusoidal modulation.

As we have discussed in previous Subsections, *n(t)* follows the intensity profile of the control signal $i_C(t)$. Therefore, a convenient form of sinusoidal refractive index profile can be expressed as

$$n(t) = n + \frac{\Delta n}{2}\left[1 + \sin(2\pi\zeta t)\right] \tag{6.118}$$

where the parameters in Equation (6.118) is defined in Table 6.4. By using the simulation parameters in Table 6.4, a plot of *n(t)* is shown in Figure 6.32.

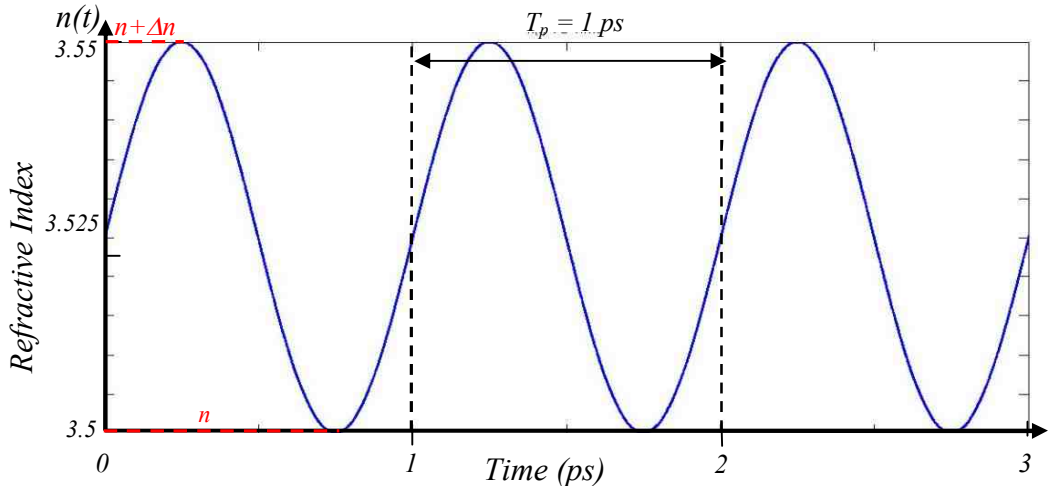

Figure 6.32: Refractive index profile induced from sinusoidal control signal.

By using the expression of $n(t)$ in (6.118), as well as relating $n(t)$ and $\omega(t)$ by Equation (6.16), $\omega_S(t)$ can be expressed as

$$\begin{aligned}\omega_S(t) &= \frac{n\omega_S}{n\left\{1+\frac{\Delta n}{2n}\left[1+\sin 2\pi\zeta t\right]\right\}} \\ &\approx \frac{n\omega_S}{n}\left[1-\frac{\Delta n}{2n}\left[1+\sin\left(2\pi\zeta t\right)\right]\right] \\ &= \omega_S - \frac{\Delta\omega}{2}\left[1+\sin\left(2\pi\zeta t\right)\right]\end{aligned} \tag{6.119}$$

In the second line of Equation (6.119), the first order Taylor series approximation has been used because $\Delta n << n$. ω_S is the frequency of the unmodulated optical field. $\Delta\omega$ is the maximum frequency deviation and is defined as $\Delta\omega = \omega_S\Delta n/n$. By substituting expression (6.119) into Equation (6.15), the modulated phase angle is given by

$$\begin{aligned}W(\omega_S,t) &= \omega_S t - \omega_S T_f + \int_{t-T_f}^{t} \omega_S - \frac{\Delta\omega}{2}\left[1+\sin\left(2\pi\zeta\tau\right)\right]d\tau \\ &= \omega_S t + \frac{\Delta\omega}{2}\left\{T_f + \frac{1}{2\pi\zeta}\left[\cos\left(2\pi\zeta t\right) - \cos\left(2\pi\zeta\left(t-T_f\right)\right)\right]\right\}\end{aligned} \tag{6.120}$$

By choosing the photon flight time inside the modulating medium to be $T_f = 1/2\zeta$, the phase offset induced from the modulator is a sinusoid [5], in which $W(\omega_S,t)$ in Equation (6.120) can be re-expressed as

$$W(\omega_S,t) = \omega_S t + \frac{\Delta\omega\cos\left(2\pi\zeta t\right)}{2\pi\zeta} + \Delta\varphi \tag{6.121}$$

where $\Delta\varphi = \Delta\omega T_f/2$.

From the theory of signal processing, the PSD denoted by $P(\omega)$, is expressed as [56]

$$P(\omega) = \left|S(\omega)\right|^2 \tag{6.122}$$

where $S(\omega)$ is the spectral amplitude, and can be determined from the Fourier Transform of the time varying signal amplitude *s(t)*

$$S(\omega) = \int_{-\infty}^{\infty} s(t)\exp(-i\omega t)\,dt \tag{6.123}$$

The time varying signal amplitude *s(t)* is related with the power flow of the signal field via. the expression [56]

$$P(t) = |s(t)|^2 \tag{6.124}$$

In QFT, the *s(t)* can be approximated as

$$s(t) \approx \sqrt{2\varepsilon_0 c_0 A}\left\langle \hat{E}_{out}^{+}(t)\right\rangle \tag{6.125}$$

where the modulated field component $\hat{E}_{out}^{+}(t)$ is related to $\hat{e}_{out}^{+}(\omega,t)$ in Equation (6.14) by

$$\hat{E}_{out}^{+}(t) = \int_{0}^{\infty} \hat{e}_{out}^{+}(\omega,t)\,d\omega \tag{6.126}$$

The time varying signal amplitude can be determined by using the expression of the modulated field operator in Equation (6.13), the relations in (6.28), and the approximation in (6.125), where we arrived at

$$\begin{aligned} s(t) &\approx \sqrt{2\varepsilon_0 c_0 A}\left\langle \hat{E}_{out}^{+}(t)\right\rangle \\ &= \sqrt{\hbar\omega_S F_S}\left[\alpha(\omega_S,t)+\beta^*(\omega_S,t)\right]\exp\left[-i\left(W(\omega_S,t)-\theta_S\right)\right] \end{aligned} \tag{6.127}$$

where $W(\omega,t)$ is the modulated phase angle given by Equation (6.15) and θ_S is the mean initial phase angle of the signal field. It can be verified that the magnitude squared of the signal amplitude in Equation (6.127) does not include the last term in Equation (6.28) (i.e. spontaneous emission from modulator), therefore Equation (6.125) is an approximate expression because it does not exactly satisfy the condition in Equation (6.124). Given that the power of the transmit laser is in the order of *1 mW*, the photoelectron flux contributed from the process of spontaneous emission from

modulator V is much smaller than the other photon creation process, as discussed in previous Subsections. Therefore the $s(t)$ is well approximated by Equation (6.127).

By substituting the phase expression in Equation (6.121) into the signal amplitude expression in Equation (6.127), we have

$$s^{SIN}(t) = \sqrt{\hbar\omega_S F_S}\left\{\alpha(\omega_S,t) + \beta^*(\omega_S,t)\right\}\exp\left[-i\left(\omega_S t + \frac{\Delta\omega\cos(2\pi\zeta t)}{2\pi\zeta} - \varphi_{out} - \theta_S\right)\right] \tag{6.128}$$

where φ_{out} is the propagation phase delay due to field propagation, and can be expressed as $\varphi_{out} = \varphi_{in} + \Delta\varphi$. The sinusoidal component inside the complex exponential term in Equation (6.128) can be expressed as [22, 55]

$$\exp\left[K\cos(2\pi\zeta t)\right] = \sum_{m=-\infty}^{\infty} J_m(K)\exp(-i2\pi m\zeta t) \tag{6.129}$$

$J_m(K)$ is the mth order Bessel function of the first kind, and is given by [22, 55]

$$J_m(K) = \frac{1}{2\pi}\int_{-\pi}^{\pi}\exp\left[i(K\sin x - mx)\right]dx \tag{6.130}$$

where m is an integer. By using Equation (6.130) to re-express the signal amplitude $s^{SIN}(t)$ from Equation (6.128) in terms of Bessel function $J_m(K)$, we have

$$s^{SIN}(t) = \sqrt{\hbar\omega_S F_S}\left\{\alpha(\omega_S,t) + \beta^*(\omega_S,t)\right\}\sum_{m=-\infty}^{\infty} J_m\left(\frac{\Delta\omega}{2\pi\zeta}\right)\exp(-i2\pi m\zeta t) \tag{6.131}$$

If the effect of photon creation is neglected, $\alpha(\omega_S,t) = 1$ and $\beta(\omega_S,t) = 0$, the signal amplitude of the modulated field is expressed as

$$s_{CFT}^{SIN}(t) = \sqrt{\hbar\omega_S F_S}\sum_{m=-\infty}^{\infty} J_m\left(\frac{\Delta\omega}{2\pi\zeta}\right)\exp\left[-i(\omega_S t + i2\pi m\zeta t - \varphi_{out} - \theta_S)\right] \tag{6.132}$$

By using Equation (6.132), (6.123) and (6.122), the PSD of the modulated field for which the effect of photon is neglected, is expressed as

$$P_{CFT}^{SIN}(\omega) = \hbar\omega_S F_S\sum_{m=-\infty}^{\infty} J_m{}^2\left(\frac{\Delta\omega}{2\pi\zeta}\right)\left[\delta(\omega+\omega_S+2\pi m\zeta) + \delta(\omega-\omega_S-2\pi m\zeta)\right] \tag{6.133}$$

The expression in (6.133) resembles to the quantum result presented by [9], as well as the results from classical field theory (CFT) [22 - 24]. This shows our analysis

reproduces the standard results if the effect of photon creation is neglected. Once again, this signifies the model presented by [9], does **not** give a complete quantum representation of the phase modulation process as it does not include the effect of photon creation from modulator.

A comparison between the PSD determined from QFT (effect of photon creation included), with the standard PSD obtained from CFT, is shown in Figure 6.33.

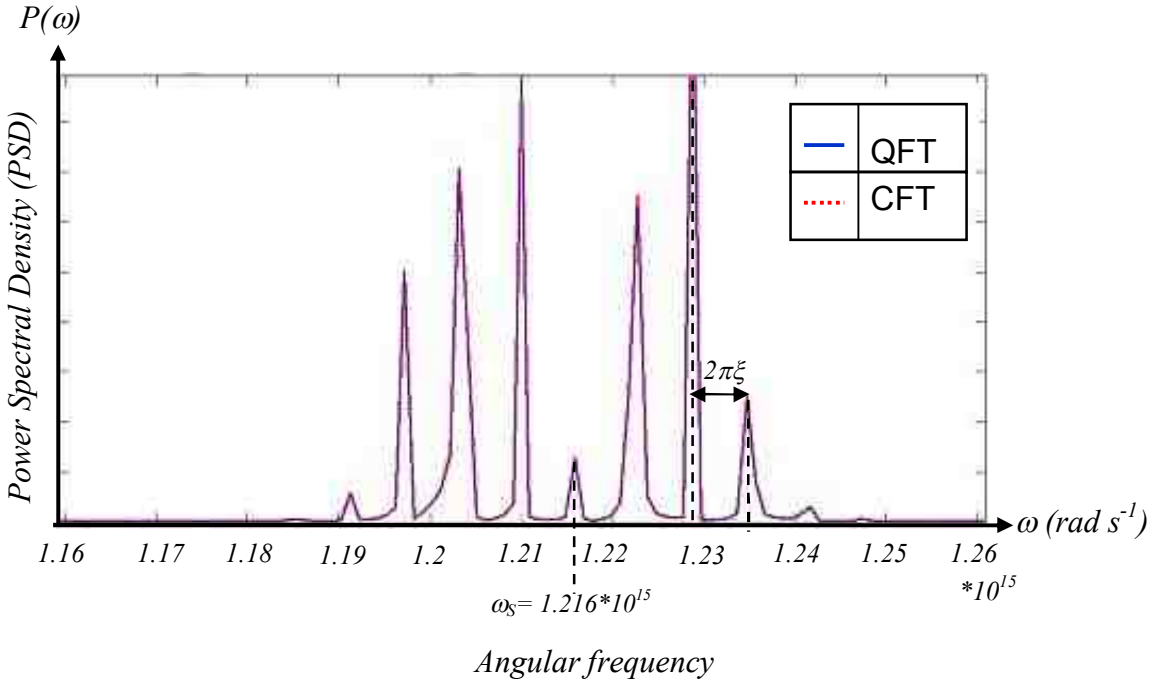

Figure 6.33: Comparison of PSD between QFT (photon creation included) and SCFT (photon creation not included) for sinusoidal modulation.

The red dotted line in Figure 6.33 is a plot of expression (6.133). It shows the spectrum of a phase modulated field contains a carrier frequency component ω_S and an infinite set of sidebands, i.e. side frequencies, located symmetrically on either side of ω_S. Each sideband is equally separated from one another by an angular frequency of $2\pi\zeta$. The amplitude for each sideband is roughly governed by the square of the absolute value of Bessel function i.e. $|J_m(\Delta\omega/2\pi\xi)|^2$. The blue solid line represents

PSD determined from QFT. From Figure 6.33, we can identify the blue dotted line is almost an overlap of the solid red line, because the effect of photon creation is small, as indicated from expression (6.117).

6.7 Conclusions

In this Chapter, we have investigated the key properties of the phase modulated field by accounting for the effect of photon creation from the modulator in the analysis. We identify there is a power flow mismatch at the input and output of a lossless modulator during the modulation process. The mismatch in power flow is accounted for by noting that an external agent alters the refractive index of the modulator which excites the vacuum state of the field so that photons are created or removed from the optical field during the modulation process. It is shown the process of photon creation affects the mean and variance of photoelectron arrival statistics observed by the detector. If the detection time is relatively long as compared with the repetition rate of the control signal, the effect of photon creation increases the mean and variance of photoelectron arrival statistics. However, the increase in variance is greater than the mean, thus photon creation degrades the SNR of phase modulated field.

The process of photon creation also alters the state of the modulated field. If the effect of photon creation is neglected, the modulated field can be described by continuum coherent state. However, if the effect of photon creation is included in the analysis, the modulated field should be described by two photon coherent state and the photon arrival statistics is no longer Poissonian.

The phenomenon of photon creation can be classified into three independent processes, spontaneous emission and stimulated emission from modulator as well as

energy exchange between the optical field and the modulator. Simulation results in Section 6.5 shows although the mean photon flux created from the modulator is dominated by the energy exchange process Γ, however the total mean photoelectron count detected is governed by the process of stimulated emission from modulator. This is because the energy exchange process will average out to zero due to the presence of phase noise and the time varying phase angle of Bogoliubov coefficients. Numerical results also show the phenomenon of photon creation has an effect in the order of *1 part to* 10^9 for tera-bit per second *(Tbps)* rectangular pulse modulation, and thus this implies the effect of photon creation has an insignificant impact to a phase modulated optical system. The effect of photon creation on optical detection can be enhanced by decreasing the frequency of the input optical field ω_S, as well as increasing the photon flight time of the modulator T_f, the change in nonlinear refractive index Δn and the bit transition rate.

Finally, we have shown if the effect of photon creation from modulator is neglected, the PSD of a sinusoidal phase modulated field given by our model reproduces the Bessel function profile determined from CFT [22 - 24]. Furthermore, even if the effect of photon creation is included, the PSD for a *THz* sinusoidal phase modulated field closely resembles to the CFT results (Bessel function profile), which once again suggests that the impact of photon creation is small.

7 Quantum Modelling of Communication Systems

7.1 Chapter Objectives

In this Chapter, quantum field models of the commonly used modulation formats in optical communication systems are presented. These modulation formats include homodyne and heterodyne binary phase shift keyed system (BPSK-HO, BPSK-HE), as well as homodyne and heterodyne amplitude shift keyed system (ASK-HO, ASK-HE). The quantum field expression of the phase modulated signal, derived in Chapter 5, will be used in these models.

This Chapter is organized as follows. In Section 7.2, the signal amplitude and the noise detected from the BPSK-HO and BPSK-HE systems are derived from the quantum field analysis. Similarly in Section 7.3, the signal amplitude and the noise detected from the ASK-HO and ASK-HE systems are derived. The expressions obtained in these two Sections reveal the differences between the results given by semi-classical field theory (SCFT) [1, 25] and quantum field theory (QFT).

In Section 7.4, the optical detection theory presented in Chapter 2, is used to determine the bit error rate (BER) quantum limit and the signal to noise ratio (SNR) of the modulation systems considered, operating at a bit-rate of *2 Tbps*. Furthermore, this Section reveals the effect of bit transition on quantum limit by considering a continuous alternating bit pattern, for which a bit transition occurs in every bit period *'1010..'*. A comparison is drawn between the results obtain from SCFT and QFT for

this bit pattern. The effect of photon creation and its relative impact to the communication system is distinguished from these comparisons.

In Section 7.5, the dependence between the BER quantum limit and the bit-rate will be shown from the simulation results.

7.2 Quantum Field model of BPSK System

In a BPSK system, the transmitted data is encoded onto the phase of the optical field by the use of an external phase modulator at the transmitter. The optical field is generated from the transmit laser operating in steady state. A coherent receiver is used to detect the encoded data in order to determine the information being sent. In this Section, a quantum field model for the BPSK system is developed in order to consider the impact of photon creation on the system, an effect that cannot be incorporated using semi-classical field theory (SCFT).

7.2.1 Analysis of BPSK Transmitter

A BPSK transmitter consists of a laser and a phase modulator as shown in Figure 7.1. The laser generates an optical field typically at a wavelength of *1500 nm*. The phase of the optical field will be modulated by the phase modulator. The phase change of the optical field is governed by the control signal. When a bit *'1'* is sent the phase of the optical field is unchanged, and when a bit *'0'* is sent, the phase of the field will experience an 180^0 phase shift. The phase modulated optical field will then propagate to the receiver.

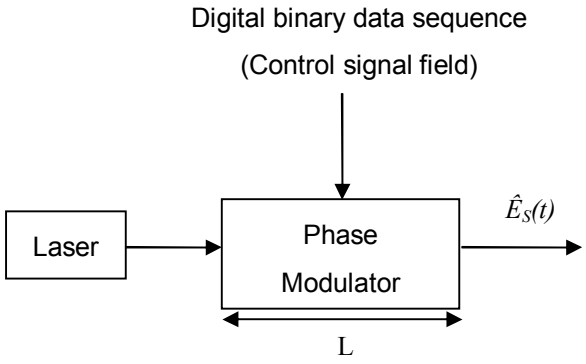

Figure 7.1: Configuration of BPSK transmitter.

In this Chapter, we shall represent the optical field in terms of quantum field operator instead of mathematical function as in SCFT presented in Chapter 2. The effect of laser phase noise $\varphi_{SN}(\omega,t)$ will be considered in this analysis. We shall use the Heisenberg picture in which the field operator changes as a consequence of modulation, but the state of the field remains unchanged. In Chapter 5.5, we have shown the phase modulated signal field operator $\hat{E}_S(t)$ after propagating through the phase modulator can be expressed as

$$\begin{aligned}\hat{E}_S(t) &= \hat{E}_S^{+}(t) + \hat{E}_S^{-}(t) \\ &= \int_0^{\infty} \hat{e}_S^{+}(\omega,t) + \hat{e}_S^{-}(\omega,t) d\omega \\ &= \int_0^{\infty} \left(\frac{\hbar\omega}{4\pi\varepsilon_0 c_0 A}\right)^{1/2} \left\{\hat{b}_S(\omega,t)\exp\left(-i\left[W(\omega,t)-\varphi\right]\right) + H.c.\right\} d\omega\end{aligned} \tag{7.1}$$

where ω is the angular frequency, $\hat{b}_S(\omega,t)$ is the annihilator of the phase modulated field, $W(\omega,t)$ represents the time varying phase as a consequence of modulation, φ is the propagation phase delay, and *H.c.* is an abbreviation for Hermitian conjugate. By comparing the second line and the last line of Equation (7.1), it can be identified that the expression of $\hat{e}_S^{+}(\omega,t)$ takes the form

$$\hat{e}_S^{\,+}(\omega,t)=\left(\frac{\hbar\omega}{4\pi\varepsilon_0 c_0 A}\right)^{1/2}\hat{b}_S(\omega,t)\exp\left(-i\left[W(\omega,t)-\varphi\right]\right) \tag{7.2}$$

The time varying phase due to modulation can be expressed as

$$W(\omega,t)=\omega t-\omega T_f+\int_{t-T_f}^{t}\omega(\tau)\,d\tau \tag{7.3}$$

where T_f is the photon flight time inside the modulating medium.

In Chapter 6, we have shown the annihilation operator of phase modulated field $\hat{b}_S(\omega,t)$ is related to the phase noise input unmodulated field annihilation and creation operator, $\hat{a}_{S\varphi}(\omega,t)$ and $\hat{a}_{S\varphi}^{\,+}(\omega,t)$, by the time and frequency dependent Bogoliubov transform

$$\hat{b}_S(\omega,t)=\alpha(\omega,t)\hat{a}_{S\varphi}(\omega,t)+\beta^*(\omega,t)\hat{a}_{S\varphi}^{\,+}(\omega,t) \tag{7.4}$$

where $\alpha(\omega,t)$ and $\beta(\omega,t)$ are the time dependent Bogoliubov coefficients. In Chapter 5.2, we have derived their approximate expression to 1st order to be

$$\alpha(\omega,t)=1+i\int_{t-T_f}^{t}\left(\frac{1}{\omega(\tau)}\right)^{1/2}\frac{d}{d\tau}\left(\frac{d\omega/d\tau}{4\omega^{3/2}(\tau)}\right)d\tau \tag{7.5}$$

$$\beta(\omega,t)=-i\int_{t-T_f}^{t}\left(\frac{1}{\omega(\tau)}\right)^{1/2}\frac{d}{d\tau}\left(\frac{d\omega/d\tau}{4\omega^{3/2}(\tau)}\right)\exp\left(-2i\left[\omega\tau-\omega T_f+\int_{\tau-T_f}^{\tau}\omega(t')dt'\right]\right)d\tau \tag{7.6}$$

where the Bogoliubov coefficients satisfy the identity,

$$\left|\alpha(\omega,t)\right|^2-\left|\beta(\omega,t)\right|^2=1 \tag{7.7}$$

Using the transformation in Equation (7.4), the Bogoliubov identity in Equation (7.7), and the equal time commutation relation for $\hat{a}_{S\varphi}(\omega,t)$ and $\hat{a}_{S\varphi}^{\,+}(\omega,t)$ introduced in Chapter 6.2 i.e.,

$$\begin{aligned}\left[\hat{a}_{S\varphi}(\omega,t),\hat{a}_{S\varphi}^{\,+}(\omega',t)\right]&=\hat{a}_{S\varphi}(\omega,t)\hat{a}_{S\varphi}^{\,+}(\omega',t)-\hat{a}_{S\varphi}^{\,+}(\omega',t)\hat{a}_{S\varphi}(\omega,t)\\&=\delta(\omega-\omega')\end{aligned} \tag{7.8}$$

the commutation relation of phase modulated field annihilator $\hat{b}_S(\omega,t)$ and creator $\hat{b}_S^{+}(\omega',t)$ is determined to be

$$\left[\hat{b}_S(\omega,t),\hat{b}_S^{+}(\omega',t)\right]=\delta(\omega-\omega') \tag{7.9}$$

In Chapter 6, we have shown the phase noise annihilation operator $\hat{a}_{S\varphi}(\omega,t)$ is related to the input annihilation operator $\hat{a}(\omega)$ (without phase noise) by

$$\hat{a}_{S\varphi}(\omega,t)=\hat{a}_S(\omega)\exp\left[i\varphi_{SN}(t)\right] \tag{7.10}$$

In an optical communication system, a single mode laser is generally employed to avoid signal degradation as a result of modal dispersion [25]. The optical field generated from the single mode laser can be represented by a continuous-mode coherent state $|\{\rho_S(\omega)\}>$ with the wavepacket function $\rho_S(\omega)$ expressed as [33, 46]

$$\rho_S(\omega)=(2\pi F_S)^{1/2}\exp(i\theta_S)\delta(\omega-\omega_S) \tag{7.11}$$

where F_S is the time independent mean photon flux, θ_S is the mean of initial phase, and ω_S is the frequency of the optical field. By operating the input annihilation operator $\hat{a}_S(\omega)$ on the continuous-mode coherent state we have

$$\begin{aligned}\hat{a}_S(\omega)\,|\{\rho_S(\omega)\}>&=\rho_S(\omega)\,|\{\rho_S(\omega)\}>\\&=(2\pi F_S)^{1/2}\exp(i\theta_S)\delta(\omega-\omega_S)\,|\{\rho_S(\omega)\}>\end{aligned} \tag{7.12}$$

Since the Heisenberg picture is adopted, the state of the modulated field is unaffected by the modulation process so that Equation (7.11) will also characterize the wavepacket function of the modulated field.

7.2.2 Analysis of BPSK Homodyne Receiver

In this Subsection, we consider the modulated field is detected by a balanced homodyne receiver, as shown in Figure 7.2.

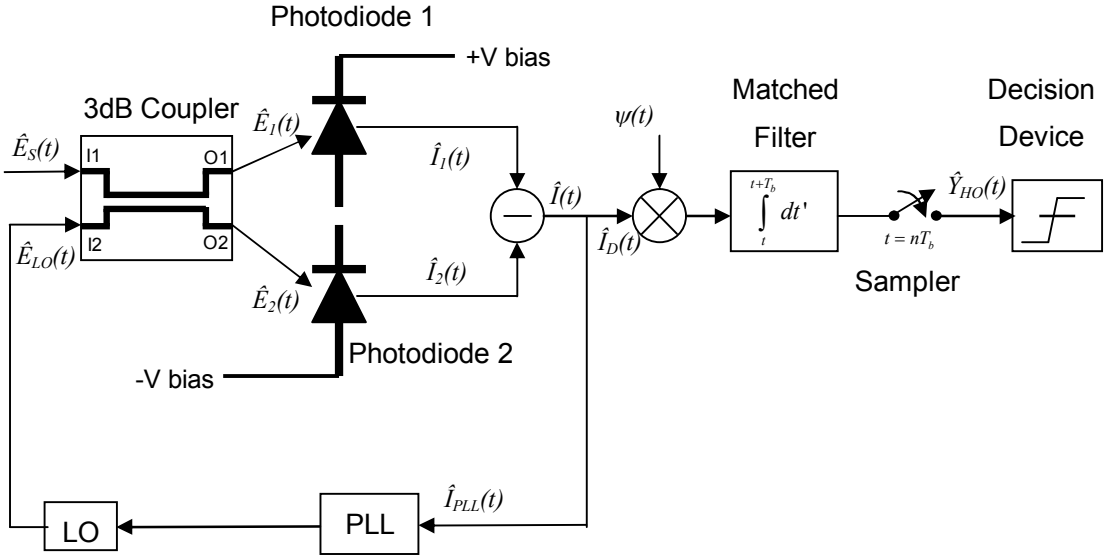

Figure 7.2: Balanced homodyne receiver structure.

Before we proceed with the quantum analysis of optical detection, we shall make the following assumptions:

1. The two photodiodes of the balanced receiver are identical.
2. The dynamics of the PLL is fast enough to track the phase variation of the signal and LO field.
3. The state of polarization (SOP) of the LO optical field is identical to the received signal.
4. The optical and electronic devices of the coherent receiver are lossless.

The operation of a BPSK receiver has been discussed in Chapter 2.2. It consists of a local oscillator (LO) laser at the receiving end so that the receiver is shot noise limited. The phase of the LO field is controlled by the phase locked loop (PLL) to optimize the SNR [22 - 25].

Similarly to the transmit laser, the LO laser is a single mode laser, and thus the wavepacket function of the LO field state $\rho_L(\omega)$ can be expressed as

$$\begin{aligned}\rho_L(\omega) &= (2\pi F_L)^{1/2}\exp(i\theta_{LO})\delta(\omega-\omega_{LO}) \\ &= (2\pi F_L)^{1/2}\exp(i\theta_{LO})\delta(\omega-\omega_S)\end{aligned} \tag{7.13}$$

where F_L is the time independent mean photon flux, θ_S is the mean initial phase angle, and ω_{LO} is the frequency of the optical field. In homodyne detection, the LO field frequency is the same as the signal frequency of the transmit laser *(ω_{LO} = ω_S)*. The power of the LO field is an order of magnitude greater than the power of the signal field, therefore $F_L >> F_S$.

The LO field is corrupted by laser phase noise due to spontaneous emission in the laser cavity. The LO field operator that includes the presence of phase noise is expressed as

$$\begin{aligned}\hat{E}_{LO}(t) &= \hat{E}_{LO}^{+}(t) + \hat{E}_{LO}^{-}(t) \\ &= \int_0^\infty \hat{e}_{LO}^{+}(\omega,t) + \hat{e}_{LO}^{-}(\omega,t)\,d\omega \\ &= \int_0^\infty \left(\frac{\hbar\omega}{4\pi\varepsilon_0 c_0 A}\right)^{1/2} \left\{\hat{a}_{L\varphi}(\omega,t)\exp\left(-i\left[\omega t - \chi_{LO}(t)\right]\right) + H.c\right\} d\omega\end{aligned} \tag{7.14}$$

where $\chi_{LO}(t)$ is the phase controlled by the PLL and $\hat{e}_{LO}^{+}(\omega,t)$ is expressed as

$$\hat{e}_{LO}^{+}(\omega,t) = \left(\frac{\hbar\omega}{4\pi\varepsilon_0 c_0 A}\right)^{1/2} \hat{a}_{L\varphi}(\omega,t)\exp\left(-i\left[\omega t - \chi_{LO}(t)\right]\right) \tag{7.15}$$

Using the approach in [33], the annihilation operator that incorporates the phase noise of the LO field, $\hat{a}_{L\varphi}(\omega,t)$, can be expressed as

$$\hat{a}_{L\varphi}(\omega,t) = \hat{a}_L(\omega)\exp\left[i\varphi_{LN}(\omega,t)\right] \tag{7.16}$$

where $\varphi_{LN}(\omega,t)$ is the phase noise of the LO field and $\hat{a}_L(\omega)$ is the annihilation operator of the LO field (phase noise neglected). By operating $\hat{a}_L(\omega)$ onto the state of the LO field in Equation (7.13), we have

$$\begin{aligned}\hat{a}_L(\omega)\left|\{\rho_L(\omega)\}\right\rangle &= \rho_L(\omega)\left|\{\rho_L(\omega)\}\right\rangle \\ &= (2\pi F_L)^{1/2}\exp(i\theta_{LO})\delta(\omega-\omega_S)\left|\{\rho_L(\omega)\}\right\rangle\end{aligned} \tag{7.17}$$

where we have used the property $\omega_{LO} = \omega_S$ for homodyne detection. The commutation relation between $\hat{a}_{L\varphi}(\omega,t)$ and $\hat{a}_{L\varphi}^{+}(\omega',t)$, and $\hat{a}_L(\omega)$ and $\hat{a}_L^{+}(\omega,t)$, is

$$\left[\hat{a}_{L\varphi}(\omega,t),\hat{a}_{L\varphi}^{+}(\omega',t)\right]=\left[\hat{a}_L(\omega),\hat{a}_L^{+}(\omega')\right]=\delta(\omega-\omega') \tag{7.18}$$

Because the LO field and signal field is generated from two different lasers, therefore the signal annihilator $\hat{a}_S(\omega)$ does not operate on the LO field state $|\{\rho_L(\omega)\}>$, and vice-versa. The commutation relation between $\hat{a}_S(\omega)$ and $\hat{a}_L^{+}(\omega)$ is [33, 35]

$$\left[\hat{a}_S(\omega),\hat{a}_L^{+}(\omega')\right]=0 \tag{7.19}$$

and therefore

$$\left[\hat{b}_S(\omega,t),\hat{a}_{L\varphi}^{+}(\omega',t)\right]=\left[\hat{a}_{S\varphi}(\omega,t),\hat{a}_{L\varphi}^{+}(\omega',t)\right]=0 \tag{7.20}$$

For simplicity of the analysis, the effect of photon creation as a consequence of controlling the phase of the LO field has been ignored. This is because the phase drift of $\chi_L(t)$ is small as compared with the bit transition rate [1], therefore $\beta(\omega,t) \approx 0$ for LO field operator.

The signal field enters into an input port (I1) of *3 dB* optical coupler while the LO field enters into the other input port (I2), as shown in Figure 7.2. The field at the couplers output port O1, can be expressed as

$$\begin{aligned}\hat{E}_1(t)&=\frac{\hat{E}_S(t)+\hat{E}_{LO}(t)}{\sqrt{2}}\\&=\int_0^{\infty}d\omega\left(\frac{\hbar\omega}{4\pi\varepsilon_0 c_0 A}\right)^{1/2}\left\{\hat{b}_1(\omega,t)\exp(-i\omega t)+H.c.\right\}\end{aligned} \tag{7.21}$$

while the field at output port O2 is

$$\begin{aligned}\hat{E}_2(t)&=\frac{\hat{E}_S(t)-\hat{E}_{LO}(t)}{\sqrt{2}}\\&=\int_0^{\infty}d\omega\left(\frac{\hbar\omega}{4\pi\varepsilon_0 c_0 A}\right)^{1/2}\left\{\hat{b}_2(\omega,t)\exp(-i\omega t)+H.c.\right\}\end{aligned} \tag{7.22}$$

where

$$\hat{b}_1(\omega,t)=\frac{1}{\sqrt{2}}\left\{\hat{b}_S(\omega,t)\exp\left(-i\left[W(\omega,t)-\omega t-\varphi\right]\right)+\hat{a}_{L\varphi}(\omega,t)\exp\left[i\chi_{LO}(t)\right]\right\} \tag{7.23}$$

$$\hat{b}_2(\omega,t)=\frac{1}{\sqrt{2}}\left\{\hat{b}_S(\omega,t)\exp\left(-i\left[W(\omega,t)-\omega t-\varphi\right]\right)-\hat{a}_{L\varphi}(\omega,t)\exp\left[i\chi_{LO}(t)\right]\right\} \tag{7.24}$$

Using the commutation relations in Equations (7.9), (7.18) and (7.20) it can be verify that

$$\left[\hat{b}_1(\omega,t),\hat{b}_1^{+}(\omega',t)\right]=\left[\hat{b}_2(\omega,t),\hat{b}_2^{+}(\omega',t)\right]=\delta(\omega-\omega') \tag{7.25}$$

A practical p-i-n photodiode is imperfect; therefore it does not achieve complete conversion of incident photons to electric current. The fraction of incident photons that on average generate a photoelectric current is called quantum efficiency, denoted by η. The losses in photoelectric process due to an inefficient photodiode can be represented as a beam splitter followed by an ideal photodiode [33], as shown in Figure 7.3.

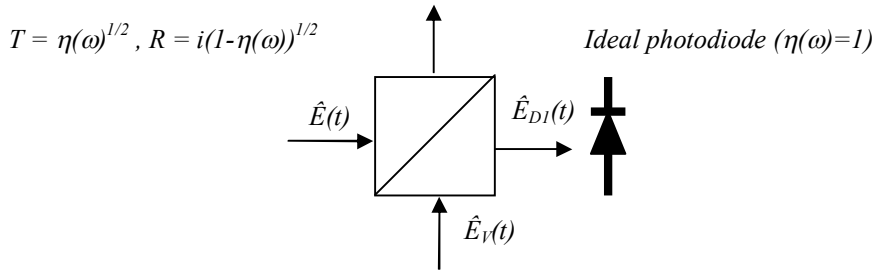

Figure 7.3: Beam splitter representation of inefficient photodiode.

The beam splitter in Figure 7.3 has a transmission coefficient, $T = \eta(\omega)^{1/2}$, and reflection coefficient, $R = i[1-\eta(\omega)]^{1/2}$. $\hat{E}_V(t)$ in Figure 7.3, is the vacuum field operator. By assuming the photodiode 1 and 2 are identical, the quantum efficiencies for photodiode 1 and 2 are both represented by $\eta(\omega)$. The detected field operator at photodiode 1 and 2, $\hat{E}_{D1}(t)$ and $\hat{E}_{D2}(t)$, can therefore be expressed as

$$\begin{aligned}\hat{E}_{D1}(t) &= \eta(\omega)^{1/2}\hat{E}_1(t) + i\left[1-\eta(\omega)\right]^{1/2}\hat{E}_{V1}(t) \\ &= \int_0^\infty \hat{e}_{D1}^{-}(\omega,t) + \hat{e}_{D1}^{+}(\omega,t)\,d\omega \\ &= \int_0^\infty \left(\frac{\hbar\omega}{4\pi\varepsilon_0 c_0 A}\right)^{1/2}\left\{\hat{b}_{D1}(\omega,t)\exp(-i\omega t) + H.c.\right\}d\omega\end{aligned} \tag{7.26}$$

$$\begin{aligned}\hat{E}_{D2}(t) &= \eta(\omega)^{1/2}\hat{E}_2(t) + i\left[1-\eta(\omega)\right]^{1/2}\hat{E}_{V2}(t) \\ &= \int_0^\infty \hat{E}_{D2}^{-}(\omega,t) + \hat{E}_{D2}^{+}(\omega,t)d\omega \\ &= \int_0^\infty \left(\frac{\hbar\omega}{4\pi\varepsilon_0 c_0 A}\right)^{1/2}\left\{\hat{b}_{D2}(\omega,t)\exp(-i\omega t) + H.c.\right\}d\omega\end{aligned} \tag{7.27}$$

where

$$\hat{e}_{D1}^{+}(\omega,t) = \left(\frac{\hbar\omega}{4\pi\varepsilon_0 c_0 A}\right)^{1/2}\hat{b}_{D1}(\omega,t)\exp(-i\omega t) \tag{7.28}$$

$$\hat{e}_{D2}^{+}(\omega,t) = \left(\frac{\hbar\omega}{4\pi\varepsilon_0 c_0 A}\right)^{1/2}\hat{b}_{D2}(\omega,t)\exp(-i\omega t) \tag{7.29}$$

and

$$\hat{b}_{D1}(\omega,t) = \eta(\omega)^{1/2}\hat{b}_1(\omega,t) + i\left[1-\eta(\omega)\right]^{1/2}\hat{a}_{V1}(\omega) \tag{7.30}$$

$$\hat{b}_{D2}(\omega,t) = \eta(\omega)^{1/2}\hat{b}_2(\omega,t) + i\left[1-\eta(\omega)\right]^{1/2}\hat{a}_{V2}(\omega) \tag{7.31}$$

The expression of vacuum field operator, $\hat{E}_{V1}(t)$ and $\hat{E}_{V2}(t)$, is given by

$$\hat{E}_{V1}(t) = \int_0^\infty d\omega\left(\frac{\hbar\omega}{4\pi\varepsilon_0 c_0 A}\right)^{1/2}\left\{\hat{a}_{V1}(\omega)\exp(-i\omega t) + H.c.\right\} \tag{7.32}$$

$$\hat{E}_{V2}(t) = \int_0^\infty d\omega\left(\frac{\hbar\omega}{4\pi\varepsilon_0 c_0 A}\right)^{1/2}\left\{\hat{a}_{V2}(\omega)\exp(-i\omega t) + H.c.\right\} \tag{7.33}$$

where the annihilation operator $\hat{a}_{V1}(\omega)$ and $\hat{a}_{V2}(\omega)$ satisfies the commutation relation

$$\left[\hat{a}_{V1}(\omega), \hat{a}_{V1}^{+}(\omega')\right] = \left[\hat{a}_{V2}(\omega), \hat{a}_{V2}^{+}(\omega')\right] = \delta(\omega-\omega') \tag{7.34}$$

$\hat{E}_{V1}(t)$ and $\hat{E}_{V2}(t)$ are denoted as the vacuum field operator, because they operate on a vacuum state $|0_{V1}\rangle$ and $|0_{V2}\rangle$, respectively. It should be noted $\hat{a}_{V1}(t)$ does not operate

on vacuum state $|0_{V2}>$ and likewise $\hat{a}_{V2}(t)$ does not operate on state $|0_{V1}>$. Furthermore, both $\hat{a}_{V1}(\omega)$ and $\hat{a}_{V2}(\omega)$ does not operate on state $|\{\rho_S(\omega)\}>$ and $|\{\rho_L(\omega)\}>$ because they are independent to the signal and LO field [33]. The vacuum field operator $\hat{E}_{V1}(t)$ and $\hat{E}_{V2}(t)$, are introduced to preserve the commutation relation so that

$$\left[\hat{a}_1(\omega),\hat{a}_1^{+}(\omega')\right]=\left[\hat{a}_{D1}(\omega),\hat{a}_{D1}^{+}(\omega')\right]=\delta(\omega-\omega') \tag{7.35}$$

and

$$\left[\hat{a}_2(\omega),\hat{a}_2^{+}(\omega')\right]=\left[\hat{a}_{D2}(\omega),\hat{a}_{D2}^{+}(\omega')\right]=\delta(\omega-\omega') \tag{7.36}$$

For simplicity of the analysis, we assume the photodiode has a simple frequency profile, as shown in Figure 7.4.

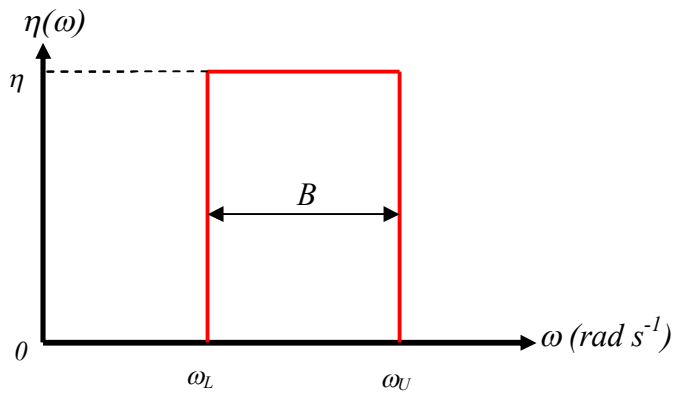

Figure 7.4: Frequency profile of an imperfect photodiode.

ω_L is the lower cutoff frequency while ω_U is the upper cutoff frequency. The input signal frequency ω_S, and LO frequency ω_{LO}, lies well within the passband of photodiode i.e $\omega_L < \omega_S < \omega_U$.

Using the frequency profile of $\eta(\omega)$ in Figure 7.4, the photocurrent operator, $\hat{I}_1(t)$ and $\hat{I}_2(t)$, that describes the photocurrent generated from the photoelectric process at photodiode 1 and 2, respectively, can be expressed as [33]

$$\begin{aligned}\hat{I}_1(t) &= 2\varepsilon_0 c_0 A \int_0^\infty \int_0^\infty R^{1/2}(\omega) R^{1/2}(\omega') \hat{e}_{D1}^{-}(\omega,t) \hat{e}_{D1}^{+}(\omega',t) d\omega d\omega' \\ &= 2\varepsilon_0 c_0 A \int_{\omega_U}^{\omega_U} \int_{\omega_L}^{\omega_U} \left(\frac{\eta q}{\hbar\omega}\right)^{1/2} \left(\frac{\eta q}{\hbar\omega'}\right)^{1/2} \hat{e}_{D1}^{-}(\omega,t) \hat{e}_{D1}^{+}(\omega',t) d\omega d\omega'\end{aligned} \tag{7.37}$$

$$\begin{aligned}\hat{I}_2(t) &= 2\varepsilon_0 c_0 A \int_0^\infty \int_0^\infty R^{1/2}(\omega) R^{1/2}(\omega') \hat{e}_{D2}^{-}(\omega,t) \hat{e}_{D2}^{+}(\omega',t) d\omega d\omega' \\ &== 2\varepsilon_0 c_0 A \int_{\omega_U}^{\omega_U} \int_{\omega_L}^{\omega_U} \left(\frac{\eta q}{\hbar\omega}\right)^{1/2} \left(\frac{\eta q}{\hbar\omega'}\right)^{1/2} \hat{e}_{D2}^{-}(\omega,t) \hat{e}_{D2}^{+}(\omega',t) d\omega d\omega'\end{aligned} \tag{7.38}$$

The parameter $R(\omega)$ is the responsitivity for an ideal photodiode and is expressed as $R(\omega) = \eta(\omega)q/\hbar\omega$, where q is the charge of an electron ($q = 1.6*10^{-19}$ C) and $\hbar$ is the reduced Planck constant ($\hbar = 1.054*10^{-34}$ Js). Figure 7.2 shows the current generated from photodiode 1 is subtracted from photodiode 2. The resultant current operator is therefore expressed as

$$\begin{aligned}\hat{I}(t) &= \hat{I}_1(t) - \hat{I}_2(t) \\ &= 2\varepsilon_0 c_0 A \int_{\omega_L}^{\omega_U} \int_{\omega_L}^{\omega_U} \left(\frac{\eta q}{\hbar\omega}\right)^{1/2} \left(\frac{\eta q}{\hbar\omega'}\right)^{1/2} \left[\hat{e}_{D1}^{-}(\omega,t) \hat{e}_{D1}^{+}(\omega',t) - \hat{e}_{D2}^{-}(\omega,t) \hat{e}_{D2}^{+}(\omega',t)\right] d\omega d\omega' \\ &= 2\varepsilon_0 c_0 A \eta \int_{\omega_L}^{\omega_U} \int_{\omega_L}^{\omega_U} \left(\frac{\eta q}{\hbar\omega}\right)^{1/2} \left(\frac{\eta q}{\hbar\omega'}\right)^{1/2} \left[\hat{e}_{LO}^{-}(\omega,t) \hat{e}_S^{+}(\omega',t) + H.c.\right] d\omega d\omega'\end{aligned} \tag{7.39}$$

In the last line of Equation (7.39), we have expressed $\hat{e}_{D1}(\omega,t)$ and $\hat{e}_{D2}(\omega,t)$ in terms of $\hat{e}_S(\omega,t)$ and $\hat{e}_{LO}(\omega,t)$ using expressions (7.21), (7.22), (7.26) and (7.27), where the expression of $\hat{e}_S(\omega,t)$ and $\hat{e}_{LO}(\omega,t)$ is given by Equation (7.2) and (7.15). Using the expression in (7.39), and expressing $\hat{e}_S^{+}(\omega,t)$ and $\hat{e}_{LO}^{+}(\omega,t)$ in terms of $\hat{a}_{L\varphi}(\omega,t)$ and $\hat{a}_{S\varphi}(\omega,t)$ from (7.2), (7.7) and (7.15), the expectation value of the photocurrent in the BPSK homodyne (BPSK-HO) receiver $\langle \hat{I}_{BPSK\text{-}HO}(t) \rangle$ is expressed as

$$\begin{aligned}\left\langle \hat{I}_{BPSK-HO}(t)\right\rangle &= \langle v|\hat{I}(t)|v\rangle \\ &= \langle v|2\varepsilon_0 c_0 A\eta \int_{\omega_L}^{\omega_U}\int_{\omega_L}^{\omega_U}\left(\frac{\eta q}{\hbar\omega}\right)^{1/2}\left(\frac{\eta q}{\hbar\omega'}\right)^{1/2}\left[\hat{e}_{LO}^{-}(\omega,t)\hat{e}_S^{+}(\omega',t)+H.c.\right]d\omega d\omega'|v\rangle \\ &= \frac{\eta q}{2\pi}\langle v|\int_{\omega_L}^{\omega_U}\int_{\omega_L}^{\omega_U} d\omega d\omega'\left\{\hat{a}_{L\varphi}^{+}(\omega,t)\left[\alpha(\omega',t)\hat{a}_{S\varphi}(\omega',t)+\beta^*(\omega',t)\hat{a}_{S\varphi}^{+}(\omega',t)\right]\right. \\ &\left.*\exp\left(-i\left[W(\omega',t)-\omega t-\varphi_{out}+\chi_{LO}(t)\right]\right)+H.c.\right\}|v\rangle\end{aligned} \tag{7.40}$$

where $|v\rangle=|\{\rho_S(\omega)\},\{\rho_L(\omega)\},0_{V1},0_{V2}\rangle$. Notice that the expression in Equation (7.40) is independent on the vacuum field parameter because $\hat{a}_{V1}(\omega)|0_{V1}\rangle = \hat{a}_{V2}(\omega)|0_{V2}\rangle = 0$. By applying the annihilation operator $\hat{a}_{L\varphi}(\omega,t)$ and $\hat{a}_{S\varphi}(\omega,t)$ onto the state $|v\rangle$ and $\langle v|$ in Equation (7.40) and then used the expression in (7.17) and (7.12), Equation (7.40) can be simplified to

$$\begin{aligned}\left\langle \hat{I}_{BPSK-HO}(t)\right\rangle = 2\eta q\sqrt{F_S F_L}\left\{\sqrt{1+|\beta(\omega_S,t)|}\cos\left[W(\omega_S,t)-\omega_S t-\varphi_{out}+\chi_{LO}(t)+\varphi_{LN}(\omega_S,t)-\varphi_{SN}(\omega_S,t)-\theta_S+\theta_{LO}\right]\right. \\ \left.+|\beta(\omega_S,t)|\cos\left[W(\omega_S,t)-\omega_S t-\varphi_{out}+\chi_{LO}(t)+\varphi_{LN}(\omega_S,t)+\varphi_{SN}(\omega_S,t)+\theta_S+\theta_{LO}+B(\omega_S,t)\right]\right\}\end{aligned} \tag{7.41}$$

where $B(\omega_S,t)$ is the phase angle of $\beta(\omega_S,t)$. In this equation, we have use the identity in Equation (7.7) to express $|\alpha(\omega_S,t)|^2$ in terms of $|\beta(\omega_S,t)|^2$. Furthermore we have assumed $A(\omega_S,t) = 0$ in Equation (7.41), because from the expression of $\alpha(\omega_S,t)$ in Equation (7.5), we can identify the imaginary term is small when the frequency changes adiabatically with respect to the carrier frequency (i.e. $d\omega_S/dt << \omega_S^2$). The dependence on the Bogoliubov coefficient $|\beta(\omega_S,t)|$ in Equation (7.41) represents the effect of photon creation from modulator as a result of phase modulation.

From Figure 7.2, we see a portion of the photocurrent is directed to the PLL to control the phase of the LO. This is related to current operator $\hat{I}(t)$ by $\hat{I}_{PLL}(t) = K_e\hat{I}(t)$ where K_e is the proportionality constant. In an optical system K_e is generally small [32], and for simplicity of the analysis, we neglect the current flowing to the PLL i.e. $\hat{I}_{PLL}(t)\approx 0$ and $\hat{I}(t) = \hat{I}_D(t)$. The PLL attempts to control the phase of the LO field $\chi_{LO}(t)$ so that the magnitude of the signal current $\left\langle \hat{I}_{BPSK-HO}(t)\right\rangle$ is

maximized for all time. Using expression (7.41), it can be verified that the controlled phase angle $\chi_{LO}(t)$ that yields a maximum value of $<\hat{I}_{BPSK\text{-}HO}(t)>$ is

$$\tan\left[\chi_{LO}(t')\right]=\frac{\sqrt{1+\beta(\omega_S,t)}\sin\left[-\varphi+\varphi_{LN}(\omega_S,t)-\varphi_{SN}(\omega_S,t)-\theta_S+\theta_{LO}\right]+\left|\beta(\omega_S,t)\right|\sin\left[-\varphi+\varphi_{LN}(\omega_S,t)+\varphi_{SN}(\omega_S,t)+\theta_S+\theta_{LO}+B(\omega_S,t)\right]}{\sqrt{1+\beta(\omega_S,t)}\cos\left[-\varphi+\varphi_{LN}(\omega_S,t)-\varphi_{SN}(\omega_S,t)-\theta_S+\theta_{LO}\right]+\left|\beta(\omega_S,t)\right|\cos\left[-\varphi+\varphi_{LN}(\omega_S,t)+\varphi_{SN}(\omega_S,t)+\theta_S+\theta_{LO}+B(\omega_S,t)\right]}$$
$$\chi_{LO}(t)\approx\varphi-\varphi_{LN}(\omega_S,t)+\varphi_{SN}(\omega_S,t)-\theta_S+\theta_{LO} \tag{7.42}$$

where the approximation in the second line of Equation (7.42) is valid when $|\beta(\omega_S,t)| << 1$.

In this analysis, we assume all the signal current $\hat{I}(t)$ is fed into a matched filter as $\hat{I}_{PLL}(t)\approx 0$. The matched filter for BPSK system can be realized by an integrator [1, 22 - 25]. The resulting output is sampled at every bit period T_b. The signal $\psi(t)$, that gets multiply by the current operator $\hat{I}_D(t)$ takes the form [1]

$$\psi(t)=\psi_{HO}(t)=1/\sqrt{T_b} \tag{7.43}$$

The homodyne detection operator $\hat{Y}_{HO}(t)$ can be represented as

$$\begin{aligned}\hat{Y}_{HO}(t)&=\int_t^{t+T_b}\hat{I}_D(t')\psi_{HO}(t')\,dt'\\&=\frac{1}{\sqrt{T_b}}\int_t^{t+T_b}\hat{I}(t')dt'\end{aligned} \tag{7.44}$$

By expressing $\hat{I}(t)$ in terms of $\hat{e}_S(\omega,t)$ and $\hat{e}_{LO}(\omega,t)$ from Equation (7.39), using the field expression $\hat{e}_S(\omega,t)$ and $\hat{e}_{LO}(\omega,t)$ in Equation (7.2) and (7.15), as well as the relation between $\hat{b}_S(\omega,t)$ and $\hat{a}_{S\varphi}(\omega,t)$ and $\hat{a}_{S\varphi}{}^{+}(\omega,t)$ in Equation (7.4), the mean signal amplitude detected from the homodyne BPSK system $<\hat{Y}_{BPSK\text{-}HO}(t)>$, can be expressed as

$$\begin{aligned}\left\langle\hat{Y}_{BPSK-HO}(t)\right\rangle&=\left\langle v\middle|\hat{Y}_{HO}(t)\middle|v\right\rangle\\&=\left\langle v\middle|\frac{\eta q}{2\pi}\int_t^{t+T_b}\psi_{HO}(t')dt'\int_0^{\infty}\int_0^{\infty}d\omega d\omega'\left\{\hat{a}_{L\varphi}{}^{+}(\omega,t')\left[\alpha(\omega',t')\hat{a}_{S\varphi}(\omega',t')+\beta^{*}(\omega',t')\hat{a}_{S\varphi}{}^{+}(\omega',t')\right]\right.\right.\\&\left.\left.*\exp\left(-i\left[W(\omega',t')-\omega t'-\varphi+\chi_{LO}(t')\right]\right)+H.c.\right\}\middle|v\right\rangle\end{aligned} \tag{7.45}$$

where the state $|v\rangle = |\{\rho_S(\omega)\},\{\rho_L(\omega)\},0_{V1},0_{V2}\rangle$. Similarly to the calculation of $\langle\hat{I}_{BPSK\text{-}HO}(t)\rangle$, by applying the annihilation operator onto the field state $|v\rangle$ as well as substituting the expression of the controlled phase angle $\chi_{LO}(t)$ in Equation (7.42), the signal amplitude detected from homodyne detection $\langle\hat{Y}_{BPSK\text{-}HO}(t)\rangle$ can be simplified to

$$\begin{aligned}\left\langle\hat{Y}_{BPSK-HO}(t)\right\rangle = 2\eta q\sqrt{\frac{F_S F_L}{T_b}}\int_t^{t+T_b}\Big\{&\sqrt{1+\left|\beta(\omega_S,t')\right|}\cos\left[W(\omega_S,t')-\omega_S t'\right]\\&+\left|\beta(\omega_S,t')\right|\cos\left[W(\omega_S,t')-\omega_S t'+2\theta_S+2\varphi_{SN}(\omega_S,t')+B(\omega_S,t')\right]\Big\}dt'\end{aligned} \tag{7.46}$$

The detected signal amplitude in Equation (7.46) shows the effect of photon creation as a consequence of phase modulation gives rise to two extra non-zero $|\beta(\omega_S,t)|$ terms. The last term is dependent on the phase angle, and when the phase angle is $0 < 2\theta_S + 2\varphi_{SN}(\omega_S,t) + B(\omega_S,t) < \pi/2$ within T_b, the process of photon creation will increase the signal amplitude on average, else the average signal amplitude will decrease. In fact, the last term in Equation (7.46) represents the energy exchange between the optical field and the modulator, as discussed in Chapter 6.3.

By definition, the shot noise variance (signal amplitude variance) that influences the homodyne detection is given by [33]

$$\begin{aligned}(\Delta Y_{HO})^2 &= \left\langle\hat{Y}_{HO}{}^2\right\rangle - \left\langle\hat{Y}_{HO}\right\rangle^2\\&= \frac{1}{T_b}\left[\int_t^{t+T_b}\int_t^{t+T_b}\langle v|\hat{I}(t')\hat{I}(t'')|v\rangle dt'dt'' - \left(\int_t^{t+T_b}\langle v|\hat{I}(t')|v\rangle dt'\right)^2\right]\\&= \frac{(2\varepsilon_0 c_0 A)^2}{T_b}\langle v|\int_t^{t+T_b}\int_t^{t+T_b}dt'dt''\int_0^\infty\int_0^\infty R^{1/2}(\omega)R^{1/2}(\omega')\left[\hat{e}_{D1}{}^-(\omega,t')\hat{e}_{D1}{}^+(\omega',t') - \hat{e}_{D2}{}^-(\omega,t')\hat{e}_{D2}{}^+(\omega',t')\right]d\omega d\omega'\\&\quad *\int_0^\infty\int_0^\infty R^{1/2}(\omega'')R^{1/2}(\omega''')\left[\hat{e}_{D1}{}^-(\omega''',t'')\hat{e}_{D1}{}^+(\omega''',t'') - \hat{e}_{D2}{}^-(\omega'',t'')\hat{e}_{D2}{}^+(\omega''',t'')\right]d\omega''d\omega'''|v\rangle\\&\quad -\left(\langle v|\int_t^{t+T_b}\int_0^\infty\int_0^\infty R^{1/2}(\omega)R^{1/2}(\omega')\left[\hat{e}_{D1}{}^-(\omega,t')\hat{e}_{D1}{}^+(\omega',t') - \hat{e}_{D2}{}^-(\omega,t')\hat{e}_{D2}{}^+(\omega',t')\right]d\omega d\omega' dt'|v\rangle\right)^2\end{aligned} \tag{7.47}$$

After some laborious algebra, it can be verified that $\hat{e}_{D1}{}^+(\omega,t)$ and $\hat{e}_{D1}{}^-(\omega,t)$ satisfies the commutation relation [33]

$$\int_0^\infty\int_0^\infty 2\varepsilon_0 c_0 AR^{1/2}(\omega)R^{1/2}(\omega')\left[\hat{e}_{D1}^{+}(\omega,t),\hat{e}_{D1}^{-}(\omega',t')\right]d\omega d\omega' = \int_0^\infty\int_0^\infty 2\varepsilon_0 c_0 AR^{1/2}(\omega)R^{1/2}(\omega')\left[\hat{e}_{D2}^{+}(\omega,t),\hat{e}_{D2}^{-}(\omega',t')\right]d\omega d\omega' \quad (7.48)$$
$$= q\delta(t-t')$$

By expressing $\hat{e}_{D1}(\omega,t)$ and $\hat{e}_{D2}(\omega,t)$ in Equation (7.47), in terms of $\hat{e}_S(\omega,t)$ and $\hat{e}_{LO}(\omega,t)$ from Equation (7.21), (7.22), (7.26) and (7.27), employing the commutation relation in Equation (7.48), and expressing $\hat{e}_S(\omega,t)$and $\hat{e}_{LO}(\omega,t)$ in terms of $\hat{b}_S(\omega,t)$ and $\hat{b}_S^{+}(\omega,t)$ using Equation (7.1) and Equation (7.14), the shot noise variance of a BPSK-HO system is given by

$$\begin{aligned}\left[\Delta Y_{BPSK-HO}(t)\right]^2 &= \eta q^2\int_t^{t+T_b}dt'\int_{\omega_L}^{\omega_U}\int_{\omega_L}^{\omega_U}d\omega d\omega'\left\{\langle v|\hat{a}_{L\varphi}^{+}(\omega,t')\hat{a}_{L\varphi}(\omega',t')\exp\left[i(\omega-\omega')t'\right]\right.\\ &\left.+\hat{b}_S^{+}(\omega,t')\hat{b}_S(\omega',t')\exp\left(i\left[W(\omega,t')-W(\omega',t')\right]\right)|v\rangle\right\} \quad (7.49)\\ &= \eta q^2\left\{F_L+\frac{1}{T_b}\int_t^{t+T_b}F_S\left(1+2\left|\beta(\omega_S,t')\right|^2+2\sqrt{1+\left|\beta(\omega_S,t')\right|}\left|\beta(\omega_S,t')\right|\cos\left[2\theta_S+2\varphi_{SV}(\omega_S,t')+B(\omega_S,t')\right]\right)dt'\right.\\ &\left.+\frac{1}{2\pi T_b}\int_t^{t+T_b}\int_{\omega_L}^{\omega_U}\left|\beta(\omega,t')\right|^2 d\omega dt'\right\}\end{aligned}$$

$[\Delta Y_{BPSK-HO}(t)]^2$ represents the effect of shot noise when photon creation is included in the analysis. If the effect of photon creation from modulator is neglected, i.e. $|\beta(\omega_S,t)| = 0$, Equation (7.49) reduces to the result in SCFT [1, 25]. Similar to SCFT, an increase in signal and LO field power will increase the amount of shot noise entering the system [1, 25]. Notice that in Equation (7.49), $|\beta(\omega_S,t)|$ is not associated with F_L, because we have neglected the effect photon creation of the LO field for simplicity. The frequency integral in the last term of Equation (7.49) is an effect of spontaneous emission from modulator. The integral limits have a lower and upper cutoff frequency, ω_L to ω_U respectively, because the photodiode is bandwidth limited (see Figure 7.3). This effect changes the noise variance at frequencies nearby ω_S.

The homodyne receiver is shot noise limited, which requires the LO field power to be much greater than the signal field power i.e. $F_L >> F_S$ [1]. As a result, the time

averaged noise current of the BPSK-HO system in Equation (7.49) can be well approximated as

$$\left[\Delta Y_{BPSK-HO}(t)\right]^2 \approx \eta q^2 F_L \tag{7.50}$$

The approximation in Equation (7.50) corresponds to the shot noise variance expression in traditional communication system literatures [1, 25]. This implies the influence of photon creation on the noise statistics is suppressed when the power of the LO field is large. Therefore, the shot noise determined from QFT converges to the results in SCFT [1, 25].

7.2.3 Analysis of BPSK Heterodyne Receiver

As we have explained in Chapter 2, the configuration of the heterodyne receiver is very similar to the homodyne receiver except that the optical frequency of the LO laser is **not the same** as the laser frequency at the transmitter $(\omega_{LO} \neq \omega_S)$ for a heterodyne receiver. The LO field and the signal field operator, $\hat{E}_{LO}(t)$ and $\hat{E}_S(t)$, for heterodyne receiver is the same as the homodyne receiver and is expressed in (7.14) and (7.1) respectively. It is the state of the LO field that distinguishes the frequency mismatch between the LO field and the modulated signal field. In heterodyne receiver, the LO field state is expressed using

$$\rho_L(\omega) = (2\pi F_L)^{1/2} \exp(i\theta_{LO})\,\delta(\omega - \omega_{LO}) \tag{7.51}$$

where the last line in Equation (7.13) does not apply to heterodyne receiver as $(\omega_{LO} \neq \omega_S)$. The mixed signal for heterodyne receiver $\psi_{HE}(t)$ that is being multiplied with the detector current $\hat{I}(t)$, is different from the homodyne detector $\psi_{HO}(t)$ expressed in Equation (7.43). This is a consequence of the frequency difference between the LO laser and the transmit laser. The multiplied signal is expressed as [1]

$$\psi(t) = \psi_{HE}(t) = \sqrt{\frac{2}{T_b}}\cos(\omega_{IF}t) \tag{7.52}$$

where ω_{IF} is the intermediate frequency and is the frequency difference between the LO laser and the laser at the transmitter $(\omega_{IF} = \omega_S - \omega_{LO})$. The homodyne receiver can be considered as a special case where $\omega_{IF} = 0$. In general, ω_{IF} is roughly an order of magnitude greater than the bit rate of the communication system [25].

Since the heterodyne receiver configuration is identical to the homodyne receiver before the matched filter, therefore the current operator $\hat{I}(t)$ continue to be represented by Equation (7.39). The mean of the photocurrent in the BPSK-HE receiver $\left\langle \hat{I}_{BPSK-HE}(t) \right\rangle$ can be determined by operating $\hat{I}(t)$ onto bra-ket state vector, $|v\rangle$ and $\langle v|$, where we have

$$\begin{aligned}
\left\langle \hat{I}_{BPSK-HE}(t) \right\rangle &= \langle v|\hat{I}(t)|v\rangle \\
&= \frac{\eta q}{2\pi}\langle v|\int_{\omega_L}^{\omega_U}\int_{\omega_L}^{\omega_U} d\omega d\omega' \hat{a}_{L\varphi}^{+}(\omega)\left[\alpha(\omega',t')\hat{a}_{S\varphi}(\omega') + \beta^{*}(\omega',t')\hat{a}_{S\varphi}^{+}(\omega')\right]\exp\left(-i\left[W(\omega',t') - \omega' t - \varphi + \chi_{LO}(t')\right]\right) + H.c.|v\rangle \\
&= 2\eta q\sqrt{F_S F_L}\left\{\sqrt{1+|\beta(\omega_S,t)|}\cos\left[W(\omega_S,t) - \omega_S t + \omega_{IF} t - \varphi_{out} + \chi_{LO}(t) + \varphi_{LN}(\omega_{LO},t) - \varphi_{SN}(\omega_S,t) - \theta_S + \theta_{LO}\right]\right. \\
&\quad \left. + |\beta(\omega_S,t')|\cos\left[W(\omega_S,t) - \omega_S t + \omega_{IF} t - \varphi_{out} + \chi_{LO}(t) + \varphi_{LN}(\omega_{LO},t) + \varphi_{SN}(\omega_S,t) + \theta_S + \theta_{LO} + B(\omega_S,t)\right]\right\}
\end{aligned} \tag{7.53}$$

The state vector $|v\rangle$ is $|v\rangle = |\{\rho_S(\omega)\},\{\rho_L(\omega)\},0_{V1},0_{V2}\rangle$. In this equation, the phase of $\alpha(\omega_S,t)$ denoted as $A(\omega_S,t)$, has been neglected. The mean signal current expression for BPSK-HE receiver in Equation (7.53) is similar to the expression of BPSK-HO receiver in Equation (7.41), except that there is a frequency offset of ω_{IF} for the heterodyne receiver. By following a similar procedure in the calculation of the phase controlled by the PLL, we find that $\chi_{LO}(t)$ for a BPSK-HE system is very similar to that of BPSK-HO in Equation (7.42), but with the frequency argument ω_S replaced by ω_{LO} in the φ_{LN} term in expression (7.42).

From Figure 7.5, we can represent the detection heterodyne operator $\hat{Y}_{HE}(t)$ as

$$\begin{aligned}\hat{Y}_{HE}(t) &= \int_{t}^{t+T_b} \hat{I}(t')\psi_{HE}(t')dt' \\ &= \sqrt{\frac{2}{T_b}}\int_{t}^{t+T_b} \hat{I}(t')\cos(\omega_{IF}t')dt'\end{aligned} \tag{7.54}$$

By operating $\hat{I}(t)$ onto the state vector $|v\rangle = |\{\rho_S(\omega)\},\{\rho_L(\omega)\},0_{V1},0_{V2}\rangle$, with $|\{\rho_L(\omega)\}\rangle$ now represented by Equation (7.51) for heterodyne receiver, and using the expression of $\chi_{LO}(t)$ in Equation (7.42), the mean signal amplitude detected from the BPSK-HE system is

$$\begin{aligned}\left\langle \hat{Y}_{BPSK-HE}(t)\right\rangle = \eta q\sqrt{\frac{2F_SF_L}{T_b}}\int_{t}^{t+T_b} dt'\Big\{&\sqrt{1+\left|\beta(\omega_S,t')\right|}\cos\left[W(\omega_S,t')-\omega_S t'\right] \\ &+\left|\beta(\omega_S,t')\right|\cos\left[W(\omega_S,t')-\omega_S t'+2\theta_S+2\varphi_{SN}(\omega_S,t')+B(\omega_S,t')\right]\Big\}\end{aligned} \tag{7.55}$$

The high frequency term $\cos(W(\omega_S,t) - \omega_S t + 2\omega_{IF}t)$ has been omitted in expression (7.55) as it averages out to zero in a time duration of a bit period T_b. By comparing signal amplitude detected from the BPSK-HE $\left\langle \hat{Y}_{BPSK-HE}(t)\right\rangle$ in Equation (7.55) with the BPSK-HO receiver $\left\langle \hat{Y}_{BPSK-HO}(t)\right\rangle$ in Equation (7.46), we can identify $\left\langle \hat{Y}_{BPSK-HO}(t)\right\rangle = \sqrt{2}\left\langle \hat{Y}_{BPSK-HE}(t)\right\rangle$.

Similar to the definition of the homodyne noise variance in Equation (7.47), the shot noise variance (signal amplitude variance) of the heterodyne receiver is defined as

$$\begin{aligned}(\Delta Y_{HE})^2 &= \left\langle \hat{Y}_{HE}{}^2\right\rangle - \left\langle \hat{Y}_{HE}\right\rangle^2 \\ &= \frac{2}{T_b}\left[\int_{t}^{t+T_b}\int_{t}^{t+T_b}\langle v|\hat{I}(t')\hat{I}(t'')\cos(\omega_{IF}t')\cos(\omega_{IF}t'')|v\rangle dt'dt'' - \left[\int_{t}^{t+T_b}\langle v|\hat{I}(t')\cos(\omega_{IF}t')|v\rangle dt'\right]^2\right]\end{aligned} \tag{7.56}$$

Using the relation in Equation (7.48), the shot noise variance that influences the detection of the BPSK-HE system can be expressed as

$$\left[\Delta Y_{BPSK-HE}(t)\right]^2 = \frac{2\eta q^2}{2\pi T_b}\int_t^{t+T_b}\frac{1}{2}\left[1+\cos(2\omega_{IF}t')\right]dt'\int_{\omega_L}^{\omega_U}\int_{\omega_L}^{\omega_U}d\omega d\omega'\left\{\langle v|\hat{a}_{L\varphi}^{+}(\omega,t')\hat{a}_{L\varphi}(\omega',t')\exp\left[i(\omega-\omega')t'\right]\right.$$
$$\left.+\hat{b}_S^{+}(\omega,t)\hat{b}_S(\omega',t)\exp\left(i\left[W(\omega,t')-W(\omega',t')\right]\right)|v\rangle\right\} \quad (7.57)$$

The high frequency term $cos(2\omega_{IF}t)$ inside the time integral of Equation (7.57) will get averaged out to zero in a duration of one bit period T_b. When the intermediate frequency ω_{IF} term is omitted, and the annihilation and creation operator operates onto the field state $|v\rangle$ in expression (7.57), $[\Delta Y_{BPSK-HE}(t)]^2$ can be re-expressed as

$$\left[\Delta Y_{BPSK-HE}(t)\right]^2 = \eta q^2\left\{F_L+\frac{F_S}{T_b}\int_t^{t+T_b}1+2\left|\beta(\omega_S,t')\right|^2+2\sqrt{1+\left|\beta(\omega_S,t')\right|}\left|\beta(\omega_S,t')\right|\cos\left[2\theta_S+2\varphi_{SN}(\omega_S,t')+B(\omega_S,t')\right]\right\}$$
$$+\frac{\eta q^2}{2\pi}\int_{\omega_L}^{\omega_U}d\omega\int_t^{t+T_b}\left|\beta(\omega,t')\right|^2dt' \quad (7.58)$$

Notice that the expression of $[\Delta Y_{BPSK-HE}(t)]^2$ in Equation (7.58) is equivalent to the expression of $[\Delta Y_{BPSK-HO}(t)]^2$ in Equation (7.49), therefore the shot noise variance for the heterodyne detector is the same as the homodyne detector. Similarly, by using the fact $F_L >> F_S$, and the spontaneous contribution (last term of (7.58)) is small, the shot noise variance for BPSK-HE can be simplified into

$$\left[\Delta Y_{BPSK-HE}(t)\right]^2 = \left[\Delta Y_{BPSK-HO}(t)\right]^2 \approx \eta q^2 F_L \quad (7.59)$$

7.3 Quantum Field Model of ASK System

In an ASK system, the transmitted data is encoded onto the amplitude of the optical field. In Chapter 2.2, we show this can be realized by the use of external phase modulator for which the optical signal generated from the steady state laser at the transmitter interferes constructively or destructively, depending on the control signal (transmitted data). Similarly to the BPSK system, the ASK system can be detected using homodyne and heterodyne receiver. In this Section, a quantum field model for the ASK-HO and ASK-HE system using external phase modulator will be presented.

7.3.1 Analysis of ASK Transmitter

In an externally modulated system, the ASK transmitter consists of a laser, and a Mach Zehnder interferometer (MZI) as shown in Figure 7.5.

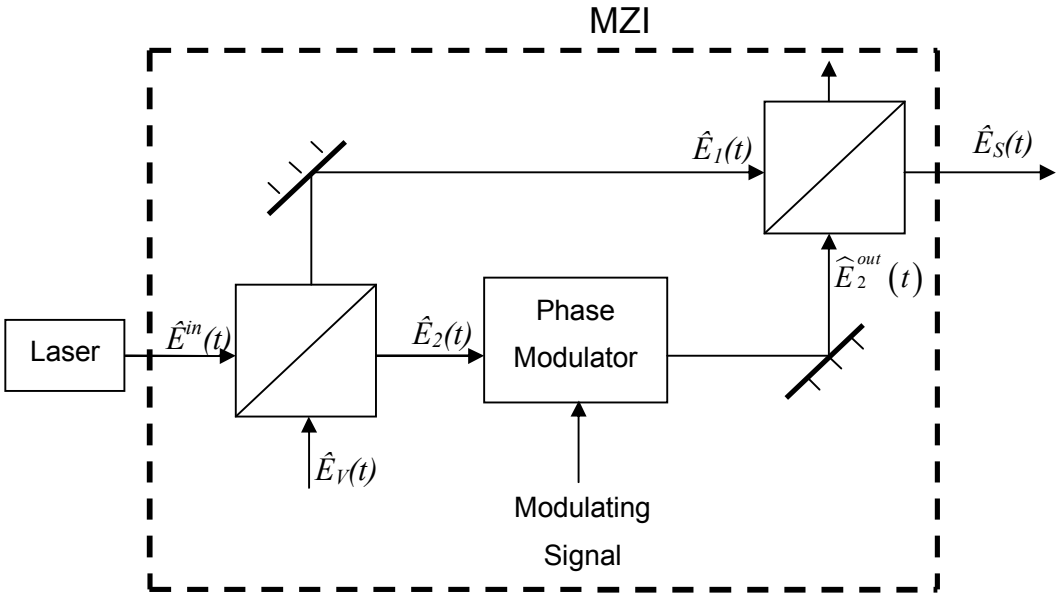

Figure 7.5: Block diagram of ASK Transmitter.

The field operator of the transmit laser $\hat{E}^{in}(t)$ is given by

$$\begin{aligned}\hat{E}^{in}(t) &= \hat{E}^{in+}(t) + \hat{E}^{in-}(t) \\ &= \int_0^{\infty} d\omega \left(\frac{\hbar\omega}{4\pi\varepsilon_0 c_0 A}\right)^{1/2} \left\{\hat{a}_{S\varphi}(\omega,t)\exp(-i\omega t) + H.c.\right\}\end{aligned} \tag{7.60}$$

where $\hat{a}_{S\varphi}(\omega,t)$ is the annihilation operator that includes the effect of laser phase noise and is defined in Equation (7.10).

The power of the optical field will be divided equally by the 50:50 beam splitter at the input of the MZI, and thus the magnitude of the amplitude reflection coefficient is $|R|$, and transmission coefficient $|T|$, of the beam splitter is, $|R| = |T| = 1/\sqrt{2}$. The

phase difference between the reflection coefficient φ_R and the transmission coefficient φ_T is $\pi/2$ ($\varphi_R - \varphi_T = \pi/2$) [33]. The optical field at arm 1 is represented as

$$\begin{aligned}\hat{E}_1(t) &= R\hat{E}(t) + T\hat{E}_V(t) \\ &= \frac{1}{\sqrt{2}}\left(i\hat{E}(t) + \hat{E}_V(t)\right)\end{aligned} \tag{7.61}$$

while the optical field at arm 2 is

$$\begin{aligned}\hat{E}_2(t) &= T\hat{E}(t) + R\hat{E}_V(t) \\ &= \frac{1}{\sqrt{2}}\left(\hat{E}(t) + i\hat{E}_V(t)\right)\end{aligned} \tag{7.62}$$

In Equation (7.61) and (7.62), the transmission coefficient phase angle φ_T has been chosen to be *0* to simplify the analysis. The vacuum field $\hat{E}_V$ is introduced so that the commutation relation so that $\left[\hat{E}^{in+}(t), \hat{E}^{in-}(t)\right] = \left[\hat{E}_1^{+}(t), \hat{E}_1^{-}(t)\right] = \left[\hat{E}_2^{+}(t), \hat{E}_2^{-}(t)\right]$. The vacuum field operator is expressed as

$$\hat{E}_V(t) = \int_0^\infty d\omega \left(\frac{\hbar\omega}{4\pi\varepsilon_0 c_0 A}\right)^{1/2} \left\{\hat{a}_V(\omega)\exp(-i\omega t) + H.c.\right\} \tag{7.63}$$

where the vacuum field annihilation and creation operator, $\hat{a}_V(\omega)$ and $\hat{a}_V^{+}(\omega)$, satisfies the usual commutation relation

$$\left[\hat{a}_V(\omega), \hat{a}_V^{+}(\omega')\right] = \delta(\omega - \omega') \tag{7.64}$$

The state of the vacuum field is described by a vacuum number state $|0_V\rangle$. The phase modulator placed at arm 2 is to control the interference process and hence the amplitude of the optical field. The field operator at arm 2 after propagating through the phase modulator is represented by (see Equation (7.1))

$$\hat{E}_2^{out}(t) = \frac{1}{2}\int_0^\infty d\omega \left(\frac{\hbar\omega}{4\pi\varepsilon_0 c_0 A}\right)^{1/2} \left\{\left[\hat{b}_S(\omega,t) + i\hat{b}_V(\omega,t)\right]\exp\left(-i\left[W(\omega,t) - \varphi\right]\right) + H.c.\right\} \tag{7.65}$$

where φ is the propagation phase delay, $W(\omega,t)$ is the modulated phase angle and is defined in Equation (7.3). $\hat{b}_S(\omega,t)$ and $\hat{b}_V(\omega,t)$ are the modulated annihilation

operator for the signal and vacuum field, respectively, and are related to $\hat{a}_{S\varphi}(\omega,t)$ and $\hat{a}_V(\omega)$, by the Bogoliubov transformation in Equation (7.4).

The signal field at the output of the second 50:50 beam splitter (output of the MZI) is related to the field at arm 1 and arm 2 by

$$\begin{aligned}\hat{E}_S(t) &= \frac{1}{\sqrt{2}}\left(\hat{E}_1(t) + i\hat{E}_2^{out}(t)\right) \\ &= \int_0^\infty \hat{e}_S^{\,+}(\omega,t) + \hat{e}_S^{\,-}(\omega,t)\,d\omega \\ &= \frac{1}{2}\int_0^\infty d\omega\left(\frac{\hbar\omega}{4\pi\varepsilon_0 c_0 A}\right)^{1/2}\left\{\left[i\hat{a}_{S\varphi}(\omega,t) + \hat{a}_V(\omega)\right]\exp\left[-i(\omega t-\varphi)\right]\right. \\ &\quad \left.+\left[i\hat{b}_S(\omega,t) + \hat{b}_V(\omega,t)\right]\exp\left(-i\left[W(\omega,t)-\varphi\right]\right) + H.c.\right\}\end{aligned} \tag{7.66}$$

where

$$\begin{aligned}\hat{e}_S^{\,+}(\omega,t) &= \frac{1}{2}\int_0^\infty d\omega\left(\frac{\hbar\omega}{4\pi\varepsilon_0 c_0 A}\right)^{1/2}\left\{\left[i\hat{a}_{S\varphi}(\omega,t) + \hat{a}_V(\omega)\right]\exp\left[-i(\omega t-\varphi)\right]\right. \\ &\quad \left.+\left[i\hat{b}_S(\omega,t) + \hat{b}_V(\omega,t)\right]\exp\left(-i\left[W(\omega,t)-\varphi\right]\right) + H.c.\right\}\end{aligned} \tag{7.67}$$

In the absence of field modulation, the optical path length at arm 1 and arm 2 are identical to one another. Therefore, the complex exponential component associated with the unmodulated field annihilator $\hat{a}_{S\varphi}(\omega,t)$ is the same as the complex exponential associated with the modulated field annihilator $\hat{b}_S(\omega,t)$ i.e. $W(\omega,t) - \varphi = \omega t + \varphi$. In this situation, the field at arm 1 will constructively interfere with the field at arm 2 after they recombine at the output of the second beam splitter. This corresponds to a bit *'1'* being transmitted. In contrast, when a bit *'0'* is transmitted, a field is applied at the control terminal of the modulator in order to create a π phase delay at arm 2. Thus the phase of the complex exponential associated with $\hat{a}_{S\varphi}(\omega,t)$ leads the corresponding phase angle of $\hat{b}_S(\omega,t)$ by π i.e. $W(\omega,t) - \varphi = \omega t + \pi + \varphi$. In this situation, the field from arm 1 will destructively interfere with the field from arm 2 at the output of the

MZI, hence the transmitted optical signal is effectively switched off (optical signal power ~ *0*) at this instant.

Using the Bogoliubov identity in expression (7.7) and the commutation relation in expression (7.64), the following commutation can be verified

$$\left[\hat{b}_V(\omega,t),\hat{b}_V^{+}(\omega',t)\right]=\delta(\omega-\omega') \tag{7.68}$$

7.3.2 Analysis of ASK Homodyne Receiver

The configuration of balanced homodyne receiver for ASK system is the same as BPSK system shown in Figure 7.2. Therefore, the detector current $\hat{I}(t)$ can be represented by expression (7.39). Using Equation (7.39), and expressing $\hat{e}_S^{+}(\omega,t)$ and $\hat{e}_{LO}^{+}(\omega,t)$ in terms of annihilation and creation operator in expression (7.67) and (7.15) respectively, the mean photocurrent for the ASK homodyne system (ASK-HO) $<\hat{I}_{ASK\text{-}HO}(t)>$ is expressed as

$$\begin{aligned}\left\langle \hat{I}_{ASK-HO}(t)\right\rangle &= \left\langle v'\left|2\varepsilon_0 c_0 A\eta\int_0^{\infty}\int_0^{\infty} R^{1/2}(\omega)R^{1/2}(\omega')\left[\hat{e}_{LO}^{+}(\omega,t)\hat{e}_S^{-}(\omega',t)+H.c.\right]d\omega d\omega'\right|v'\right\rangle \\ &= i\left\langle v'\left|\frac{\eta q}{2\pi}\int_{\omega_L}^{\omega_U}\int_{\omega_L}^{\omega_U}\left\{\hat{a}_{L\varphi}^{+}(\omega',t)\exp\left[i(\omega' t-\varphi)\right]\left\{\hat{a}_{S\varphi}(\omega)\exp\left[-i(\omega t-\varphi)\right]\right.\right.\right. \\ &\quad \left.\left.\left.+\hat{b}_S(\omega,t)\exp\left(-i\left[W(\omega,t)-\varphi\right]\right)+H.c.\right\}d\omega d\omega'\right|v'\right\rangle\end{aligned} \tag{7.69}$$

where $|v'> = |\{\rho_S(\omega)\},\{\rho_L(\omega)\},0_V,0_{V1},0_{V2}>$. The vacuum field operators i.e. $\hat{b}_V(\omega,t)$ and $\hat{a}_V(\omega)$, is not included in Equation (7.69) because they give a null result once they operate on the state vector $|v'>$ or $<v'|$. We shall simplify expression (7.69) by operating $\hat{a}_{S\varphi}(\omega,t)$ and $\hat{b}_S(\omega,t)$ onto the state $|v'>$ where we have

$$\begin{aligned}\left\langle \hat{I}_{ASK-HO}(t)\right\rangle &= \langle v'|\hat{I}(t)|v'\rangle \\ &= \eta q\sqrt{F_S F_L}\left\{\cos\left[\varphi_{LN}(\omega_S,t)-\varphi_{SN}(\omega_S,t)+\theta_{LO}-\theta_S-\varphi+\chi_{LO}(t)-\frac{\pi}{2}\right]\right. \\ &+\sqrt{1+\left|\beta(\omega_S,t)\right|^2}\cos\left[W(\omega_S,t)-\omega_S t+\varphi_{LN}(\omega_S,t)-\varphi_{SN}(\omega_S,t)+\theta_{LO}-\theta_S-\varphi+\chi_{LO}(t)-\frac{\pi}{2}\right] \\ &\left.+\left|\beta(\omega_S,t')\right|\cos\left[W(\omega_S,t)-\omega_S t+\varphi_{LN}(\omega_S,t)+\varphi_{SN}(\omega_S,t)+\theta_{LO}+\theta_S-\varphi+\chi_{LO}(t)-\frac{\pi}{2}+B(\omega_S,t)\right]\right\}\end{aligned} \tag{7.70}$$

where $B(\omega_S,t)$ is the phase of $\beta(\omega_S,t)$. In this Equation, we have neglected the phase of $A(\omega_S,t)$. Although the current operator $\hat{I}(t)$ for both ASK and BPSK system is given by Equation (7.39), the expression for the mean signal current detected by the ASK-HO receiver $\langle\hat{I}_{ASK\text{-}HO}(t)\rangle$ in Equation (7.70), is different from the current of the BPSK receiver $\langle\hat{I}_{BPSK\text{-}HO}(t)\rangle$ in Equation (7.40).

Similarly to the BPSK analysis, we shall simplify the problem by neglecting the current flowing to the PLL, thus $\hat{I}_{PLL}(t) = 0$ and $\hat{I}(t) = \hat{I}_D(t)$. The controlled LO phase angle $\chi_{LO}(t)$, that maximizes $|\langle\hat{I}_{ASK\text{-}HO}(t)\rangle|$ is given by

$$\begin{aligned}-\tan\left[\chi_{LO}(t)\right] &= \frac{\sin\left[\Lambda(t)\right]+\sqrt{1+\left|\beta(\omega_S,t)\right|^2}\sin\left[\Lambda(t)\right]+\left|\beta(\omega_S,t)\right|\sin\left[\Lambda'(t)\right]}{\cos\left[\Lambda(t)\right]+\sqrt{1+\left|\beta(\omega_S,t)\right|^2}\cos\left[\Lambda(t)\right]+\left|\beta(\omega_S,t)\right|\cos\left[\Lambda'(t)\right]} \\ &\approx \frac{\left(\sqrt{1+\left|\beta(\omega_S,t)\right|^2}+1\right)\sin\left[\Lambda(t)\right]}{\left(\sqrt{1+\left|\beta(\omega_S,t)\right|^2}+1\right)\cos\left[\Lambda(t)\right]} \\ \chi_{LO}(t) &= \Lambda(t) = \varphi_{LN}(\omega_S,t)-\varphi_{SN}(\omega_S,t)+\theta_{LO}-\theta_S-\varphi-\frac{\pi}{2}\end{aligned} \tag{7.71}$$

where $\Lambda(t) = \varphi_{LN}(\omega_S,t) - \varphi_{SN}(\omega_S,t) + \theta_{LO} - \theta_S - \varphi - \pi/2$ and $\Lambda'(t) = \varphi_{LN}(\omega_S,t) + \varphi_{SN}(\omega_S,t) + \theta_{LO} + \theta_S - \varphi + B(\omega_S,t) - \pi/2$. In the second line approximation of Equation (7.71), we have omitted the $|\beta(\omega_S,t)|$ term because $|\beta(\omega_S,t)|<<1$.

Since the receiver structure is represented by Figure 7.2, therefore the homodyne operator of ASK receiver $\hat{Y}_{ASK\text{-}HO}(t)$, is given by Equation (7.44). By substituting the signal and LO field operator, $\hat{e}_S(\omega,t)$ and $\hat{e}_{LO}(\omega,t)$, from Equation (7.66) and (7.14) respectively, into expression (7.39), applying them onto the state vector $|v'\rangle$, and

finally using the expression of $\chi_{LO}(t)$ in Equation (7.71), the mean signal amplitude detected by the ASK-HO receiver is

$$\begin{aligned}\left\langle \hat{Y}_{ASK-HO}(t)\right\rangle &= \frac{1}{\sqrt{T_b}}\langle v'|\int_{t}^{t+T_b}\hat{I}(t')dt'|v'\rangle \\ &= \eta q\sqrt{\frac{F_S F_L}{T_b}}\int_{t}^{t+T_b}\left\{1+\sqrt{1+\left|\beta(\omega_S,t')\right|^2}\cos\left[W(\omega_S,t')-\omega_S t'\right]\right. \\ &\left.+\left|\beta(\omega_S,t')\right|\cos\left[W(\omega_S,t')-\omega_S t'+2\left[\varphi_{SN}(\omega_S,t')+\theta_S\right]+B(\omega_S,t')\right]\right\}dt'\end{aligned} \tag{7.72}$$

From (7.72), we can identify the effect of photon creation gives rise to 2 extra $|\beta(\omega_S,t)|$ terms. The presence of these two extra terms causes the mean signal amplitude detected when a bit *'0'* is sent (i.e. $W(\omega_S,t')-\omega_S t'=\pi$) to be non-zero. This is a consequence of the field component $\hat{E}_1(t)$ and $\hat{E}_2^{out}(t)$, cannot be completely cancelled out at the output of the MZI in Figure 7.5. This is because the signal field amplitude at arm 2 is no longer equivalent to that in arm 1 due to phenomenon of photon creation during the process of phase modulation.

We shall now determine the impact of shot noise that influences the outcome of the detection process. By using the mathematical definition of variance in Equation (7.47), the commutation relation in Equation (7.48), expressing $\hat{e}_S(\omega,t)$ and $\hat{e}_{LO}(\omega,t)$ in terms of annihilation and creation operator in Equation (7.67) and Equation (7.15) respectively, the shot noise variance of ASK system is expressed as

$$\begin{aligned}\left[\Delta Y_{ASK-HO}(t)\right]^2 &= \frac{1}{T_b}\left[\int_{t}^{t+T_b}\int_{t}^{t+T_b}\langle v'|\hat{I}(t')\hat{I}(t'')|v'\rangle dt'dt''-\left(\int_{t}^{t+T_b}\langle v'|\hat{I}(t')|v'\rangle dt'\right)^2\right] \\ &= \frac{\eta q^2}{2\pi T_b}\int_{t}^{t+T_b}dt'\int_{\omega_L}^{\omega_U}\int_{\omega_L}^{\omega_U}\langle v'|\hat{a}_{L\varphi}^{+}(\omega,t')\hat{a}_{L\varphi}(\omega',t')\exp\left[i(\omega-\omega')t'\right]+\frac{1}{4}\left\{\hat{a}_{S\varphi}^{+}(\omega,t')\hat{a}_{S\varphi}(\omega',t')\exp\left[i(\omega-\omega')t'\right]\right. \\ &+\left[\hat{b}_S^{+}(\omega,t')\hat{b}_S(\omega',t')+\hat{b}_V^{+}(\omega,t')\hat{b}_V(\omega',t')\right]\exp\left[i\left(W(\omega,t')-W(\omega',t')\right)\right] \\ &\left.+2\hat{a}_{S\varphi}^{+}(\omega,t')\hat{b}_S(\omega',t')\cos\left[W(\omega',t')-\omega t'\right]\right\}d\omega d\omega'|v'\rangle\end{aligned} \tag{7.73}$$

By operating the annihilation and creation operator onto state vector $|v'\rangle$ and $\langle v'|$, the shot noise variance expression in Equation (7.73) can be simplified to

$$\begin{aligned}\left[\Delta Y_{ASK-HO}(t)\right]^2 = \eta q^2 F_L + \frac{\eta q^2}{2T_b}\int_{t}^{t+T_b}\Big(F_S\{1+2\sqrt{1+\left|\beta(\omega_S,t')\right|}\left|\beta(\omega_S,t')\right|\cos\left[2\left(\theta_S+\varphi_{SN}(\omega_S,t')\right)-B(\omega_S,t')\right] \\ +2\left|\beta(\omega_S,t')\right|^2+\left|\beta(\omega_S,t')\right|\cos\left[W(\omega_S,t')-\omega t'+2\left(\theta_S+\varphi_{SN}(\omega_S,t')\right)+B(\omega_S,t')\right] \\ +\sqrt{1+\left|\beta(\omega_S,t')\right|}\cos\left[W(\omega_S,t')-\omega t'\right]\}+\frac{1}{2\pi}\int_{\omega_L}^{\omega_U}\left|\beta(\omega,t')\right|^2 d\omega\Big)dt'\end{aligned} \tag{7.74}$$

The first and second term in Equation (7.74) corresponds to the shot noise variance presented by traditional communication literatures [1, 25] using SCFT. The quantum effect of photon creation gives rise to the remaining $|\beta(\omega_S,t)|$ terms. However, the ASK-HO noise variance $[Y_{ASK\text{-}HO}(t)]^2$ in Equation (7.74) is expressed differently to the noise variance of BPSK-HO system $[Y_{BPSK\text{-}HO}(t)]^2$ in (7.49). This is because only half of the transmitted laser power is fed into the modulator for the ASK system, while for the BPSK system, all the laser power is injected into the modulator. As a result, different photon numbers are stimulated out of the modulator during the phase modulation process between these two systems, and hence lead to a different impact on the shot noise variance.

Because $F_L >> F_S$ for a shot noise limited receiver, therefore the first term in (7.74) dominates over all the other terms and thus Equation (7.74) can be approximated as

$$\left[Y_{ASK-HO}(t)\right]^2 \approx \eta q^2 F_L \tag{7.75}$$

Similar to the BPSK system, the effect of photon creation on the shot noise variance is suppressed when the power of the LO field is large. Once the quantum effect is omitted, the noise variance of BPSK and ASK system becomes identical i.e. $\left[Y_{BPSK-HO}(t)\right]^2 = \left[Y_{ASK-HO}(t)\right]^2$. This agrees with the results from SCFT [1, 25].

7.3.3 ASK Heterodyne Receiver Analysis

The configuration of the ASK heterodyne (ASK-HE) receiver is the same as the BPSK-HE receiver, therefore the current operator $\hat{I}(t)$ can be expressed in the general form in Equation (7.39). The LO field and the signal field operator, $\hat{E}_{LO}(t)$ and $\hat{E}_S(t)$, for ASK-HE receiver is the same as the ASK-HO receiver and is expressed as (7.14) and (7.66), respectively. Since $\omega_{LO} \neq \omega_S$, the wavepacket function of the signal and LO field, $\rho_S(\omega)$ and $\rho_L(\omega)$, is given by Equation (7.11) and (7.51), respectively. By expressing $\hat{I}(t)$ from Equation (7.39), in terms of annihilation and creation operators using Equation (7.67) and (7.15), and then operated onto bra-ket state vector $|v'\rangle$ and $\langle v'|$ defined in Equation (7.69) ($|v'\rangle = |\{\rho_S(\omega)\},\{\rho_L(\omega)\},0_V,0_{V1},0_{V2}\rangle$), we have

$$\begin{aligned}\left\langle \hat{I}_{ASK-HE}(t)\right\rangle &= i\langle v'|\frac{\eta q}{2\pi}\int_0^\infty\int_0^\infty\left\{\left[\hat{a}_{S\varphi}(\omega,t)\exp\left[-i(\omega t-\varphi)\right]+\hat{b}_S(\omega,t)\exp\left(-i\left[W(\omega,t)-\varphi\right]\right)\right]\hat{a}_{L\varphi}^{+}(\omega',t)\exp\left[i(\omega' t-\varphi)\right]+H.c.\right\}d\omega d\omega'|v'\rangle \\ &= \eta q\sqrt{F_S F_L}\left\{\cos\left[-\omega_{IF}t+\varphi_{LN}(\omega_{LO},t)-\varphi_{SN}(\omega_S,t)+\theta_{LO}-\theta_S-\varphi+\chi_{LO}(t)-\frac{\pi}{2}\right]\right. \\ &+\sqrt{1+|\beta(\omega_S,t)|^2}\cos\left[W(\omega_S,t)-\omega_S t+\omega_{IF}t+\varphi_{LN}(\omega_{LO},t)-\varphi_{SN}(\omega_S,t)+\theta_{LO}-\theta_S-\varphi+\chi_{LO}(t)-\frac{\pi}{2}\right] \\ &\left.+|\beta(\omega_S,t)|\cos\left[W(\omega_S,t)-\omega_S t+\omega_{IF}t+\varphi_{LN}(\omega_{LO},t)+\varphi_{SN}(\omega_S,t)+\theta_{LO}+\theta_S-\varphi+\chi_{LO}(t)-\frac{\pi}{2}+B(\omega_S,t)\right]\right\}\end{aligned} \tag{7.76}$$

The expression of the mean heterodyne current in Equation (7.76) corresponds to the mean homodyne current in Equation (7.70) with an additional ω_{IF} frequency offset. It can be verified that the phase angle controlled by the PLL is similar to Equation (7.71), but with ω_S replaced with ω_{LO} in the φ_{LN} term.

The heterodyne receiver operator $\hat{Y}_{HE}(t)$ is defined in Equation (7.54), where the expression of the mixing signal $\psi_{HE}(t)$ is given by (7.52). By operating $\hat{Y}_{HE}(t)$ onto the field state $|v'\rangle = |\{\rho_S(\omega)\},\{\rho_L(\omega)\},0_V,0_{V1},0_{V2}\rangle$, with $|\{\rho_L(\omega)\}\rangle$ now given by Equation (7.51) for heterodyne detection, and using the approximate expression of $\chi_{LO}(t)$ in (7.71), the mean signal amplitude detected from the ASK-HE system $\left\langle \hat{Y}_{ASK-HE}(t)\right\rangle$ can be expressed as

$$\left\langle \hat{Y}_{ASK-HE}(t) \right\rangle = \eta q \sqrt{\frac{F_S F_L}{2T_b}} \int_t^{t+T_b} 1 + \sqrt{1+\left|\beta(\omega_S,t')\right|^2} \cos\left[W(\omega_S,t') - \omega_S t'\right] + \left|\beta(\omega_S,t')\right| \cos\left[W(\omega_S,t') - \omega_S t' + 2\left(\varphi_{SN}(\omega_S,t') + \theta_S\right) + B(\omega_S,t')\right] dt' \tag{7.77}$$

where the high frequency terms associated with the intermediate frequency ω_{IF} has been omitted in Equation (7.55) as it averages out to zero within the time duration of a bit period T_b. Similar to BPSK detection, the mean signal current detected by the heterodyne receiver is a factor of $\sqrt{2}$ smaller than the homodyne receiver in the ASK system i.e. $\left\langle \hat{Y}_{ASK-HO}(t) \right\rangle = \sqrt{2} \left\langle \hat{Y}_{ASK-HE}(t) \right\rangle$.

The shot noise variance detected by the ASK-HE receiver is defined in Equation (7.56). Therefore, by using the definition in Equation (7.56), the commutation relation in (7.48), and after some laborious algebraic manipulation, we have

$$\begin{aligned} \left[\Delta Y_{ASK-HE}(t)\right]^2 = \eta q^2 F_L + \frac{\eta q^2}{2T_b} \int_t^{t+T_b} F_S \{ & 1 + 2\sqrt{1+\left|\beta(\omega_S,t')\right|} \left|\beta(\omega_S,t')\right| \cos\left[2\left(\theta_S + \varphi_{SN}(\omega_S,t')\right) + B(\omega_S,t')\right] \\ & + 2\left|\beta(\omega_S,t')\right|^2 + \left|\beta(\omega_S,t')\right| \cos\left[W(\omega_S,t') - \omega_S t' + 2\left(\theta_S + \varphi_{SN}(\omega_S,t')\right) + B(\omega_S,t')\right] \\ & + \sqrt{1+\left|\beta(\omega_S,t')\right|} \cos\left[W(\omega_S,t') - \omega_S t'\right] \} dt' + \frac{1}{2\pi} \int_t^{t+T_b} \int_{\omega_L}^{\omega_U} \left|\beta(\omega,t')\right|^2 dt' d\omega \end{aligned} \tag{7.78}$$

where the terms associated with the intermediate frequency ω_{IF} averaged out to *0* within the bit period T_b, and are neglected in the expression. Note that the shot noise expression for ASK-HO and ASK-HE are the same i.e. $\left[\Delta Y_{ASK-HO}(t)\right]^2 = \left[\Delta Y_{ASK-HE}(t)\right]^2$. Using the fact that $F_L >> F_S$, the expression for $[Y_{ASK-HE}(t)]^2$ can be approximated as

$$\left[\Delta Y_{ASK-HE}(t)\right]^2 = \left[\Delta Y_{ASK-HO}(t)\right]^2 \approx \eta q^2 F_L \approx \left[\Delta Y_{BPSK-HE}(t)\right]^2 = \left[\Delta Y_{BPSK-HO}(t)\right]^2 \tag{7.79}$$

From Equation (7.79), we see that the shot noise variance is the same for ASK and BPSK coherent system. In fact, Equation (7.79) corresponds to the results given by SCFT [1, 25].

7.4 BER Quantum Limit of Communication Systems

The BER quantum limit dictates the minimum signal power required to achieve a given BER. In the analysis presented in Chapter 2.2, we have derived the quantum limits for BPSK-HO, BPSK-HE, ASK-HO, ASK-HE systems using SCFT with the effect of bit transition neglected. In this Section, we shall determine the impact of bit transition and photon creation from modulator on the BER quantum limit using the quantum field models developed for the modulation systems considered in Section 7.2 and Section 7.3. A continuous alternating bit pattern is considered i.e. *'1010...'*, in which a bit transition occurs in every bit period so that the effect of bit transition is maximized. Two important comparisons will be drawn in this analysis. Firstly, we compare the traditional results (results from Chapter 2 OR [1, 25]) in which the effect of bit transition is neglected, with the results obtained from an alternating bit pattern where the effect of bit transition is included but the effect of photon creation is neglected i.e. $|\beta(\omega,t)| = 0$. Subsequently, a comparison between the SCFT and QFT will be made, in order to determine the impact of photon creation from modulator on the types of communication systems considered. Note that, the impact of photon creation is also maximized for an alternating bit pattern because a pulse of photon flux is excited from the modulator at every bit transition (see simulation results in Chapter 6.5).

In Chapter 2.2.3, we have shown the receiver will determine whether a bit *'1'* or bit *'0'* is sent based on the received signal and the threshold set by the decision device X. For the modulation formats considered in this thesis (BPSK-HO, BPSK-HE, ASK-HO, ASK-HE), the probability of transmitting a *'1'* and *'0'* for an alternating bit pattern is equally probable and that the impact of mistaking a *'0'* for a *'1'* is the same

as its converse [22 - 25]. Under these conditions, the optimum threshold can be expressed as [1]

$$X = \frac{\left\langle \hat{Y}[0] \right\rangle (\Delta Y[1]) + \left\langle \hat{Y}[1] \right\rangle (\Delta Y[0])}{(\Delta Y[0]) + (\Delta Y[1])} \tag{7.80}$$

where $<\hat{Y}[0]>$ and $<\hat{Y}[1]>$ are the mean signal amplitude detected from a *'1'* bit and *'0'* bit respectively, and $(\Delta Y[0])$ and $(\Delta Y[1])$ is the standard deviation for a received *'1'* bit and a received *'0'* bit respectively. In Chapter 2.2.3, we have shown provided the photon flux for the signal field and LO field is large i.e. F_S and $F_L >> 1$, the probability density function (PDF) for a received *'0'* bit and a received *'1'* bit can be approximated as a Gaussian distribution. A decision error is made when the signal amplitude detected is greater than X given that a *'0'* bit is sent (i.e. $P(Y|0) > X$) OR when the signal amplitude detected is smaller than X given that a *'1'* bit is sent (i.e. $P(Y|1) < X$), as shown in the shaded area of Figure 7.6.

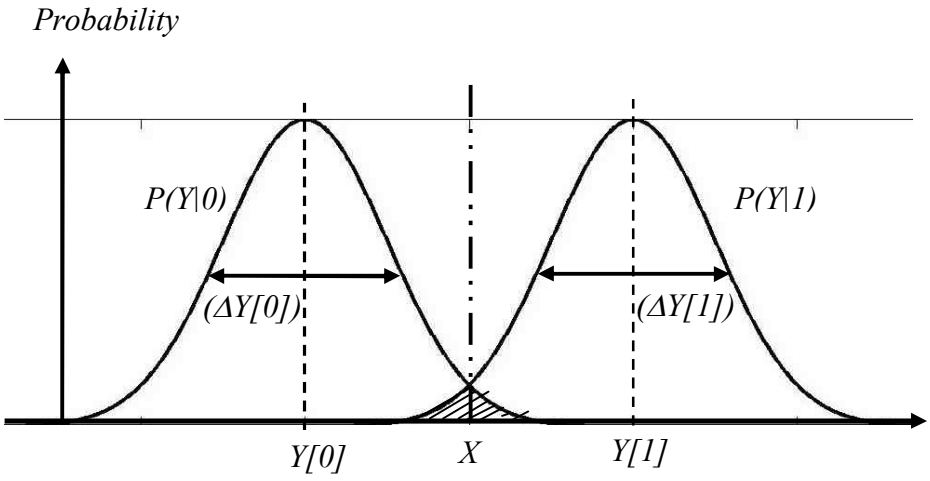

Figure 7.6: Probability density functions for Y, conditioned on *'1'* and *'0'*.

It is shown in Chapter 2.2.3 that the relation between the decision threshold X and the BER is given by

$$BER = Q(\gamma) = Q\left(\frac{X - \left\langle \hat{Y}[0] \right\rangle}{(\Delta Y[0])}\right) = Q\left(\frac{X - \left\langle \hat{Y}[1] \right\rangle}{(\Delta Y[1])}\right) \tag{7.81}$$

where the Q function represents the tail probability of a Gaussian PDF and can be expressed as [25]

$$\begin{aligned} Q(\gamma) &= \frac{1}{2} erfc\left(\frac{\gamma}{\sqrt{2}}\right) \\ &= \frac{1}{\sqrt{2\pi}} \int_{\gamma}^{\infty} \exp\left(\frac{-\xi^2}{2}\right) d\xi \\ &\approx \frac{1}{\sqrt{2\pi\gamma}} \exp\left(-\frac{\gamma^2}{2}\right) \end{aligned} \tag{7.82}$$

The approximation in the second line of Equation (7.82) is valid provided $\gamma > 3$ [25]. By substituting the expression of X in Equation (7.80) into Equation (7.81), the BER can be re-expressed as

$$BER = Q(\gamma) = Q\left(\frac{\left\langle \hat{Y}[1] \right\rangle - \left\langle \hat{Y}[0] \right\rangle}{(\Delta Y[1]) + (\Delta Y[0])}\right) \tag{7.83}$$

where the parameter γ is defined by

$$\gamma = \frac{\left\langle \hat{Y}[1] \right\rangle - \left\langle \hat{Y}[0] \right\rangle}{(\Delta Y[1]) + (\Delta Y[0])} \tag{7.84}$$

γ^2 can be identified as the SNR [1, 25]. Using the expression of the Q-function in Equation (7.82), we can identify the BER is exponentially related to the SNR γ^2.

When the bit pattern is alternating, the refractive index of the modulating medium fluctuates periodically between n and $n + \Delta n$ with respect to time t. A refractive index profile $n(t)$ that describes this situation is given by

$$n(t) = n + \frac{\Delta n}{2}\left\{1 + \sum_{j=0}^{\infty}\left[\tanh\left(2.2\Omega\left(t - 2jT_b\right)\right) - \tanh\left(2.2\Omega\left(t - (2j+1)T_b\right)\right)\right]\right\} \tag{7.85}$$

where j is an integer. The simulation parameters used in this analysis is given by Table 7.1.

Parameters	Symbol	Value
Wavelength	λ_S	*1500 nm*
Bit rate	$1/T_b$	*2 Tbps*
Photon flight time in modulator	T_f	*0.15 ps* ($0.3*T_b$)
10 – 90 % bit transition rate	Ω	$1.5*10^{14}\ s^{-1}$ ($75*1/T_b$)
Modulator refractive index	n	*3.5*
Change in refractive index	Δn	*0.059*
Laser spectral width	$\Delta \nu$	*50 MHz*

Table 7.1: List of simulation parameters.

By using the simulation parameter given in Table 7.1, a plot of alternating bit pattern with its corresponding refractive index profile of the modulating medium is shown in Figure 7.7.

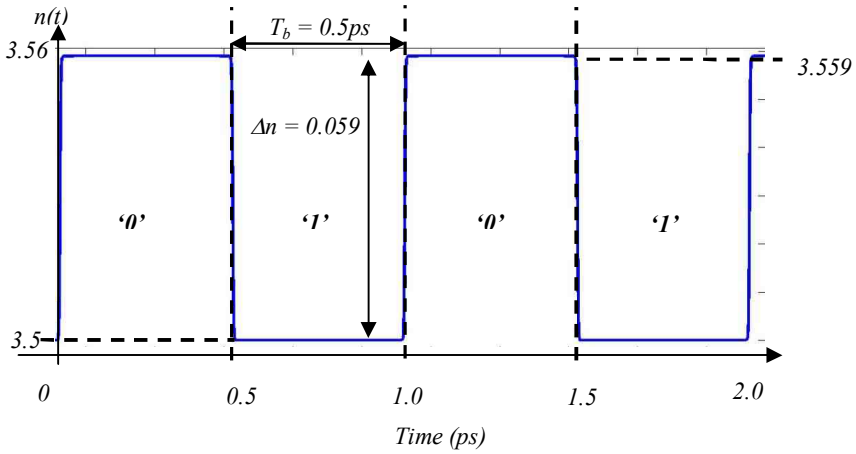

Figure 7.7: Refractive index profile for alternating bit pattern.

The photon flight time in the modulator T_f and the change in refractive index Δn are chosen so that there will be an additional phase delay of π when a *'0'* bit is transmitted in both BPSK and ASK systems. If a *'1'* bit is transmitted; there will be

no additional phase shift. The additional phase delay $\Delta\varphi$ due to modulation is expressed as

$$\Delta\varphi = \frac{2\pi\Delta nL}{\lambda_S} \tag{7.86}$$

where L is the length of the modulator, and is related to the flight time T_f by

$$L = \frac{c_0}{n+\Delta n} T_f \tag{7.87}$$

n is the refractive index of the modulator, and c_0 is the speed of light in vacuum. Since $\Delta\varphi$ must be set to π ($\Delta\varphi = \pi$) in order to satisfy the design specification, and by substituting Equation (7.87) into Equation (7.88), we arrive at

$$\frac{2\pi\Delta n c_0 T_f}{(n+\Delta n)\lambda_0} = \pi \tag{7.89}$$

By setting the photon flight time T_f to be *0.3* of the bit period ($T_f = 0.3*T_b = 0.15$ ps) in Table 7.1, and solving for Δn in Equation (7.89), we found that Δn must satisfy the condition

$$\Delta n = \frac{n\lambda_0}{0.6c_0T_b - \lambda_0} \tag{7.90}$$

to give an additional phase delay of π.

Using Equation (7.46), (7.55), (7.72) and (7.77), the mean signal amplitude of BPSK-HO, BPSK-HE, ASK-HO and ASK-HE systems can be rewritten as

$$\left\langle \hat{Y}_{BPSK-HO}(t) \right\rangle = 2\eta q \sqrt{\frac{F_S F_L}{T_b}} \int_t^{t+T_b} \left(\sqrt{1+\left|\beta(\omega_S,t')\right|^2} \cos\left[W(\omega_S,t') - \omega_S t'\right] + \left|\beta(\omega_S,t')\right| \cos\left[W(\omega_S,t') - \omega_S t' + 2\theta_S + 2\varphi_{SN}(\omega_S,t') + B(\omega_S,t')\right] \right) dt' \tag{7.91}$$

$$\approx 2\eta q \sqrt{\frac{F_S F_L}{T_b}} \left(MT_b + \int_t^{t+T_b} \frac{P(t')}{2} \left|\beta(\omega_S,t')\right|^2 + \left|\beta(\omega_S,t')\right| \cos\left[W(\omega_S,t') - \omega_S t' + 2\theta_S + 2\varphi_{SN}(\omega_S,t') + B(\omega_S,t')\right] dt' \right)$$

$$\left\langle \hat{Y}_{BPSK-HE}(t) \right\rangle = \eta q \sqrt{\frac{2F_S F_L}{T_b}} \int_t^{t+T_b} \left(\sqrt{1+\left|\beta(\omega_S,t')\right|^2} \cos\left[W(\omega_S,t') - \omega_S t'\right] + \left|\beta(\omega_S,t')\right| \cos\left[W(\omega_S,t') - \omega_S t' + 2\theta_S + 2\varphi_{SN}(\omega_S,t') + B(\omega_S,t')\right] \right) dt' \tag{7.92}$$

$$\approx \eta q \sqrt{\frac{2F_S F_L}{T_b}} \left(M + \int_t^{t+T_b} \frac{P(t')}{2} \left|\beta(\omega_S,t')\right|^2 + \left|\beta(\omega_S,t')\right| \cos\left[W(\omega_S,t') - \omega_S t' + 2\theta_S + 2\varphi_{SN}(\omega_S,t') + B(\omega_S,t')\right] dt' \right)$$

$$\left\langle \hat{Y}_{ASK-HO}(t) \right\rangle = \eta q \sqrt{\frac{F_S F_L}{T_b}} \int_t^{t+T_b} 1 + \sqrt{1+\left|\beta(\omega_S,t')\right|^2} \cos\left[W(\omega_S,t') - \omega_S t'\right] + \left|\beta(\omega_S,t')\right| \cos\left[W(\omega_S,t') - \omega_S t' + 2\left(\varphi_{SN}(\omega_S,t') + \theta_S\right) + B(\omega_S,t')\right] dt' \tag{7.93}$$

$$\approx \eta q \sqrt{\frac{F_S F_L}{T_b}} \left(T_b(1+M) + \int_t^{t+T_b} \frac{P(t')}{2} \left|\beta(\omega_S,t')\right|^2 + \left|\beta(\omega_S,t')\right| \cos\left[W(\omega_S,t') - \omega_S t' + 2\theta_S + 2\varphi_{SN}(\omega_S,t') + B(\omega_S,t')\right] dt' \right)$$

$$\left\langle \hat{Y}_{ASK-HE}(t) \right\rangle = \eta q \sqrt{\frac{F_S F_L}{2T_b}} \int_t^{t+T_b} 1 + \sqrt{1+\left|\beta(\omega_S,t')\right|^2} \cos\left[W(\omega_S,t') - \omega_S t'\right] + \left|\beta(\omega_S,t')\right| \cos\left[W(\omega_S,t') - \omega_S t' + 2\left(\varphi_{SN}(\omega_S,t') + \theta_S\right) + B(\omega_S,t')\right] dt' \quad (7.94)$$

$$\approx \eta q \sqrt{\frac{F_S F_L}{2T_b}} \left(T_b(1+M) + \int_t^{t+T_b} \frac{P(t')}{2} \left|\beta(\omega_S,t')\right|^2 + \left|\beta(\omega_S,t')\right| \cos\left[W(\omega_S,t') - \omega_S t' + 2\theta_S + 2\varphi_{SN}(\omega_S,t') + B(\omega_S,t')\right] dt' \right)$$

where we have used the 1st order Taylor series approximation in the last line of Equation (7.91) - (7.94), because $|\beta(\omega_S,t)|^2 << 1$. The modulation factor M in the above Equations is defined as

$$M = \frac{1}{T_b} \int_t^{t+T_b} \cos\left[W(\omega_S,t') - \omega_S t'\right] dt' = \frac{1}{T_b} \int_t^{t+T_b} P(t') dt' \quad (7.95)$$

where $W(\omega_S,t)$ is the modulated phase angle, defined in Equation (7.3), and $P(t)$ is given by

$$P(t) = \cos\left[W(\omega_S,t) - \omega_S t\right] \quad (7.96)$$

From Equation (7.95), we can identify the modulation factor $|M|$ is bounded between *-1* and *1*. In the case of an alternating bit pattern, M becomes time dependent. This is because the phase of $P(t)$, is varying between *0* and π during the bit transition. A plot of the phase of $P(t)$, defined in Equation (7.96), is shown in Figure 7.8, while the modulation factor defined in Equation (7.95) is plotted in Figure 7.9.

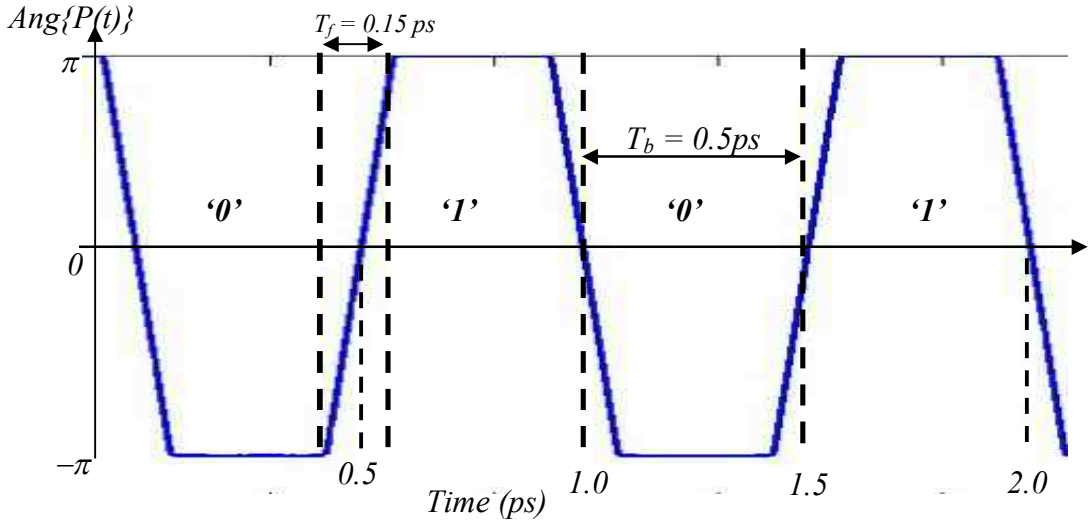

Figure 7.8: Phase of $P(t)$ against time.

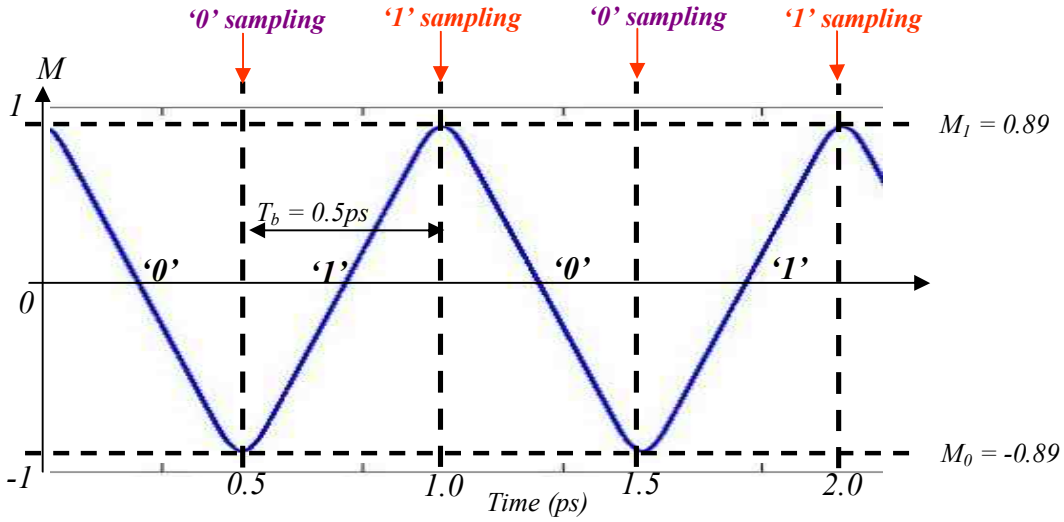

Figure 7.9: Modulation factor M against time.

Notice that when the bit pattern is alternating, the absolute value of the modulation factor never reaches 1, as shown in Figure 7.9. This is because it requires some time for the phase to transit from *0* to π due to the finite T_f of the modulator. The data is sampled at the extrema of M, as shown in Figure 7.9. This gives the maximum difference between the mean signal amplitude of bit *'1'* and bit *'0'* , i.e. the numerator in Equation (7.84) is maximized, and hence minimizes the BER. The maximum and the minimum M value are separated by 1 bit period for an alternating bit sequence. The maximum value of M represents the sampling time of *'1'* bit, this value is

$$M[1] = 0.89 \tag{7.97}$$

Conversely, the minimum value of M represents the sampling time of *'0'* bit, its value is

$$M[0] = -0.89 \tag{7.98}$$

in which $M[1] = -M[0]$. The magnitude of *M[1]* and *M[0]* are the same (i.e. |*M[1]*| = |*M[0]*|) because the profile of leading edge transition is symmetrical to the falling edge transition. The value of M in Equation (7.97) and Equation (7.98) was

determined from the results plotted in Figure 7.9. Referring to Table 7.1, the value of M in Equation (7.97) and (7.98) corresponds to a photon flight time of $T_f = 0.15\ ps$.

The $|\beta(\omega_S,t)|$ term is non-zero in the case of alternating bit pattern for the signal amplitude expressions in Equation (7.91) - (7.94). This is because during the bit transition, $n(t)$ varies with time, thus $d\omega_S/dt$ is non-zero, giving $|\beta(\omega_S,t)|$ also non-zero, as indicated by Equation (7.6). The simulation result of $|\beta(\omega_S,t)|$ against time for alternating bit pattern is shown in Figure 7.10.

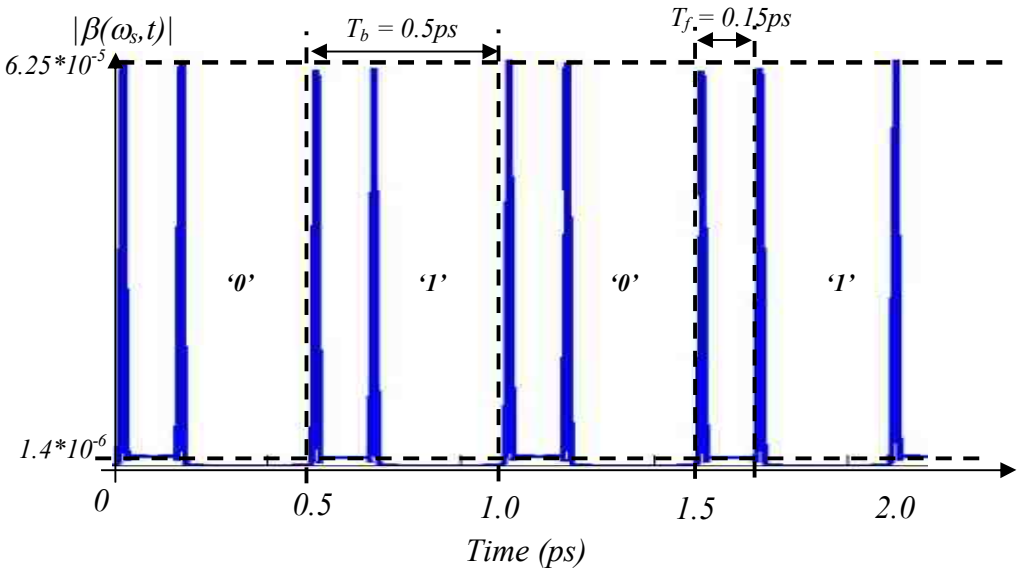

Figure 7.10: $|\beta(\omega_S,t)|$ against time for alternating bit pattern.

In the case of alternating bit pattern, $|\beta(\omega_S,t)|$ is non-zero for some periods of time as shown in Figure 7.10. We see that $|\beta(\omega_S,t)|$ becomes non-zero at the time when bit transition occurs. This non-zero value persists for approximately the photon flight time period inside the modulator T_f because the field will experience a change in refractive index (i.e. $d\omega/dt \neq 0$) over its time of flight inside the modulator, giving a $\beta(\omega_S,t) > 0$ as indicated in Equation (7.6). A detailed explanation for the pulse shape of $\beta(\omega_S,t)$ is given in Chapter 6.3.

The BER is experimentally determined from a large number of bit samples, thus the time for a BER measurement normally greatly exceeds the coherence time of the transmit laser. Therefore, the phase noise $\varphi_{SN}(\omega_S,t)$ can be represented as a random variable with a uniform distribution, as discussed in Chapter 6.3. Using the result in Equation (6.54), we can determine the last term in Equation (7.91) - (7.94) averages out to zero over the period of a BER measurement. The long time averaged detected signal amplitude for the modulation systems considered can therefore be expressed as

$$\overline{\left\langle \hat{Y}_{BPSK-HO}(t) \right\rangle} = 2\eta q \sqrt{\frac{F_S F_L}{T_b}} \left(MT_b + \int_t^{t+T_b} \frac{P(t')}{2} \left| \beta(\omega_S, t') \right|^2 dt' \right) \tag{7.99}$$

$$\overline{\left\langle \hat{Y}_{BPSK-HE}(t) \right\rangle} = 2\eta q \sqrt{\frac{F_S F_L}{T_b}} \left(MT_b + \int_t^{t+T_b} \frac{P(t')}{2} \left| \beta(\omega_S, t') \right|^2 dt' \right) \tag{7.100}$$

$$\overline{\left\langle \hat{Y}_{ASK-HO}(t) \right\rangle} = \eta q \sqrt{\frac{F_S F_L}{T_b}} \left(T_b(1+M) + \int_t^{t+T_b} \frac{P(t')}{2} \left| \beta(\omega_S, t') \right|^2 dt' \right) \tag{7.101}$$

$$\overline{\left\langle \hat{Y}_{ASK-HE}(t) \right\rangle} = \eta q \sqrt{\frac{F_S F_L}{T_b}} \left(T_b(1+M) + \int_t^{t+T_b} \frac{P(t')}{2} \left| \beta(\omega_S, t') \right|^2 dt' \right) \tag{7.102}$$

where the overbar represents the long time averaging quantities. The long time averaged detected signal amplitude for *'1'* bit of the modulation formats can be determined by replacing M by $M[1]$ in Equations (7.99) - (7.102), where we obtained

$$\overline{\left\langle \hat{Y}_{BPSK-HO}[1] \right\rangle} = 2\eta q \sqrt{\frac{F_S F_L}{T_b}} \left(M[1]T_b + \int_{T_{S1}-T_b}^{T_{S1}} \frac{P(t')}{2} \left| \beta(\omega_S, t') \right|^2 dt' \right) \tag{7.103}$$

$$\overline{\left\langle \hat{Y}_{BPSK-HE}[1] \right\rangle} = \eta q \sqrt{\frac{2F_S F_L}{T_b}} \left(M[1]T_b + \int_{T_{S1}-T_b}^{T_{S1}} \frac{P(t')}{2} \left| \beta(\omega_S, t') \right|^2 dt' \right) \tag{7.104}$$

$$\overline{\left\langle \hat{Y}_{ASK-HO}[1] \right\rangle} = \eta q \sqrt{\frac{F_S F_L}{T_b}} \left(T_b(1+M[1]) + \int_{T_{S1}-T_b}^{T_{S1}} \frac{P(t')}{2} \left| \beta(\omega_S, t') \right|^2 dt' \right) \tag{7.105}$$

$$\overline{\left\langle \hat{Y}_{ASK-HE}[1] \right\rangle} = \eta q \sqrt{\frac{F_S F_L}{T_b}} \left(T_b \left(1 + M[1]\right) + \int_{T_{S1}-T_b}^{T_{S1}} \frac{P(t')}{2} \left|\beta(\omega_S, t')\right|^2 dt' \right) \quad (7.106)$$

where T_{S1} is the sampling time of *'1'* bit. Similarly, the long time averaged detected signal amplitude for *'0'* bit for the modulation formats considered can be determined by replacing M with $M[0]$ in Equation (7.99) - (7.102), where we have

$$\overline{\left\langle \hat{Y}_{BPSK-HO}[0] \right\rangle} = 2\eta q \sqrt{\frac{F_S F_L}{T_b}} \left(M[0] T_b + \int_{T_{S0}-T_b}^{T_{S0}} \frac{P(t')}{2} \left|\beta(\omega_S, t')\right|^2 dt' \right) \quad (7.107)$$

$$\overline{\left\langle \hat{Y}_{BPSK-HE}[0] \right\rangle} = \eta q \sqrt{\frac{2F_S F_L}{T_b}} \left(M[0] T_b + \int_{T_{S0}-T_b}^{T_{S0}} \frac{P(t')}{2} \left|\beta(\omega_S, t')\right|^2 dt' \right) \quad (7.108)$$

$$\overline{\left\langle \hat{Y}_{ASK-HO}[0] \right\rangle} = \eta q \sqrt{\frac{F_S F_L}{T_b}} \left(T_b \left(1 + M[0]\right) + \int_{T_{S0}-T_b}^{T_{S0}} \frac{P(t')}{2} \left|\beta(\omega_S, t')\right|^2 dt' \right) \quad (7.109)$$

$$\overline{\left\langle \hat{Y}_{ASK-HE}[0] \right\rangle} = \eta q \sqrt{\frac{F_S F_L}{2T_b}} \left(T_b \left(1 + M[0]\right) + \int_{T_{S0}-T_b}^{T_{S0}} \frac{P(t')}{2} \left|\beta(\omega_S, t')\right|^2 dt' \right) \quad (7.110)$$

where T_{S0} is the sampling time of *'0'* bit.

Because the LO field power is much greater than the signal field power $F_L >> F_S$, the dependence between the noise variance and $|\beta(\omega_S,t)|$ for the modulation formats considered in Equations (7.49), (7.58), (7.74), (7.78) is suppressed and can be represented by Equation (7.79). By substituting the expressions from (7.103) - (7.110) into Equation (7.80), the optimum decision threshold for the modulation systems considered for an alternating *'1010...'* transmit bit pattern with the effect of photon creation included is

$$X_{BPSK-HO} = \eta q \sqrt{\frac{F_S F_L}{T_b}} \left(\left(M[1] + M[0]\right) T_b + \int_{T_{S1}-T_b}^{T_{S1}} \frac{P(t')}{2} \left|\beta(\omega_S, t')\right|^2 dt' + \int_{T_{S0}-T_b}^{T_{S0}} \frac{P(t')}{2} \left|\beta(\omega_S, t')\right|^2 dt' \right) \quad (7.111)$$

$$X_{BPSK-HE} = \eta q \sqrt{\frac{F_S F_L}{2T_b}} \left(\left(M[1] + M[0]\right) T_b + \int_{T_{S1}-T_b}^{T_{S1}} \frac{P(t')}{2} \left|\beta(\omega_S, t')\right|^2 dt' + \int_{T_{S0}-T_b}^{T_{S0}} \frac{P(t')}{2} \left|\beta(\omega_S, t')\right|^2 dt' \right) \quad (7.112)$$

$$X_{ASK-HO} = \frac{\eta q}{2} \sqrt{\frac{F_S F_L}{T_b}} \left(\left(2 + M[1] + M[0]\right) T_b + \int_{T_{S1}-T_b}^{T_{S1}} \frac{P(t')}{2} \left|\beta(\omega_S, t')\right|^2 dt' + \int_{T_{S0}-T_b}^{T_{S0}} \frac{P(t')}{2} \left|\beta(\omega_S, t')\right|^2 dt' \right) \quad (7.113)$$

$$X_{ASK-HE}=\frac{\eta q}{2}\sqrt{\frac{F_S F_L}{2T_b}}\left((2+M[1]+M[0])T_b+\int_{T_{S1}-T_b}^{T_{S1}}\frac{P(t')}{2}\left|\beta(\omega_S,t')\right|^2dt'+\int_{T_{S0}-T_b}^{T_{S0}}\frac{P(t')}{2}\left|\beta(\omega_S,t')\right|^2dt'\right) \quad (7.114)$$

From expression (7.115) - (7.118), we see that the thresholds of the modulation formats considered is dependent on the effect of photon creation $|\beta(\omega_S,t)|$. Furthermore, the thresholds are governed by the modulation factor *M* and the phase transition of the optical field *P(t)*. From Figure 7.8, Figure 7.9 and Figure 7.10, we can identify *M*, *P(t)*, and $\beta(\omega_S,t)$ are all dependent on the shape of the refractive index profile, as shown in Figure 7.7. Because the $|\beta(\omega_S,t)|$ profile for a leading edge transition (bit '*0*' to bit '*1*') is symmetrical to that for a falling edge transition ('*1*' to '*0*'), therefore the phase transition *P(t)* and the modulation factor *M* for *'0'* bit, is negative to *'1'* bit, as shown in Figure 7.8. As a result, *M[1] = -M[0]* and the integral $\int_{T_{S0}-T_b}^{T_{S0}}P(t')\left|\beta(\omega_S,t')\right|^2dt'$ has an opposite sign to the integral $\int_{T_{S1}-T_b}^{T_{S1}}P(t')\left|\beta(\omega_S,t')\right|^2dt'$. Using these relations, the expressions in (7.111) - (7.114) can be simplified to

$$X_{BPSK-HO}=\eta q\sqrt{F_S F_L T_b} \quad (7.115)$$

$$X_{BPSK-HE}=\eta q\sqrt{\frac{F_S F_L T_b}{2}} \quad (7.116)$$

$$X_{ASK-HO}=\eta q\sqrt{F_S F_L T_b} \quad (7.117)$$

$$X_{ASK-HE}=\eta q\sqrt{\frac{F_S F_L T_b}{2}} \quad (7.118)$$

The decision thresholds for an alternating bit pattern, expressed in Equation (7.115) - (7.118), is the same as the traditional results [25] in which the effect of bit transition and photon creation is neglected. This is due to the symmetry of the leading edge transition and the falling edge transition of the control signal profile.

By substituting the expressions of the optimum decision thresholds in Equations (7.115) - (7.118) into Equation (7.81), the BER expressions of the modulation systems considered for an alternating bit pattern transmitted is given by

$$BER_{BPSK-HO} = Q\left[\frac{2\eta q\sqrt{\frac{F_S F_L}{T_b}}\left(\left(M[1]-M[0]\right)T_b + \frac{1}{2}\left(\int_{T_{S1}-T_b}^{T_{S1}} P(t')\left|\beta(\omega_S,t')\right|^2 dt' - \int_{T_{S0}-T_b}^{T_{S0}} P(t')\left|\beta(\omega_S,t')\right|^2 dt'\right)\right)}{2\sqrt{\eta q^2 F_L}}\right] \quad (7.119)$$

$$= Q\left[\sqrt{\eta F_S T_b}\left(2M[1] + \frac{1}{T_b}\int_{T_{S1}-T_b}^{T_{S1}} P(t')\left|\beta(\omega_S,t')\right|^2 dt'\right)\right]$$

$$BER_{BPSK-HE} = Q\left[\sqrt{\frac{\eta F_S T_b}{2}}\left(2M[1] + \frac{1}{T_b}\int_{T_{S1}-T_b}^{T_{S1}} P(t')\left|\beta(\omega_S,t')\right|^2 dt'\right)\right] \quad (7.120)$$

$$BER_{ASK-HO} = Q\left[\frac{\sqrt{\eta F_S T_b}}{2}\left(2M[1] + \frac{1}{T_b}\int_{T_{S1}-T_b}^{T_{S1}} \frac{P(t')}{2}\left|\beta(\omega_S,t')\right|^2 dt'\right)\right] \quad (7.121)$$

$$BER_{ASK-HE} = Q\left[\frac{1}{2}\sqrt{\frac{\eta F_S T_b}{2}}\left(2M[1] + \frac{1}{T_b}\int_{T_{S1}-T_b}^{T_{S1}} \frac{P(t')}{2}\left|\beta(\omega_S,t')\right|^2 dt'\right)\right] \quad (7.122)$$

In these expressions, we have used the properties $\int_{T_{S0}-T_b}^{T_{S0}} P(t')\left|\beta(\omega_S,t')\right|^2 dt' = -\int_{T_{S1}-T_b}^{T_{S1}} P(t')\left|\beta(\omega_S,t')\right|^2 dt'$ and *M[1] = -M[0]*. By using the expressions in (7.119) - (7.122) and the definition of SNR in Equation (7.84), the SNR of the considered modulation formats for an alternate bit pattern transmitted is

$$SNR_{BPSK-HO} = \left(\gamma_{BPSK-HO}\right)^2 = \eta F_S T_b\left(2M[1] + \frac{1}{T_b}\int_{T_{S1}-T_b}^{T_{S1}} P(t')\left|\beta(\omega_S,t')\right|^2 dt'\right)^2 \quad (7.123)$$

$$SNR_{BPSK-HE} = \left(\gamma_{BPSK-HE}\right)^2 = \frac{\eta F_S T_b}{2}\left(2M[1] + \frac{1}{T_b}\int_{T_{S1}-T_b}^{T_{S1}} P(t')\left|\beta(\omega_S,t')\right|^2 dt'\right)^2 \quad (7.124)$$

$$SNR_{ASK-HO} = \left(\gamma_{ASK-HO}\right)^2 = \frac{\eta F_S T_b}{4}\left(2M[1] + \frac{1}{T_b}\int_{T_{S1}-T_b}^{T_{S1}} \frac{P(t')}{2}\left|\beta(\omega_S,t')\right|^2 dt'\right)^2 \quad (7.125)$$

$$SNR_{ASK-HE} = \left(\gamma_{ASK-HE}\right)^2 = \frac{\eta F_S T_b}{8}\left(2M[1] + \frac{1}{T_b}\int_{T_{S1}-T_b}^{T_{S1}} \frac{P(t')}{2}\left|\beta(\omega_S,t')\right|^2 dt'\right)^2 \quad (7.126)$$

The terms that are dependent on $|\beta(\omega_S,t)|$ from the BER and SNR expressions in Equations (7.119) - (7.122), and Equations (7.123) - (7.126), respectively, characterizes the effect of photon creation from modulator during the modulation

process. The terms that are dependent on the modulation factor *M[1]*, describes the effect of bit transition on the performance of the communication systems. If a steady state bit pattern *'1111...'* (i.e. no bit transition) is transmitted, we can verify from Equation (7.6) and Equation (7.95) that $|\beta(\omega_S,t)|^2 = 0$ and $M[1] = 1$, respectively. Therefore, the BER equations in (7.119) - (7.122) **reduces to the traditional results** given by [1, 25], if a **steady state bit pattern** is transmitted because there is no transition in refractive index i.e. $n(t) = n$.

The reduction in M is due to a finite propagation time inside the modulator and finite bit transition time. Because this is not a consequence of the non-zero commutation relation between quantum field operators i.e. $\hat{a}(\omega)$ and $\hat{a}^+(\omega)$, therefore this is **not a quantum effect** and can be predicted by SCFT.

However, the presence of $|\beta(\omega_S,t)|$ term is a **quantum effect** because the Bogoliubov coefficients are required in order for the modulated annihilation and creation operator, $\hat{b}(\omega,t)$ and $\hat{b}^+(\omega,t)$, to satisfy the usual commutation relations given in Equation (7.9). (See Chapter 5.5 for further details). When $|\beta(\omega_S,t)|$ is non-zero, the SNR will increase and the BER will decrease.

The only difference between the results from SCFT and QFT is the $|\beta(\omega_S,t)|$ terms are not included in the SCFT analysis. Therefore, setting $|\beta(\omega_S,t)|$ to zero in (7.119) – (7.122) would yield the SCFT results for the BER expressions for an alternate bit pattern, where we have

$$BER_{BPSK-HO}^{SCFT} = Q\left(2M[1]\sqrt{\eta F_S T_b}\right) \tag{7.127}$$

$$BER_{BPSK-HE}^{SCFT} = Q\left(M[1]\sqrt{2\eta F_S T_b}\right) \tag{7.128}$$

$$BER_{ASK-HO}^{SCFT} = Q\left[M[1]\sqrt{\eta F_S T_b}\right] \tag{7.129}$$

$$BER_{ASK-HE}^{SCFT} = Q\left(M[1]\sqrt{\frac{\eta F_S T_b}{2}} \right) \tag{7.130}$$

Using the expression of the *Q*-function in Equation (7.82), a BER of 10^{-9} *(error/bit)* is achieved when $\gamma \approx 6$ (γ is square root of SNR), while to achieve a BER of 10^{-15}, $\gamma \approx 8$. The parameters $F_S T_b$ in Equations (7.127) - (7.130) represents the photon number required in a bit period i.e. $N = F_S T_b$. Using the simulation parameters in Table 7.1, as well as substituting the value of *M[1]* and *M[0]* from Equation (7.97) and Equation (7.98) respectively into expressions (7.127) - (7.130), SCFT shows the number of photons required in a bit period, to achieve a BER quantum limit of 10^{-9} for the modulation formats considered, are given by

$$\begin{aligned} &2 * 0.891\sqrt{N_{BPSK-HO}^{SCFT}\Big|_{BER=10^{-9}}} = 6 \\ &\therefore N_{BPSK-HO}^{SCFT}\Big|_{BER=10^{-9}} = 11.36 \ photons \ per \ bit \ period \end{aligned} \tag{7.131}$$

$$N_{BPSK-HE}^{SCFT}\Big|_{BER=10^{-9}} = 22.72 \ photons \ per \ bit \ period \tag{7.132}$$

$$N_{ASK-HO}^{SCFT}\Big|_{BER=10^{-9}} = 45.45 \ photons \ per \ bit \ period \tag{7.133}$$

$$N_{ASK-HE}^{SCFT}\Big|_{BER=10^{-9}} = 90.88 \ photons \ per \ bit \ period \tag{7.134}$$

where the quantum efficiency η is assumed to be *1* in the calculation. Similarly using SCFT, the number of photons required in a bit period to achieve a BER quantum limit of 10^{-15} ($\gamma = 8$) of the modulation formats considered are

$$\begin{aligned} &(2 * 0.891)\sqrt{N_{BPSK-HO}^{SCFT}\Big|_{BER=10^{-15}}} = 8 \\ &\therefore N_{BPSK-HO}^{SCFT}\Big|_{BER=10^{-15}} = 20.2 \ photons \ per \ bit \ period \end{aligned} \tag{7.135}$$

$$N_{BPSK-HE}^{SCFT}\Big|_{BER=10^{-15}} = 40.4 \ photons \ per \ bit \ period \tag{7.136}$$

$$N_{BPSK-HE}^{SCFT}\Big|_{BER=10^{-15}} = 80.8 \ photons \ per \ bit \ period \tag{7.137}$$

$$N_{BPSK-HE}^{SCFT}\Big|_{BER=10^{-15}} = 161.6 \ photons \ per \ bit \ period \tag{7.138}$$

Table 7.2 summarizes the differences between traditional (effect of bit transition not included), SCFT (effect of) and QFT results for the BER quantum limit for an alternating bit pattern.

Modulation Format	Quantum limit 10^{-9} (ph/bit) (traditional)	Quantum limit 10^{-15} (ph/bit) (traditional)	Quantum limit 10^{-9} (ph/bit) (SCFT)	Quantum limit 10^{-15} (ph/bit) (SCFT)	Quantum limit 10^{-9} (ph/bit) (QFT)	Quantum limit 10^{-9} (ph/bit) (QFT)
BPSK-HO	9	16	11.36	20.2	$1.136*10^{1}$ - $2.8*10^{-10}$	$2.02*10^{1}$ - $3.8*10^{-10}$
BPSK-HE	18	32	22.72	40.4	$2.272*10^{1}$ - $2.8*10^{-10}$	$4.04*10^{1}$ - $3.8*10^{-10}$
ASK-HO	36	64	45.45	80.8	$4.545*10^{1}$ - $2.8*10^{-10}$	$8.08*10^{1}$ - $3.8*10^{-10}$
ASK-HE	72	128	90.88	161.2	$9.088*10^{1}$ - $2.8*10^{-10}$	$1.612*10^{2}$ - $3.8*10^{-10}$

Table 7.2: Quantum limit comparisons between traditional, SCFT (effect of bit transition included) and QFT analysis for alternating bit pattern.

Table 7.2 shows the quantum limit to achieve a BER of 10^{-15} is greater than 10^{-9} because the performance of the system improves by increasing the power of the transmit laser. The quantum limit relation between different modulation systems in Table 7.2 continue to hold by including the effect of bit transition i.e. $N_{BPSK-HO}^{SCFT} = N_{BPSK-HE}^{SCFT}/2 = N_{ASK-HO}^{SCFT}/4 = N_{ASK-HE}^{SCFT}/8$. From this relation we see that the BPSK-HO receiver is twice as sensitive as BPSK-HE, 4 times as sensitive as ASK-HO, and 8 times more sensitive than ASK-HE receiver. The results in Table 7.2 also show by including the effect of bit transition in SCFT analysis, the number of photon per bit period required to achieve the same BER is greater than the traditional analysis.

This is because traditional analysis [1, 25] assume *M[1] = 1*, while including the effect of bit transition gives *M[1] < 1* in Equation (7.97). Therefore we can conclude the effect of bit transition degrades the systems performance. Using the simulation parameters in Table 7.1, results in Table 7.2 shows the additional photon number required to achieve a given BER is over *10%*, thus the degradation due to bit transition is noticeable. The degradation is illustrated in the signal space diagram in Figure 7.11 where the signal point distance between *'1'* bit and *'0'* bit decreases.

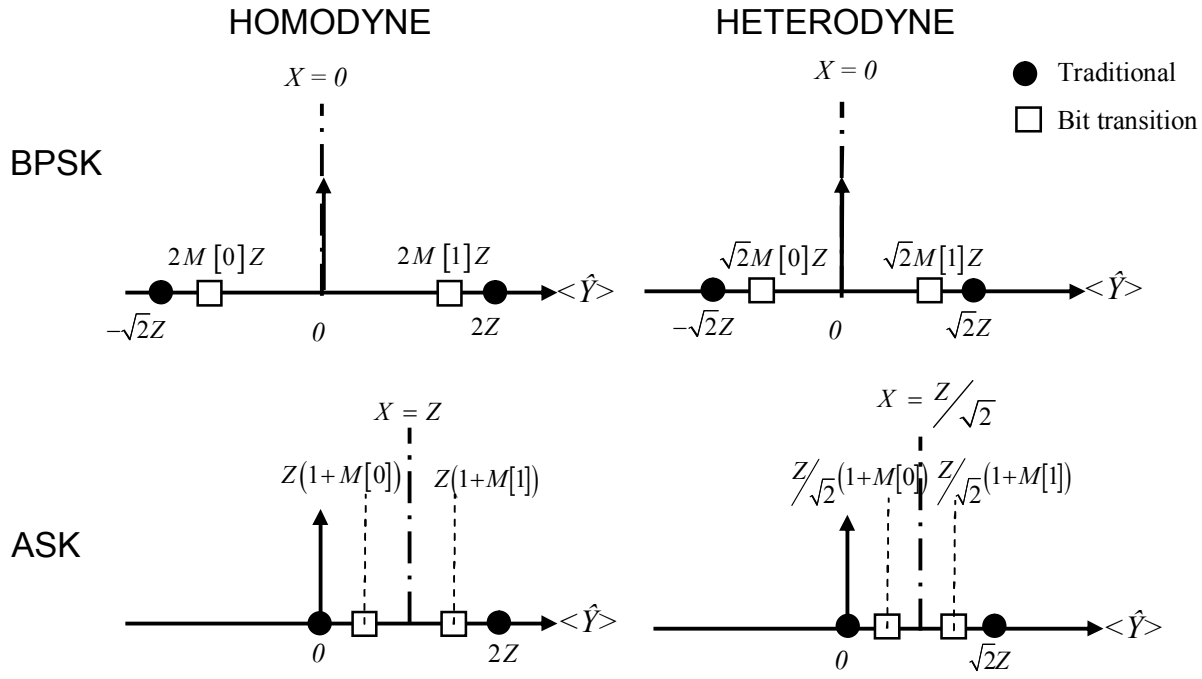

Figure 7.11: Signal space diagram for alternate bit pattern from SCFT, with variable $Z = \eta q\sqrt{F_S F_L T_b}$.

Equation (7.95) shows the modulation factor *M* can be improved (i.e. Increase in *M*) by decreasing the photon flight time T_f i.e. Reducing the size of the modulator. However, the trade off is an increase in the control field power that is required to provide a greater change in refractive index Δn, as suggested by Equation (7.87). The increase in *M* will eventually be limited by damaging the material of the modulator

due to an intense control field. Another option to improve M is to use a traveling wave modulator in which the impact of energy-size tradeoff can be reduced [5, 28].

The $|\beta(\omega_S,t)|$ term is now considered in order to determine the impact of photon creation from modulator on the communication system. Using the results in Equations (7.127) - (7.130) and the QFT BER relation in Equation (7.119) - (7.122) of the modulation formats considered, we can verify the photon number differences between the QFT and SCFT results to achieve a BER of 10^{-9} ($\gamma = 6$) is given by

$$\begin{aligned}\Delta N_{BPSK-HO}\Big|_{BER=10^{-9}} &= \Delta N_{BPSK-HE}\Big|_{BER=10^{-9}} = \Delta N_{ASK-HO}\Big|_{BER=10^{-9}} = \Delta N_{ASK-HE}\Big|_{BER=10^{-9}} \\ &= N^{SCFT}_{BPSK-HO}\Big|_{BER=10^{-9}} - N_{BPSK-HO}\Big|_{BER=10^{-9}} \\ &= \frac{\sqrt{N_{BPSK-HO}\Big|_{BER=10^{-9}}}}{T_b}\int_{T_{S1}-T_b}^{T_{S1}} P(t')\left|\beta(\omega_S,t')\right|^2 dt' \\ &= 2.8*10^{-10}\ photons\ per\ bit\ period\end{aligned} \tag{7.139}$$

Similarly, using the results from Equation (7.135) - (7.138) and the expressions in (7.119) - (7.122), the photon number difference between the SCFT and QFT results to achieve a BER of 10^{-15} ($\gamma = 8$) can be expressed as

$$\begin{aligned}\Delta N_{BPSK-HO}\Big|_{BER=10^{-15}} &= \Delta N_{BPSK-HE}\Big|_{BER=10^{-15}} = \Delta N_{ASK-HO}\Big|_{BER=10^{-15}} = \Delta N_{ASK-HE}\Big|_{BER=10^{-15}} \\ &= N^{SCFT}_{BPSK-HO}\Big|_{BER=10^{-15}} - N_{BPSK-HO}\Big|_{BER=10^{-15}} \\ &= \frac{\sqrt{N^{SCFT}_{BPSK-HO}\Big|_{BER=10^{-15}}}}{T_b}\int_{T_{S1}-T_b}^{T_{S1}} P(t')\left|\beta(\omega_S,t')\right|^2 dt' \\ &= 3.8*10^{-10}\ photons\ per\ bit\ period\end{aligned} \tag{7.140}$$

A positive ΔN in expression (7.139) and (7.140) suggests the number of photons required in a bit period given by the QFT results are less than the SCFT result, which implies the BER is improved. This improvement is due to the process of photon creation from modulator, where these excited photons are added onto the signal strength of the modulated optical field. As a result, the amplitude differences between

a *'1'* bit and *'0'* bit increases, as shown in Figure 7.12, which leads to a decrease in BER, and hence improves the system performance.

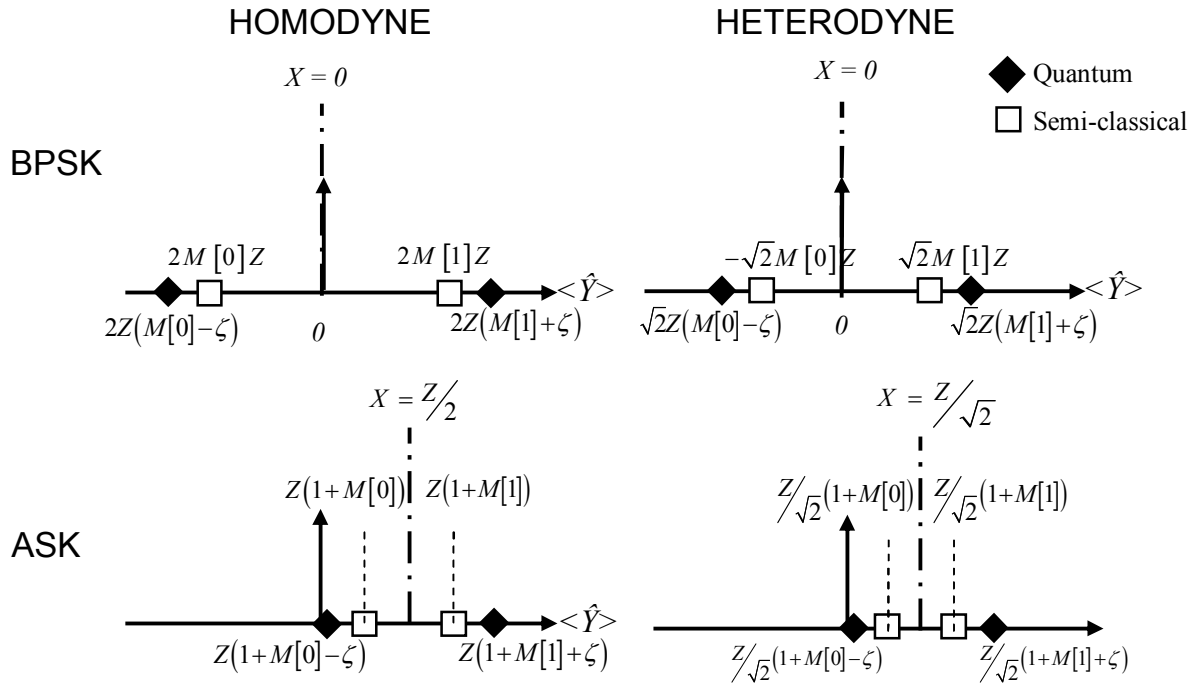

Figure 7.12: Signal space diagram for alternate bit pattern (quantum analysis), with variable $Z = \eta q\sqrt{F_S F_L T_b}$ and $\zeta = \frac{1}{T_b}\int_{T_{S1}-T_b}^{T_{S1}} P(t')\left|\beta(\omega_S, t')\right|^2 dt'$.

From Figure 7.12, we see that the photons created from a *'0'* to *'1'* transition has an opposite phase angle to photons created from a *'1'* to *'0'* transition, therefore the signal point for *'1'* bit and *'0'* bit shifts in an opposite direction. The results in expression (7.139) and (7.140) that are summarized in Table 7.2, which show the photon number difference between SCFT and QFT detection is the same for all of the modulation systems considered. This is because the photon number required to attain a specific BER N^{SCFT} is inversely proportional to the receiver sensitivity. The value of ΔN for systems with a BER of 10^{-15} is greater than systems with a BER of 10^{-9}. This is because to achieve a BER of 10^{-15}, more photons is required in a bit period, as

a result the signal photon flux is greater, and hence more photons are stimulated from the modulator.

Similar to Chapter 6, we introduce the quantum ratio Φ to give a measure for the impact of photon creation on the communication systems. The quantum ratio Φ is defined as

$$\Phi = \frac{\Delta N}{N^{SCFT}} \tag{7.141}$$

A large Φ signifies the effect of photon creation from modulator is large. Using the expressions in (7.139) and (7.140), the value of Φ for various modulation formats at a bit-rate of *2 Tbps* is given by

$$\Phi_{BPSK-HO}\Big|_{BER=10^{-9}} = \Phi_{BPSK-HO}\Big|_{BER=10^{-15}} = 2.5*10^{-11} \tag{7.142}$$

$$\Phi_{BPSK-HE}\Big|_{BER=10^{-9}} = \Phi_{BPSK-HE}\Big|_{BER=10^{-15}} = 1.25*10^{-11} \tag{7.143}$$

$$\Phi_{ASK-HO}\Big|_{BER=10^{-9}} = \Phi_{ASK-HO}\Big|_{BER=10^{-15}} = 6.2*10^{-12} \tag{7.144}$$

$$\Phi_{ASK-HE}\Big|_{BER=10^{-9}} = \Phi_{ASK-HE}\Big|_{BER=10^{-15}} = 3.1*10^{-12} \tag{7.145}$$

The expressions in (7.142) - (7.145) shows the effect of photon creation is independent on the systems BER. This is because ΔN in expression (7.139) and (7.140) increases by the same factor as N^{SCFT} in (7.135) - (7.138), and the trend applies to other BER. However the value of Φ is different for different modulation format and follows the trend of the receiver sensitivity. The effect of photon creation is the greatest for BPSK-HO system and the smallest for ASK-HE system. Note that Φ is maximized when an alternate bit pattern is transmitted because there is a bit transition in every bit period T_b, thus $|\beta(\omega_S,t)|$ is non-zero in every T_b as indicated in expression (7.6), and hence the process of photon creation from modulator has an effect for every bit. In contrast, Φ is minimized for a steady state bit pattern as refractive index is static, where we have $\Phi = 0$. At a bit rate of *2 Tbps*, the quantum

effect of photon creation is very small (ranging from *1 part in 3.2*10^10* for ASK-HE – *1 part in 4*10^10* for BPSK-HO) for the optical communication systems considered.

The issue on whether the effect of photon creation can be observed in an optical communication system can be clarified by determining the BER differences between the QFT and SCFT model. Using the expression in (7.119) - (7.122) and (7.127) - (7.130), the BER difference of various modulation formats for an alternating bit pattern is expressed as

$$\begin{aligned}\Delta BER_{BPSK-HO} &= BER^{SCFT}_{BPSK-HO} - BER^{QFT}_{BPSK-HO} \\ &= Q\left[2M[1]\sqrt{N^{SCFT}_{BPSK-HO}}\right] - Q\left[2M[1]\sqrt{N^{SCFT}_{BPSK-HO}} + \Delta N_{BPSK-HO}\right]\end{aligned} \tag{7.146}$$

$$\Delta BER_{BPSK-HE} = Q\left[M[1]\sqrt{2N^{SCFT}_{BPSK-HE}}\right] - Q\left[M[1]\sqrt{2N^{SCFT}_{BPSK-HE}} + \Delta N_{BPSK-HE}\right] \tag{7.147}$$

$$\Delta BER_{ASK-HO} = Q\left[M[1]\sqrt{N^{SCFT}_{ASK-HO}}\right] - Q\left[M[1]\sqrt{N^{SCFT}_{ASK-HO}} + \Delta N_{ASK-HO}\right] \tag{7.148}$$

$$\Delta BER_{ASK-HE} = Q\left[M[1]\sqrt{\frac{N^{SCFT}_{ASK-HE}}{2}}\right] - Q\left[M[1]\sqrt{\frac{N^{SCFT}_{ASK-HE}}{2}} + \Delta N_{ASK-HE}\right] \tag{7.149}$$

By substituting the corresponding value of N^{SCFT} from (7.131) - (7.134) and ΔN from (7.139) into (7.146) - (7.149), the BER difference between the QFT and SCFT model for the modulation systems that has a SCFT BER of 10^{-9} i.e. $BER^{SCFT}_{BPSK-HO} = 10^{-9}$, is

$$\begin{aligned}\Delta BER_{BPSK-HO}\Big|_{BER=10^{-9}} = \Delta BER_{BPSK-HE}\Big|_{BER=10^{-9}} = \Delta BER_{ASK-HO}\Big|_{BER=10^{-9}} = \Delta BER_{ASK-HE}\Big|_{BER=10^{-9}} &= 2.4*10^{-18} \\ &= -176dB\end{aligned} \tag{7.150}$$

A logarithm unit in *dB* is used for the purpose of convenience of a small BER difference. Similarly using the value of N^{SCFT} and expression and ΔN from (7.140), the BER difference between the QFT and SCFT model for the modulation systems that has a SCFT BER of 10^{-15} i.e. $BER^{SCFT} = 10^{-15}$, is

$$\begin{aligned}\Delta BER_{BPSK-HO}\Big|_{BER=10^{-15}} = \Delta BER_{BPSK-HE}\Big|_{BER=10^{-15}} = \Delta BER_{ASK-HO}\Big|_{BER=10^{-15}} = \Delta BER_{ASK-HE}\Big|_{BER=10^{-15}} &= 3.6*10^{-24} \\ &= -234dB\end{aligned} \tag{7.151}$$

Notice that the BER difference is independent on the modulation systems considered. This is because the photon number difference ΔN due to the effect of photon creation

for the modulation systems considered is the same, as indicated in Equation (7.139) and (7.140). A positive value of ΔBER suggests the BER from the QFT result is **smaller** than the SCFT result, and hence the BER difference corresponds to the BER improvement. Once again, this reveals the fact that the effect of photon creation improves the performance of the system. We shall use the terminology of BER difference and BER improvement interchangeably. However, the improvement is extremely small and is in the order of *-176 dB* for systems with $BER^{SCFT} = 10^{-9}$, and -234 *dB* for systems with $BER^{SCFT} = 10^{-15}$ at *2 Tbps*. This resolution of accuracy is difficult to observe using standard optical communication system equipment. Furthermore, for systems with a BER of 10^{-15}, the BER improvement due to the effect of photon creation from modulator is roughly 6 orders of magnitude (*60 dB*) smaller than systems with a BER of 10^{-9}. This is because the rate of change of the Q function in Equation (7.82) exponentially decreases with an increase in photon number per bit. This implies the BER improvement due to the effect of photon creation will become insignificant as the transmit laser power increases. The relation between the BER difference and the transmitted laser power, for BPSK-HO, BPSK-HE, ASK-HO and ASK-HE systems operating at *2 Tbps*, is shown in Figure 7.13 (a), (b), (c) and (d) respectively.

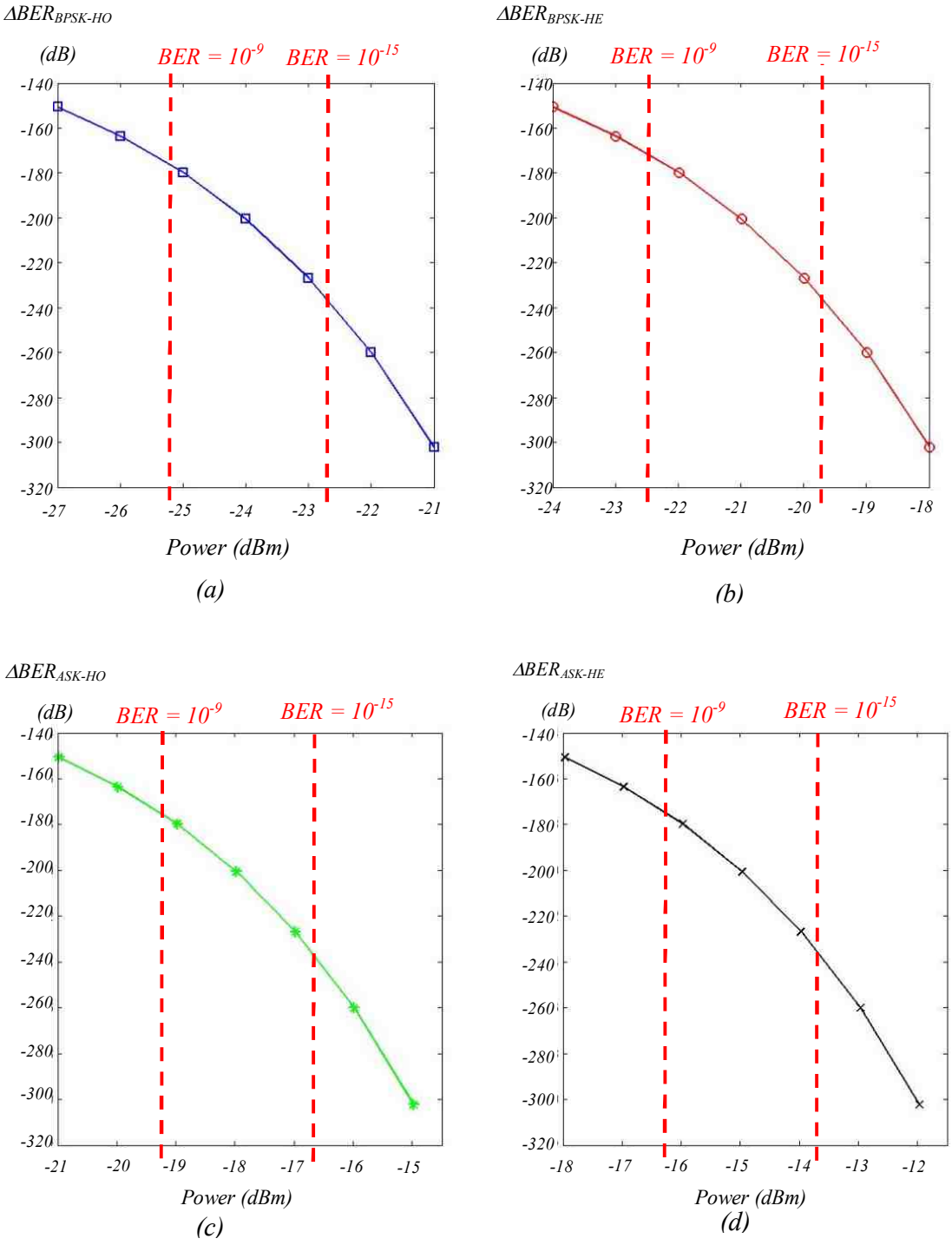

Figure 7.13: Relation between BER improvement and transmitted laser power for the modulation systems considered at *2 Tbps*. (a) BPSK-HO system (b) BPSK-HE system (c) ASK-HO system (d) ASK-HE system.

Figure 7.13 shows the BER improvement rapidly decays as the optical power of the transmit laser increases. The plots show BPSK-HO system requires the least transmit power to achieve the same BER improvement and the same BER. This is because BPSK-HO system has the lowest quantum limit to achieve a given BER as shown in Table 7.2. In addition, the plots show BPSK-HE, ASK-HO and ASK-HE systems require *3 dBm*, *6 dBm*, and *9 dBm* more transmit power, respectively to achieve the same BER and ΔBER. This is because BPSK-HO receiver is twice as sensitive as BPSK-HE, 4 times as sensitive as ASK-HO, and 8 times more sensitive than ASK-HE receiver i.e. $N_{BPSK-HO}^{SCFT} = N_{BPSK-HE}^{SCFT} / 2 = N_{ASK-HO}^{SCFT} / 4 = N_{ASK-HE}^{SCFT} / 8$.

7.5 BER Quantum Limit and Bit rate Relation

In this Section, we reveal the relation between BER quantum limit and bit-rate of the communication system. When an alternating bit pattern *'1010..'* is transmitted, the modulation factor M is not necessarily bit-rate independent because M is dependent on T_b as indicated in Equation (7.95). However, M could become bit-rate independent if all of the following conditions are satisfied:

1. Bit transition rate (Ω in Table 7.1) changes by the same proportion as bit-rate $1/T_b$.
2. Optical wavelength of the transmitted laser λ_S remains the same.
3. Photon flight time inside the modulator T_f changes by the same proportion as the bit period.

The above conditions can be verified from the relation in Equation (7.3). Therefore, by referring to Table 7.1, if the transition rate remains at a fixed multiple *(75)* of times greater than the bit-rate, the ratio of T_f and T_b stays at *0.3*, and the optical wavelength remains at *1500 nm*, the value of *M[1]* and *M[0]* in expression (7.97) and (7.98) is

applicable for systems operating at any bit-rate. The plot in Figure 7.14 shows the transition rate Ω is linearly related to the bit-rate $1/T_b$ and the gradient of the line is *75*.

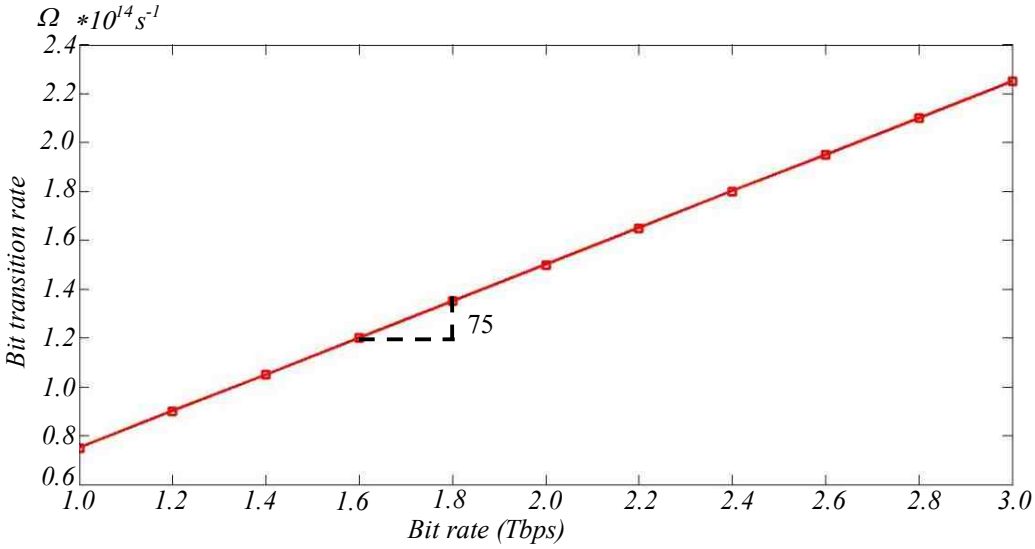

Figure 7.14: Bit transition rate against bit rate.

Note that the adiabatic condition,

$$\left(\frac{d\omega / dt}{\omega_S^{\,2}(t)} \right)_{\max} << 1 \qquad (7.152)$$

introduced in Chapter 5.2, applies at these transition rates. The Bogoliubov coefficients may not be well approximated by Equation (7.5) and (7.6) when the systems bit rate is above *3 Tbps*, as the ratio in expression (7.152) approaches 1. The inverse relation between the photon flight time T_f and the bit-rate, is shown in Figure 7.15.

Using the relation in Equation (7.87), the corresponding modulator length L against bit-rate is plotted in Figure 7.16. The length of the modulator for systems operating in the order of *Tbps* is in the order of *10 μm*.

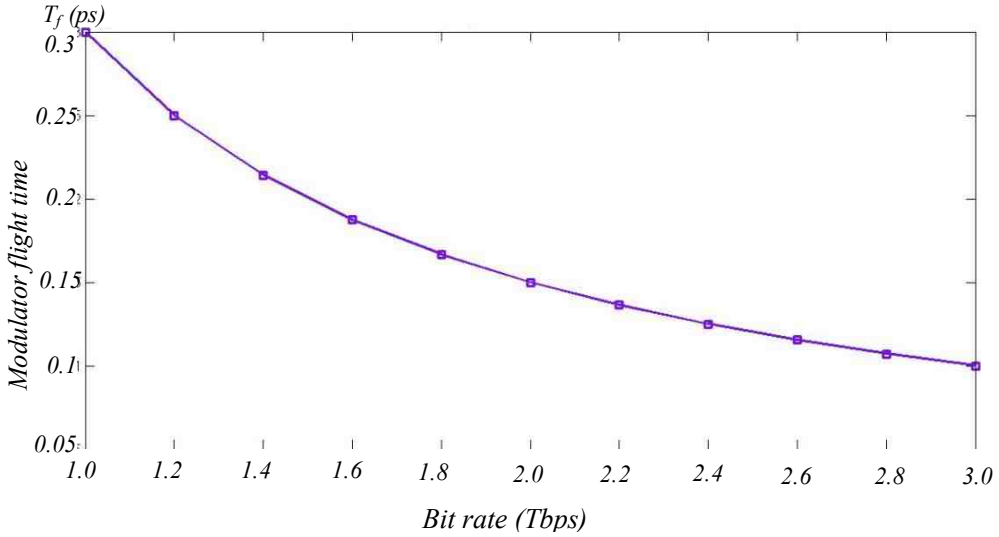

Figure 7.15: Photon flight time in the modulator against bit rate.

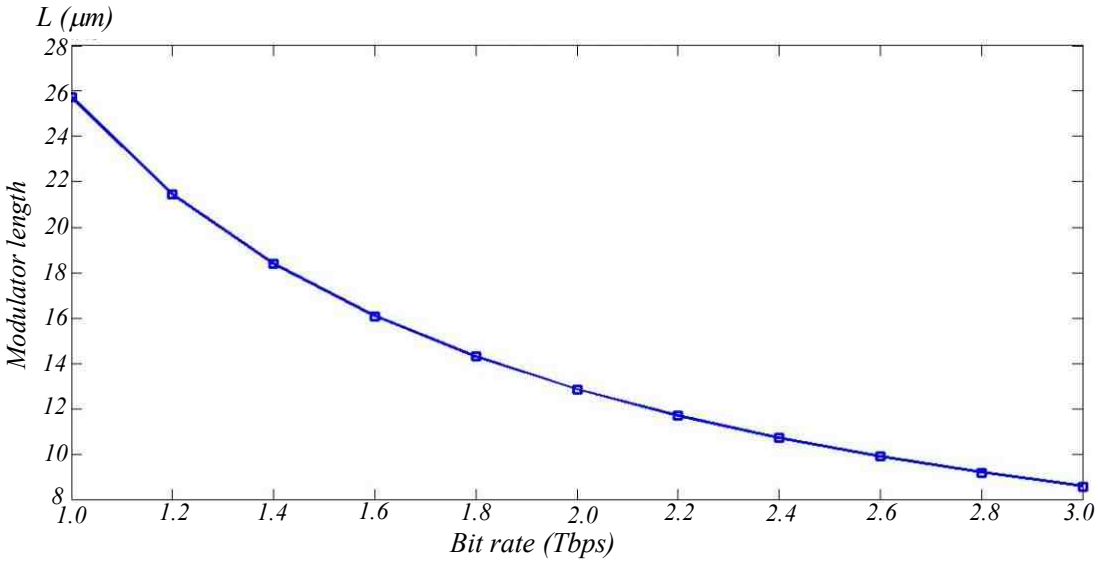

Figure 7.16: Modulator length against bit rate.

Of course the refractive index change Δn needs to be modified when the modulator length L alters with respect to bit-rate as indicated in Equation (7.86). According to expression (7.90), Δn is expected to increase when there is an increase in systems bit-rate. A plot of Equation (7.90) in Figure 7.17 shows the bit rate $1/T_b$ is linearly related to the refractive index change Δn.

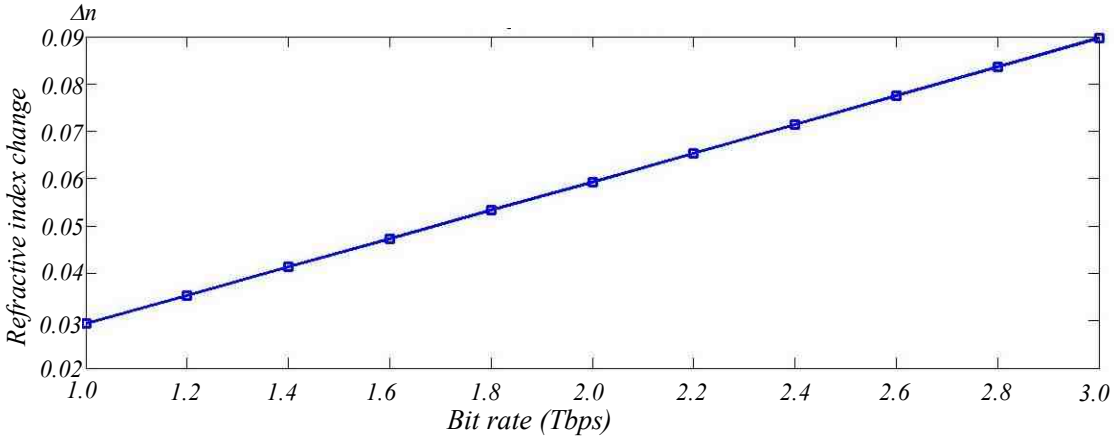

Figure 7.17: Refractive index change against bit rate.

The SCFT results in Equation (7.127) - (7.130) shows **BER becomes bit-rate independent provided the photon number in a T_b remains the same, and the modulation factor M is independent of bit-rate**. However, the results obtained from **QFT disagree with this**. This is because the extra $|\beta(\omega_S,t)|$ in (7.119) - (7.122), which governs the number of photons created during the modulation process is bit-rate dependent, as $\beta(\omega_S,t)$ is governed by $d\omega/dt$, which is related to transition rate Ω, and the change in refractive index Δn. As a result, the **BER is dependent on bit-rate even though M is bit-rate independent**. Therefore, the effect of photon creation from modulator inevitably leads to a difference between SCFT and QFT result on the BER quantum limit.

In Section 7.4, we have introduced the quantum ratio Φ in Equation (7.141) as a measure of the effect of photon creation from modulator. The semi-log plot of the quantum ratio Φ against bit-rate is shown in Figure 7.18.

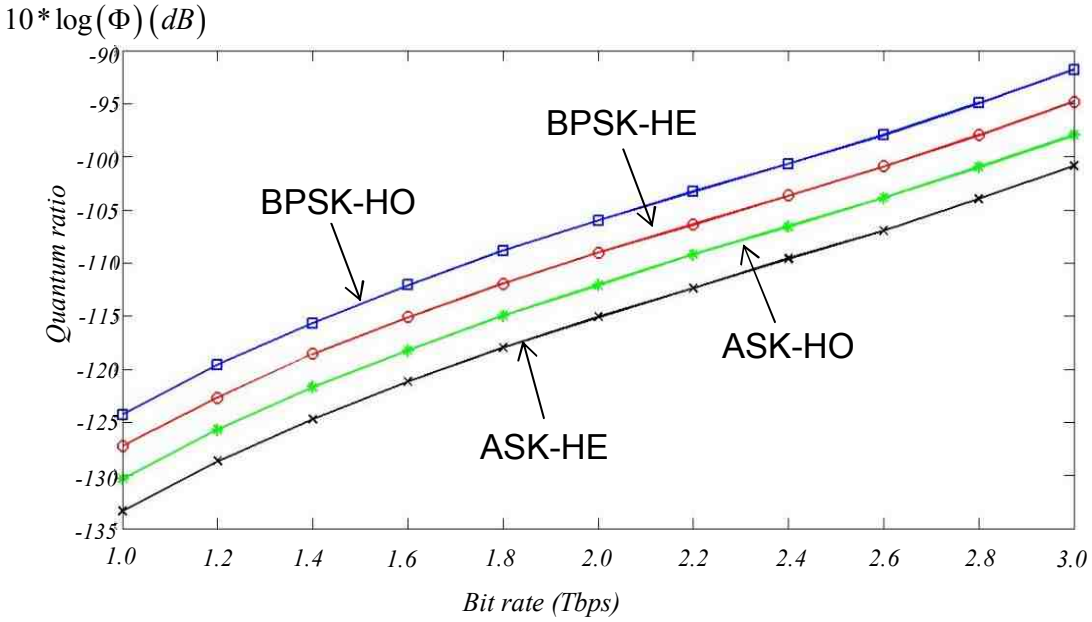

Figure 7.18: Semi-log plot of quantum ratio against bit-rate for modulation systems considered.

From Figure 7.18, we can identify Φ increases by roughly 3 orders of magnitude *30 dB* for an increase in bit-rate of the modulation systems. This indicates the difference in photon number count between the results from SCFT and QFT increases with bit-rate. This is because increasing the bit rate increases both the Ω and Δn as shown in Figure 7.14 and Figure 7.17, where an increase in either of these parameters increases $|\beta(\omega_S,t)|$, as discussed in Chapter 6. The plot shows Φ is the greatest for BPSK-HO, followed by BPSK-HE, ASK-HO and ASK-HE, as Φ is dependent on the photon number required in a bit period N to achieve a specific BER. In Chapter 7.4, we have explained the effect of photon creation from modulator improves the systems performance and Figure 7.18 shows such improvement is bit rate dependent. Furthermore, we have shown in Section 7.4 that Φ is independent on systems BER provided the number of photons in a bit period remains the same. For current optical communication system that operates at a bit-rate of *10 – 40 Gbps*, the quantum effect

is irrelevant ($\Phi < 10^{-35}$). At a bit rate of *3 Tbps*, Figure 7.18 shows the difference is still very small (~ *1 part in* 10^9 for BPSK-HO system). This implies the quantum limit predicted by the SCFT is adequate even at very high bit rates. Therefore we can conclude the quantum effect of **photon creation from modulator has negligible impact on high bit rate optical communication system, thus no extra design consideration is required to incorporate this effect into account**. This is because there are many external factors, such as imperfection of devices and temperature variation, which could obscure the effect of photon creation during the time in which the BER measured. Therefore, we can conclude it is **difficult to detect the impact of photon creation from modulator for high bit-rate *(Tbps)* optical communication systems**.

Detecting the effect of photon creation from modulator requires the phase modulated optical system to be extremely stable so that it is almost independent of external disturbances. Furthermore, the system must have high precision and sensitive measurement devices. An example of a stable phase modulated optical system that utilizes high precision measurement is an optical clock, which could measure down to an accuracy of *1 part in* 10^{18} [57]. The femtosecond pulses that produce periodic event or "clock ticks" at a repetition rate in the order of *GHz* have a high optical intensity, where this leads to the effect of self phase modulation [57], and hence the effect of photon creation from phase modulation may be observed in an atomic clock system owing to its high precision.

7.6 Conclusions

This Chapter presents a quantum field analysis of BPSK-HO, BPSK-HE, ASK-HO, ASK-HE optical communication systems. These analyses show the difference between SCFT and QFT results is due to the phenomenon of photon creation during the phase modulation process. The effect of photon creation increases both signal amplitude and the shot noise of the system. However, the change in shot noise statistics is suppressed and can be neglected given that the power of the LO field is much greater than the signal field.

The optical detection theory presented in this Chapter shows the BER quantum limit is dependent on bit pattern transmitted. This is because the effect of bit transition reduces the modulation factor, and hence degrades the system's performance. Furthermore photons are created from modulator at every bit transition which leads to the difference between QFT and SCFT results. Analysis shows the effect of photon creation from modulator improves the performance of the modulation system considered. For modulation systems operating at a bit-rate of *2 Tbps*, the difference in the number of photons required in a bit period between SCFT and QFT results to achieve a BER of 10^{-9}, is $2.8*10^{-10}$, and for systems with a BER of 10^{-15}, it is $3.8*10^{-10}$. This difference is the same for the modulation formats considered. The photon number difference due to photon creation gives rise to a BER difference between the SCFT and QFT results.

The effect of photon creation from modulator can be measured by the quantum ratio Φ. It is shown that the quantum ratio is bit-rate dependent as the transition rate and the refractive index change increases by the same proportion to maintain the same modulation factor. Φ is the greatest for BPSK-HO followed by BPSK-HE, ASK-HO and ASK-HE, and is independent to systems BER. The results show for modulation

systems operating at *1 – 3 Tbps,* the quantum ratio exponentially increases roughly by *30 dB* (i.e. from $\sim 10^{-12}$ - $\sim 10^{-9}$ for BPSK-HO system, and from $\sim 10^{-14}$ - $\sim 10^{-11}$ for ASK-HE system). Based on this resolution, we can conclude the effect of **photon creation from modulator has negligible impact on high bit rate optical communication system,** and it is **difficult to detect the BER difference as a result of photon creation**. However, the effect of photon creation maybe observed for high precision phase modulated systems such as atomic clock [57].

8 Conclusion

8.1 Summary

We have developed a quantum field model of a phase modulated optical field that includes the quantum effect of photon creation from modulator. In this thesis, we considered the field is modulated by an all optical transverse phase modulator (AO-TPM) operating in the order of *Tbps*. The equations of motion that governs propagation of the optical field in the modulating medium and anti-reflective coating (ARC) of the phase modulator were derived. By matching the boundary conditions of the general solutions between these different media in the modulator, the quantum field representation for a phase modulated optical field was derived.

Using the expression for the phase modulated field derived from our quantum model, we identified a power flow mismatch between the input and output of a lossless modulator during the modulation process. The mismatch in power flow is accounted for by noting that the modulating agent alters the refractive index of the modulator and exciting the vacuum state of the field. Depending on the initial phase angle, phase noise, and the phase of the Bogoliubov coefficients (α and β), the power of the input field can be added or removed by the modulator, which gives rise to the power flow difference between the input and the output of the modulator. We have shown the process of photon creation changes the state of the input optical field from a coherent state to a two photon coherent state, for which the mean and variance of the photoelectron arrival statistics observed by the detector for a modulated field is different to that of an unmodulated field. Simulation results have shown photons are

excited from the modulator during the transition of the modulating medium's refractive index.

The effect of photon creation from modulator can be enhanced by decreasing the frequency of the input optical field ω_S, or increasing the photon flight time of the modulator T_f, the nonlinear refractive index Δn, or the bit transition rate.

From the expression for the phase modulated field, we see the effect of bit transition reduces the modulation factor, which leads to a noticeable degradation in the system's performance. However, the effect of photon creation improves the performance of the modulation systems considered (BPSK-HO, BPSK-HE, ASK-HO and ASK-HE systems) because the energy excited from modulator are added onto the signal field, while the effect of photon creation on the power of the shot noise is suppressed by the strong LO field. By maintaining the modulation factor while increasing the bit rate of the system, simulation results have shown the influence of photon creation from modulator on the optical communication system is exponentially increasing with a linear increase in bit rate. However, it is shown that for optical communication systems operating in the order of *Tbps*, the effect of photon creation from modulator has an insignificant impact to the systems performance. Therefore we conclude the effect of photon creation is unlikely to be detected in high speed optical communication systems.

8.2 Future works

In this thesis, the quantum model that we have constructed describes the operation of a transverse phase modulator. The model presented here is not applicable to the description of a traveling wave phase modulator, another common type of phase modulator in which the control field co-propagates with the signal field. The

refractive index change of a traveling wave phase modulator is time and spatially dependent while in this thesis the refractive index change is only dependent on time for a transverse phase modulator. This work can be extended by developing a quantum model that describes the operation of a traveling wave phase modulator so that the extent of the impact of photon/energy excitation from the travelling wave modulator could be deduced.

Another possible future direction for this work is to consider the impact of photon creation in ultra-high speed clock systems such as proposed by [57]. The system uses femto-second pulses within a high precision phase modulated system that can measure down to the accuracy of *1 part to* 10^{18}, thus the effect of photon creation may be detectable.

Bibliography and References

[1] J. R. Barry and E. A. Lee, "Performance of Coherent Optical Receivers" Proceedings of IEEE, Vol. 8, No. 8, pp. 1369-1394, 1990.

[2] J. Baliga, et al., "Energy Consumption in Optical IP Networks," *J. Lightwave Technol.*, Vol. 27, pp. 2391-2403, 2009.

[3] K. G. Coffman and A. M. Odlyzko, "The size and growth rate of the Internet," *AT & T Labs - Research*, 1998.

[4] R. S. Tucker, "High-speed modulation of semiconductor lasers," (Invited Paper), *IEEE Trans. Electron Devices*, pp. 2572-2584, Dec. 1985.

[5] A. Yariv, "Optical Electronics in Modern Communications," 5th ed.", Oxford Uni. Press, 1997.

[6] W. Shieh, Q. Yang, and Y. Ma, "107 Gb/s coherent optical OFDM transmission over 1000-km SSMF fiber using orthogonal band multiplexing," Opt. Express, Vol. 16, pp. 6378-6386, 2008.

[7] L. Zhao and H. Shankar "40G QPSK and DQPSK Modulation," *Inphi - Research*, 2007.

[8] K. Kikuchi, "Coherent optical communication systems," in *Optical Fiber Telecommunications V,* I. P. Kaminow, T. Li and A. E. Willner, eds., Elsevier Vol. B. Chap. 3, 2008.

[9] P. Kumar and A. Prabhakar, "Evolution of Quantum States in an Electro-optic Phase Modulator," *IEEE J. of Quantum Electronics*, Vol. 45, pp. 149–156, 2009.

[10] E. Schrödinger, Physica, Vol. 6, pp. 899–912, 1939.

[11] K. Husumi, “Miscellanea in elementary quantum mechanics II”, Prog. Theor. Phys., Vol 9, pp. 381–402, 1953.

[12] L. Parker, “Quantized fields and particle creation in expanding universes. I,” Phys. Rev., Vol. 183, Issue 5, pp. 1057-1068, 1969.

[13] G. T. Moore, “Quantum Theory of the Electromagnetic Field in a Variable-Length One-Dimensional Cavity,” *J. Math. Phys.*, Vol. 11, pp. 2679–2691, 1970.

[14] S. W. Hawking, “Black hole explosions?,” *Nature*, Vol. 248, pp. 30-31, 1974.

[15] W. G. Unruh, “Notes on black-hole evaporation,” *Phys. Rev. D*, Vol. 14, pp. 870-892, 1976.

[16] E. Yablonotivitch, “Accelerating Reference Frame for Electromagnetic Waves in a Rapidly Growing Plasma: Unruh-Davies-Fulling-DeWitt Radiation and the Nonadiabtic Casimir Effect,” *Phys. Rev. Letter*, Vol. 62, pp. 1742-1745, 1989.

[17] V. V. Dodonov, et Al. “Quantum phenomena in nonstationary media,” *Phys. Rev. A*, Vol. 47, pp. 4422-4429, 1993.

[18] C. K. Law, “Effective Hamiltonian for the radiation in a cavity with a moving mirror and a time-varying dielectric medium,” *Phys. Rev. A*, Vol. 49, pp. 433-437, 1994.

[19] V. V. Hizhnyakov, “Quantum emission of a medium with a time-dependent refractive index,” *Quantum Opt. Letter*, Vol. 4, pp. 277-280, 1992.

[20] J. T. Mendonca, et al., “Temporal beam splitter and temporal interference,” *Phys. Rev. A*, Vol. 68, 043801, 2003.

[21] A. V. Dodonov, V. V. Dodonov, "Resonance generation of photons from vacuum in cavities due to strong periodical changes of conductivity in a thin semiconductor boundary layer," *J. Opt. B*, Vol 7, pp. S47-S58, 2005.

[22] S. Haykin, "Communication Systems," Fourth eds., John Wiley and Sons, 2001.

[23] B. P. Lathi, "Modern Digital and Analog Communication Systems," 3rd eds., Oxford Uni. Press, 1998.

[24] H. P. Hsu, "Analog and Digital Communication Systems," 2nd eds., in *Schaum's outlines*, McGraw-Hill Co., 2003.

[25] P.E. Green, "Fiber Optic Networks," Prentice Hall, 1993.

[26] N. Birrell and P. C. W. Davies, "Quantum Fields in Curved Space," Cambridge Uni. Press, 1982.

[27] S. L. Braunstein, "A quantum optical shutter," *J. Opt. B*, Vol.7, pp. S28-S31, 2005.

[28] E. L. Wooten, et al., "A Review of Lithium Niobate Modulators for Fiber-Optic Communication Systems," *IEEE J. of Sel. Topics in Quantum Electronics*, Vol. 6, pp. 69-82, 2000.

[29] E. Bahaar, A. Saleh and M. C. Teich, "Fundamentals of Photonics", Wiley Interscience, 1991.

[30] S. Yamataki and K. Emura, "Feasibility study on QPSK optical-heterodyne detection system," Vol. 8, pp. 1646-1653, 1990.

[31] A. Arvizu, et al., "Balanced photoreceiver for coherent optical communications," *J. of Mexian Soc. of Instr.*, Vol. 3, pp. 3-14, 1998.

[32] G. Einarsson, "Principles of Lightwave Communications," Wiley, 1996.

[33] R. Loudon, "The Quantum Theory of Light," 3rd eds., Oxford Uni. Press, 2000.

[34] A. Papoulis, "Probability, Random Variables, and Stochastic Processes," 2nd ed., McGraw Hill, 1984.

[35] D. Marcuse, "Principles of quantum electronics," Academic Press, 1980.

[36] F. T. Ulaby, "Fundamentals of Applied Electromagnetics," 2004 Media ed., Pearson Prentice Hall, 2004.

[37] G. F. Miner, "Lines and Electromagnetic Fields for Engineers," Oxford Uni. Press, 1996.

[38] D. McMahon, "Quantum Field Theory Dymystified," McGraw Hill, 2008.

[39] L. S. Brown and L. J. Carson, "Quantum-mechanical parametric amplification," *Phys. Rev. A*, Vol. 20, pp. 2486 – 2497, 1979.

[40] V. Mukhanov and S. Winitski, "Introduction to Quantum Effects in Gravity," Cambridge Uni. Press, 2007.

[41] V. L. Ginzburg, "The Propagation of Electromagnetic Waves in Plasmas," Oxford, New York, Pergamon Press, 1970.

[42] E. Sassaroli, et al., "Photon production by the dynamical Casimir effect," *Phys. Rev. A,* Vol. 50, pp. 1027-1034, 1994

[43] C. Bernard and A. Duncan, "Regularization and renormalization of quantum field theory in curved space-time," *Annals of Phys.*, Vol. 107, pp. 201-221, 1977.

[44] M. R. Setare, "Cosmological Particle Creation and Dynamical Casimir Effect," *Int. J. of Theo. Phys.*, Vol. 43, pp. 2237 – 2242, 2004.

[45] D. Bohm, "Quantum Theory," Dover Publications Inc., 1989.

[46] K. J. Blow, et al., "Continuum Fields in Quantum Optics," *Phys. Rev. A*., Vol. 42, pp. 4102-4114, 1990.

[47] L. L. Jeromin and V. W. S. Chan, "Modulation design for heterodyne optical communication system," in *Proc. IEEE Global Commun. Conf.*, pp. 412-415, 1983.

[48] G. J. Foschini, et al., "Noncoherent detection of coherent lightwave signals corrupted by phase noise," *IEEE Trans. Commun.,* Vol. 36, pp. 306-314, 1988.

[49] J. Salz, "Coherent lightwave communications," *AT&T Tech. J.*, Vol. 64, pp. 2153-2209, 1985.

[50] H. P. Yuen, "Two-photon coherent states of the radiation field," *Phys. Rev. A.*, Vol. 13, pp. 2226-2243.

[51] J. V. Neumann, "Die Eindeutigkeit der Schrödingerschen Operator," *Math. Ann.*, Vol. 104, pp. 570-578, 1931.

[52] R. Loudon and P. L. Knight, "Squeezed light," *J. Mod. Opt.*, Vol. 34, pp. 709-759, 1987.

[53] M. Miri and S. Khorasani, "Displacement and Squeezed Operators of a Three-Dimensional Harmonic Oscillator and Their Associated Quantum States," *Int. J. Opt. and Photonics,* Vol. 4, pp. 9-22, 2010.

[54] J. S. Peng and G. X. Li, "Introduction to Modern Quantum Optics," World Scienitifc, 1998.

[55] M. Abramowitz and I. Stegun, "Handbook of Mathematical Functions with Formulas, Graphs, and Mathematical Tables," New York: Dover, 1972.

[56] A. V. Oppenheim, A. S. Willsky and S.H. Nawab, "Signals and Systems," 2nd Ed., Prentice Hall, 1997.

[57] S. A. Diddam, et al., "An Optical Clock Based on a Single Trapped $^{199}Hg^{+}$ Ion," *Science Research Articles*, Vol. 293, pp. 825-828, 2001.

Appendix A: List of Publications

1. A. Tam, et al., "Quantum Model of Optical Phase Modulator," *Australasian Conf. on Opt., Laser and Spec.*, Adelaide, paper 441, 2009
2. A. Tam, et al., "Quantum model of phase modulated optical field," submitted to *Int. Quantum Elec. Conf.*, 2011.